NONLINEAR COMBUSTION INSTABILITY IN LIQUID PROPELLANT ROCKET ENGINES

A THESIS

Presented to

The Faculty of the Division of Graduate

Studies and Research

by

Eugene Alexander Powell

In Partial Fulfillment

of the Requirements for the Degree

Doctor of Philosophy

in the School of Aerospace Engineering

Georgia Institute of Technology

September, 1970

NONLINEAR COMBUSTION INSTABILITY IN LIQUID PROPELLANT ROCKET ENGINES

Approved:

Chairman

Date approved by Chairman: May 28, 1970

In presenting the dissertation as a partial fulfillment of the requirements for an advanced degree from the Georgia Institute of Technology, I agree that the Library of the Institute shall make it available for inspection and circulation in accordance with its regulations governing materials of this type. I agree that permission to copy from, or to publish from, this dissertation may be granted by the professor under whose direction it was written, or, in his absence, by the Dean of the Graduate Division when such copying or publication is solely for scholarly purposes and does not involve potential financial gain. It is understood that any copying from, or publication of, this dissertation which involves potential financial gain will not be allowed without written permission.

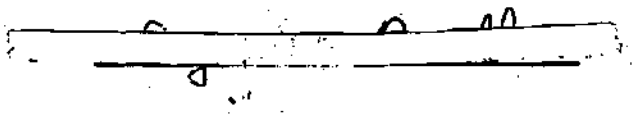

7/25/68

ACKNOWLEDGMENTS

I would like to express my appreciation to Dr. Ben T. Zinn for his suggestion of the thesis topic and for his guidance during the course of this research. I would also like to thank Dr. Warren C. Strahle and Professor James E. Hubbartt for their careful examination of the manuscript, and Dr. Michael Stallybrass for his advice on the mathematical aspects of the problem.

The numerous discussions with my colleagues, in particular Mr. Allan J. Smith, Jr., have provided me with valuable insight into the various aspects of the problem from time to time. Their advice is greatly appreciated. In addition I would like to thank the staff of the Rich Electronic Computer Center for the use of the Univac 1108 Computer facility which made possible the numerical computations presented in this thesis.

The financial support of the National Aeronautics and Space Administration (under NASA grant NGR 11-002-083), the National Science Foundation, and the Georgia Institute of Technology are gratefully acknowledged.

I wish to express my appreciation to Mrs. Anne Fisher for the typing of the manuscript.

Finally, I wish to thank my parents, Mr. and Mrs. Eugene Powell, for their assistance and wholehearted support during the years of my education.

TABLE OF CONTENTS

LIST OF TABLES

LIST OF ILLUSTRATIONS

LIST OF ILLUSTRATIONS (Continued)

LIST OF ILLUSTRATIONS (Continued)

LIST OF ILLUSTRATIONS (Continued)

NOMENCLATURE

$A_{lmn}(t)$, $B_{lmn}(t)$	mode-amplitude functions (see Eq. (215))
B_i	boundary residuals
c^*	velocity of sound
c_p	specific heat at constant pressure
c_v	specific heat at constant volume
e	specific internal energy
E_i	equations residuals
f	rate of physical processes (see Eq. (90))
F_E	energy generation per unit volume
F_{Mass}	mass generation per unit volume
$\vec{F}_{Mom}$	momentum generation per unit volume
h	specific enthalpy
i	imaginary unit, $\sqrt{-1}$
$\vec{J}$	mass flux vector

J_m	Bessel function of the first kind, order m
L^*	characteristic length
m	azimuthal mode number
n	interaction index
$\underrightarrow{n}$	unit outward normal vector
p	pressure
Q_E	concentrated energy source at the boundary
Q'_m	unsteady mass source at nozzle boundary
Q_{Mass}	concentrated mass source at the boundary
$\underrightarrow{Q}_{Mom}$	concentrated momentum source at the boundary
r	radial coordinate
R^*	chamber radius
s	boundary of combustor, complex frequency
S	entropy
S_{mn}	dimensionless transverse mode frequency
t	time
T	temperature

u	axial velocity component
v	volume of combustor, radial velocity component
$\underset{\rightarrow}{V}$	velocity vector
w	tangential velocity component
W_m	mass source due to combustion
x	axial coordinate for one-dimensional problem
$\underset{\rightarrow}{x}$	position vector
z	axial coordinate
γ	ratio of specific heats
ϵ	ordering parameter
ζ	tangential quasi-potential function
η	radial quasi-potential function
θ	azimuthal coordinate
Λ	amplification factor, i.e. real part of s
ρ	density
τ	sensitive time lag
Φ	velocity potential, axial quasi-potential function

Φ_{mn}, Ψ_{mn}	transverse acoustic mode functions
ω	frequency of oscillation
Ω	imaginary part of the complex frequency
$\underset{\sim}{\Omega}$	vorticity

Superscripts

$( )'$	perturbation quantity
$(\bar{})$	steady state quantity
$( )^*$	dimensional quantity, complex conjugate
$(\tilde{})$	approximate solution

Subscripts

e	evaluated at the nozzle entrance
L	pertaining to the liquid phase
n	radial mode number
r	reference quantity
s	stagnation quantity
0	evaluated at the injector

SUMMARY

In an effort to overcome the mathematical difficulties associated with the solution of nonlinear combustion instability problems, a new approximate method based on the Galerkin method is developed. This method is used to study the nonlinear behavior of combustion driven oscillations in cylindrical combustion chambers in which the liquid propellants are injected uniformly across the injector face and the combustion process is distributed throughout the combustion chamber. Crocco's time-lag (n, τ) hypothesis is used to describe the unsteady combustion process, and the hot combustion products are assumed to leave the combustion chamber through a quasi-steady nozzle.

In a second order analysis the steady state Mach number is assumed to be small and the conservation equations are combined to obtain a single nonlinear partial differential equation which describes the behavior of the velocity potential. The velocity potential is expanded in a series of acoustic modes, each of which is multiplied by an unknown time-dependent coefficient. Using this series and applying the Galerkin orthogonality criteria yields a system of nonlinear ordinary differential equations which are solved numerically. Numerical calculations are used to predict the following phenomena: (1) the final amplitude attained in an unstable engine, (2) "triggering" of instability by finite amplitude disturbances in a linearly stable engine, and (3) the shape of the nonlinear pressure waves. The dependence of the resulting oscillation upon the engine parameters is

also determined.

Restrictions imposed on the second order theory include small Mach number mean flow, irrotational flow, and the presence of waves of moderate amplitude. In order to relax some of these restrictions a third order theory is developed. The resulting conservation equations can no longer be reduced to a single equation governing the behavior of the velocity potential; instead a system of partial differential equations must be solved. Because of the complexity of these equations, the behavior of a single transverse mode is studied by approximating each of the dependent variables as the product of an amplitude function and the spatial dependence of that mode. The resulting solutions are then compared with those obtained from the second order analysis.

On the basis of results obtained from the second and third order theories the following nonlinear mechanisms were found to be important in determining the nonlinear stability characteristics of the system: (1) the transfer of energy between modes, (2) the self-coupling of a mode with itself, and (3) a nonlinear combustion mass source. The self-coupling mechanism was found to be very important in the initiation of triggered instability, while the nonlinear driving mechanism was important in the determination of the final amplitude of triggered instability.

CHAPTER I

INTRODUCTION

Description of the Problem

During steady operation of a liquid-propellant rocket engine the injected propellants are converted by various physical and chemical processes into hot burned gases which are subsequently accelerated to supersonic velocity by passing through a converging-diverging nozzle. The operation of such an engine, however, is seldom perfectly smooth. Instead the quantities which describe the conditions inside the combustor (i.e., pressure, density, temperature, etc.) are time-dependent. Such oscillations can be of either a destructive or nondestructive nature. Nondestructive unsteadiness is characterized by random fluctuations in the flow properties and includes the phenomena of turbulence and combustion noise. Unsteady operation of a destructive nature, on the other hand, is characterized by organized oscillations in which there is a definite correlation between the fluctuations at two different locations in the combustor. Such oscillations have a definite frequency and result in additional thermal and mechanical loads that the system must withstand.

Unsteady operation of the destructive variety, known as combustion instability, was first encountered in 1940[1]. At that time a British group testing a small solid-propellant rocket motor observed sudden increases of pressure to twice the expected level, enough to destroy a motor of flight weight. Since that time every major rocket development

program has been plagued by combustion instability of some form. These oscillations in the combustion chamber can have several detrimental effects. In some cases, particularly in solid-propellant rockets, instability can cause the steady-state pressure to increase to a point at which the rocket motor will explode. In liquid-propellant rocket chambers experiencing unstable combustion, heat transfer rates to the walls considerably exceed the corresponding steady state heat transfer rates, resulting in burn-out of the walls. If the chamber can survive these effects, mechanical vibrations in the rocket system can cause mechanical failure or destroy the effectiveness of the delicate control and guidance systems.

The phenomenon of combustion instability depends heavily upon the unsteady behavior of the combustion process. The organized oscillations of the gas within the chamber must be coupled with the combustion process in such a way as to form a feedback loop. In this manner part of the energy stored in the propellants becomes available to drive large amplitude oscillations. An understanding of this coupling between the combustion process and the wave motion is necessary in order to predict the stability characteristics of rocket engines.

Combustion instability problems in liquid propellant rocket motors usually fall into one of three categories according to the frequency of oscillation. Low frequency combustion instability, also known as chugging, is characterized by frequencies ranging from ten to several hundred cycles per second, nearly spatially uniform properties, and coupling with the feed system of the rocket. This type of instability is less detrimental than other forms, and the means of preventing it are well understood.

Low frequency instability will not be considered in this investigation.

A second type of combustion instability, which is less frequently observed, has a frequency of several hundred cycles per second. This type of oscillation is associated with the appearance of entropy waves inside the combustion chamber.

The third and most important form of combustion instability is known as high frequency or acoustic instability. As the name suggests, this type of instability represents the case of forced oscillations of the combustion chamber gases which are driven by the unsteady combustion process and interact with the resonance properties of the combustor geometry. The observed frequencies, which are as high as 10,000 cycles per second, are very close to those of the natural acoustic modes of a closed-ended chamber of the same geometry as the one experiencing unstable combustion. High frequency combustion instability is by far the most destructive and is the type to be considered in the present investigation.

High frequency combustion instability can resemble any of the following acoustic modes: (1) longitudinal, (2) transverse, and (3) combined longitudinal-transverse modes. Longitudinal oscillations are usually observed in chambers whose length to diameter ratio is much greater than one; in this case the velocity fluctuations are parallel to the axis of the chamber and the disturbances depend only on one space dimension. For much shorter chambers the transverse mode of instability is most frequently observed. Transverse oscillations in rocket motors are characterized by a component of the velocity perturbation which is perpendicular to the axis of the chamber and a three-dimensional disturbance field.

Such oscillations can take either of two forms: (1) the standing form in which the nodal surfaces are stationary, and (2) the spinning form in which the nodal surfaces rotate in either the clockwise or counter-clockwise direction. Transverse combustion instability, particularly that resembling the first tangential mode, has been frequently encountered in modern rocket development programs and has been the subject of much current research[2].

Previous Work in the Field

Since the early 1950's much experimental and analytical research has been devoted to better understanding the phenomenon of high frequency combustion instability. Most of the theories presented prior to 1966 were restricted to circumstances in which the amplitudes of the pressure oscillations were infinitesimally small, that is, in the linear regime. Prominent among these are the pioneering studies of longitudinal instability by Crocco[3] as well as the studies of transverse instability by Scala[4], Reardon[5], and Culick[6]. A complete discussion of these theories is given in the work of Zinn[7] and will not be repeated here.

Although linear theories provide the propulsion engineer with considerable insight into the problem, their applicability and usefulness in design is limited. The linear theories cannot provide answers to such important problems as the limiting value of the pressure amplitude attained by a small disturbance in the case of a linearly unstable engine, or the effect of a finite-amplitude disturbance upon the behavior of a linearly stable engine. In the latter case the results of many tests indicate that under certain conditions the introduction of sufficiently

large disturbances into a linearly stable engine can "trigger" combustion instability. Another shortcoming of linear theories is the fact that their predictions cannot be compared directly with available experimental data; for, in the majority of cases, the experimental data is obtained under conditions in which the combustion instability is fully developed (i.e., in the nonlinear regime). To provide answers to these questions theories accounting for the nonlinearities associated with combustion instability are needed. A more detailed discussion of the nonlinear aspects of combustion instability can be found in the work by Zinn[7].

In the field of finite amplitude (nonlinear) combustion instability, mathematical difficulties have precluded any exact solutions, and approximate methods and numerical analysis have been used almost exclusively. For this reason publications in this field are relatively scarce. Notable among these is the work of Maslen and Moore[8] who studied the behavior of finite amplitude transverse waves in a circular cylinder. Their major conclusion was that, unlike longitudinal oscillations, transverse waves do not steepen to form shock waves. Maslen and Moore, however, considered only fluid mechanical effects; they did not consider the influences of the combustion process, the steady state flow, and the nozzle which are so important in the analysis of combustion instability problems. Nevertheless pressure recordings taken from engines experiencing transverse instability reveal the presence of continuous pressure waves similar in form to those predicted by Maslen and Moore.

One of the first nonlinear analyses to include the effects of the combustion process and the resulting steady state flow was performed by Priem and Guentert[9]. In this investigation the problem was made one-

dimensional by considering the behavior of tangential waves traveling in an annular section of the combustor of a liquid propellant rocket motor. They used a computer to solve numerically the resulting nonlinear equations for various values of the parameters involved. Due to the many assumptions involved in the derivation of the one-dimensional equations, the results of this investigation are open to question.

The successful use of the time-lag concept (see Crocco[3]) in the linear theories prompted a number of researchers to apply this model to the analysis of nonlinear combustion instability. By considering a chamber with a concentrated combustion zone and a short nozzle, Sirignano[10] demonstrated the existence of continuous, finite-amplitude, longitudinal periodic waves. These solutions were shown to be unstable, however, thus indicating the possibility of triggering longitudinal oscillations. Mitchell[11] extended the work of Sirignano to include the possibility of discontinuous solutions. In this manner he was able to show that the final form of triggered longitudinal instability consisted of shock waves moving back and forth along the combustion chamber. Mitchell also considered the more realistic case of distributed combustion.

In the analyses of Priem, Sirignano, and Mitchell the oscillations were dependent on only one space dimension. One of the first researchers to study finite-amplitude three-dimensional combustion oscillations was Zinn[7] whose work is an extension of the linear transverse theories and the analysis of Maslen and Moore. Using Crocco's time-lag model Zinn investigated the nonlinear behavior of transverse waves in a chamber with a concentrated combustion zone at the injector end and an arbitrary converging-diverging nozzle at the other end. In this case it was necessary

to extend Crocco's burning rate expression and transverse nozzle admittance relation to obtain the appropriate boundary conditions for the case when the flow oscillations are of finite size. As a result of this analysis Zinn was able to prove the existence of three-dimensional, finite-amplitude continuous waves which are periodic in time. In addition he was able to prove the possibility of triggering combustion oscillations. An analytical criterion for the determination of the stability of such waves was derived, but because of its complicated form and the limited capacity of available computers no specific numerical results were obtained.

In more recent years other investigators such as Burstein[12] have attempted to solve numerically the equations describing instabilities that depend on two space dimensions. Although the resulting solutions resemble experimentally observed combustion instability, this method requires excessive computer time, and studies of this type for three-dimensional oscillations will have to await the development of a much faster breed of computers.

Objectives of the Present Investigation

Experimental studies indicate that nonlinearities play an important role in the phenomenon of combustion instability. In spite of this knowledge, most of the theoretical analyses in the past have been restricted to the linear regime, and those nonlinear analyses that have been done were restricted to one or two dimensions or to special limiting cases. For example, only in the case of longitudinal oscillations have nonlinear stability limits been found (see Mitchell[11]). This state of affairs

exists because of the mathematical difficulties associated with the solution of nonlinear problems in general, especially when the unsteady solutions depend on two or three space dimensions.

In attempting to solve a combustion instability problem by analytical techniques, the engineer is always faced with the difficult task of solving a system of nonlinear coupled partial differential equations whose solutions must satisfy a complicated set of boundary conditions. These boundary conditions may describe the unsteady burning process at the wall of a solid propellant rocket motor; the conditions at an idealized concentrated combustion zone of a liquid-propellant rocket engine; or the unsteady flow at the entrance of a converging-diverging nozzle. In an effort to obtain analytical solutions to various combustion instability problems, previous investigators have often been forced to simplify the original problem to such an extent that it no longer resembled the real problem that they had originally set out to solve.

In an effort to overcome these mathematical difficulties numerous sophisticated mathematical techniques have been developed. These theories involve complicated perturbation techniques coupled with eigenfunction expansions and numerical integration schemes (e.g., see References (5), (7), (10), and (11)). In some cases solutions were obtained by using straight-forward numerical integration methods[9,12,13]. Due to memory size limitations and relatively high cost of operation of available computers the applications of the numerical techniques have been primarily limited to the analysis of combustion instability problems where the oscillations depended on one space dimension. While the above-mentioned works provide considerable understanding of the phenomenon of nonlinear

combustion instability, they fail to provide the propulsion engineer with a useful and relatively simple analytical tool that could be used in future engine design.

At present there is a definite need for a new theoretical approach that will enable the propulsion engineer to perform a nonlinear stability analysis with relative ease. This method should be applicable to both linear and nonlinear problems and should be capable of handling the complicated boundary conditions which so often arise in combustion instability problems. It is therefore the primary objective of this investigation to develop such a new theoretical technique.

On the basis of an extensive search of the literature it was found that the Galerkin method has the potential for satisfying the above needs. The Galerkin method is an approximate mathematical technique which has been successfully employed in the solution of various engineering problems, many of which belonged to the field of acoustics. Indeed it was the similarities between acoustics and combustion instability that suggested the possibility of using the Galerkin method in the analysis of combustion instability problems. However it was the existence of complicated boundary conditions that the solutions are required to satisfy that pointed to the fact that the classical Galerkin method had to be considerably modified before it could be used in the solution of combustion instability problems. A review of the classical Galerkin method and its modification to accommodate these complicated boundary conditions forms the subject of Chapter II.

The equations that describe the flow conditions inside liquid-propellant rocket motors will be derived and discussed in Chapter III.

These equations will be used to determine the nonlinear stability characteristics of a cylindrical combustor with a quasi-steady nozzle and a distributed combustion process, where the response of the burning rate to the pressure oscillations is assumed to be described by Crocco's sensitive time lag hypothesis. The appropriate nonlinear expressions for the burning rate and the nozzle boundary condition are then derived in Chapter IV.

The remaining chapters of this thesis are devoted to demonstrating the applicability of the modified Galerkin method in the solution of both linear and nonlinear combustion instability problems, with special emphasis on the problem of nonlinear transverse instability. In Chapter V the Galerkin method is used to obtain approximate solutions to various linear combustion instability problems. These are necessary in order to test the validity of the modified Galerkin method by comparing the approximate solutions with those obtained by available exact techniques. The nonlinear analyses will be presented in Chapters VI and VII. In the second order analysis of Chapter VI it is assumed that the amplitude of the waves is not too large and that the Mach number of the steady state flow is small. Under these conditions the unsteady flow in the combustor is described by a single nonlinear partial differential equation which is derived in Chapter III. In Chapter VII a third order analysis is performed and the Galerkin method is used to obtain approximate solutions to the full system of wave equations (also derived in Chapter III). In both cases the approximate nonlinear solutions will be used to obtain the nonlinear waveforms and the nonlinear stability characteristics of the engine as a function of the relevant system parameters. The major conclusions of this research are then presented in Chapter VIII.

CHAPTER II

THE GALERKIN METHOD

Classical Galerkin Method

The Galerkin Method is a special application of the Method of Weighted Residuals (usually referred to as MWR). Since its development around the turn of the century, the Galerkin method has been extensively used in the solution of various stability and aeroelasticity problems (see ref. (14) for a review of this method and an extensive list of references). In these instances the Galerkin method proved itself as a useful tool for the solution of both linear and nonlinear problems. Although it is an approximate mathematical technique, it has nevertheless produced results which were in excellent agreement with available exact solutions. These approximate solutions are usually simpler in form than the exact solutions obtained by numerical integration, and their quantitative evaluation requires considerably less computation time.

The Method of Weighted Residuals and the classical Galerkin Method will now be briefly described. If x is the vector of independent variables, the problem may be formulated in the domain D as

$$N(u) = f(x) \qquad (x \text{ in } D) \tag{1}$$

$$B_i(u) = g_i(x) \qquad i = 1,2,\ldots p \qquad (x \text{ on boundary})$$

where N is a nonlinear differential operator, B_i represents the ith boundary condition, while f and g_i are known functions of the independent variables.

An approximate solution of the following type is assumed

$$\tilde{u}(x) = \sum_{j=0}^{n} C_j \Phi_j \tag{2}$$

where the Φ_j are "trial" functions chosen beforehand and the coefficients C_j are to be determined by the method. The functions Φ_j are often chosen to be the first n+1 components of a complete set of functions (see ref. (15) for definition of completeness). It is desirable that these functions satisfy as many known properties of the solution to be found as possible; such as monotonicity or periodicity. For example these functions may be solutions to a linearized version of the problem being considered, or they may be chosen on the basis of experimental data. The Φ_j's may be functions of all the independent variables in which case the C_j's are unknown constants, or the Φ_j's may be functions of a lesser number of independent variables in which case the C_j's are undetermined functions of the remaining independent variables. In the case where the C_j's are constants, the application of the MWR converts the original equation into a system of n+1 nonlinear algebraic equations to be solved for the C_j's. When the C_j's are unknown functions the application of the MWR yields a system of n+1 nonlinear differential equations that control the behavior of the unknown functions. In either case the solution of the resulting system of equations is simpler than the solution

of the original problem.

In applying the MWR, the approximating solutions (2) are substituted into the differential equations and boundary conditions to form the following residuals.

$$R_N(\tilde{u}) = N(\tilde{u}) - f(x) = N\left[\sum_{j=0}^{n} C_j \Phi_j\right] - f(x) \tag{3}$$

$$R_{B_i}(\tilde{u}) = B_i(\tilde{u}) - g_i(x)$$

If $\tilde{u}$ were an exact solution of Eq. (1) then the residual R_N would be identically zero. This, however, is not usually the case, and the coefficients C_j are determined in such a way that the error R_N is minimized in some sense. If the boundary conditions are simple, it is often possible to find an approximate solution $\tilde{u}$ that satisfies the boundary conditions, in which case the boundary residuals R_{B_i} are identically zero.

According to the MWR the unknown constants (or functions) C_j are determined by requiring that the following condition be satisfied.

$$\int_D W_k R_N dD = 0 \qquad k = 0,1,2,\ldots n \tag{4}$$

In the above relation R_N is the residual to be minimized and W_k is a specified weighting function. Various special cases of MWR, such as the

method of moments and the method of collocation, are derived by using special types of weighting functions (see ref. (16)).

The Galerkin method is the special case of the MWR obtained by letting $W_k = \Phi_k$; that is, the weighting functions are chosen to be the same functions as those used in constructing the approximate solution $\tilde{u}$. In this case the functions Φ_k must form a complete orthogonal set. The unknown coefficients are then found from the relations

$$\int_D R_N \Phi_k dD = 0 \qquad k = 0,1,2,\ldots n \tag{5}$$

which requires the residual R_N to be orthogonal to all the trial functions Φ_k.

In classical applications of the Galerkin Method the approximate solutions are chosen to satisfy all the boundary conditions, so that all boundary residuals vanish. When the boundary conditions are cumbersome, as in the case of combustion instability problems, it is often impossible to find an approximating solution that satisfies all the boundary conditions. Therefore the boundary residuals must also be considered, and the Galerkin Method must be modified to properly accommodate these boundary conditions. This will now be done for the equations and boundary conditions that describe the unsteady flow in rocket combustors.

Modification of the Galerkin Method

Before proceeding to modify the classical Galerkin method, the appropriate equations and boundary conditions must be derived. In the

analysis of solid-propellant and some liquid-propellant rocket engines it is often assumed that the hot products of combustion, with time dependent properties, are generated at the combustor's boundary. Under these conditions the boundary may be regarded as a distribution of unsteady sources (or sinks) of mass, momentum, and energy that are concentrated within an infinitesimally thin zone. Such a concentrated combustion zone is depicted schematically in Fig. (1). Here $\underrightarrow{n}$ is a unit vector in the direction of the outward normal to the combustor's boundary, and the subscripts (1) and (2) respectively represent conditions on the "outside" and "inside" sides of the concentrated combustion zone. For the moment the thickness of the zone is considered to be small but finite. Within this zone F_{Mass}, $\underrightarrow{F}_{Mom}$, and F_E represent the rates of mass, momentum, and energy generation per unit volume. Following the procedure used by Williams[17] the equations describing the conservation of mass, momentum, and energy are written in integral form. Allowing the thickness of the zone to approach zero and assuming that no accumulation occurs within the zone, the following conservation relations are obtained:

$$Q_{Mass} + \left(\rho_2 \underrightarrow{V}_2\right)\cdot\underrightarrow{n} - \left(\rho_1 \underrightarrow{V}_1\right)\cdot\underrightarrow{n} = 0 \tag{6a}$$

$$\underrightarrow{Q}_{Mom} + \left[\underrightarrow{V}_2\left(\rho_2 \underrightarrow{V}_2 \cdot \underrightarrow{n}\right) + p_2\underrightarrow{n}\right] - \left[\underrightarrow{V}_1\left(\rho_1 \underrightarrow{V}_1 \cdot \underrightarrow{n}\right) + p_1\underrightarrow{n}\right] = 0 \tag{6b}$$

$$Q_E + \left[\rho_2 \underrightarrow{V}_2\left(e_2 + \frac{p_2}{\rho_2} + \frac{1}{2}V_2^2\right)\right]\cdot\underrightarrow{n} - \left[\rho_1 \underrightarrow{V}_1\left(e_1 + \frac{p_1}{\rho_1} + \frac{1}{2}V_1^2\right)\right]\cdot\underrightarrow{n} = 0 \tag{6c}$$

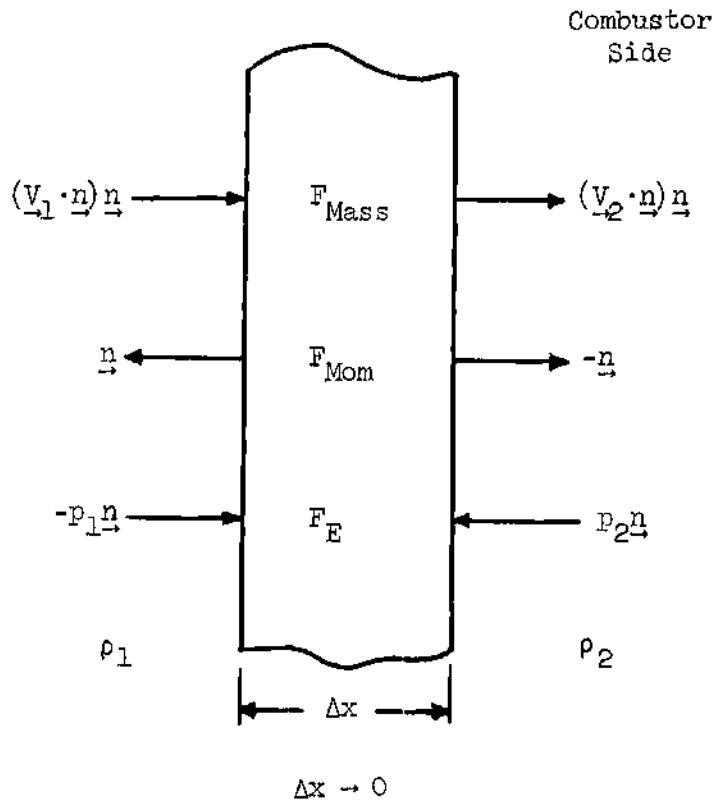

Figure 1. Schematic Diagram of Concentrated Combustion Zone.

where Q_{Mass}, $\underline{Q}_{Mom}$, and Q_E represent the rates of mass, momentum, and energy generation per unit surface area. These quantities depend on the physical conditions at the combustor's boundary and they can be expressed as follows: $Q_{Mass} = Q_{Mass}(\rho, p, \underline{V}, \ldots)$. This functional dependence is determined by a detailed analysis of the complicated combustion zone dynamics. In the present discussion it will be sufficient to assume that these functional relationships are known. The above relations are not limited to considerations of combustion zones only and they can be used to describe other boundary conditions such as those that result from the presence of a nozzle at one end of the combustion chamber.

The conservation equations, which will be treated by the Galerkin Method, can now be written subject to some simplifying assumptions which will be used in all analyses to follow. The presence of diffusion, viscosity, heat conduction, and body forces will be neglected, and the gas phase will be assumed to be thermally and calorically perfect. The presence of sources of mass, momentum, and energy distributed throughout the volume of the chamber will be included. Under these conditions the flow field is described by the following equations:

$$E_1 = \frac{\partial \rho}{\partial t} + \nabla \cdot (\rho \underline{V}) - F_{Mass} = 0 \tag{7}$$

$$E_2 = \frac{\partial}{\partial t}(\rho \underline{V}) + \nabla \cdot (\underline{V} \rho \underline{V}) + \nabla p - \underline{F}_{Mom} = 0 \tag{8}$$

$$E_3 = \frac{\partial}{\partial t}\left[\frac{1}{\gamma - 1} p + \frac{1}{2} \rho V^2\right] + \nabla \cdot \left[\frac{\gamma}{\gamma - 1} p \underline{V} + \frac{1}{2} \rho V^2 \underline{V}\right] - F_E = 0 \tag{9}$$

In the energy equation the thermal and caloric equations of state have been used to eliminate the internal energy.

Following the Galerkin method the dependent variables are assumed to have the following series solutions:

$$\tilde{V}_i = \sum_{n=0}^{N} A_{n_i} \varphi_n(\underset{\rightarrow}{x},t) \qquad i = 1,2,3 \tag{10}$$

$$\tilde{\rho} = \sum_{n=0}^{N} B_n \varphi_n(\underset{\rightarrow}{x},t)$$

$$\tilde{p} = \sum_{n=0}^{N} C_n \varphi_n(\underset{\rightarrow}{x},t)$$

where $\tilde{V}_i$ is the component of velocity in the ith direction, the $\varphi_n(\underset{\rightarrow}{x},t)$ are known functions which form a complete set in the $(\underset{\rightarrow}{x},t)$ space, and A_{n_i}, B_n, and C_n are the unknown constants that must be determined. As an alternative form the functions φ could be only spatially dependent with the coefficients becoming functions of time.

For the moment, it will be assumed that the expansions of the dependent variables have been properly chosen and that the boundary conditions are identically satisfied, that is

$$B_1(\tilde{\rho},\underset{\rightarrow}{\tilde{V}},\tilde{p}) = Q_{Mass}(\tilde{\rho},\underset{\rightarrow}{\tilde{V}},\tilde{p}) + (\tilde{\rho}\underset{\rightarrow}{\tilde{V}})\cdot\underset{\rightarrow}{n} - (\rho_1\underset{\rightarrow}{V}_1)\cdot\underset{\rightarrow}{n} = 0 \tag{11}$$

$$B_2(\tilde{\rho},\underset{\rightarrow}{\tilde{V}},\tilde{p}) = \underset{\rightarrow}{Q}_{Mom}(\tilde{\rho},\underset{\rightarrow}{\tilde{V}},\tilde{p}) + \left[\underset{\rightarrow}{\tilde{V}}(\tilde{\rho}\underset{\rightarrow}{\tilde{V}}\cdot\underset{\rightarrow}{n}) + \tilde{p}\underset{\rightarrow}{n}\right] - \left[\underset{\rightarrow}{V}_1(\rho_1\underset{\rightarrow}{V}_1\cdot\underset{\rightarrow}{n}) + p_1\underset{\rightarrow}{n}\right] = 0 \tag{12}$$

$$B_3(\tilde{\rho},\tilde{\underline{V}},\tilde{p}) = Q_E(\tilde{\rho},\tilde{\underline{V}},\tilde{p}) + \left[\frac{\gamma}{\gamma-1}\,\tilde{p}\,\tilde{\underline{V}} + \frac{1}{2}\tilde{\rho}\,\tilde{\underline{V}}\tilde{V}^2\right]\cdot\underline{n} \qquad (13)$$

$$- \left[\frac{\gamma}{\gamma-1}\,p_1\underline{V}_1 + \frac{1}{2}\,\rho_1\underline{V}_1 V_1^2\right]\cdot\underline{n} = 0$$

In the above equations, ρ_1, $\underline{V}_1$, and p_1 (the conditions on the "outside" side of the combustion zone) are considered to be known. Next the expansions given in Eqs. (10) are substituted into Eqs. (7) through (9) to yield the following residuals:

$$E_1(\tilde{\rho},\tilde{\underline{V}},\tilde{p}) = \frac{\partial\tilde{\rho}}{\partial t} + \nabla\cdot(\tilde{\rho}\,\tilde{\underline{V}}) - F_{Mass}(\tilde{\rho},\tilde{\underline{V}},\tilde{p}) \qquad (14)$$

$$E_2(\tilde{\rho},\tilde{\underline{V}},\tilde{p}) = \frac{\partial}{\partial t}\,(\tilde{\rho}\,\tilde{\underline{V}}) + \nabla\cdot(\tilde{\underline{V}}\tilde{\rho}\,\tilde{\underline{V}}) + \nabla\tilde{p} - \underline{F}_{Mom}(\tilde{\rho},\tilde{\underline{V}},\tilde{p}) \qquad (15)$$

$$E_3(\tilde{\rho},\tilde{\underline{V}},\tilde{p}) = \frac{\partial}{\partial t}\left[\frac{1}{\gamma-1}\,\tilde{p} + \frac{1}{2}\,\tilde{\rho}\tilde{V}^2\right] + \nabla\cdot\left[\frac{\gamma}{\gamma-1}\,\tilde{p}\,\tilde{\underline{V}} + \frac{1}{2}\,\tilde{\rho}\tilde{V}^2\tilde{\underline{V}}\right] - F_E(\tilde{\rho},\tilde{\underline{V}},\tilde{p}) \qquad (16)$$

To determine the unknown coefficients which occur in the expansions of the dependent variables, each of the residuals is required to be orthogonal to all of the trial functions $\varphi_n(\underline{x},t)$, that is

$$\int_0^{t^*}\int_V E_i(\underline{x},t)\,\varphi_n(\underline{x},t)\,dv\,dt = 0 \qquad i = 1,2,3 \qquad (17)$$

$$n = 0,1,2,\ldots N$$

where v represents the space under consideration and t^* a properly specified time. For example if periodic solutions are being sought, t^* would be the period of oscillation. Performing the integrations implied in Eqs. (17) yields 3(N+1) nonlinear algebraic equations for the 3(N+1) unknown coefficients which appear in the expansions (10).

The Galerkin procedure outlined above can be justified as follows. If the assumed solutions exactly satisfy Eqs. (7) through (9), then the residuals (14) through (16) are identically zero and the validity of Eqs. (17) is evident. If, however, the assumed solutions are not exact, then Eq. (17) states that the residuals must be orthogonal to the first N+1 members of a complete set of functions. In the limit as N approaches infinity, the residuals are required to be orthogonal to a complete set of functions in $(\underset{\sim}{x},t)$ which by definition of completeness implies that the residuals are identically equal to zero. The approximating solutions then become identical to the exact solution of the problem.

The Galerkin Method will now be modified for the case when the approximate solutions do not satisfy the boundary conditions. Substituting the assumed solutions (10) into the conservation of mass boundary condition (6a) yields the following nonzero boundary residual:

$$B_1(\tilde{\rho},\underset{\sim}{\tilde{V}},\tilde{p}) = Q_{Mass}(\tilde{\rho},\underset{\sim}{\tilde{V}},\tilde{p}) + (\tilde{\rho}\,\underset{\sim}{\tilde{V}})\cdot\underset{\sim}{n} - (\rho_1\underset{\sim}{V}_1)\cdot\underset{\sim}{n} \qquad (18)$$

Of course similar relations are obtained for the momentum and energy boundary conditions, Eqs. (6b) and (6c). There is now a need to minimize the residuals generated by both the differential equations

and the boundary conditions. If the orthogonality conditions are applied to the equations and boundary conditions separately, the boundary conditions give 3(N+1) additional equations,

$$\int_o^{t^*}\int_s \left[B_i(\tilde{\rho},\tilde{\underline{V}},\tilde{p})\varphi_n(\underline{x},t)\right]ds\,dt = 0 \qquad i = 1,2,3 \qquad (19)$$

$$n = 0,1,2,\ldots N$$

making a total of 6(N+1) equations.

Since there are only 3(N+1) unknowns, a straightforward solution of Eqs. (17) and (19) requires that 3(N+1) redundant equations be discarded. In the past this problem was unsatisfactorily resolved by arbitrarily discarding either the equation or boundary residuals[18]. An alternative method employed by Shulesko[19] was to expand the dependent variables in terms of two sets of functions, each of which satisfied a different set of conditions.

The difficulties mentioned above can be avoided if a way is found to combine the expressions resulting from the orthogonalization of an equation residual with the corresponding expression for the boundary residual. This way the number of equations is reduced without discarding any information. Similar procedures were used by Finlayson and Scriven[20,21] who analysed the heat conduction equation. Finlayson and Scriven justified their approach on the basis of a variational principle. In the absence of a variational principle for the equations of fluid dynamics, the proposed approach will be justified by making use of the

relationship between the conservation equations and their corresponding boundary conditions.

The modified Galerkin orthogonality condition for the continuity equation will now be obtained. First consider the case in which the unknown coefficients in the expansions of the dependent variables are functions of time and the weighting function is a constant (the first member of the set of trial functions φ_o is on many occasions a constant). Applying the Galerkin method to the continuity equation (Eq. (17) with i = 1) and converting the volume integral of the divergence term to a surface integral yields:

$$\int_V \frac{\partial \tilde{\rho}}{\partial t} dv = \int_V \tilde{F}_{Mass} dv - \int_S \tilde{\rho}\tilde{\vec{V}}\cdot\vec{n} ds \tag{20}$$

Equation (20) states that the instantaneous net accumulation of mass within the combustor is equal to the sum of the mass generated within the combustor and the net mass flux into the combustor. In a similar manner by applying the Galerkin method to the boundary condition (i.e., Eq. (19) with i = 1) one obtains:

$$- \int_S \tilde{\rho}\tilde{\vec{V}}\cdot\vec{n} ds = \int_S \left[\tilde{Q}_{Mass} - \rho_1 \vec{V}_1 \cdot \vec{n}\right] ds \tag{21}$$

which has the interpretation that the instantaneous net mass flux into the system is given by the expression on the right hand side. Equations (20) and (21) are easily combined to give:

$$\int_v \frac{\partial \tilde{\rho}}{\partial t} dv = \int_v \tilde{F}_{Mass} dv + \int_s \left[\tilde{Q}_{Mass} - \rho_l \underline{V}_l \cdot \underline{n}\right] ds \qquad (22)$$

which is the total mass balance of the system. The operations performed in deriving Eq. (22) are equivalent tc subtracting the boundary residual (i.e., Eq. (19)) from the corresponding equation residual (i.e., Eq. (17)). Thus subtracting the boundary residual is equivalent in this case to requiring the approximate solutions to satisfy the total mass balance of the system. Obviously this result would not be obtained if the weighted residuals were combined in a different manner (such as by adding them).

The manner in which the residuals should be combined has just been demonstrated for the special case when φ is a constant and the unknown coefficients are time dependent. In the more general case when φ_n is a function of both time and space, the residuals should be combined in the same manner, in order that the resulting general expression will satisfy the mass conservation law in the special case when φ = constant. Generalizing the results obtained in the case when φ is a constant will provide one with a consistent and uniform approach for the solution of this type of problems. Following the suggested approach, the orthogonality condition for the continuity equation and its boundary condition becomes:

$$\int_o^{t^*} \left\{ \int_v \left[\frac{\partial \tilde{\rho}}{\partial t} + \nabla \cdot (\tilde{\rho}\, \underline{\tilde{V}}) - \tilde{F}_{Mass}\right] \varphi_n dv \right. \qquad (23)$$

$$- \int_s \left[\tilde{Q}_{Mass} + (\tilde{\rho}\,\tilde{\underline{V}})\cdot\underline{n} - (\rho_1 \underline{V}_1)\cdot\underline{n} \right] \varphi_n \, ds \Big\} dt = 0$$

Another justification of the above procedure is based upon the concept of natural boundary conditions used in the calculus of variations. In applying the Galerkin method to a problem for which a variational principle exists, there is a unique way in which the weighted residuals of the differential equations and natural boundary conditions should be combined. In various problems in elasticity (see Bolotin[22]) these natural boundary conditions express conditions of equilibrium at the boundary. The analogous conditions in fluid dynamics are mass, momentum, and energy balances at the boundary. Even though no true variational principle has been found for the conservation equations of fluid mechanics, it appears that Eqs. (6) are the "natural" boundary conditions for these equations.

It must be emphasized that no rigorous proof has been given for Eq. (23). It would be much more satisfying if the applicability of the expression given by Eq. (23) could be demonstrated with a properly derived variational principle. In the absence of such a principle, however, the correctness of the approach leading to the derivation of Eq. (23) will be further demonstrated in Chapter V by showing that its application in the analysis of linear combustion instability problems produces results that are in excellent agreement with available exact solutions.

From the definition of the residuals it is seen that Eq. (23) as well as the corresponding expressions derived from the momentum and

energy equations can be written in the following form:

$$\int_o^{t^*} \left\{ \int_v E_i(\tilde{\rho},\tilde{\underset{\sim}{V}},\tilde{p})\varphi_n dv - \int_s B_i(\tilde{\rho},\tilde{\underset{\sim}{V}},\tilde{p})\varphi_n ds \right\} dt = 0 \qquad i = 1,2,3 \qquad (24)$$

$$n = 0,1,2,\ldots N$$

where the E_i are given by Eqs. (14), (15), and (16) and the corresponding B_i are given by Eqs. (11), (12), and (13). These equations state that the equations and boundary residuals are minimized by requiring that the difference between their weighted residuals vanish. If the boundary conditions are satisfied the boundary residuals vanish and the modified Galerkin method reduces to the classical Galerkin method.

The expressions given by Eqs. (24) give 3(N+1) relations which can be used to determine the 3(N+1) unknown coefficients which appear in the expansions of the dependent variables. Once the indicated integrations are performed the resulting set of algebraic equations is simpler and requires less computation time than the original set of partial differential equations. A somewhat different approach will be followed in the nonlinear analysis. The coefficients which appear in the expansions of the dependent variables will be unknown functions of time, and the trial functions will be only spatially dependent. Omitting the integration over the time interval, the modified Galerkin method then reduces the original system of partial differential equations to a system of ordinary differential equations that describes the behavior of the time dependent coefficients. Using the specified

initial conditions to obtain initial values of the unknown coefficients, these differential equations can be integrated by standard numerical techniques (e.g., Runge-Kutta) to determine the time history of the unknown amplitudes.

CHAPTER III

COMBUSTOR EQUATIONS

Due to the mathematical complexity of the conservation equations that describe the unsteady flow field inside unstable liquid-propellant rocket motors it is desirable to obtain a simplified version of these equations. It is the objective of the discussions presented in this chapter to analyze the combustor conservation equations and reduce them to an analytical form that is amenable to mathematical solution. The simplification will be done in a manner that will allow the resultant equations to preserve both the mathematical and physical essence of the original problem.

The combustion chamber medium will be considered as a two phase mixture of liquid propellant droplets and gaseous combustion products. The primary reaction between the fuel and oxidizer is assumed to occur immediately upon vaporization of the propellant droplets, that is, the vaporization process is rate controlling. Therefore the gas phase can be treated as a single constituent, which will furthermore be assumed to be thermally and calorically perfect. The presence of burning liquid droplets in the chamber will be represented as a continuous distribution of mass, momentum, and energy sources which will influence the propagation of waves in the chamber medium.

In deriving the conservation equations it will be assumed that transport phenomena such as diffusion, viscosity, and heat conduction are

negligible. The absence of diffusion is consistent with the single species approximation for the burned gases. Since viscosity and heat conduction result in damping of the pressure waves, their elimination from the analysis results in a conservative estimate of the stability of the system.

The following equations are derived in the usual manner by applying the laws of conservation of mass, momentum, and energy to an arbitrary stationary control volume[5,6]. They are presented first in dimensional form and will be nondimensionalized later.

Continuity:

$$\frac{\partial \rho^*}{\partial t^*} + \nabla^* \cdot (\rho^* \underset{\rightarrow}{V}^*) = - \left(\frac{\partial \rho_L^*}{\partial t^*} + \nabla^* \cdot \rho_L^* \underset{\rightarrow}{V}_L^* \right) = W_m^* \tag{25}$$

Momentum:

$$\frac{\partial}{\partial t^*} (\rho^* \underset{\rightarrow}{V}^*) + \nabla^* \cdot (\rho^* \underset{\rightarrow}{V}^* \underset{\rightarrow}{V}^*) = - \left\{ \frac{\partial}{\partial t^*} \left(\rho_L^* \underset{\rightarrow}{V}_L^* \right) + \nabla^* \cdot \left(\rho_L^* \underset{\rightarrow}{V}_L^* \underset{\rightarrow}{V}_L^* \right) \right\} - \nabla^* p^* \tag{26}$$

Energy:

$$\frac{\partial}{\partial t^*} \left[\rho^* \left(e^* + \frac{\underset{\rightarrow}{V}^* \cdot \underset{\rightarrow}{V}^*}{2} \right) \right] + \nabla^* \cdot \left[\rho^* \left(e^* + \frac{\underset{\rightarrow}{V}^* \cdot \underset{\rightarrow}{V}^*}{2} \right) \underset{\rightarrow}{V}^* \right] + \nabla^* \cdot (p^* \underset{\rightarrow}{V}^*) \tag{27}$$

$$= - \left\{ \frac{\partial}{\partial t^*} \left(\rho_L^* e_{L_s}^* \right) + \nabla \cdot \left(\rho_L^* e_{L_s}^* \underset{\rightarrow}{V}_L^* \right) \right\}$$

In the energy equation $e^*_{L_s}$ represents the liquid droplet stagnation internal energy and is given by

$$e^*_{L_s} = e^*_L + \frac{\underset{\rightarrow}{V}^*_L \cdot \underset{\rightarrow}{V}^*_L}{2}$$

where e^*_L contains both the thermal and chemical energy of the propellants.

The conservation equations will now be combined and rearranged into a more convenient form. By using the vector identity

$$\nabla\cdot(a\underset{\rightarrow}{A}\underset{\rightarrow}{A}) = a\underset{\rightarrow}{A}\cdot\nabla\underset{\rightarrow}{A} + \underset{\rightarrow}{A}\nabla\cdot a\underset{\rightarrow}{A}$$

and the continuity equation (eq. (25)) the momentum equation can be written in a form similar to the Euler equation.

$$\rho^*\left[\frac{\partial \underset{\rightarrow}{V}^*}{\partial t^*} + \underset{\rightarrow}{V}^*\cdot\nabla^*\underset{\rightarrow}{V}^*\right] = W^*_m\left(\underset{\rightarrow}{V}^*_L - \underset{\rightarrow}{V}^*\right) - \rho^*_L\left[\frac{\partial \underset{\rightarrow}{V}^*_L}{\partial t^*} + \underset{\rightarrow}{V}^*_L\cdot\nabla^*\underset{\rightarrow}{V}^*_L\right] - \nabla^* p^* \qquad (28)$$

Since W^*_m is the rate of generation of gas from the liquid phase, the first term on the right represents the force required to accelerate this gas from the velocity of the droplets to the velocity of the gas. The second term on the right represents the drag force experienced by the droplets due to their interations with the gas phase. This second term is usually approximated by $C^*(\underset{\rightarrow}{V}^* - \underset{\rightarrow}{V}^*_L)$ where the constant C^* depends on the Reynolds number of the drops[5,6]. In view of the above comments, the

momentum equation can be rewritten in the following form:

$$\rho^{*}\left\{\frac{\partial \underset{\rightarrow}{V}^{*}}{\partial t^{*}} + \underset{\rightarrow}{V}^{*}\cdot\nabla^{*}\underset{\rightarrow}{V}^{*}\right\} + \nabla^{*}p^{*} = -\left(\underset{\rightarrow}{V}^{*} - \underset{\rightarrow}{V}_{L}^{*}\right)\left(C^{*} + W_{m}^{*}\right) \qquad (29)$$

To simplify the energy equation the liquid specific stagnation internal energy (i.e. $e_{L_s}^{*}$) is replaced by the corresponding enthalpy. This substitution is allowed because of the low specific volume of the liquid phase. Introducing the relation $e_{s}^{*} = h_{s}^{*} - p^{*}/\rho^{*}$ into Eq. (27) and expanding terms gives

$$\rho^{*}\left[\frac{\partial h_{s}^{*}}{\partial t^{*}} + \underset{\rightarrow}{V}^{*}\cdot\nabla^{*}h_{s}^{*}\right] + h_{s}^{*}\left[\frac{\partial \rho^{*}}{\partial t^{*}} + \nabla^{*}\cdot\left(\rho^{*}\underset{\rightarrow}{V}^{*}\right)\right] - \frac{\partial p^{*}}{\partial t^{*}}$$

$$= -\rho_{L}^{*}\left[\frac{\partial h_{L_s}^{*}}{\partial t^{*}} + \underset{\rightarrow}{V}_{L}^{*}\cdot\nabla^{*}h_{L_s}^{*}\right] - h_{L_s}^{*}\left[\frac{\partial \rho_{L}^{*}}{\partial t^{*}} + \nabla^{*}\cdot\left(\rho_{L}^{*}\underset{\rightarrow}{V}_{L}^{*}\right)\right]$$

The continuity equation is then used to replace the expressions in the second and last brackets to yield the following much simplified form of the energy equation.

$$\rho^{*}\left[\frac{\partial h_{s}^{*}}{\partial t^{*}} + \underset{\rightarrow}{V}^{*}\cdot\nabla^{*}h_{s}^{*}\right] - \frac{\partial p^{*}}{\partial t^{*}} = -\rho_{L}^{*}\left[\frac{\partial h_{L_s}^{*}}{\partial t^{*}} + \underset{\rightarrow}{V}_{L}^{*}\cdot\nabla^{*}h_{L_s}^{*}\right] - W_{m}^{*}\left(h_{s}^{*} - h_{L_s}^{*}\right) \qquad (30)$$

In the above energy equation the first term on the right repre-

sents a loss of energy from the gas phase due to heating and acceleration of the liquid phase. The second term represents an energy source that results from the evaporation and combustion of the liquid droplets. This source vanishes if the stagnation enthalpies of the gas and liquid are equal.

The governing equations will now be nondimensionalized with respect to a steady reference state, which will be denoted by the subscript "r". Usually this reference state is taken to be the stagnation condition at the injector face, but if the variation of steady state properties is negligible the reference condition can be the corresponding constant steady state condition. All lengths will be referred to some characteristic length, such as the chamber radius. The characteristic velocity is the speed of sound at the reference state, and the characteristic time is the wave travel time c_r^*/L^*. The dimensionless quantities are defined below:

$$\underset{\rightarrow}{x} = \frac{\underset{\rightarrow}{x}^*}{L^*} \quad ; \quad t = c_r^* \frac{t^*}{L^*} \quad ; \quad \underset{\rightarrow}{V} = \frac{\underset{\rightarrow}{V}^*}{c_r^*} \quad ; \quad \underset{\rightarrow}{V}_L = \frac{\underset{\rightarrow}{V}_L^*}{c_r^*}$$

$$\rho = \frac{\rho^*}{\rho_r^*} \quad ; \quad p = \frac{\gamma p^*}{\rho_r^* c_r^{*2}} \quad ; \quad h = \frac{h^*}{c_p^* T_r^*} = \frac{(\gamma-1)h^*}{c_r^{*2}}$$

$$W_m = W_m^* \frac{L^*}{\rho_r^* c_r^*} \quad ; \quad C = c^* \frac{L^*}{\rho_r^* c_r^*}$$

Using the above definitions the stagnation enthalpy is given by

$$h_s = h + \frac{\gamma-1}{2} V^2$$

and the dimensionless conservation equations become:

Continuity

$$\frac{\partial \rho}{\partial t} + \nabla\cdot(\rho \underline{V}) = W_m \tag{31}$$

Momentum

$$\rho\left[\frac{\partial \underline{V}}{\partial t} + \underline{V}\cdot\nabla\underline{V}\right] + \frac{1}{\gamma}\nabla p = -\left(\underline{V}-\underline{V}_L\right)\left(C+W_m\right) \tag{32}$$

Energy

$$\rho\left[\frac{\partial h_s}{\partial t} + \underline{V}\cdot\nabla h_s\right] - \frac{\gamma-1}{\gamma}\frac{\partial p}{\partial t} = -\rho_L\left[\frac{\partial h_{L_s}}{\partial t} + \underline{V}_L\cdot\nabla h_{L_s}\right] - W_m\left(h_s - h_{L_s}\right) \tag{33}$$

In addition to the conservation equations, an expression relating h_s to the gas velocity and the appropriate state variables is needed. This relation is obtained by combining the thermal and caloric equations of state with the definition of the stagnation enthalpy, and is given by the following expression:

$$h_s = \frac{p}{\rho} + \frac{\gamma-1}{2} V^2 \tag{34}$$

Equations Governing the Wave Motion

Since it is desired to investigate the propagation of waves in a combustion chamber and the effect of mean flow and combustion on the growth or decay of these waves, general equations governing the wave motion in the combustor will now be derived. To obtain the wave equations each dependent variable is expressed as a sum of a steady state quantity and a time dependent perturbation. The behavior of the steady state quantities is governed by the time independent versions of Eqs. (31) through (34). Setting the time derivatives equal to zero, the following system of steady state equations can be derived:

$$\nabla\cdot(\bar{\rho}\underline{\bar{V}}) = \bar{W}_m \tag{31a}$$

$$\bar{\rho}\underline{\bar{V}}\cdot\nabla\underline{\bar{V}} + \frac{1}{\gamma}\nabla\bar{p} = -\left(\underline{\bar{V}}-\underline{\bar{V}}_L\right)\left(C+\bar{W}_m\right) \tag{32a}$$

$$\bar{\rho}\underline{\bar{V}}\cdot\nabla\bar{h}_s = -\bar{\rho}_L\underline{\bar{V}}_L\cdot\nabla\bar{h}_{L_s} - \bar{W}_m\left(\bar{h}_s-\bar{h}_{L_s}\right) \tag{33a}$$

$$\bar{h}_s = \frac{\bar{p}}{\bar{\rho}} + \frac{\gamma-1}{2}\bar{V}^2 \tag{34a}$$

To derive the wave equations the assumed form of the dependent variables is substituted into the full unsteady equations (i.e. Eqs. (31) through (34)) and the corresponding steady state equations are subtracted out. The resulting set of equations that controls the behavior of the wave motion is:

Continuity

$$\frac{\partial \rho'}{\partial t} + \nabla\cdot(\bar{\rho}\underset{\rightarrow}{V}') + \nabla\cdot(\rho'\underset{\rightarrow}{\bar{V}}) + \nabla\cdot(\rho'\underset{\rightarrow}{V}') = W_m' \tag{31b}$$

Momentum

$$\bar{\rho}\frac{\partial \underset{\rightarrow}{V}'}{\partial t} + \bar{\rho}\underset{\rightarrow}{\bar{V}}\cdot\nabla\underset{\rightarrow}{V}' + \bar{\rho}\underset{\rightarrow}{V}'\cdot\nabla\underset{\rightarrow}{\bar{V}} + \rho'\underset{\rightarrow}{\bar{V}}\cdot\nabla\underset{\rightarrow}{\bar{V}} + \frac{1}{\gamma}\nabla p' + \tag{32b}$$

$$\rho'\frac{\partial \underset{\rightarrow}{V}'}{\partial t} + \bar{\rho}\underset{\rightarrow}{V}'\cdot\nabla\underset{\rightarrow}{V}' + \rho'\underset{\rightarrow}{\bar{V}}\cdot\nabla\underset{\rightarrow}{V}' + \rho'\underset{\rightarrow}{V}'\cdot\nabla\underset{\rightarrow}{\bar{V}} + \rho'\underset{\rightarrow}{V}'\cdot\nabla\underset{\rightarrow}{V}' =$$

$$-\left\{\left(\underset{\rightarrow}{\bar{V}}-\underset{\rightarrow}{\bar{V}}_L\right)W_m' + \left(\underset{\rightarrow}{V}'-\underset{\rightarrow}{V}_L'\right)\bar{W}_m + \left(\underset{\rightarrow}{V}'-\underset{\rightarrow}{V}_L'\right)W_m' + C\left(\underset{\rightarrow}{V}'-\underset{\rightarrow}{V}_L'\right)\right\}$$

Energy

$$\bar{\rho}\frac{\partial h_s'}{\partial t} + \bar{\rho}\underset{\rightarrow}{\bar{V}}\cdot\nabla h_s' + \bar{\rho}\underset{\rightarrow}{V}'\cdot\nabla\bar{h}_s + \rho'\underset{\rightarrow}{\bar{V}}\cdot\nabla\bar{h}_s + \rho'\frac{\partial h_s'}{\partial t} + \tag{33b}$$

$$+\bar{\rho}\underset{\rightarrow}{V}'\cdot\nabla h_s' + \rho'\underset{\rightarrow}{\bar{V}}\cdot\nabla h_s' + \rho'\underset{\rightarrow}{V}'\cdot\nabla\bar{h}_s + \rho'\underset{\rightarrow}{V}'\cdot\nabla h_s' - \frac{\gamma-1}{\gamma}\frac{\partial p'}{\partial t} =$$

$$-\left\{\bar{\rho}_L\frac{\partial h_{L_s}'}{\partial t} + \bar{\rho}_L\underset{\rightarrow}{\bar{V}}_L\cdot\nabla h_{L_s}' + \bar{\rho}_L\underset{\rightarrow}{V}_L'\cdot\nabla\bar{h}_{L_s} + \rho_L'\underset{\rightarrow}{\bar{V}}_L\cdot\nabla\bar{h}_{L_s} + \rho_L'\frac{\partial h_{L_s}'}{\partial t}\right.$$

$$+ \bar{\rho}_L \underset{\rightarrow}{V}_L' \cdot \nabla h_{L_s}' + \rho_L' \underset{\rightarrow}{\bar{V}}_L \cdot \nabla h_{L_s}' + \rho_L' \underset{\rightarrow}{V}_L' \cdot \nabla \bar{h}_{L_s} + \rho_L' \underset{\rightarrow}{V}_L' \cdot \nabla h_{L_s}' \Big\}$$

$$- \left\{ \bar{W}_m \left(h_s' - h_{L_s}' \right) + W_m' \left(\bar{h}_s - \bar{h}_{L_s} \right) + W_m' \left(h_s' - h_{L_s}' \right) \right\}$$

Equation of state

$$p' = \bar{\rho} h_s' + \rho' \bar{h}_s + \rho' h_s' \tag{34b}$$

$$- \frac{\gamma - 1}{2} \left[2\bar{\rho} \underset{\rightarrow}{\bar{V}} \cdot \underset{\rightarrow}{V}' + \bar{\rho} (\underset{\rightarrow}{V}')^2 + \rho' (\underset{\rightarrow}{\bar{V}}^2) + 2\rho' \underset{\rightarrow}{\bar{V}} \cdot \underset{\rightarrow}{V}' + \rho' (\underset{\rightarrow}{V}')^2 \right]$$

Approximation Procedure

Due to their highly nonlinear and mathematically complicated nature, the system of wave equations (Eqs. (31b) through (34b)) cannot be solved exactly. In order to obtain simpler, but approximate, equations which can hopefully be solved, an order of magnitude analysis will be performed to determine which terms can be neglected. In this approximation scheme each perturbation quantity will be assigned the order of magnitude $O(\epsilon)$ where ϵ is an ordering parameter (roughly a measure of the wave amplitude). It then follows that products of perturbation quantities are of second order or $O(\epsilon^2)$. To obtain an equation that is correct to a given order all terms of higher order are neglected. For example an equation is valid to second order if all quadratically nonlinear perturbation terms are retained, but products

of three or more perturbation quantities are neglected. By this definition it is seen that first order equations are necessarily linear.

The equations derived from this perturbation analysis are expected to be valid as long as the amplitude of the perturbation quantities is finite but smaller than unity. If in addition it is assumed that the Mach number of the steady state flow is small (i.e. $\bar{u}$ is $O(\epsilon)$), additional terms can be neglected. Under these conditions the product of the mean flow velocity and a perturbation quantity would be of second order.

The approximation procedures described above have been used by Lighthill[23] and Blackstock[24] in their investigations of the propagation of finite amplitude waves in thermally conducting, viscous media. They also employed a substitution principle which follows logically from the basic approximation procedure. This principle, called the "Substitution Corollary" by Lighthill, is best described by the use of a simple example. Consider the perturbed continuity equation (i.e. Eq. (31b)) for the special case of no steady state flow or combustion (i.e. $\bar{V} = W_m' = 0$ and $\bar{\rho} = 1$). Introducing the velocity potential defined by $V' = \nabla\Phi$ yields the following equation:

$$\frac{\partial \rho'}{\partial t} + \nabla^2\Phi + \nabla\cdot(\rho'\nabla\Phi) = 0$$

Suppose it is desired to express the second order nonlinear term $\nabla\cdot(\rho'\nabla\Phi)$ in terms of the velocity potential only. From a first order (linear) analysis of the wave equations it will be shown later in this

chapter that the density perturbation can be expressed as:

$$\rho' = - \frac{\partial \Phi}{\partial t} + O(\epsilon^2)$$

Substituting this expression into the second order term gives the following result:

$$\nabla \cdot (\rho' \nabla \Phi) = \nabla \cdot \left[- \nabla \Phi \frac{\partial \Phi}{\partial t} + O(\epsilon^3) \right]$$

The third order term can be neglected when compared to the second order term, hence the continuity equation can be expressed in terms of the velocity potential in the following form correct to second order.

$$\frac{\partial \rho'}{\partial t} + \nabla^2 \Phi - \nabla \cdot \left(\nabla \Phi \frac{\partial \Phi}{\partial t} \right) = 0$$

It has thus been demonstrated that any factor of a second order term may be replaced by its equivalent first order expression, because any more precise substitution would result in the appearance of higher order terms.

The approximation procedure that has just been described can be used to derive first and second order wave equations for the following two cases: (1) the mean flow Mach number is unrestricted, and (2) the mean flow Mach number is small (i.e. $O(\epsilon)$). Allowing for the possibility of high subsonic mean flow velocities, the Mach number cannot be used in

the ordering scheme. In this case only third order products of perturbation quantities can be neglected. The resulting system of wave equations is nearly as complex as the original wave equations (i.e. Eqs. (31b) through (34b)). In this case only one term can be dropped from the momentum and state equations, two from the energy equation, and none from the continuity equation. In order to obtain significant simplification of the wave equations it will be necessary to assume that the mean flow Mach number is small, or make some other suitable approximation which will be described in the next section.

Simplified Wave Equations

By making some additional assumptions regarding the unsteady behavior of the liquid droplets it is possible to obtain greatly simplified wave equations without restricting the size of the mean flow Mach number. It will be assumed that: (1) the unsteady momentum source may be neglected and (2) that the specific stagnation enthalpy of the liquid droplets does not change as they move through the combustor. Both of these assumptions have previously been utilized in various combustion instability studies. Since the presence of a momentum source (droplet drag) is expected to cause damping of the pressure waves, the use of assumption (1) in the analysis is expected to result in a conservative estimate of the engine stability. The justification for the use of assumption (2) is discussed in Ref. 3 (see p. 105) where it was originally used by Crocco in his analysis of longitudinal instability. This assumption implies that the increase in droplet enthalpy due to droplet heating compensates for the loss of kinetic energy that is caused by

viscous drag. The droplet energy balance equation can then be replaced by the following expression:

$$\frac{\partial h_{L_s}}{\partial t} + \underline{V}_L \cdot \nabla h_{L_s} = 0 \tag{35}$$

It will be assumed that deviations from the constancy of h_{L_s} would only introduce higher order effects into the following developments. It will also be assumed that the velocity and thermodynamic properties of the liquid at injection do not vary with time; that is, only the case of intrinsic instability will be considered.

Before proceeding with the development of the simplified wave equations, the steady state equations will be examined to obtain some results that will be useful in deriving these equations. Under the above restrictions the steady state equations become:

$$\nabla \cdot (\bar{\rho}\underline{\bar{V}}) = \bar{W}_m \tag{36}$$

$$\bar{\rho}\underline{\bar{V}} \cdot \nabla \underline{\bar{V}} + \frac{1}{\gamma} \nabla \bar{p} = 0$$

$$\bar{\rho}\underline{\bar{V}} \cdot \nabla \bar{h}_s = - \bar{W}_m \left(\bar{h}_s - \bar{h}_{L_s} \right)$$

$$\underline{\bar{V}}_L \cdot \nabla \bar{h}_{L_s} = 0$$

If it is assumed that the mean flow is one-dimensional then the steady

state equations can easily be integrated subject to the boundary conditions on the mean flow properties at the injector face. Letting z represent the axial coordinate and $\bar{u}$ the mean flow velocity, the steady state equations become:

$$\frac{d}{dz}\left(\overline{\rho u}\right) = \bar{W}_m = -\frac{d}{dz}\left(\bar{\rho}_L \bar{u}_L\right) \tag{37}$$

$$\overline{\rho u}\,\frac{d\bar{u}}{dz} + \frac{1}{\gamma}\frac{d\bar{p}}{dz} = 0$$

$$\overline{\rho u}\,\frac{d\bar{h}_s}{dz} = -\bar{W}_m\left(\bar{h}_s - \bar{h}_{L_s}\right)$$

$$\frac{d\bar{h}_{L_s}}{dz} = 0$$

subject to the following boundary conditions at z = 0.

$$\bar{u}(0) = 0 \tag{38}$$

$$\bar{u}_L(0) = \bar{u}_{L_o}$$

$$\bar{\rho}_L(0) = \bar{\rho}_{L_o}$$

$$\bar{p}(0) = \bar{\rho}(0) = \bar{T}(0) = 1$$

$$\bar{h}_s(0) = \bar{h}_{s_o} \quad ; \quad \bar{h}_{L_s}(0) = \bar{h}_{L_{s_o}}$$

$$\bar{W}_m(0) = 0$$

Integrating the steady state continuity equation and applying the boundary conditions gives:

$$\bar{\rho}\bar{u} = \bar{\rho}_{L_o}\bar{u}_{L_o} - \bar{\rho}_L\bar{u}_L \tag{39}$$

while the droplet energy balance yields:

$$\bar{h}_{L_s} = \bar{h}_{L_{s_o}} \tag{40}$$

Using the continuity equation to replace $\bar{W}_m$, the energy equation becomes:

$$\frac{d}{dz}\left(\bar{\rho}\bar{u}\bar{h}_s\right) = -\frac{d}{dz}\left(\bar{\rho}_L\bar{u}_L\bar{h}_{L_{s_o}}\right) \tag{41}$$

which can be integrated to obtain:

$$\bar{\rho}\bar{u}\bar{h}_s = \left(\bar{\rho}_{L_o}\bar{u}_{L_o} - \bar{\rho}_L\bar{u}_L\right)\bar{h}_{L_{s_o}} \tag{42}$$

while substituting Eqs. (39) and (40) into the above expression yields:

$$\bar{\rho}\bar{u}\left(\bar{h}_s - \bar{h}_{L_s}\right) = 0 \tag{43}$$

Since $\overline{\rho u}$ is different from zero, it follows that

$$\bar{h}_s - \bar{h}_{L_s} = 0 \tag{44}$$

a result which will be later used to simplify the perturbed energy equation.

Before analyzing the perturbed equations the droplet energy relation (i.e. Eq. (35)) will be examined to obtain an additional simplifying result. Perturbing Eq. (35) and using Eq. (40) yields the following expression.

$$\frac{\partial h'_{L_s}}{\partial t} + \underline{V}_L \cdot \nabla h'_{L_s} = 0 \tag{45}$$

This equation states that under the assumptions of the present study the perturbation of the liquid droplet stagnation enthalpy does not change as a droplet moves downstream. Since it has been assumed that all droplets are injected with the same properties, the perturbation of the droplet properties is zero at the injector face, and Eq. (45) implies that $h'_{L_s} = 0$ throughout the combustor.

The appropriate equations governing the wave motion can now be derived from Eqs. (31b) through (33b). The continuity equation (i.e. Eq. (31b)) remains unchanged, and the momentum equation (Eq. (32b)) is simplified by dropping the momentum source terms. The resulting equations are:

Continuity

$$\frac{\partial \rho'}{\partial t} + \nabla\cdot(\bar{\rho}\underset{\rightarrow}{V}') + \nabla\cdot(\rho'\underset{\rightarrow}{\bar{V}}) + \nabla\cdot(\rho'\underset{\rightarrow}{V}') = W_m' \tag{46}$$

Momentum

$$\bar{\rho}\frac{\partial \underset{\rightarrow}{V}'}{\partial t} + \bar{\rho}\underset{\rightarrow}{\bar{V}}\cdot\nabla\underset{\rightarrow}{V}' + \bar{\rho}\underset{\rightarrow}{V}'\cdot\nabla\underset{\rightarrow}{\bar{V}} + \rho'\underset{\rightarrow}{\bar{V}}\cdot\nabla\underset{\rightarrow}{\bar{V}} + \frac{1}{\gamma}\nabla p' \tag{47}$$

$$+ \rho'\frac{\partial \underset{\rightarrow}{V}'}{\partial t} + \bar{\rho}\underset{\rightarrow}{V}'\cdot\nabla\underset{\rightarrow}{V}' + \rho'\underset{\rightarrow}{\bar{V}}\cdot\nabla\underset{\rightarrow}{V}' + \rho'\underset{\rightarrow}{V}'\cdot\nabla\underset{\rightarrow}{\bar{V}} + \rho'\underset{\rightarrow}{V}'\cdot\nabla\underset{\rightarrow}{V}' = 0$$

In treating the energy equation (Eq. (33b)) use is made of Eqs. (40), (44), (45), and the result $h'_{L_s} = 0$ which together yield the following result:

$$\bar{\rho}\frac{\partial h_s'}{\partial t} + \bar{\rho}\underset{\rightarrow}{\bar{V}}\cdot\nabla h_s' + \rho'\frac{\partial h_s'}{\partial t} + \bar{\rho}\underset{\rightarrow}{V}'\cdot\nabla h_s' + \rho'\underset{\rightarrow}{\bar{V}}\cdot\nabla h_s' \tag{48}$$

$$+ \rho'\underset{\rightarrow}{V}'\cdot\nabla h_s' - \frac{\gamma-1}{\gamma}\frac{\partial p'}{\partial t} = -\bar{W}_m h_s' - W_m' h_s'$$

The above equations are considerably simpler than Eqs. (31b) through (33b) because all liquid droplet terms have been removed, and it is no longer necessary to obtain solutions for the unsteady behavior of the liquid droplets. It is important to note that at this point in the analysis no restriction has been placed on the size of the perturba-

tions or the mean flow Mach number. These equations will therefore be used as the basis for the nonlinear stability analysis to be presented in later chapters.

Entropy and Vorticity Production

It will be of considerable help in the solution of the system of governing partial differential equations (i.e. Eqs. (46) through (48)) if a first integral of the momentum equation can be found. This can be accomplished if the flow is isentropic and irrotational, because the velocity vector can then be expressed as the gradient of a scalar potential, and the density becomes a function of pressure alone. Under these conditions it is possible to combine the perturbed equations to obtain a single partial differential equation governing the behavior of the velocity potential. The pressure is then related to the velocity potential by the integrated momentum equation. Such an equation has been used by Maslen and Moore[8] to describe the behavior of finite amplitude transverse waves in a circular cylinder, and by Blackstock[24] to describe the propagation of finite amplitude waves in viscous, thermally conducting media. It is the objective of the following analysis to determine under what conditions a similar equation can be derived, that will be valid for the investigation of the behavior of finite amplitude waves in a rocket combustor with mean flow, nozzle damping, and a distributed combustion process.

The energy equation Eq. (48) is easily seen to be a perturbation of the following equation:

$$\rho^* \frac{D}{Dt^*}\left(h^* + \frac{1}{2} V^{*2}\right) - \frac{\partial p^*}{\partial t^*} = \rho^* q^* = - W_m^*\left(h_s^* - h_{L_s}^*\right)$$

where q^* is the rate of heat addition per unit mass (see Ref. 25). This heat is provided by the combustion of the liquid droplets and it gives rise to an entropy change given by

$$\frac{DS^*}{Dt^*} = \frac{q^*}{T^*} = - \frac{W_m^*}{\rho^* T^*}\left(h_s^* - h_{L_s}^*\right) \tag{49}$$

Thus it is seen that, unless the right hand side of Eq. (48) vanishes, the perturbed flow cannot be isentropic. To determine how these entropy variations affect the rotationality of the unsteady flow, the unperturbed momentum equation (i.e. Eq. (32) without its right hand side) is transformed using the relation

$$\underset{\rightarrow}{V}\cdot\nabla\underset{\rightarrow}{V} = \nabla\left(\frac{1}{2}\underset{\rightarrow}{V}\cdot\underset{\rightarrow}{V}\right) - \underset{\rightarrow}{V}\times(\nabla\times\underset{\rightarrow}{V})$$

to obtain the following result:

$$\frac{\partial \underset{\rightarrow}{V}}{\partial t} + \nabla\left(\frac{1}{2}\underset{\rightarrow}{V}\cdot\underset{\rightarrow}{V}\right) - \underset{\rightarrow}{V}\times(\nabla\times\underset{\rightarrow}{V}) = - \frac{1}{\gamma}\frac{\nabla p}{\rho} \tag{50}$$

Taking the curl of both sides of Eq. (50) and introducing the definition of the vorticity $\underset{\rightarrow}{\Omega} = \nabla\times\underset{\rightarrow}{V}$ yields an equation which describes

the generation of vorticity in the flow.

$$\frac{\partial \vec{\Omega}}{\partial t} + \vec{V}\cdot\nabla\vec{\Omega} - \vec{\Omega}\cdot\nabla\vec{V} + \vec{\Omega}(\nabla\cdot\vec{V}) = -\frac{1}{\gamma}\nabla x\left(\frac{\nabla p}{\rho}\right) \tag{51}$$

In order to obtain a relation between the vorticity and entropy production, the dimensionless form of the First Law of Thermodynamics is used to obtain the result:

$$\nabla x\left(\frac{\nabla p}{\rho}\right) = -\frac{1}{\gamma-1}\nabla T x \nabla S \tag{52}$$

where $S = S^*/c_v^*$ and $T = T^*/T_r^*$

Substituting Eq. (52) into the vorticity equation yields the following equivalent form:

$$\frac{\partial \vec{\Omega}}{\partial t} + \vec{V}\cdot\nabla\vec{\Omega} - \vec{\Omega}\cdot\nabla\vec{V} + \vec{\Omega}(\nabla\cdot\vec{V}) = \frac{1}{\gamma(\gamma-1)}\nabla T x \nabla S \tag{53}$$

Unless $\nabla T x \nabla S = 0$, Eq. (53) implies that the flow is rotational. In the developments to follow it will be shown that if the mean flow Mach number is assumed to be small and the order of magnitude scheme described earlier is used, then in equations correct to second order the vorticity can be neglected.

The vorticity equation (Eq. (53)) is now perturbed and the steady state equations are subtracted out. Using the assumption that the mean flow is one-dimensional (and hence irrotational) it follows that $\bar{\vec{\Omega}} = 0$

and the vorticity equation describing the unsteady flow becomes:

$$\frac{\partial \vec{\Omega}'}{\partial t} + \bar{\vec{V}}\cdot\nabla\vec{\Omega}' + \vec{V}'\cdot\nabla\vec{\Omega}' - \vec{\Omega}'\cdot\nabla\bar{\vec{V}} - \vec{\Omega}'\cdot\nabla\vec{V}' + \vec{\Omega}'\nabla\cdot\bar{\vec{V}} \tag{54}$$

$$+ \vec{\Omega}'\nabla\cdot\vec{V}' = \frac{1}{\gamma(\gamma-1)}\left[\nabla\bar{T}x\nabla S' + \nabla T'x\nabla\bar{S} + \nabla T'x\nabla S'\right]$$

Since the right hand side of Eq. (54) represents a vorticity source, it is expected that the vorticity generated is of the same order of magnitude as this source term. Therefore the order of magnitude of the vorticity can be determined after the order of magnitude of $\bar{S}$ and S' are found.

Writing Eq. (49) in dimensionless form, one obtains

$$\frac{DS}{Dt} = -\frac{\gamma}{\rho T} W_m\left(h_s - h_{L_s}\right) \tag{55}$$

and setting the time derivatives equal to zero yields the corresponding steady flow equation.

$$\bar{\vec{V}}\cdot\nabla\bar{S} = -\frac{\gamma}{\rho\bar{T}} \bar{W}_m\left(\bar{h}_s - \bar{h}_{L_s}\right) \tag{56}$$

It has already been shown that under the assumptions of the present study $\bar{h}_s - \bar{h}_{L_s} = 0$, so it is easily seen from Eq. (56) that $\bar{\vec{V}}\cdot\nabla\bar{S} = 0$. This result implies that either the entropy gradient $\nabla\bar{S}$ vanishes or

that it is perpendicular to the velocity vector $\bar{\underset{\rightarrow}{V}}$. This latter possibility is clearly inconsistent with the assumption that the mean flow is one-dimensional, therefore the mean flow must be isentropic.

Perturbing Eq. (55) yields

$$\frac{DS'}{Dt} = -\frac{\gamma}{\rho T}\left[\bar{W}_m h_s' + W_m' h_s'\right] \tag{57}$$

where the previously derived result $h_{I_s}' = 0$ has been used. In the above expression the density and temperature are not perturbed because this would only introduce higher order quantities. From the steady state continuity equation (see Eqs. (36)) it is seen that $\bar{W}_m$ is of the same order of magnitude as the mean flow Mach number, therefore Eq. (57) implies that the entropy perturbation is of first order (i.e. $O(\epsilon)$) if no restriction is made on the Mach number and of second order if the Mach number is small.

Introducing the results of Eqs. (56) and (57) into Eq. (54) reveals that the vorticity perturbation $\underset{\rightarrow}{\Omega}'$ is of first order for flows with high subsonic Mach number. However for low Mach number flow it can be shown that $\nabla\bar{T}$ is $O(\bar{u}^2)$, and it thus follows that $\underset{\rightarrow}{\Omega}'$ is of third order (i.e. $O(\epsilon^3)$) and can be neglected in equations correct to second order. As a result only the low Mach number case will be considered in the second order analysis to follow. Under these conditions it is permissible to express the velocity in terms of the velocity potential.

Second Order Equations

Under the assumption of small mean flow Mach number, a second

order analysis will be performed on the simplified wave equations (i.e. Eqs. (46) through (48)) to obtain a set of second order equations involving the velocity potential. After a first integral of the momentum equation is obtained, these equations will be combined to yield a single nonlinear partial differential equation governing the behavior of the velocity potential.

Several additional implications of the low Mach number assumption will be used in the second order analysis. By integrating the steady state equations it can be shown that the mean flow pressure and density are described by expressions of the form[3]

$$\bar{\rho}(z) = 1 + O(\bar{u}^2) \qquad \bar{p}(z) = 1 + O(\bar{u}^2)$$

therefore if the Mach number is small these quantities can be considered uniform throughout the combustion chamber. The steady state can be used as the reference state (i.e. $\rho_r^* = \bar{\rho}^* = \text{const.}$) so that $\bar{\rho} = \bar{p} = \bar{h}_s = 1$. Since the steady state burning rate $\bar{W}_m$ is of the same order of magnitude as the Mach number*, its perturbation is an order of magnitude smaller; that is, $W_m' \sim O(\epsilon^2)$. This last result can be demonstrated more rigorously for the special case of a burning rate perturbation described by Crocco's sensitive time-lag model.

Since it has been shown that under the assumption of small Mach number the flow is irrotational to second order, a velocity potential

---

* It has been assumed that the mean flow Mach number and its gradient are of the same order of magnitude. Thus, from the steady state continuity equation, one obtains $\bar{W}_m = \nabla\cdot(\bar{\rho}\bar{\underline{V}}) = O(\epsilon)$.

defined by $\underset{\rightarrow}{V}' = \nabla\Phi$ will be introduced into the simplified wave equations. Using the results discussed above and neglecting terms of third order, Eqs. (46) through (48) become:

Continuity

$$\frac{\partial\rho'}{\partial t} + \nabla^2\Phi + \nabla\cdot(\rho'\underset{\rightarrow}{\bar{V}}) + \rho'\nabla^2\Phi + \nabla\rho'\cdot\nabla\Phi = \dot{W}_m' \tag{58}$$

Momentum

$$\nabla\left(\frac{\partial\Phi}{\partial t}\right) + \underset{\rightarrow}{\bar{V}}\cdot\nabla(\nabla\Phi) + \nabla\Phi\cdot\nabla\underset{\rightarrow}{\bar{V}} + \frac{1}{\gamma}\nabla p' + \tag{59}$$

$$+ \rho'\nabla\left(\frac{\partial\Phi}{\partial t}\right) + \nabla\Phi\cdot\nabla(\nabla\Phi) = 0$$

Energy

$$\frac{\partial h_s'}{\partial t} + \underset{\rightarrow}{\bar{V}}\cdot\nabla h' + \nabla\Phi\cdot\nabla h' + \rho'\frac{\partial h'}{\partial t} - \frac{\gamma-1}{\gamma}\frac{\partial p'}{\partial t} = -\bar{\dot{W}}_m h' \tag{60}$$

In the derivation of the energy equation the relation

$$h_s' = h' + O(\epsilon^2)$$

has been substituted into the second order terms and the resulting higher order terms were neglected. The momentum equation can be trans-

formed by using the following vector identity

$$\nabla(\underset{\rightarrow}{U}\cdot\underset{\rightarrow}{V}) = (\underset{\rightarrow}{V}\cdot\nabla)\underset{\rightarrow}{U} + (\underset{\rightarrow}{U}\cdot\nabla)\underset{\rightarrow}{V} + \underset{\rightarrow}{V}x(\nabla x\underset{\rightarrow}{U}) + \underset{\rightarrow}{U}x(\nabla x\underset{\rightarrow}{V})$$

which by letting $\underset{\rightarrow}{V} = \bar{\underset{\rightarrow}{V}}$ and $\underset{\rightarrow}{U} = \nabla\Phi$ and using the assumption of one-dimensional mean flow (which implies that $\nabla x\bar{\underset{\rightarrow}{V}} = 0$) becomes

$$\bar{\underset{\rightarrow}{V}}\cdot\nabla(\nabla\Phi) + \nabla\Phi\cdot\nabla\bar{\underset{\rightarrow}{V}} = \nabla(\bar{\underset{\rightarrow}{V}}\cdot\nabla\Phi)$$

The same identity with $\underset{\rightarrow}{U} = \underset{\rightarrow}{V} = \nabla\Phi$ gives the result

$$\nabla\Phi\cdot\nabla(\nabla\Phi) = \nabla\left(\frac{1}{2}\nabla\Phi\cdot\nabla\Phi\right)$$

Substituting both of these relations into the momentum equation (i.e. Eq. (59)) yields the following expression:

$$\nabla\left[\frac{\partial\Phi}{\partial t} + \frac{1}{\gamma}p' + \bar{\underset{\rightarrow}{V}}\cdot\nabla\Phi + \frac{1}{2}\nabla\Phi\cdot\nabla\Phi\right] + \rho'\nabla\left(\frac{\partial\Phi}{\partial t}\right) = 0 \qquad (61)$$

Before Eq. (61) can be integrated, certain first order expressions must be obtained so that, by using the substitution principle described earlier, all second order terms can be expressed in terms of the velocity potential alone. Neglecting all second order terms in Eqs. (58), (60), and (61) yields the following system of first order equations:

$$\frac{\partial \rho'}{\partial t} + \nabla^2 \Phi = 0 \tag{62a}$$

$$\nabla\left[\frac{\partial \Phi}{\partial t} + \frac{1}{\gamma} p'\right] = 0 \tag{62b}$$

$$\frac{\partial}{\partial t}\left[h' - \frac{\gamma-1}{\gamma} p'\right] = 0 \tag{62c}$$

The first order form of the equation of state (i.e. Eq. (34b)) is

$$p' = h' + \rho' \tag{63}$$

These first order expressions are simply the acoustic wave equations, which is not surprising since, under the assumptions of this analysis, both linear terms involving the steady state flow or combustion mass source and quadratically nonlinear terms are of second order. They are of no use in studying the linear instability problem, and will be used only for simplifying the second order equations. In order to express to first order the perturbation quantities p', ρ', and h' in terms of the velocity potential, Eqs. (62) must be integrated.

The first integral of the momentum equation (i.e. Eq. (62b)) is

$$\frac{\partial \Phi}{\partial t} + \frac{1}{\gamma} p' = F(t) \tag{64}$$

Burns[26] uses a lengthy and complicated argument to show that $F(t) = 0$. However $F(t)$ can be eliminated by redefining the velocity potential.

Since the velocity is the space derivative of Φ, it is permissible to add to Φ any arbitrary function of time. Therefore replacing Φ by $\Phi + \int F(t)\,dt$ in Eq. (64) yields the following equivalent form of the momentum equation.

$$\frac{\partial \Phi}{\partial t} + \frac{1}{\gamma} p' = 0 \tag{65}$$

Integrating the energy equation (i.e. Eq. (62c)) gives

$$h' - \frac{\gamma-1}{\gamma} p' = G(\underset{\rightarrow}{x})$$

where $G(\underset{\rightarrow}{x})$ is a function of space only, but at a time when the medium is undisturbed $G(\underset{\rightarrow}{x})$ must vanish. Since $G(\underset{\rightarrow}{x})$ is not dependent on time, it must therefore be identically equal to zero, and the energy equation becomes:

$$h' - \frac{\gamma-1}{\gamma} p' = 0 \tag{66}$$

Solving Eq. (65) for p' yields

$$p' = - \gamma \frac{\partial \Phi}{\partial t} \tag{67}$$

and substituting Eq. (67) into Eq. (66) gives

$$h' = -(\gamma-1)\frac{\partial\Phi}{\partial t} \tag{68}$$

while by introducing Eqs. (67) and (68) into the equation of state (i.e. Eq. (63)) one obtains

$$\rho' = -\frac{\partial\Phi}{\partial t} \tag{69}$$

Finally by differentiating Eq. (69) with respect to time and substituting the result into the continuity equation (i.e. Eq. (62a)) yields the linear wave equation

$$\nabla^2\Phi - \frac{\partial^2\Phi}{\partial t^2} = 0 \tag{70}$$

With the knowledge that the resulting error is of third order, Eqs. (67) through (70) are substituted into the second order terms of Eqs. (58), (60), and (61). The resulting second order equations are (where subscripts are used to denote partial differentiation):

Continuity

$$\frac{\partial\rho'}{\partial t} + \nabla^2\Phi = W_m' + \Phi_t\nabla^2\Phi + \nabla\Phi\cdot\nabla\Phi_t + \nabla\cdot\left(\vec{V}\Phi_t\right) \tag{71}$$

Momentum

$$\nabla\left[\frac{\partial\Phi}{\partial t} + \frac{1}{\gamma}\, p' + \bar{\underline{V}}\cdot\nabla\Phi + \frac{1}{2}\,\nabla\Phi\cdot\nabla\Phi - \frac{1}{2}\,\Phi_t^2\right] = 0 \tag{72}$$

In simplifying the energy equation the steady state continuity equation (i.e. the first of Eqs. (36)) is used to replace $\bar{W}_m$ in the right hand side of Eq. (60). This substitution together with the small Mach number approximation yields the following result

$$-\bar{W}_m h' \approx (\gamma-1)(\nabla\cdot\bar{\underline{V}})\,\Phi_t$$

where h' has been replaced by Eq. (68). Thus the energy equation becomes:

$$\frac{\partial h_s'}{\partial t} - (\gamma-1)\,\bar{\underline{V}}\cdot\nabla\Phi_t - (\gamma-1)\,\nabla\Phi\cdot\nabla\Phi_t + (\gamma-1)\,\Phi_t\Phi_{tt} - \tag{73}$$

$$-\frac{\gamma-1}{\gamma}\,\frac{\partial p'}{\partial t} = (\gamma-1)(\nabla\cdot\bar{\underline{V}})\,\Phi_t$$

The momentum equation can be integrated once to obtain

$$\frac{\partial\Phi}{\partial t} + \frac{1}{\gamma}\, p' + \bar{\underline{V}}\cdot\nabla\Phi + \frac{1}{2}\,\nabla\Phi\cdot\nabla\Phi - \frac{1}{2}\,\Phi_t^2 = 0 \tag{74}$$

where the function of integration was eliminated by using the same argument as in the first order analysis. The energy equation can be rewritten by introducing the second order equation defining the stagnation enthalpy; that is,

$$h_s' = h' + (\gamma-1)\underline{\bar{V}}\cdot\nabla\Phi + \frac{\gamma-1}{2}\nabla\Phi\cdot\nabla\Phi \tag{75}$$

and combining terms to yield

$$\frac{\partial h'}{\partial t} + (\gamma-1)\Phi_t\Phi_{tt} - (\gamma-1)(\nabla\cdot\underline{\bar{V}})\Phi_t - \frac{(\gamma-1)}{\gamma}\frac{\partial p'}{\partial t} = 0 \tag{76}$$

The equation of state (i.e. Eq. (34b)) can be expressed in the following form correct to second order

$$h' = p' - \rho' - (\gamma-1)\Phi_t^2 \tag{77}$$

where again first order relations have been substituted into the second order terms.

The partial differential equation describing the behavior of the velocity potential will now be derived by combining Eqs. (71), (74), (76), and (77). Differentiating Eq. (77) with respect to time and substituting the result into Eq. (76) yields

$$\frac{1}{\gamma}\frac{\partial p'}{\partial t} - \frac{\partial \rho'}{\partial t} - (\gamma-1)\Phi_t\Phi_{tt} - (\gamma-1)(\nabla\cdot\underline{\bar{V}})\Phi_t = 0 \tag{78}$$

The momentum equation (i.e. Eq. (74)) is then differentiated with respect to time to obtain

$$\frac{1}{\gamma}\frac{\partial p'}{\partial t} = -\Phi_{tt} - \bar{\underset{\rightarrow}{V}}\cdot\nabla\Phi_t - \nabla\Phi\cdot\nabla\Phi_t + \Phi_t\Phi_{tt} \tag{79}$$

Substituting Eqs. (71) and (79) into Eq. (78), collecting and rearranging terms, and using Eq. (70) in the appropriate second order term yields the following partial differential equation:

$$\nabla^2\Phi - \Phi_{tt} = 2\bar{\underset{\rightarrow}{V}}\cdot\nabla\Phi_t + \gamma(\nabla\cdot\bar{\underset{\rightarrow}{V}})\Phi_t + 2\nabla\Phi\cdot\nabla\Phi_t + (\gamma-1)\Phi_t\nabla^2\Phi + W_m' \tag{80}$$

The above equation is similar to the one used by Maslen and Moore[8] to describe the behavior of finite amplitude waves in a circular cylinder. Maslen and Moore, however, included third order (cubic) nonlinearities in their equation. These are assumed to be negligible in this analysis. It should be pointed out that Maslen and Moore were able to assume isentropic and irrotational flow, since no mean flow, combustion process, or shock waves were allowed in their analysis. This assumption enabled them to obtain a first integral of the momentum equation and a single partial differential equation describing the velocity potential without making any order of magnitude assumptions or neglecting any terms. When steady state flow and a combustion process are present one cannot a priori assume that the flow is isentropic and irrotational, and an order of magnitude approximation must be made in order to combine the wave equations. If a third order analysis is desired, then one must solve a system of coupled nonlinear partial differential equations, that from a mathematical point of view is considerably more complex.

It is to be noted that Eq. (80) has the form of an inhomogeneous wave equation. In this equation the first two terms on the right hand side result from the presence of steady state flow, the next two terms occur due to gasdynamical nonlinearities, and the last term describes the unsteady mass source due to combustion of liquid propellants. In order to solve this equation, the steady state flow distribution $\vec{V} = \bar{u}(z)$ must be known, and the mass source must be expressible as a function of the velocity potential (i.e. $W_m' = W_m'(\Phi)$). To account for the presence of the nozzle, the solution of Eq. (80) must satisfy the appropriate boundary conditions at the nozzle entrance.

Approximate solutions of Eq. (80) will be obtained with the aid of the modified Galerkin method. The resulting solutions will then be used to obtain a better understanding of the nonlinear behavior of unstable liquid propellant rocket engines.

Galerkin Orthogonality Conditions

The manner in which the residual of Eq. (80) and the boundary residual at the nozzle entrance should be combined will now be determined. From the first of Eqs. (24) the Galerkin orthogonality condition for the continuity equation can be expressed as

$$\int_0^{\frac{2\pi}{\omega}} \left\{ \int_V \left[\frac{\partial \tilde{\rho}'}{\partial t} + \nabla \cdot \vec{\tilde{J}}' - \tilde{W}_m' \right] \Psi_n \, dV - \int_S \left[\tilde{Q}_m' + \vec{\tilde{J}}' \cdot \underline{n} \right] \Psi_n \, ds \right\} dt = 0 \qquad (81)$$

where $\underline{J}'$ is the perturbation of the mass flux vector and is given by

$$\underset{\rightarrow}{J}' = \nabla\Phi - \underset{\rightarrow}{\bar{V}}\Phi_t - \Phi_t\nabla\Phi \tag{82}$$

The approximate solution for the velocity potential is expressed in terms of a complete set of functions as follows:

$$\tilde{\Phi} = \sum_{n=0}^{N} C_n \Psi_n(\underset{\rightarrow}{x},t)$$

The approximate solutions of the other properties such as $\tilde{\rho}'$, $\tilde{p}'$, and $\tilde{h}'_s$ are not expanded in terms of Ψ_n, but are determined by substituting the expansion for $\tilde{\Phi}$ into the remaining equations (i.e. momentum, energy, and state). It is therefore permissible to use these equations to derive an expression for $\partial\tilde{\rho}'/\partial t$ in terms of $\tilde{\Phi}$ which is substituted directly into Eq. (81) to obtain the desired orthogonality condition.

To express $\partial\tilde{\rho}'/\partial t$ in terms of $\tilde{\Phi}$ Eq. (79) is substituted into Eq. (78) to eliminate $\partial\tilde{p}'/\partial t$ and the resulting equation is solved for $\partial\tilde{\rho}'/\partial t$ to obtain

$$\frac{\partial\tilde{\rho}'}{\partial t} = -\tilde{\Phi}_{tt} + (2-\gamma)\tilde{\Phi}_t\nabla^2\tilde{\Phi} - \nabla\tilde{\Phi}\cdot\nabla\tilde{\Phi}_t - (\gamma-1)(\nabla\cdot\underset{\rightarrow}{\bar{V}})\tilde{\Phi}_t - \underset{\rightarrow}{\bar{V}}\cdot\nabla\tilde{\Phi}_t \tag{83}$$

Introducing Eqs. (82) and (83) into Eq. (81) yields the modified Galerkin orthogonality condition for the velocity potential.

$$\int_0^{\frac{2\pi}{\omega}} \Big\{ \int_v \Big[\nabla^2\tilde{\Phi} - \tilde{\Phi}_{tt} - 2\vec{\bar{V}}\cdot\nabla\tilde{\Phi}_t - \gamma(\nabla\cdot\vec{\bar{V}})\tilde{\Phi}_t \tag{84}$$

$$- 2\nabla\tilde{\Phi}\cdot\nabla\tilde{\Phi}_t - (\gamma-1)\tilde{\Phi}_t\nabla^2\tilde{\Phi} - \tilde{W}_m' \Big] \Psi_n dV$$

$$- \int_s \Big[\tilde{Q}_m' + \Big(\nabla\tilde{\Phi} - \vec{\bar{V}}\tilde{\Phi}_t - \tilde{\Phi}_t\nabla\tilde{\Phi} \Big)\cdot\vec{n} \Big] \Psi_n ds \Big\} dt = 0$$

It is to be noted that the integrand of the volume integral of Eq. (84) is simply the residual of Eq. (80) multiplied by the appropriate weighting function. The surface integral is the weighted residual of the condition which expresses conservation of mass at the combustor's boundary.

CHAPTER IV

COMBUSTION RESPONSE AND NOZZLE BOUNDARY CONDITION

In the present study attention will be restricted to the nonlinear behavior of transverse mode instabilities in a cylindrical combustion chamber with uniform injection of liquid propellants at one end and a multi-orifice (quasi-steady) nozzle at the other end (see Fig. 2). The contraction ratio of this nozzle is sufficiently large that the assumption of small mean flow Mach number is applicable. It will be assumed that the unsteady combustion process is represented by fluctuating mass sources distributed throughout the rocket's combustion chamber, and that perturbations of the burning rate will be described by Crocco's sensitive time-lag hypothesis (see Chapter I of Ref. 3 for a discussion of this model). Using these assumptions, expressions relating the burning rate perturbation W_m' and the nozzle boundary condition Q_m' to oscillations in chamber properties will now be derived.

Nonlinear Expression for the Burning Rate

In his monograph, Crocco has derived linearized expressions for the burning rate which are applicable to the case of small amplitude oscillations in combustors with distributed combustion. Under the restriction of small Mach number, Crocco's analysis will now be extended to obtain a nonlinear expression correct to third order that relates the burning rate to the pressure perturbations. Although transverse oscillations are present, no attempt will be made in this analysis

to account for the effect of transverse velocity components or displacements on the burning rate.

The dependence of the fractional burning rate on the time rate of change of the sensitive time lag is given by the following expression (see Ref. 3, p. 24, Eq. 1.11.18)

$$\delta\dot{m}_b = \delta\bar{\dot{m}}_b\left(1 - \frac{d\tau}{dt}\right) \tag{85}$$

where $\delta\dot{m}_b$ is a small fraction of the total burning rate (in units of mass/time). This quantity is related to the local burning rate (mass generation per unit volume) by

$$\delta\dot{m}_b = W_m(r,\theta,z,t)\,r\,dr\,d\theta\,dz$$

The local burning rate is then given by

$$W_m(r,\theta,z,t)\,\delta z = \bar{W}_m(r,\theta,\bar{z})\,\bar{\delta}z\left(1 - \frac{d\tau}{dt}\right) \tag{86}$$

where a propellant element that burns at the location $\bar{z}$ in the steady state burns at a different location z in the presence of pressure oscillations. For the case of longitudinal oscillations, Crocco has derived an expression for the total burning rate, which consists of three terms (see Eq. 3.08.14, p. 113 of Ref. 3). The first term originates directly from the time variations of the local burning rate and is called the timewise contribution; the remaining two terms result from the displace-

ment of the location at which a given element burns and is called the spacewise contribution. It has been shown by Crocco[3] (see pp. 115-6) that if the Mach number of the mean flow is small the timewise contribution is an order of magnitude larger than the spacewise contribution and is therefore the more important effect. In the present study, therefore, this spacewise contribution will be neglected by making the assumption

$$z = \bar{z}, \qquad \delta z = \bar{\delta} z$$

The expression relating the local burning rate to the time-lag fluctuations becomes simply

$$W_m(r,\theta,z,t) = \bar{W}_m(r,\theta,z)\left(1 - \frac{d\tau}{dt}\right) \tag{87}$$

which is perturbed to give

$$W_m' = - \bar{W}_m \frac{d\tau}{dt} \tag{88}$$

If the steady state Mach number is small, the steady state burning rate $\bar{W}_m$ can be related directly to the mean flow velocity distribution $\bar{u}(z)$. From the first of Eqs. (36) $\bar{W}_m$ is given by

$$\bar{W}_m(z) = \bar{\rho}(z) \frac{d\bar{u}}{dz} + \bar{u}(z) \frac{d\bar{\rho}}{dz}$$

and the burning rate perturbation becomes

$$W_m' = - \left[\bar{\rho} \frac{d\bar{u}}{dz} + \bar{u} \frac{d\bar{\rho}}{dz} \right] \frac{d\tau}{dt}$$

Since the perturbation quantities and the mean flow Mach number are $O(\epsilon)$ it is expected that $d\tau/dt$ is $O(\epsilon)$ and $\bar{\rho} = 1 + O(\epsilon^2)$ so that $d\bar{\rho}/dz$ is $O(\epsilon^2)$. Under these conditions the above equation becomes

$$W_m' = - \left[\frac{d\bar{u}}{dz} \frac{d\tau}{dt} + O(\epsilon^2) \frac{d\bar{u}}{dz} \frac{d\tau}{dt} + \bar{u} O(\epsilon^2) \frac{d\tau}{dt} \right]$$

The last two terms on the right hand side of this equation are of fourth order (i.e. $O(\epsilon^4)$) and can be neglected in comparison to the first term which is of second order. The resulting expression for the burning rate perturbation is correct to third order.

$$W_m' = - \frac{d\bar{u}}{dz} \frac{d\tau}{dt} \tag{89}$$

It is now necessary to derive a nonlinear expression relating $d\tau/dt$ to fluctuations in the local pressure during the time-lag. In this development terms of higher order than $O(\epsilon^2)$ will be neglected. Due to the presence of $d\bar{u}/dz$ in Eq. (89) this degree of approximation is sufficient to yield a third order expression for W_m'.

According to Crocco the rate of physical processes (i.e. vaporization of liquid propellants, gas phase reactions, etc.) occurring

during the pressure sensitive time-lag is correlated to the pressure by

$$f \propto p^n$$

where n is the interaction index (for the linear development see pp. 22-3 of Ref. 3). Introducing the constant of proportionality and using $p = \bar{p} + p'$ yields

$$f = \bar{f}\left[1 + \frac{p'}{\bar{p}}\right]^n \tag{90}$$

With the aid of the binomial theorem, Eq. (90) is expanded in powers of $p'/\bar{p}$ to obtain the following second order expression for the rate of physical processes:

$$f = \bar{f}\left[1 + n\left(\frac{p'}{\bar{p}}\right) + \frac{n(n-1)}{2}\left(\frac{p'}{\bar{p}}\right)^2\right] \tag{91}$$

Following the method of Crocco, it is assumed that the transformation of unburned liquid propellants into burned gases occurs instantaneously when the preparatory processes have accumulated to a certain level E_a. For a propellant element that burns at the instant t this condition is expressed by

$$\int_{t-\tau}^{t} f(t')\,dt' = E_a \tag{92}$$

where $f(t')$ is the rate of accumulation experienced by the element as it moves through the chamber. Neglecting the unsteady motion of the propellant elements and using the assumption of one-dimensional steady state flow, the propellant elements are found to move along lines parallel to the axis of the combustor. The rate of accumulation can then be expressed as

$$f(t') = f\{p[r,\theta,z(t'),t']\}$$

where $z(t')$ gives the location of the element at some time t' during the time-lag.

For the case of steady flow, Eq. (92) becomes

$$\int_{t-\bar{\tau}}^{t} \bar{f}(t')\,dt' = E_a \tag{93}$$

where

$$\bar{f}(t') = \bar{f}\{\bar{p}[z(t')]\}$$

This latter expression can be expanded in a Taylor series about $t' = t-\bar{\tau}$ to obtain

$$\bar{f}(t') = \bar{f}(t-\bar{\tau}) + \frac{d\bar{f}}{dt'}\bigg|_{t-\bar{\tau}} [t' - (t-\bar{\tau})]$$

It is easily seen that

$$\frac{d\bar{f}}{dt'} = \frac{d\bar{f}}{d\bar{p}} \frac{d\bar{p}}{dz} \frac{dz}{dt'},$$

where dz/dt' is the velocity of the propellant element. Except in the region very near the injector, the liquid velocity is of the same order of magnitude as the gas velocity, therefore under the assumption of small Mach number, dz/dt' is of $O(\epsilon)$. Since $d\bar{f}/d\bar{p}$ is $O(1)$ and the steady state pressure gradient is $O(\epsilon^2)$, the term containing $d\bar{f}/dt'$ is of third order. Neglecting this term, which is equivalent to assuming that $\bar{f}$ is constant, will therefore result in an error of $O(\epsilon^4)$ in the expression for the burning rate. Thus the integration of Eq. (93) can be performed to obtain:

$$\bar{f}\bar{\tau} = E_a \tag{94}$$

Combining Eqs. (92) and (94) to eliminate E_a yields the following result:

$$\int_{t-\tau}^{t} f(t')dt' = \bar{f}\bar{\tau} \tag{95}$$

The time-lag is then expressed in the form $\tau = \bar{\tau}+\tau'$ where the steady state value $\bar{\tau}$ is of $O(1)$ and the perturbation τ' is $O(\epsilon)$. Introducing this result into Eq. (95), the integral over the time-lag is separated

into two parts to yield:

$$\int_{t-\tau}^{t-\bar{\tau}} f(t')\,dt' + \int_{t-\bar{\tau}}^{t} f(t')\,dt' = \bar{f}\bar{\tau} \tag{96}$$

In order to evaluate the first integral on the left hand side of Eq. (96) the integrand is expanded in a Taylor series about $t' = t-\bar{\tau}$ to give:

$$f(t') = f_o + f_1[t' - (t-\bar{\tau})] + f_2[t' - (t-\bar{\tau})]^2 + \ldots \tag{97}$$

where the coefficients are given by

$$f_o = f(t-\bar{\tau}) \tag{98}$$

$$f_1 = \frac{df}{dt'}\,(t-\bar{\tau})$$

$$f_2 = \frac{1}{2}\,\frac{d^2f}{dt'^2}\,(t-\bar{\tau})$$

Since the coefficients in the Taylor expansion of $f(t')$ do not depend on the variable of integration t', the first term of Eq. (96) is readily integrated to obtain:

$$\int_{t-\tau}^{t-\bar{\tau}} f(t')\,dt' = f_o(\tau-\bar{\tau}) - \frac{f_1}{2}\,(\tau-\bar{\tau})^2 + \frac{f_2}{3}\,(\tau-\bar{\tau})^3$$

In the above expression $\tau-\bar{\tau} = \tau'$ is $O(\epsilon)$, therefore the last term is of third order and will be neglected to give:

$$\int_{t-\tau}^{t-\bar{\tau}} f(t')\,dt' = f_o(\tau-\bar{\tau}) - \frac{f_1}{2}(\tau-\bar{\tau})^2 \tag{99}$$

With the help of Eq. (91) the coefficients f_o and f_1 will be expressed in terms of the pressure perturbations. For an observer moving with a propellant element, $\bar{f}$ is a function of time as a result of the spatial variation of $\bar{p}$. The expression for $\frac{df}{dt}$, therefore, contains a term of the form $\frac{d\bar{f}}{dt}[1 + O(\epsilon)]$. Remembering that $d\bar{f}/dt$ is of third order, this term will be neglected. The coefficients in the Taylor series expansion of $f(t')$ then become:

$$f_o = \bar{f}\left[1 + n\frac{p'}{\bar{p}}(t-\bar{\tau}) + O(\epsilon^2)\right]$$

$$f_1 = \bar{f}\left[\frac{n}{\bar{p}}\frac{dp'}{dt}(t-\bar{\tau}) + O(\epsilon^2)\right]$$

Introducing these expressions into Eq. (99) and neglecting higher order terms yields:

$$\int_{t-\tau}^{t-\bar{\tau}} f(t')\,dt' = \bar{f}\left[1 + n\frac{p'}{\bar{p}}(t-\bar{\tau})\right](\tau-\bar{\tau}) \tag{100}$$

while substituting Eqs. (91) and (100) into Eq. (96) gives:

$$\bar{f}\left[1 + n\frac{\bar{p}'}{\bar{p}}(t-\bar{\tau})\right](\tau-\bar{\tau}) +$$

$$+ \int_{t-\bar{\tau}}^{t} \bar{f}\left\{1 + \frac{np'(t')}{\bar{p}} + \frac{n(n-1)}{2}\frac{[p'(t')]^2}{\bar{p}^2}\right\}dt' = \bar{f}\bar{\tau}$$

Neglecting the variation of $\bar{f}$ (the resulting error is of fourth order) and taking the time derivative of the above equation with the aid of Leibnitz' Rule, the integral over the time-lag is eliminated to yield the following expression correct to second order:

$$\frac{d\tau}{dt} + \left[\frac{n}{\bar{p}}\frac{dp'}{dt}(t-\bar{\tau})\right](\tau-\bar{\tau}) + \frac{n}{\bar{p}}p'(t-\bar{\tau})\frac{d\tau}{dt} \tag{101}$$

$$+ \frac{n}{\bar{p}}\left[p'(t) - p'(t-\bar{\tau})\right] + \frac{n(n-1)}{2\bar{p}^2}\left\{\left[p'(t)\right]^2 - \left[p'(t-\bar{\tau})\right]^2\right\} = 0$$

If only the first order terms are retained, Eq. (101) reduces, as expected, to the linear expression derived by Crocco (see Ref. 3, p. 23, Eq. 1.11.13), which is

$$\frac{d\tau}{dt} = -\frac{n}{\bar{p}}\left[p'(t) - p'(t-\bar{\tau})\right] \tag{102}$$

As it stands Eq. (101) can be solved explicitly for $d\tau/dt$, but the resulting expression is very cumbersome. This difficulty can be overcome by substituting the first order expressions for $\tau-\bar{\tau}$ and $d\tau/dt$ into these second order terms, with the knowledge that the resulting

error is of third order. The first order relation for $d\tau/dt$ is given by Eq. (102), while $\tau-\bar{\tau}$ is obtained from the integrated form of Eq. (102) which is

$$\tau - \bar{\tau} = - \frac{n}{\bar{p}} \int_{t-\bar{\tau}}^{t} p'(t')\,dt' \tag{103}$$

Introducing Eqs. (102) and (103) into the appropriate second order terms of Eq. (101) and using $\bar{p} = 1$ (the result of neglecting the spatial variation of mean flow properties) yields the following expression:

$$\frac{d\tau}{dt} + n\left[p'(t) - p'(t-\bar{\tau})\right] + \frac{n(n-1)}{2}\left\{\left[p'(t)\right]^2 - \left[p'(t-\bar{\tau})\right]^2\right\} \tag{104}$$

$$- n^2 p'(t-\bar{\tau})\left[p'(t) - p'(t-\bar{\tau})\right] - n^2 \frac{dp'}{dt}(t-\bar{\tau}) \int_{t-\bar{\tau}}^{t} p'(t')\,dt' = 0$$

In general the perturbation p' occurring in Eq. (104) is a function of both space and time so that

$$p'(t) = p'[r,\theta,z(t),t] \tag{105}$$

$$p'(t-\bar{\tau}) = p'[r,\theta,z(t-\bar{\tau}),t-\bar{\tau}]$$

where a propellant element that burns at the location z at the time t first became sensitive to pressure oscillations at the location $z(t-\bar{\tau})$. The distance traveled by this element during the time-lag is given by

$$\Delta z = \int_{t-\bar{\tau}}^{t} \bar{u}_L(t')dt'$$

Since the steady state velocities of the liquid droplets and the burned gases are of the same order of magnitude, and the sensitive time-lag is of the order of unity; the above relation implies that Δz is of $O(\epsilon)$. If it is assumed that the axial variation of the pressure perturbation for pure transverse modes is small compared to the transverse variation (i.e. $\partial p'/\partial z = O(\epsilon)\ \partial p'/\partial r$) it is permissible to use the simpler relations:

$$p'(t) = p'[r,\theta,z,t] \tag{106}$$

$$p'(t-\bar{\tau}) = p'[r,\theta,z,t-\bar{\tau}]$$

that is, the variation of the pressure perturbation over the short distance Δz can be neglected.

The total time derivative dp'/dt occurring in Eq. (104) can be expressed in terms of the partial derivatives as:

$$\frac{dp'}{dt} = \frac{\partial p'}{\partial t} + \bar{u}_L \frac{\partial p'}{\partial z} \tag{107}$$

For the case of pure transverse mode oscillations in a chamber with small mean flow Mach number, the convective term in Eq. (107) is of third order and can be neglected. Therefore the total derivative occurring in Eq. (104) can be replaced by the partial derivative to

obtain

$$\frac{d\tau}{dt} = -n\left(p'-p'_\tau\right) - \frac{n(n-1)}{2}(p')^2 + n^2 p' p'_\tau \tag{108}$$

$$- \frac{n(n+1)}{2}\left(p'_\tau\right)^2 + n^2 \frac{\partial p'_\tau}{\partial t}\int_{t-\bar{\tau}}^{t} p'(t')\,dt'$$

where $p' = p'(r,\theta,z,t)$ and $p'_\tau = p'(r,\theta,z,t-\bar{\tau})$.

Substituting Eq. (108) into Eq. (89) yields the following expression for the burning rate which is correct to third order:

$$W'_m = n\frac{d\bar{u}}{dz}\left\{\left(p'-p'_\tau\right) + \frac{n-1}{2}(p')^2 - np'p'_\tau \right. \tag{109}$$

$$\left. + \frac{n+1}{2}\left(p'_\tau\right)^2 - n\frac{\partial p'_\tau}{\partial t}\int_{t-\bar{\tau}}^{t} p'(t')\,dt'\right\}$$

It is seen that Eq. (109) describes a nonlinear response of the combustion process to finite amplitude pressure oscillations, and it will be used in the nonlinear combustion instability analyses to be presented in Chapters VI and VII.

Nonlinear Nozzle Boundary Condition

Rather than attempt a solution of the general nonlinear nozzle problem (which is beyond the scope of the present work), attention will be restricted to a quasi-steady nozzle. For the case of longitudinal oscillations the nozzle is approximately quasi-steady if the converging

section is very short compared to the wavelength or the characteristic dimension of the chamber. However if transverse or three-dimensional waves are present, the diameter of the nozzle must also be small relative to the diameter of the chamber. Such a quasi-steady condition can be approximated by the use of many small individual nozzles which are uniformly distributed over the nozzle end of the cylindrical combustion chamber. This particular nozzle geometry is known as a multi-orifice nozzle, and although it differs considerably from the conventional geometries, it can be approximated in experimental rocket motors.

Under the above assumptions the quasi-steady nozzle condition can be expressed as:

$$\frac{u}{c} = \text{const.}\left\{1 + \frac{\gamma-1}{2}\frac{v^2}{c^2}\right\}^{\frac{\gamma+1}{2(\gamma-1)}} \qquad (110)$$

where $c = (p/\rho)^{\frac{1}{2}}$ is the dimensionless sonic velocity (see Ref. 27 for the derivation of Eq. (110)). This relation implies that the Mach number of the axial velocity component is nearly constant, where the nonlinear correction term accounts for the presence of transverse velocity components at the nozzle entrance. The constant factor is readily determined by applying Eq. (110) to the steady state quantities, which yields:

$$\frac{\bar{u}_e}{\bar{c}_e}\left[1 + \frac{\gamma-1}{2}\frac{\bar{u}_e^2}{\bar{c}_e^2}\right]^{-\frac{\gamma+1}{2(\gamma-1)}} = \text{const.} \tag{111}$$

For the case of unsteady flow, Eq. (110) when combined with Eq. (111) becomes:

$$\left(\frac{\bar{u}_e+u_e'}{\bar{c}_e+c_e'}\right)\left[1 + \frac{\gamma-1}{2}\frac{\left[\left(\bar{u}_e+u_e'\right)^2 + \left(v_e'\right)^2 + \left(w_e'\right)^2\right]}{\left(\bar{c}_e+c_e'\right)^2}\right]^{-\frac{\gamma+1}{2(\gamma-1)}} \tag{112}$$

$$= \frac{\bar{u}_e}{\bar{c}_e}\left[1 + \frac{\gamma-1}{2}\frac{\bar{u}_e^2}{\bar{c}_e^2}\right]^{-\frac{\gamma+1}{2(\gamma-1)}}$$

in which the velocity vector has been expressed in terms of its axial, radial, and tangential components.

A third order nozzle boundary condition (i.e. expression for Q_m') will now be obtained from Eq. (112) under the restriction of small mean flow Mach number. Neglecting terms of higher order than $O(\epsilon^3)$ in the binomial expansion of Eq. (112) gives:

$$\left(\bar{u}_e+u_e'\right)\left\{1 - \frac{\gamma+1}{4\bar{c}_e^2}\left[\bar{u}_e^2 + 2\bar{u}_e u_e' + \left(u_e'\right)^2 + \left(v_e'\right)^2 + \left(w_e'\right)^2\right] + \ldots\right\} \tag{113}$$

$$= \frac{\bar{u}_e}{\bar{c}_e}\left\{1 - \frac{\gamma+1}{4\bar{c}_e^2}\bar{u}_e^2 + \ldots\right\}\left(\bar{c}_e+c_e'\right)$$

Performing the indicated multiplications, collecting terms, and again neglecting any higher order terms yields:

$$\bar{u}_e + u_e' = \bar{u}_e + \bar{u}_e\left(\frac{c_e'}{\bar{c}_e}\right) + \frac{\gamma+1}{4\bar{c}_e^2}\left\{3\bar{u}_e^2 u_e' + 3\bar{u}_e\left(u_e'\right)^2 + \right. \tag{114}$$

$$\left. + \bar{u}_e\left(v_e'\right)^2 + \bar{u}_e\left(w_e'\right)^2 + \left(u_e'\right)^3 + u_e'\left(v_e'\right)^2 + u_e'\left(w_e'\right)^2\right\}$$

The nozzle will be represented as an unsteady mass sink concentrated at an infinitesimally thin zone at the nozzle end of the chamber. This sink is assumed to swallow the entire mass flow leaving the chamber, therefore the velocity $\underrightarrow{V}_1$ on the nozzle side of this zone is zero, and a perturbation of the boundary condition given by Eq. (6a) yields:

$$Q_m' = -\left(\bar{\rho}\underrightarrow{V}' + \rho'\underrightarrow{\bar{V}} + \rho'\underrightarrow{V}'\right)\cdot\underrightarrow{n}$$

Expressed in terms of the axial velocity components, this relation becomes:

$$\bar{\rho}_e u_e' + \bar{u}_e\rho_e' + \rho_e' u_e' = -Q_m' \tag{115}$$

To obtain the nozzle boundary condition in terms of Q_m', both sides of Eq. (114) are multiplied by the density $\bar{\rho}_e + \rho_e'$. Introducing Eq. (115) into the left hand side of the resulting equation, neglecting higher

order terms, and rearranging terms yields the desired expression.

$$Q_m' = -\bar{u}_e\left[\rho_e' + \bar{\rho}_e\left(\frac{c_e'}{\bar{c}_e}\right) + \rho_e'\left(\frac{c_e'}{\bar{c}_e}\right)\right] - \frac{\gamma+1}{4}\frac{\bar{\rho}_e}{\bar{c}_e^2}\left[3\bar{u}_e^2 u_e' + 3\bar{u}_e\left(u_e'\right)^2\right. \quad (116)$$

$$\left. + \bar{u}_e\left(v_e'\right)^2 + \bar{u}_e\left(w_e'\right)^2 + \left(u_e'\right)^3 + u_e'\left(v_e'\right)^2 + u_e'\left(w_e'\right)^2\right]$$

The oscillations of the sonic velocity c' occurring in Eq. (116) can be directly related to the density perturbations if it is assumed that the combustion is complete before the nozzle is reached. Under this condition the unsteady flow at the nozzle entrance is found to be isentropic. The definition of the speed of sound $c^2 = p/\rho$ is then combined with the isentropic relation $p = \rho^\gamma$ to yield:

$$c = \rho^{\frac{\gamma-1}{2}}$$

which is perturbed to give:

$$1 + c_e'/\bar{c}_e = \left[1 + \rho_e'/\bar{\rho}_e\right]^{\frac{\gamma-1}{2}} \quad (117)$$

The right hand side of Eq. (117) is expanded in a binomial series and terms of higher order than $O(\epsilon^3)$ are neglected to obtain:

$$\frac{c_e'}{\bar{c}_e} = \frac{\gamma-1}{2}\left(\frac{\rho_e'}{\bar{\rho}_e}\right)\left\{1 - \frac{3-\gamma}{4}\left(\frac{\rho_e'}{\bar{\rho}_e}\right) + \frac{(3-\gamma)(5-\gamma)}{24}\left(\frac{\rho_e'}{\bar{\rho}_e}\right)^2\right\} \tag{118}$$

Substituting Eq. (118) into Eq. (116) yields the desired expression:

$$Q_m' = -\frac{\gamma+1}{2}\bar{u}_e\rho_e' - \frac{1}{8}(\gamma-1)(\gamma+1)\frac{\bar{u}_e}{\bar{\rho}_e}\left(\rho_e'\right)^2 - \frac{\gamma+1}{4}\frac{\bar{\rho}_e}{\bar{c}_e^2}\left[3\bar{u}_e^2u_e' + 3\bar{u}_e\left(u_e'\right)^2\right. \tag{119}$$

$$\left. + \bar{u}_e\left(v_e'\right)^2 + \bar{u}_e\left(w_e'\right)^2 + \left(u_e'\right)^3 + u_e'\left(v_e'\right)^2 + u_e'\left(w_e'\right)^2\right]$$

which is the third order nonlinear quasi-steady nozzle boundary condition. This relation, which describes the response of the multi-orifice nozzle to finite amplitude density and velocity fluctuations, will be employed in the nonlinear combustion instability analysis to follow.

CHAPTER V

TREATMENT OF LINEAR COMBUSTION INSTABILITY PROBLEMS BY THE MODIFIED GALERKIN METHOD

In this chapter approximate solutions for various linear combustion instability problems will be obtained with the aid of the modified Galerkin method. These linear solutions are desired for the following reasons: (1) to demonstrate how the modified Galerkin method is used to obtain the neutral stability boundary, (2) to test the validity of the modified Galerkin method by comparison of the approximate solutions with available exact solutions, and (3) to provide approximate linear stability limits that are consistent with the approximate nonlinear solutions.

First the applicability of the modified Galerkin method will be demonstrated by treating the simplest case of high frequency longitudinal instability analyzed by Crocco[3]. Approximate solutions for chambers with concentrated combustion and low steady state Mach number are then compared to the solutions obtained by a more rigorous mathematical technique. This analysis is then extended to account for some of the effects of high Mach number. Under the assumptions set forth in Chapters III and IV, the more interesting case of transverse and three-dimensional instability in chambers with distributed combustion will also be considered. Approximate neutral stability limits are then obtained which are consistent with the limiting behavior of the nonlinear solutions as the amplitude approaches zero.

Longitudinal Instability

The modified Galerkin method will now be applied in the solution of a linear, axial-mode high frequency combustion instability problem whose exact solution is available[3]. A liquid propellant rocket motor with combustion concentrated at the injector face and a short (quasi-steady) nozzle at the other end will be considered (see Fig. 2). It is assumed that the combustion process is described by Crocco's time-lag hypothesis.

Under these conditions the distributed mass and momentum sources vanish (since the hot gases are generated in an infinitesimally thin zone), which implies that the steady state pressure, density, and velocity are uniform throughout the chamber. It is then convenient to nondimensionalize the equations with respect to the steady state conditions, so that the normalized steady state density is unity. Assuming that the amplitudes of the perturbations are small, all products of perturbations occurring in Eqs. (31a) and (31b) are neglected to yield the following one-dimensional wave equations:

$$E_1(\rho',u') = \frac{\partial \rho'}{\partial t} + \bar{u}\frac{\partial \rho'}{\partial x} + \frac{\partial u'}{\partial x} = 0 \qquad (120)$$

$$E_2(\rho',u') = \frac{\partial u'}{\partial t} + \bar{u}\frac{\partial u'}{\partial x} + \frac{\partial \rho'}{\partial x} = 0 \qquad (121)$$

where the isentropic relation $p' = \gamma\rho'$ has been used to eliminate the pressure from Eq. (121).

The boundary conditions for this problem are given by a mass

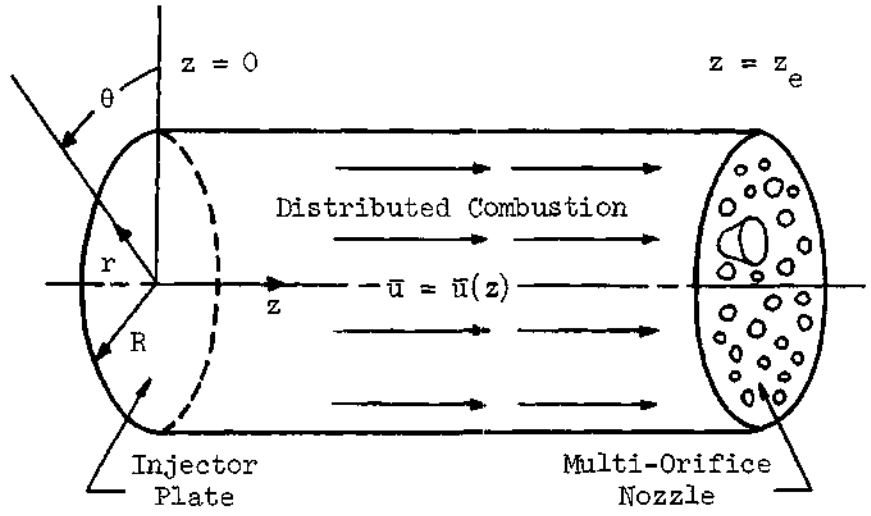

Transverse Analysis

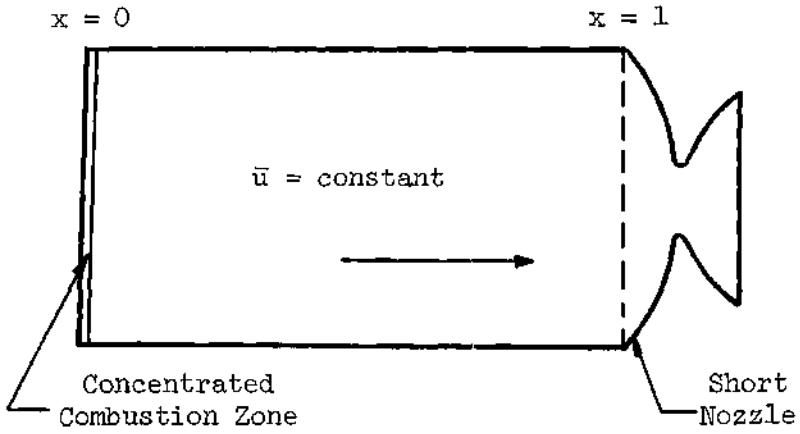

Axial Analysis

Figure 2. Combustor Configurations.

source at the injector face (x = 0) and an admittance condition at the nozzle entrance (x = 1). At x = 0 the fractional increase of the difference in mass flow rates across the concentrated combustion zone equals the fractional increase in the burning rate at the concentrated combustion zone. With the aid of Crocco's time-lag hypothesis the combustion zone boundary condition can be expressed in the following form:

$$\left[\frac{\rho'\bar{u} + \bar{\rho}u'}{\bar{\rho}\bar{u}}\right]_{x=0} = \gamma n\left[\rho'(0,t) - \rho'(0,t-\bar{\tau})\right] \tag{122}$$

where $\bar{\tau}$ is the steady state value of the sensitive time-lag τ and n is the interaction index. Since the gas phase mass flux into the concentrated combustion zone from the injector face is assumed to be zero, the result $\underset{\rightarrow}{V}_1 = u_1 = 0$ is obtained, so Eq. (6a) becomes:

$$Q_{mass} + (\rho'\underset{\rightarrow}{\bar{u}} + \underset{\rightarrow}{u}')_{x=0} \cdot \underset{\rightarrow}{n} = 0$$

where

$$Q_{mass} = \gamma n\bar{u}[\rho'(0,t) - \rho'(0,t-\bar{\tau})] \tag{123}$$

In the case of a short nozzle the Mach number at the nozzle entrance (x = 1) may be assumed to be constant. This condition leads to the following relation between the density and velocity perturbations:

$$\frac{u'}{\bar{u}} = \frac{\gamma-1}{2}\frac{\rho'}{\bar{\rho}}$$

which can be rewritten as

$$Q_{mass} + (\rho'\underline{\bar{u}} + \underline{u}')_{x=1} \cdot \underline{n} = 0$$

where

$$Q_{mass} = -\frac{\gamma+1}{2}\bar{u}\rho'(1,t) \tag{124}$$

Application of the modified Galerkin method to the continuity equation (i.e. Eq. (120)) yields

$$\int_0^{t^*}\left\{\int_0^1\left[\frac{\partial\tilde{\rho}'}{\partial t} + \bar{u}\frac{\partial\tilde{\rho}'}{\partial x} + \frac{\partial\tilde{u}'}{\partial x}\right]\varphi_n dx - \left[\left(\tilde{\rho}'\bar{u}+\tilde{u}'\right)_{x=1} - \frac{\gamma+1}{2}\bar{u}\tilde{\rho}'(1,t)\right]\varphi_n(1,t)\right. \tag{125}$$

$$\left. - \left[-\left(\tilde{\rho}'\bar{u} + \tilde{u}'\right)_{x=0} + \gamma n\bar{u}\left\{\tilde{\rho}'(0,t) - \tilde{\rho}'(0,t-\bar{\tau})\right\}\right]\varphi_n(0,t)\right\}dt = 0$$

Applying the Galerkin method tc the Euler equation, Eq. (121), is more difficult, since the Euler equation is a combination of the momentum and continuity equations. For this reason the proper boundary condition for the momentum equation does not hold for the Euler equation. Therefore the boundary residuals appropriate for the Euler equation must be derived. For this purpose the boundary momentum

source $\underset{\rightarrow}{Q}_{mom}$ occurring in Eq. (6b) will be expressed as

$$\underset{\rightarrow}{Q}_{mom} = \underset{\rightarrow}{V}Q_{mass} + \underset{\rightarrow}{M} \tag{126}$$

where $\underset{\rightarrow}{M}$ represents a momentum source due to interactions between liquid droplets and the gas in the boundary zone. If the dependent variables are expanded in terms of a complete set of functions $\varphi_n(\underset{\rightarrow}{x},t)$, it can be shown that for a flow with no volume sources the Galerkin orthogonality condition applicable to the Euler equation is given by

$$\int_0^{t^*}\left\{\int_V\left[\tilde{\rho}\frac{\partial\tilde{\underset{\rightarrow}{V}}}{\partial t} + \tilde{\rho}\tilde{\underset{\rightarrow}{V}}\cdot\nabla\tilde{\underset{\rightarrow}{V}} + \nabla\tilde{p}\right]\varphi_n dv - \int_S\left[\underset{\rightarrow}{M} + \left(\tilde{p}-p_1\right)\underset{\rightarrow}{n}\right]\varphi_n ds\right\}dt = 0 \tag{127}$$

where again $\underset{\rightarrow}{V}_1 = 0$. The derivation of Eq. (127) involves a complicated expansion technique which will be described in detail in Chapter VII. At that time the momentum and energy equations will both be treated for the more general case when volume sources are present.

In order to specialize Eq. (127) to the linear problem being analyzed, two assumptions made by Crocco[3] must be used. First the effect of liquid drops in the combustion zone is neglected, so $\underset{\rightarrow}{M} = 0$. Secondly the pressure is assumed continuous across the concentrated combustion zone, therefore $p_1 = \tilde{p}$. The same assumptions also apply at the nozzle entrance. Under these conditions the surface integral in Eq. (127) vanishes and the orthogonality condition for the one-dimensional Euler equation becomes:

$$\int_0^{t^*}\int_0^{l}\left[\frac{\partial\tilde{u}'}{\partial t} + \bar{u}\frac{\partial\tilde{u}'}{\partial x} + \frac{\partial\tilde{\rho}'}{\partial x}\right]\varphi_n dx dt = 0 \qquad (128)$$

The above equation together with Eq. (125) will now be used to obtain the neutral stability limits without having to determine the unknown coefficients in the expansions of $\tilde{\rho}'$ and $\tilde{u}'$. This will first be done for the case of small mean flow Mach number, and will later be extended to consider chambers with high subsonic Mach number.

Low Mach Number

In order to apply the Galerkin method one must select a set of functions in which to expand the dependent variables ρ' and u', that is, the functions φ_n which appear in the expansions presented in Eq. (10). Since only neutrally stable (periodic) oscillations are considered, it is required that the functions $\varphi_n(x,t)$ be periodic in time. Available experimental data indicates that in most cases of high-frequency instability the oscillations are similar to the acoustic modes that can be excited in the given combustor geometry. The acoustic modes are the solutions to Eqs. (120) and (121) with $\bar{u} = 0$; these solutions can be expressed in terms of the following complex exponential functions:

$$\varphi(x,t) = e^{i\omega(t-x)} \quad ; \quad \Psi(x,t) = e^{i\omega(t+x)} \qquad (129)$$

The real parts of these functions respectively represent a wave moving to the right and a wave moving to the left. In the instability problem, due to the presence of a mean flow, a nozzle, and a combustion

process, the frequency is expected to differ from the acoustic value $k\pi$, where k is a positive integer. Therefore the frequency ω is left unspecified and will be determined by the solution. The foregoing suggests that u' and ρ' be represented by the following expansions:

$$\tilde{\rho}' = \sum_{k=1}^{N} \left(a_k \varphi_k + b_k \Psi_k \right) \tag{130}$$

$$\tilde{u}' = \sum_{k=1}^{N} \left(c_k \varphi_k + d_k \Psi_k \right)$$

where

$$\varphi_k(x,t) = e^{ik\omega t} e^{-ik\omega x} \tag{131}$$

$$\Psi_k(x,t) = e^{ik\omega t} e^{ik\omega x}$$

Keeping only the first term in the series gives the first approximation:

$$\tilde{\rho}' = a_1 \varphi_1 + b_1 \Psi_1 \quad ; \quad \tilde{u}' = c_1 \varphi_1 + d_1 \Psi_1 \tag{132}$$

Equations relating the constants a_1, b_1, c_1, and d_1 are obtained from the Galerkin orthogonality conditions (i.e. Eqs. (125) and (128)) in which t^* is the period of oscillation $2\pi/\omega$. Since $\tilde{\rho}'$ and $\tilde{u}'$ are complex

quantities, the complex conjugates φ_1^* and Ψ_1^* should be used as weighting functions in the orthogonality conditions. The modified Galerkin orthogonality conditions for this problem can now be written as:

$$\int_0^{\frac{2\pi}{\omega}} \int_0^1 E_1(\tilde{\rho}', \tilde{u}') \varphi_1^*(x,t)\, dx dt \tag{133a}$$

$$- \int_0^{\frac{2\pi}{\omega}} B_0(t) \varphi_1^*(0,t)\, dt - \int_0^{\frac{2\pi}{\omega}} B_1(t) \varphi_1^*(1,t)\, dt = 0$$

$$\int_0^{\frac{2\pi}{\omega}} \int_0^1 E_1(\tilde{\rho}', \tilde{u}') \Psi_1^*(x,t)\, dx dt \tag{133b}$$

$$- \int_0^{\frac{2\pi}{\omega}} B_0(t) \Psi_1^*(0,t)\, dt - \int_c^{\frac{2\pi}{\omega}} B_1(t) \Psi_1^*(1,t)\, dt = 0$$

$$\int_0^{\frac{2\pi}{\omega}} \int_0^1 E_2(\tilde{\rho}', \tilde{u}') \varphi_1^*(x,t)\, dx dt = 0 \tag{133c}$$

$$\int_0^{\frac{2\pi}{\omega}} \int_0^1 E_2(\tilde{\rho}', \tilde{u}') \Psi_1^*(x,t)\, dx dt = 0 \tag{133d}$$

where E_1 and E_2 are given by Eqs. (120) and (121), B_0 and B_1 are

defined by

$$B_0(t) = - \left[\tilde{\rho}'\bar{u} + \tilde{u}'\right]_{x=0} + \gamma n\bar{u}\left[\tilde{\rho}'(0,t) - \tilde{\rho}'(0,t-\bar{\tau})\right] \qquad (134a)$$

$$B_1(t) = \left[\tilde{\rho}'\bar{u} + \tilde{u}'\right]_{x=1} - \frac{\gamma+1}{2}\,\bar{u}\tilde{\rho}'(1,t) \qquad (134b)$$

Substituting the assumed solutions given by Eqs. (132) into Eqs. (133) and performing the indicated integrations yields a set of four homogeneous linear equations in the four unknown constants. After some algebraic manipulations these four equations become:

$$K_1 a_1 + \left[K_1 - \left(1 + \frac{\gamma-1}{2}\,\bar{u}\right)\Omega_+\right]b_1 + \bar{u}(\bar{u}-2)\,i\omega c_1 + \frac{1}{2}\,\bar{u}^2\Omega_+ d_1 = 0 \qquad (135)$$

$$\left[K_1 + \left(1 - \frac{\gamma-1}{2}\,\bar{u}\right)\Omega_-\right]a_1 + K_1 b_1 + \frac{1}{2}\,\bar{u}^2\Omega_- c_1 - \bar{u}(\bar{u}+2)\,i\omega d_1 = 0$$

$$- i\omega a_1 - \frac{1}{2}\,\Omega_+ b_1 + (1-\bar{u})\,i\omega c_1 - \frac{1+\bar{u}}{2}\,\Omega_+ d_1 = 0$$

$$- \frac{1}{2}\,\Omega_- a_1 + i\omega b_1 + \frac{1-\bar{u}}{2}\,\Omega_- c_1 + (1+\bar{u})\,i\omega d_1 = 0$$

where

$$K_1 = \frac{\gamma+1}{2}\,\bar{u} - \gamma n\bar{u}\left(1 - e^{-i\omega\bar{\tau}}\right)$$

$$\Omega_+ = 1 - e^{2i\omega} \quad ; \quad \Omega_- = 1 - e^{-2i\omega}$$

In order for nontrivial solutions of Eqs. (135) to exist, the determinant of the coefficient matrix must vanish. Setting this determinant equal to zero yields a complex relation between ω, n, and $\bar{\tau}$; separating the real and imaginary parts gives two real equations in the three variables ω, n, and $\bar{\tau}$. These equations are solved for $n(\omega)$ and $\bar{\tau}(\omega)$ (if solutions exist) to obtain the curves of neutral stability in the n-$\bar{\tau}$ plane, the only points where linearly neutral (periodic) oscillations exist.

Assuming that the mean flow Mach number is small, all terms of order $\bar{u}^2$ or higher are neglected, and the real and imaginary parts of the characteristic equation become:

$$\gamma n\bar{u}[(\gamma-1)\bar{u}(1-\cos\omega\bar{\tau})(1-\cos 2\omega) + 2\sin\omega\bar{\tau}\sin 2\omega] = 2(1-\cos 2\omega) \qquad (136)$$

$$\gamma n\bar{u}[2(1-\cos\omega\bar{\tau})\sin 2\omega - (\gamma-1)\bar{u}\sin\omega\bar{\tau}(1-\cos 2\omega)] = (\gamma+1)\bar{u}\sin 2\omega \qquad (137)$$

Solving Eqs. (136) and (137) for $\gamma n\bar{u}$ and equating the results to eliminate n gives, after some trigonometric manipulations, an equation relating $\omega\bar{\tau}$ and ω.

$$\omega\bar{\tau} = (2m+1)\pi - 2\tan^{-1}\left\{\frac{1}{\bar{u}}\frac{\tan\omega}{1 + \frac{\gamma-1}{2}\sec^2\omega}\right\} \qquad (138)$$

$$m = 0, 1, 2, 3, \ldots$$

Solving Eq. (136) for n and using some trigonometric identities yields:

$$n = \frac{\gamma+1}{2\gamma}\left[1 - \cos\omega\bar{\tau} - \frac{\gamma-1}{2}\,\bar{u}\sin\omega\bar{\tau}\tan\omega\right]^{-1} \tag{139}$$

This same problem is solved by exact mathematical techniques by Crocco[3] who obtains the following pair of equations (see Eq. 3.02.01 in Ref. (3)):

$$\gamma n\cos\omega\bar{\tau} = -(1-\gamma n) - \frac{\gamma-1}{2\cos^2\omega} \tag{140}$$

$$\gamma n\sin\omega\bar{\tau} = \frac{\tan\omega}{\bar{u}}$$

The expressions presented in Eq. (140) can be manipulated to yield Eqs. (138) and (139). Thus it has just been shown that, at least for the case of small Mach number, the stability limit predicted by the modified Galerkin method, which is an approximate mathematical technique, is in complete agreement with the stability limit predicted, for the same problem, by the more rigorous analysis performed by Crocco and Cheng.

High Subsonic Mach Number

It is now desired to extend the analysis of the preceding section and consider the behavior of combustors with high Mach number mean flows. Solutions will be obtained by extending Crocco's original treat-

ment of this problem (see pp. 79-87 of Ref. (3)); the calculated stability limits will be compared with those obtained by using the Galerkin method.

In general, in studies of the stability of combustors with high Mach number mean flows it is appropriate to nondimensionalize the dependent variables with respect to some reference stagnation quantities (see Ref. 28). In this study, which considers a concentrated combustion model, it is possible to simplify the analysis by normalizing the conservation equations with respect to the combustor's mean flow properties. It should be pointed out that the results obtained in this manner are qualitatively similar to those obtained in the more general analysis of Mitchell[28].

Under these conditions it is easily seen from Eqs. (31a) and (31b) that the one-dimensional wave equations (i.e. Eqs. (120) and (121)) governing the behavior of waves in a combustor with low mean flow Mach number are also appropriate in the high Mach number analysis. This simplification results in part from the absence of volume sources, which implies that the steady state velocity as well as the density and pressure are uniform even for high Mach number flows. It is also assumed that the boundary conditions described by Eqs. (123) and (124) are applicable to this problem. The extension to high Mach number will therefore be obtained by retaining all terms involving $\bar{u}$ (i.e. terms of order $\bar{u}^2$, etc. which were previously neglected) which appear in the following developments.

An exact analytical solution to this problem must first be obtained. This solution will then be compared with the approximate

solution obtained by the Galerkin method. Following the method of Crocco, the solution to Eqs. (120) and (121) which combines leftward and rightward-running waves can be written in the following form:

$$\rho' = \sigma(x)e^{st} \quad ; \quad u' = \nu(x)e^{st} \quad ; \quad p' = \Phi(x)e^{st} \tag{141}$$

where the spatial dependence is given by

$$\nu(x) = c_r \exp\left(-\frac{sx}{1+\bar{u}}\right) + c_s \exp\left(\frac{sx}{1-\bar{u}}\right) \tag{142}$$

$$\frac{\Phi(x)}{\gamma} = \sigma(x) = c_r \exp\left(-\frac{sx}{1+\bar{u}}\right) - c_s \exp\left(\frac{sx}{1-\bar{u}}\right) \tag{143}$$

and $s = \Lambda + i\Omega$ is a complex frequency and c_r and c_s are constants to be determined by the boundary conditions.

Applying the boundary condition at the nozzle entrance gives:

$$\frac{c_r}{c_s} = -\exp\left(\frac{2s}{1-\bar{u}^2}\right)\left[\frac{1+\frac{\gamma-1}{2}\bar{u}}{1-\frac{\gamma-1}{2}\bar{u}}\right] \tag{144}$$

while the combustion zone boundary condition yields:

$$\frac{c_r}{c_s} = -\frac{1-\bar{u}+\gamma n\bar{u}(1-e^{-s\bar{\tau}})}{1+\bar{u}-\gamma n\bar{u}(1-e^{-s\bar{\tau}})} \tag{145}$$

The curves of neutral stability can be found by eliminating the ratio c_r/c_s between Eqs. (144) and (145) and then setting $s = i\omega$ (i.e. $\Lambda = 0$ for neutral stability). The resulting complex equation relating ω, n, and $\bar{\tau}$ is then separated into real and imaginary parts. In the process all terms involving $\bar{u}$ are retained, resulting in the pair of equations

$$\gamma n\bar{u}\{B[\sin\omega\bar{\tau}\sin 2\omega' - (1-\cos\omega\bar{\tau})\cos 2\omega'] - (1-\cos\omega\bar{\tau})\} \qquad (146)$$

$$= 1 - \bar{u} - (1+\bar{u})B\cos 2\omega'$$

$$\gamma n\bar{u}\{B[(1-\cos\omega\bar{\tau})\sin 2\omega' + \sin\omega\bar{\tau}\cos 2\omega'] + \sin\omega\bar{\tau}\} \qquad (147)$$

$$= (1+\bar{u})B\sin 2\omega'$$

where

$$B = \frac{1 + \frac{\gamma-1}{2}\bar{u}}{1 - \frac{\gamma-1}{2}\bar{u}} \quad ; \quad \omega' = \frac{\omega}{1 - \bar{u}^2}$$

An equation giving $\omega\bar{\tau}$ as a function of ω' is found by solving Eqs. (146) and (147) for n and equating the results to eliminate n. Applying some trigonometric identities to the result and allowing only positive values of $\omega\bar{\tau}$ yields:

$$\omega\bar{\tau} = (2m+1)\pi - 2\tan^{-1}\left[\frac{1}{\bar{u}}\frac{\sin 2\omega'}{K + \cos 2\omega'}\right] \tag{148}$$

$$m = 0, 1, 2, 3, \ldots$$

where

$$K = \frac{\gamma + \left(\frac{\gamma-1}{2}\bar{u}\right)^2}{1 - \left(\frac{\gamma-1}{2}\bar{u}\right)^2}$$

Once $\omega\bar{\tau}$ is known n can be calculated from either Eq. (146) or Eq. (147). Using Eq. (147) gives the following expression:

$$n = \frac{1+\bar{u}}{\gamma\bar{u}} \sin 2\omega'\left[\frac{1}{B}\sin\omega\bar{\tau} + \sin\omega\bar{\tau}\cos 2\omega' + (1-\cos\omega\bar{\tau})\sin 2\omega'\right]^{-1} \tag{149}$$

The Galerkin method will now be applied to this same problem, and the results compared with Eqs. (148) and (149). Since the governing differential equations and boundary conditions for the high Mach number case are identical to the corresponding low Mach number expressions, the residuals occurring in the Galerkin orthogonality conditions (i.e. Eqs. (133)) are given by Eqs. (120), (121), and (134). Again the approximate expressions for $\tilde{\rho}'$ and $\tilde{u}'$ are given by

$$\tilde{\rho}' = a\varphi(x,t) + b\Psi(x,t) \tag{150}$$

$$\tilde{u}' = c\varphi(x,t) + d\Psi(x,t)$$

where a, b, c, and d are unknown constants, but the definition of the functions φ and Ψ must be modified. While in the lower Mach number case φ and Ψ could be represented by undamped waves traveling in a stationary medium, the use of the same functions in the analysis of the high Mach number problem gave results which did not agree well with the exact solutions.

Further study of this problem has shown that the approximating functions φ and Ψ can be expressed as follows:

$$\varphi(x,t) = \exp\left[i\omega\left(t - \frac{x}{1+\bar{u}}\right)\right] \tag{151}$$

$$\Psi(x,t) = \exp\left[i\omega\left(t + \frac{x}{1-\bar{u}}\right)\right]$$

where the effect of mean flow convection on the speed of propagation of the waves has been taken into account. It should be noted that with the proper choice of the constants a, b, c, and d the approximate solution given by Eqs. (150) and (151) reduces to the solution assumed by Crocco (i.e. Eqs. (141-5)), which satisfies the continuity and Euler equations and the boundary conditions.

Substituting the approximate solutions given by Eqs. (150) and (151) into the Galerkin orthogonality conditions (i.e. Eqs. (133)) and performing the integrations yields a homogeneous linear system of equations in the four unknown coefficients a, b, c, and d. These can

be rearranged somewhat to obtain the following:

$$K_1 a + \left[K_1 - \left(1 + \frac{\gamma+1}{2}\,\bar{u}\right)\Omega_+\right] b - \bar{u}\Omega_+ d = 0 \tag{152}$$

$$\left[K_1 + \left(1 - \frac{\gamma+1}{2}\,\bar{u}\right)\Omega_-\right] a + K_1 b + \bar{u}\Omega_- c = 0$$

$$-(1-\bar{u})\,i\omega' a - \frac{1+\bar{u}}{2}\,\Omega_+ b + (1-\bar{u})\,i\omega' c - \frac{1+\bar{u}}{2}\,\Omega_+ d = 0$$

$$-\frac{(1-\bar{u})}{2}\,\Omega_- a + (1+\bar{u})\,i\omega' b + \frac{1-\bar{u}}{2}\,\Omega_- c + (1+\bar{u})\,i\omega' d = 0$$

where

$$K_1 = \frac{\gamma+1}{2}\,\bar{u} - \gamma m\bar{u}\left(1 - e^{-i\omega\bar{\tau}}\right)$$

$$\Omega_+ = 1 - e^{2i\omega'} \quad ; \quad \Omega_- = 1 - e^{-2i\omega'}$$

The condition for the existence of a neutral oscillation is that Eqs. (152) have a nontrivial solution; that is, the determinant of the system must vanish. Expanding this determinant and equating it to zero yields the following complex equation:

$$K_1\left[\left(1 - \frac{\gamma-1}{2}\,\bar{u}\right)\Omega_- - \left(1 + \frac{\gamma-1}{2}\,\bar{u}\right)\Omega_+\right] \tag{153}$$

$$-\left(1 - \frac{\gamma-1}{2}\,\bar{u}\right)\left(1 + \frac{\gamma-1}{2}\,\bar{u}\right)\Omega_+\Omega_- = 0$$

Introducing the expressions for K_1, Ω_+, and Ω_- into the above equation, expanding and separating the real and imaginary parts gives the following two relations:

$$\gamma\bar{u}n\left[\frac{\gamma-1}{2}\,\bar{u}(1-\cos\omega\bar{\tau})(1-\cos2\omega') + \sin\omega\bar{\tau}\sin2\omega'\right] \tag{154}$$

$$= \left(1 + \frac{\gamma-1}{2}\,\bar{u}^2\right)\left(1-\cos2\omega'\right)$$

$$\gamma\bar{u}n\left[\frac{\gamma-1}{2}\,\bar{u}\sin\omega\bar{\tau}(1-\cos2\omega') - (1-\cos\omega\bar{\tau})\sin2\omega'\right] \tag{155}$$

$$= -\frac{\gamma+1}{2}\,\bar{u}\sin2\omega'$$

Solving Eqs. (154) and (155) for $\gamma n\bar{u}$ and equating the results to eliminate n, and then performing some trigonometric manipulations yields the following result:

$$\omega\bar{\tau} = (2m+1)\pi - 2\tan^{-1}\frac{1}{\bar{u}}\left[\frac{\sin2\omega'}{K + \cos2\omega'}\right] \tag{156}$$

where K is the same as that in Eq. (148). It is seen that for the particular approximating functions used the modified Galerkin method yields for $\omega\bar{\tau}$ results which are identical to the exact solution given by Eq. (148).

From Eq. (155) the following expression for n is obtained:

$$n = \frac{\gamma+1}{2\gamma}\left[1 - \cos\omega\bar{\tau} - \frac{\gamma-1}{2}\,\bar{u}\,\sin\omega\bar{\tau}\tan\omega'\right]^{-1} \qquad (157)$$

This equation is not identical in form to its exact counterpart (i.e. Eq. (149)), but neutral stability curves calculated from Eqs. (156) and (157) are in excellent agreement (to five significant digits) with those computed by use of Eq. (149)*. Some representative stability limits obtained in this study are presented in Figs. (3) and (4). In these plots operating conditions represented by a point inside the loops or parabolic-looking curves are unstable. As can be seen from Fig. (3) the neutral stability curve exhibits loops which can be shown to represent instabilities with respect to consecutive longitudinal modes (i.e. the loop with $\ell = 1$ corresponds to the first longitudinal mode, $\ell = 2$ to the second longitudinal and so on). This study also indicated that as $\bar{u}$ increases the loops closed at lower values of n; this result is in agreement with the results obtained in Mitchell[28] and Zinn and Savell[29].

The effect of increasing the Mach number of the mean flow is demonstrated in Fig. (4) which shows that the unstable region markedly increases as a result of increasing $\bar{u}$. It may thus be concluded that the likelihood of the occurrence of axial combustion instability increases when the Mach number of the combustor's mean flow is increased.

Application of the Galerkin method to the case of longitudinal

---

* This result is hardly surprising since the assumed solutions are reducible to the exact solutions if the constants are chosen correctly. Thus it is suspected that Eqs. (149) and (157), although not of the same algebraic form, are in exact agreement.

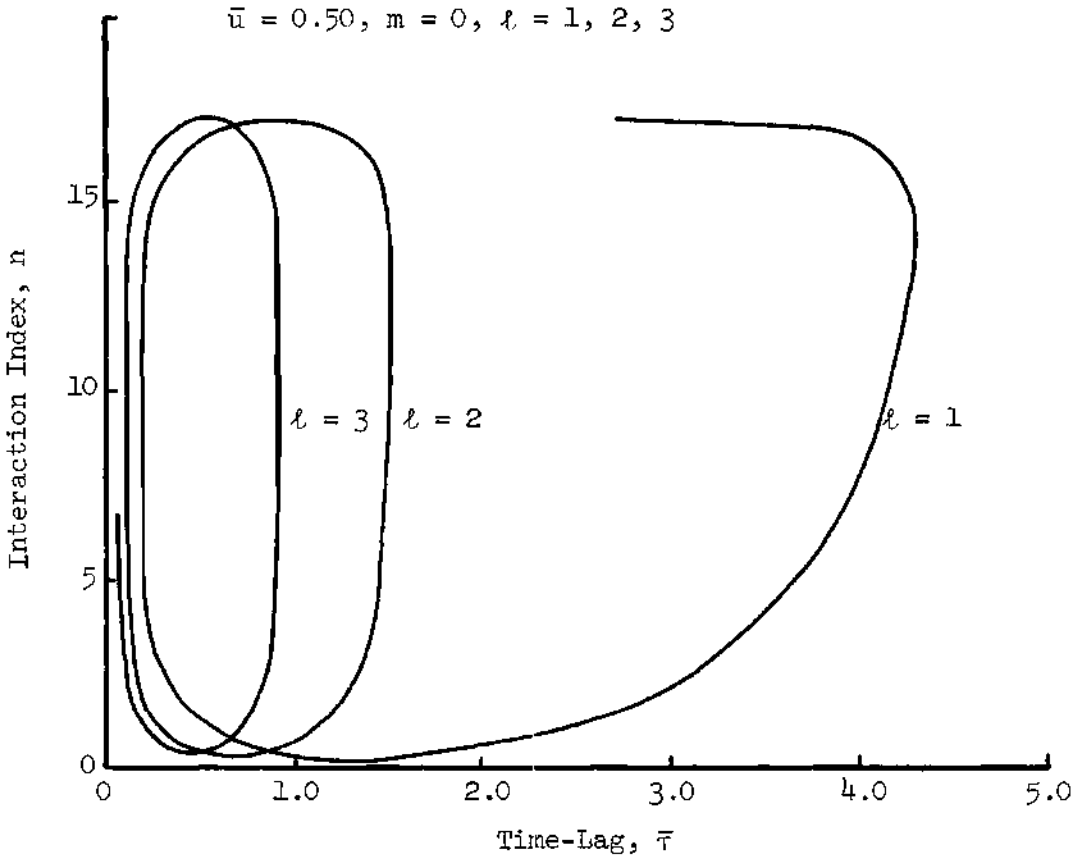

Figure 3. Stability Plot for Axial Oscillations in a Combustor with High Mach Number Mean Flow.

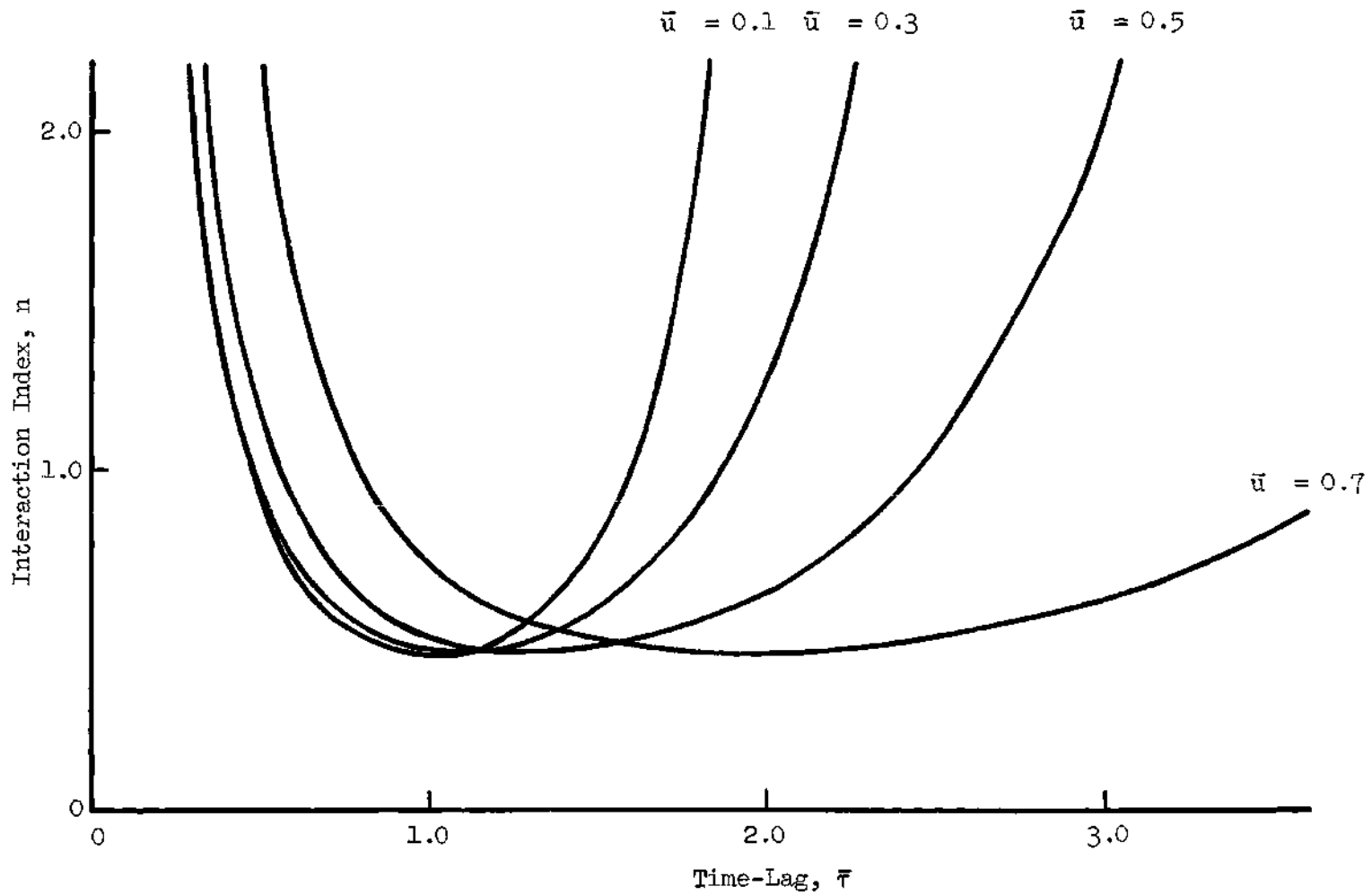

Figure 4. Dependence of the Axial Stability Limits on the Combustor's Mean Flow Velocity.

combustion instability illustrates well the fact that the accuracy of the approximation depends heavily upon a judicious choice of the functions in terms of which the dependent variables are expanded. If the more general approximate solutions given by Eqs. (151) are employed, the Galerkin method predicts neutral stability limits which are in exact agreement with those determined by more exact methods. This correspondence holds for both small and large Mach number, as Eqs. (156) and (157), with the aid of some trigonometric identities, reduce to the low Mach number expressions (i.e. Eqs. (138) and (139)) when terms of order $\bar{u}^2$ and higher are neglected. However the converse is not true; Eqs. (156) and (157) cannot be obtained with the aid of the low Mach number expansions (i.e. Eqs. (131)) simply by keeping all terms involving the steady state velocity. In particular the frequency shift arising from the convection of the waves cannot be predicted with the simpler expansions.

Transverse and Three-Dimensional Instability

The modified Galerkin method will now be employed to obtain the linear stability limits in the case of transverse mode combustion instability under the same assumptions and restrictions that are imposed on the nonlinear theory. Two situations will be examined: (1) the wave motion is irrotational and is described by a single partial differential equation involving the velocity potential, and (2) the irrotationality restriction is relaxed and the complete system of wave equations is considered. The neutral stability limits thus obtained will be useful in the proper interpretation of the second and third order

nonlinear solutions to be presented in Chapters VI and VII.

The desirability of acquiring the neutral stability boundary by the same approximate mathematical technique used to find the nonlinear solutions will now be explained. On the $(n, \bar{\tau})$ plane given in Fig. (5) a possible configuration of the exact and approximate linear stability limits is shown, where the discrepancy between the two curves is exaggerated for clarity. The solutions of the linearized equations represent the limiting case of the corresponding nonlinear solutions as the amplitude of the waves becomes vanishingly small. An exact nonlinear analysis would predict that, for an engine operating with an $(n, \bar{\tau})$ in the region above the solid surve, all small amplitude disturbances will be amplified. Since no exact theory applicable to finite amplitude oscillations is available, an approximate method must be used to determine the nonlinear behavior. For values of n and $\bar{\tau}$ lying above the dashed curve, the approximate linear and nonlinear theories both predict that infinitesimally small oscillations will grow; while, for an $(n, \bar{\tau})$ below this curve, similar disturbances will decay. At a point P between these curves the conclusions of the approximate nonlinear theory regarding small perturbations clearly contradict those of the exact linear theory, whereas the approximate linear and nonlinear theories are consistent.

Contradictions can also arise in the interpretation of strictly nonlinear phenomena. Suppose that at the point P, according to the approximate nonlinear theory, a certain initial disturbance develops into a large amplitude neutrally stable oscillation, but a somewhat smaller disturbance is damped. Referring to the approximate stability

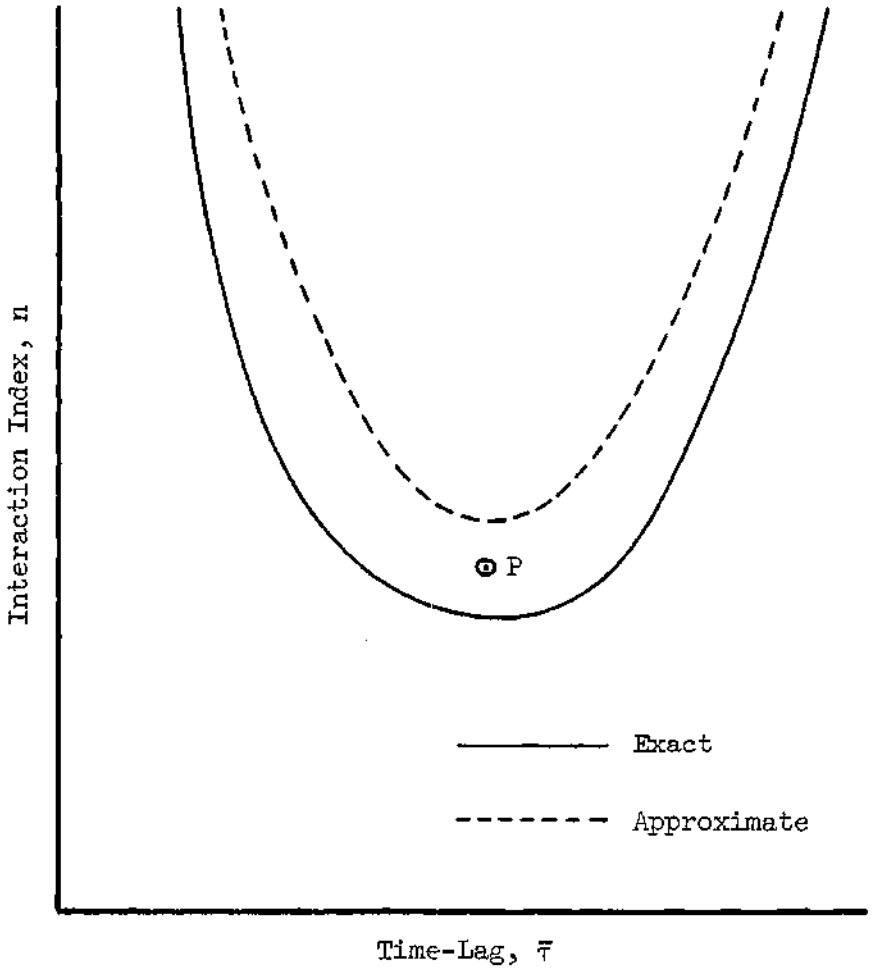

Figure 5. Exact and Approximate Neutral Stability Limits.

limit, this oscillation would be correctly interpreted as triggered or pulsed instability. However if this result is referred to the exact neutral stability curve, it would be erroneously concluded that a triggering limit or unstable limit cycle can occur in a region of spontaneous instability, which is inconsistent with linear theory.

In view of the above considerations, the approximate nonlinear solutions to be determined in Chapters VI and VII will be referred to the approximate linear stability limits to be obtained in the following sections.

The linear analysis will be conducted subject to the assumptions used to derive the simplified wave equations (i.e. Eqs. (46) through (48)). These are summarized as follows: (1) the gas phase in the combustor consists of a single constituent which is thermally and calorically perfect; (2) all transport phenomena such as diffusion, viscosity, and heat conduction can be neglected; (3) the momentum source due to droplet-gas interaction is negligible; and (4) the specific stagnation enthalpy of the liquid phase does not change as the droplets move down the chamber.

Attention is confined to a cylindrical combustion chamber with uniform propellant injection at one end ($z = 0$) and a multi-orifice (quasi-steady) nozzle at the other end ($z = z_e$). The combustor configuration and coordinate system is depicted in Fig. (2), where all lengths are normalized with respect to the chamber radius. The combustion process is assumed to be distributed throughout the rocket's combustion chamber, and the burning rate perturbations are related to the pressure fluctuations by Crocco's time-lag hypothesis.

Linear Stability Limits Consistent with the Second Order Theory

It has been shown in Chapter III that under low Mach number mean flow conditions the unsteady flow can be approximated to second order as an irrotational flow, which is described by Eq. (80). The Galerkin orthogonality condition which is appropriate to Eq. (80) is then given by Eq. (84). In order to study the stability characteristics of infinitesimally small disturbances, Eq. (84) is linearized by simply dropping all products of perturbations to obtain the following expression:

$$\int_0^{\frac{2\pi}{\omega}} \left\{ \int_V \left[\nabla^2\tilde{\Phi} - \tilde{\Phi}_{tt} - 2\bar{\underline{V}}\cdot\nabla\tilde{\Phi}_t - \gamma(\nabla\cdot\bar{\underline{V}})\tilde{\Phi}_t - \tilde{W}'_m \right] \Psi_n dv \right. \tag{158}$$

$$\left. - \int_S \left[\tilde{Q}'_m + \left(\nabla\tilde{\Phi} - \bar{\underline{V}}\tilde{\Phi}_t \right)\cdot\underline{n} \right] \Psi_n ds \right\} dt = 0$$

where partial derivatives with respect to time are indicated by subscripts.

Before approximate solutions can be obtained from Eq. (158), the burning rate perturbation W'_m and the nozzle boundary source Q'_m must be expressed in terms of the velocity potential Φ. It has been shown in Chapter IV that, subject to the small Mach number restriction, Crocco's time-lag model leads to Eq. (109), a relation between the fluctuating combustion mass source and the pressure oscillations which is correct to third order. Neglecting the third order terms and substituting the first order expression $p' = -\gamma\Phi_t$ into the remaining

second order terms yields the desired linear burning rate function:

$$W_m' = - \gamma n \frac{d\bar{u}}{dz} \left[\Phi_t(r,\theta,z,t) - \Phi_t(r,\theta,z,t-\bar{\tau}) \right] \tag{159}$$

With the aid of the first order relation $\rho' = - \Phi_t$ a similar procedure is applied to Eq. (119), and the linear quasi-steady nozzle condition becomes:

$$Q_m' = \frac{\gamma+1}{2} \bar{u}_e \Phi_t \tag{160}$$

where $\bar{u}_e$ is the steady state velocity at the nozzle entrance ($z = z_e$). Over the remainder of the combustor's boundary $Q_m' = 0$, because at the injector face ($z = 0$) and the wall ($r = 1$) the normal component of the velocity (and hence the mass flux) must vanish.

Introducing the source terms given by Eqs. (159) and (160) into Eq. (158) and writing the result in cylindrical coordinates yields the linearized Galerkin orthogonality condition:

$$\int_0^{\frac{2\pi}{\omega}} \left\{ \int_0^{z_e} \int_0^{2\pi} \int_0^1 \left[\tilde{\Phi}_{rr} + \frac{1}{r}\tilde{\Phi}_r + \frac{1}{r^2}\tilde{\Phi}_{\theta\theta} + \tilde{\Phi}_{zz} - \tilde{\Phi}_{tt} - 2\bar{u}\tilde{\Phi}_{zt} - \gamma\tilde{\Phi}_t \frac{d\bar{u}}{dz} - \tilde{W}_m' \right] \Psi_n r dr d\theta dz \right. \tag{161}$$

$$\left. - \int_0^{2\pi} \int_0^1 \left[\frac{\gamma+1}{2} \bar{u}_e \tilde{\Phi}_t + \left(\tilde{\Phi}_z - \bar{u}_e \tilde{\Phi}_t \right) \right]_{z=z_e} \Psi_n\left(r,\theta,z_e,t\right) r dr d\theta \right\} dt = 0$$

It is now necessary to choose an approximating series expansion for the velocity potential. Since the neutral stability boundary is being sought, the velocity potential is expanded in a series of periodic functions. Therefore $\tilde{\Phi}$ will be expressed in the following form:

$$\tilde{\Phi} = e^{i\omega t}\Psi_{mn}(r,\theta)\left[a_o + \sum_{k=2}^{N} a_k z^k\right] \tag{162}$$

where the $\Psi_{mn}(r,\theta)$ are the eigenfunctions corresponding to the acoustic standing transverse modes which can be excited in a circular cylinder that is closed at both ends. These functions are given by

$$\Psi_{mn}(r,\theta) = \cos m\theta J_m\left(S_{mn} r\right) \tag{163}$$

where J_m is the Bessel function of the first kind of order m, and S_{mn} is the n^{th} nonzero root of the equation $J_m'(x) = 0$. It is seen that the expansion given by Eq. (162) satisfies the rigid wall boundary conditions at $z = 0$ and $r = 1$, but the boundary condition at $z = z_e$ is left free.

For combustors experiencing transverse mode instability (i.e. no axial or mixed modes are present) previous studies have indicated that the perturbations may vary along the axial coordinate (see Ref. 5). These axial gradients arise from the influence of the nozzle, the steady state flow, and the distributed combustion process upon the wave

motion. To account for this effect the axial dependence of the assumed solution is expressed as a power series, as indicated in Eq. (162). The term $a_1 z$ is omitted from the z-expansion because it violates the solid wall boundary condition at the injector (i.e. $\Phi_z(r, \theta, 0, t) = 0$). The constants a_0, a_2, a_3, ... a_N occurring in this expansion are to be determined by the Galerkin method.

It should be observed from Eq. (162) that only one transverse eigenfunction Ψ_{mn} has been included in the assumed form of the approximate solution. This simplification can be justified by considering the consequences of expanding $\tilde{\Phi}$ in an infinite series of these eigenfunctions. Such a multi-mode expansion is substituted into Eq. (161) and the integrations are performed. Due to the orthogonality properties of the eigenfunctions Ψ_{mn} and the linearity of Eq. (161), the resulting system of algebraic equations contains no coupling between the various modes. Thus an equation describing a particular mode can be solved independently of all the others, consequently the single-mode expansion given by Eq. (162) is sufficient to determine the linear stability limits for that particular mode.

First Approximation. To investigate the stability of purely transverse (two dimensional) pressure oscillations, only the first term in the z-expansion is retained giving

$$\tilde{\Phi} = a_o e^{i\omega t} \cos m\theta J_m\left(S_{mn} r\right) \tag{164}$$

The above expression is then substituted into the Galerkin orthogonality

condition (i.e. Eq. (161)), in which the complex conjugate

$$\Psi^* = e^{-i\omega t}\cos m\theta J_m\left(S_{mn}r\right)$$

is the appropriate weighting function. Evaluating the integrals yields the following result:

$$a_o\left\{\left(\omega^2-S_{mn}^2\right)z_e - \gamma i\omega\bar{u}_e\left[1 + \frac{\gamma-1}{2\gamma} - n\left(1-e^{-i\omega\bar{\tau}}\right)\right]\right\} = 0 \qquad (165)$$

If an oscillation is present the constant a_o must be nonzero which implies that the expression in brackets must vanish. When the real and imaginary parts of the resulting complex equation are separated, two relations involving the parameters n, $\bar{\tau}$, and the unknown frequency ω are obtained:

$$\omega^2 - S_{mn}^2 - \gamma n \frac{\bar{u}_e}{z_e}\omega\sin\omega\bar{\tau} = 0 \qquad (166)$$

$$1 + \frac{\gamma-1}{2\gamma} - n(1 - \cos\omega\bar{\tau}) = 0 \qquad (167)$$

Further algebraic manipulations are performed to obtain expressions for the interaction index and the frequency as functions of the phase-lag $\omega\bar{\tau}$:

$$n = \left(1 + \frac{\gamma-1}{2\gamma}\right) \frac{1}{1 - \cos\omega\bar{\tau}} \tag{168}$$

$$\omega = \frac{1}{2}\left[G + \sqrt{4S_{mn}^2 + G^2}\right] \tag{169}$$

where $$G = \frac{\gamma n \bar{u}_e}{z_e} \sin\omega\bar{\tau}$$

To determine a point on the neutral stability curve in the $(n, \bar{\tau})$ plane, a value of $\omega\bar{\tau}$ is chosen and n is calculated from Eq. (168). With both $\omega\bar{\tau}$ and n known, ω can be computed from Eq. (169) and $\bar{\tau}$ can be found from the relation $\bar{\tau} = \omega\bar{\tau}/\omega$.

These linear stability limits are presented in Fig. (6) for the three transverse modes of lowest frequency. These modes, which are most commonly observed experimentally, are the first tangential (1T), the second tangential (2T), and the first radial (1R) modes. In the region above the parabolic curves all small disturbances grow without limit; below these curves small oscillations decay exponentially to zero. Consequently all modes are seen to be stable for values of n below the critical value given by:

$$n_{min} = \frac{1}{2}\left(1 + \frac{\gamma-1}{2\gamma}\right) \tag{170}$$

which is approximately 0.542 for $\gamma = 1.2$. It is observed that n_{min} is a function of γ only; it is independent of the chamber length or exit

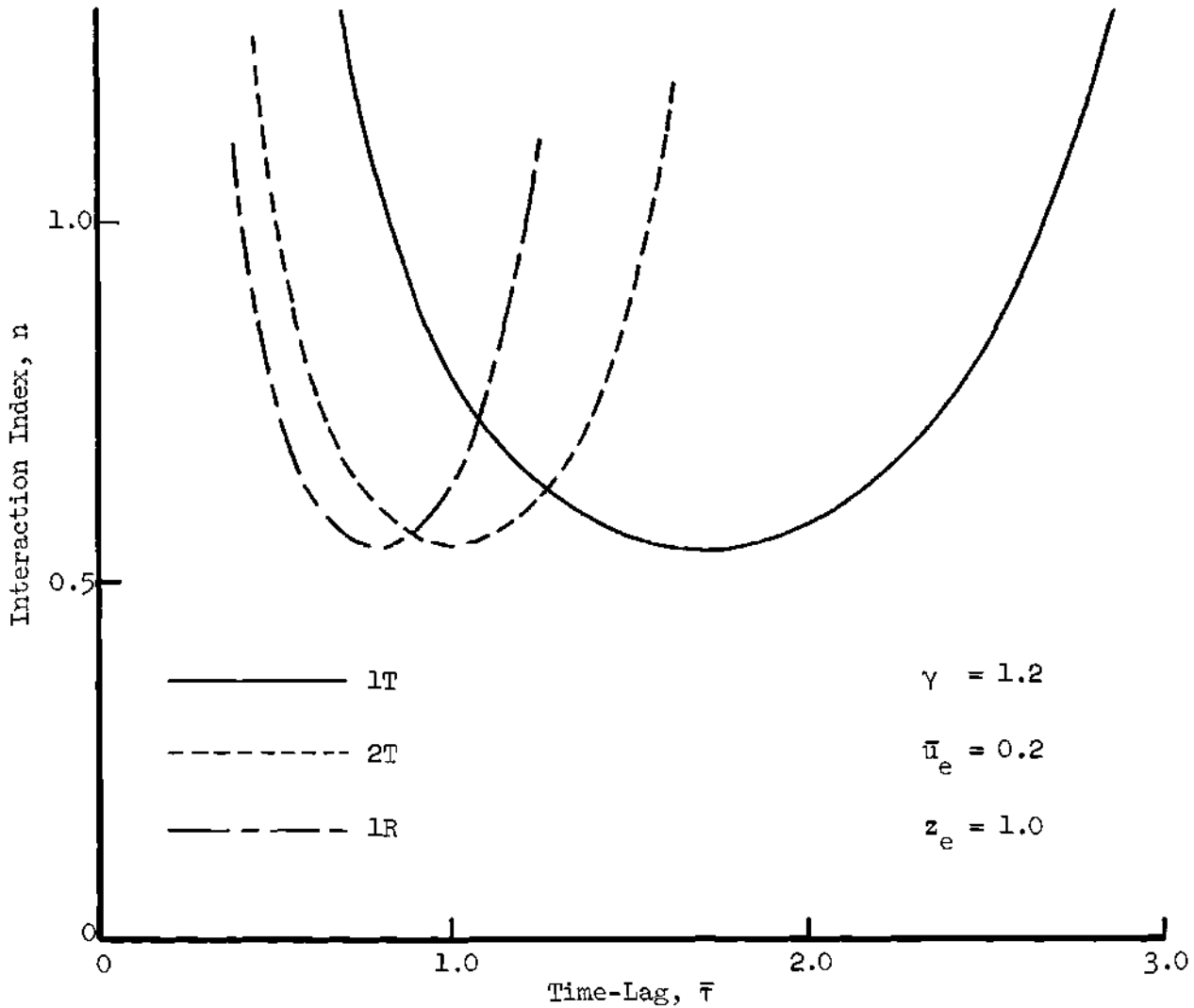

Figure 6. Linear Stability Limits for the Three Lowest Frequency Transverse Modes.

Mach number. For all modes this minimum interaction index for neutral stability occurs when $\omega\bar{\tau} = \pi$ which corresponds to $\bar{\tau} = 1.70629$ for the first tangential mode. Thus spontaneous instability is most likely to occur when the time-lag is equal to one-half of the period of oscillation.

Second Approximation. To evaluate the effect of axial gradients in the perturbations, additional terms must be retained in the z-expansion. Stability limits obtained from a two-term expansion will next be investigated. The velocity potential is then expressed as follows:

$$\tilde{\Phi} = e^{i\omega t}\cos m\theta J_m\left(S_{mn}r\right)\left[a_o + a_2 z^2\right] \tag{171}$$

where the constants a_o and a_2 are evaluated from Eq. (161) by using both of the weighting functions given by:

$$\Psi_1^* = e^{-i\omega t}\cos m\theta J_m\left(S_{mn}r\right) \tag{172}$$

$$\Psi_2^* = e^{-i\omega t} z^2 \cos m\theta J_m\left(S_{mn}r\right)$$

The resulting pair of equations to be solved for these constants is then:

$$\left\{\omega^2 - S_{mn}^2 - \frac{\gamma i\omega\bar{u}_e}{z_e}\left[1 + \frac{\gamma-1}{2\gamma} - n\left(1-e^{-i\omega\bar{\tau}}\right)\right]\right\}a_o \tag{173}$$

$$+\left\{\frac{1}{3}\left(\omega^2-S_{mn}^2\right)z_e^2-\gamma i\omega\bar{u}_e z_e\left[1+\frac{\gamma-1}{2\gamma}-n\left(1-e^{-i\omega\bar{\tau}}\right)\right]\right.$$

$$\left.-\frac{2\gamma i\omega}{z_e}\left[\frac{2-\gamma}{\gamma}+n\left(1-e^{-i\omega\bar{\tau}}\right)\right]\int_o^{z_e}\bar{u}(z)\,z\,dz\right\}a_2=0$$

$$\left\{\frac{1}{3}\left(\omega^2-S_{mn}^2\right)z_e^2-\gamma i\omega\bar{u}_e z_e\left[1+\frac{\gamma-1}{2\gamma}-n\left(1-e^{-i\omega\bar{\tau}}\right)\right]\right. \tag{174}$$

$$\left.+\frac{2i\omega\gamma}{z_e}\left[1-n\left(1-e^{-i\omega\bar{\tau}}\right)\right]\int_o^{z_e}\bar{u}(z)\,z\,dz\right\}a_o$$

$$+\left\{-\frac{4}{3}z_e^2+\frac{1}{5}\left(\omega^2-S_{mn}^2\right)z_e^4-\gamma i\omega\bar{u}_e z_e^3\left[1+\frac{\gamma-1}{2\gamma}-n\left(1-e^{-i\omega\bar{\tau}}\right)\right]\right.$$

$$\left.+\frac{4\gamma i\omega}{z_e}\left[\frac{\gamma-1}{\gamma}-n\left(1-e^{-i\omega\bar{\tau}}\right)\right]\int_o^{z_e}\bar{u}(z)\,z^3dz\right\}a_2=0$$

The above system has a nontrivial solution only if the determinant of the coefficient matrix vanishes. Expanding this determinant and setting it equal to zero gives the following complex equation valid for arbitrary mean flow velocity distributions $\bar{u}(z)$.

$$-\frac{4}{3}\Omega z_e^2+\frac{4}{45}\Omega^2 z_e^4-\frac{8}{15}i\omega\gamma\Omega\bar{u}_e z_e^3K_2+\frac{4}{3}i\omega\gamma\bar{u}_e z_e K_2 \tag{175}$$

$$-\frac{4}{3}i\omega\gamma\Omega z_e M_1\left(K_2-\frac{\gamma+1}{2\gamma}\right)+4i\omega\Omega\frac{\gamma}{z_e}M_3\left(K_2-\frac{\gamma+1}{2\gamma}\right)$$

$$+ 4\omega^2 \frac{\gamma^2}{z_e^2} \bar{u}_e M_3 K_2\left(K_2 - \frac{\gamma+1}{2\gamma}\right) - 4\omega^2\gamma^2\bar{u}_e M_1 K_2\left(K_2 - \frac{\gamma+1}{2\gamma}\right)$$

$$+ 4\omega^2 \frac{\gamma^2}{z_e^2} M_1^2\left(K_2 - \frac{\gamma+3}{2\gamma}\right)\left(K_2 - \frac{\gamma-1}{2\gamma}\right) = 0$$

where $$\Omega = \omega^2 - S_{mn}^2$$

$$K_2 = 1 + \frac{\gamma-1}{2\gamma} - n\left(1-e^{-i\omega\bar{\tau}}\right)$$

$$M_1 = \int_o^{z_e} \bar{u}(z)\, z\, dz \quad ; \quad M_3 = \int_o^{z_e} \bar{u}(z)\, z^3 dz$$

In order to obtain specific numerical results, the special case of uniformly distributed combustion will be considered; that is, it will be assumed that the steady state velocity varies linearly with axial position. Substituting the velocity distribution $\bar{u}(z) = \bar{u}_e(z/z_e)$ into the integrals occurring in Eq. (175) yields

$$M_1 = \frac{1}{3}\bar{u}_e z_e^2 \quad ; \quad M_3 = \frac{1}{5}\bar{u}_e z_e^4$$

Introducing these and the expressions for K_2 and Ω into Eq. (175) produces a complex equation relating n, $\bar{\tau}$, and ω. The real and imaginary components are separated and rearranged to give the following:

$$\left(\omega^2-S_{mn}^2\right)\left[1 - \frac{1}{15}\left(\omega^2-S_{mn}^2\right)z_e^2\right] - \frac{\omega\gamma\bar{u}_e}{z_e}\left[1 - \frac{2}{15}\left(\omega^2-S_{mn}^2\right)z_e^2\right]n\sin\omega\bar{\tau} \quad (176)$$

$$+ \frac{\omega^2\gamma^2\bar{u}_e^2}{15}\left[\frac{4\gamma^2 - 2\gamma + 3}{\gamma^2} - \frac{5\gamma + 1}{\gamma}\, n(1-\cos\omega\bar{\tau}) - 2n^2\cos\omega\bar{\tau}(1-\cos\omega\bar{\tau})\right] = 0$$

$$1 + \frac{\gamma - 1}{2\gamma} - n(1-\cos\omega\bar{\tau}) - \frac{2}{15}\left(\omega^2-S_{mn}^2\right)z_e^2\left[\frac{5\gamma + 1}{2\gamma} - n(1-\cos\omega\bar{\tau})\right] \quad (177)$$

$$+ \frac{\omega\gamma\bar{u}_e}{15}\, z_e\left[\frac{5\gamma + 1}{\gamma} - 2n(1-\cos\omega\bar{\tau})\right]n\sin\omega\bar{\tau} = 0$$

The above equations were solved by an iteration scheme using the Burroughs B-5500 computer facility at the Georgia Institute of Technology. Some examples of calculated stability limits, plotted on an $(n, \bar{\tau})$ coordinate system, are shown in Figures (7) through (9).

Stability limits computed using the two-term expansion (three-dimensional theory) will now be compared with those obtained under the single-term approximation (two-dimensional theory). For combustors with low Mach number mean flows the first tangential mode stability limits determined by the two theories are in very close agreement. For typical values of the Mach number and chamber length ($\bar{u}_e = 0.2$, $z_e = 1.0$) the three-dimensional theory yields a value of n_{min} which differs from the corresponding two-dimensional value by only 0.2 per cent. The error incurred by using the one-term approximation however is considerably larger for the higher frequency modes. In Fig. (7) a comparison between the second tangential mode stability limits pre-

dicted by the two and three-dimensional theories is presented. These results indicate that for a given engine the three-dimensional theory predicts a slightly more unstable behavior.

Numerical calculations reveal that when the perturbations are three-dimensional the minimum value of the interaction index (i.e., n_{min}) on the neutral stability curve of a particular acoustic mode depends upon the steady state velocity distribution, the velocity at the nozzle entrance, and the combustor's length to diameter ratio. Increasing $\bar{u}_e$ or z_e was found to be destabilizing; that is, the threshold of instability n_{min} is lowered. The effect of an increase in $\bar{u}_e$ was much greater for long chambers ($z_e > 2$) than for short ones ($z_e < 1$). These results are in contrast to the conclusions of the two-dimensional theory which predicts that n_{min} is a function of γ only, however in the limiting case $\bar{u}_e = 0$ the values of n_{min} determined with the two and three-dimensional approximations are in exact agreement.

These findings indicate that the single-term approximation provides sufficiently accurate stability limits for the three lowest frequency transverse modes if (1) the mean flow Mach number is small ($\bar{u}_e < 0.3$) and (2) the chamber is relatively short ($z_e < 2$). Otherwise consideration of property variation in the axial direction should be included in future analyses of similar problems.

Figures (8) and (9) show the effect of increasing the Mach number of the combustor's mean flow and of decreasing the combustor's length to diameter ratio. For most values of the time-lag, both of these effects are shown to be destabilizing, however for values of $\bar{\tau}$ in the immediate vicinity of n_{min} decreasing z_e is seen to have the oppo-

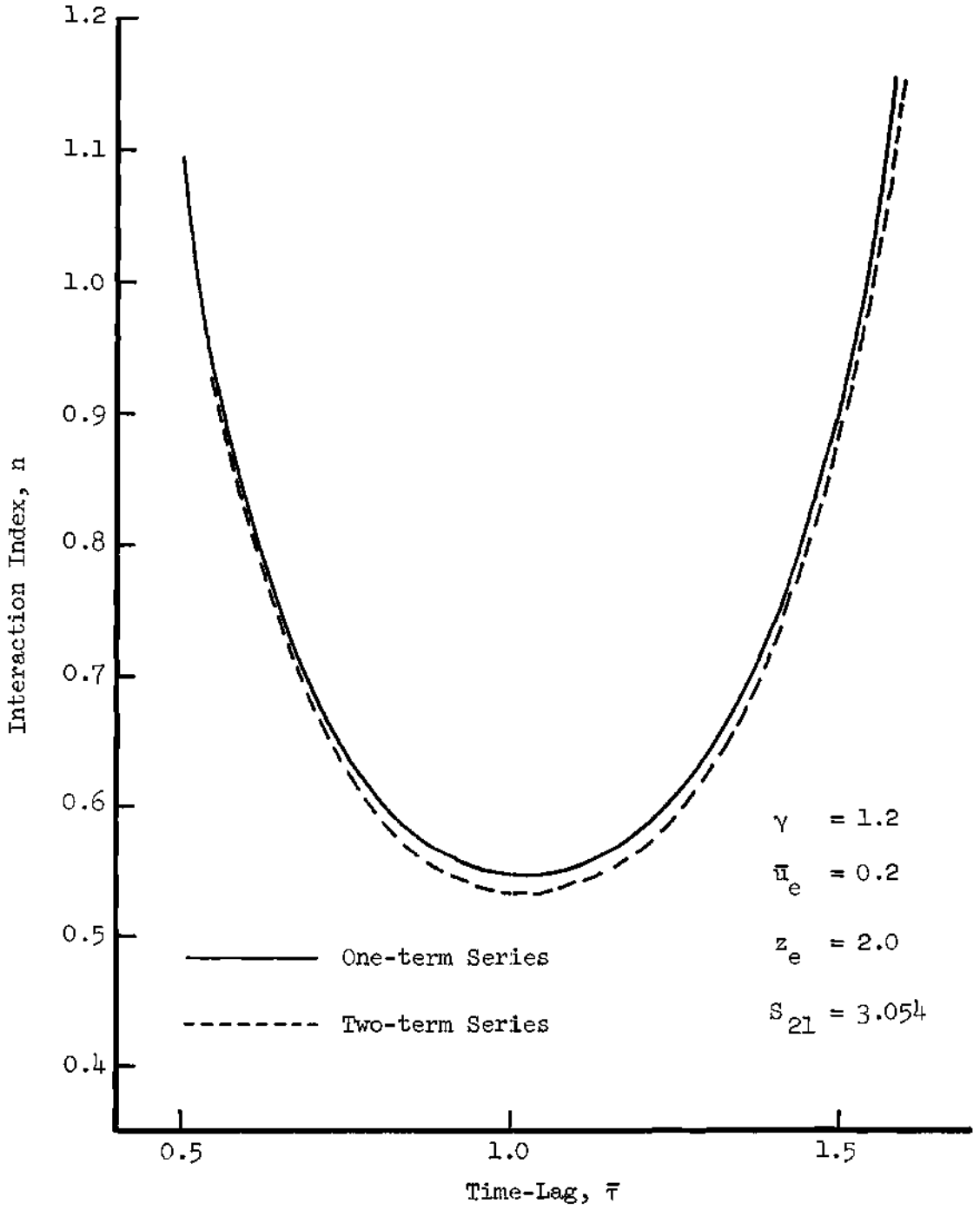

Figure 7. Comparison of Stability Limits Obtained with One- and Two-Term Expansions.

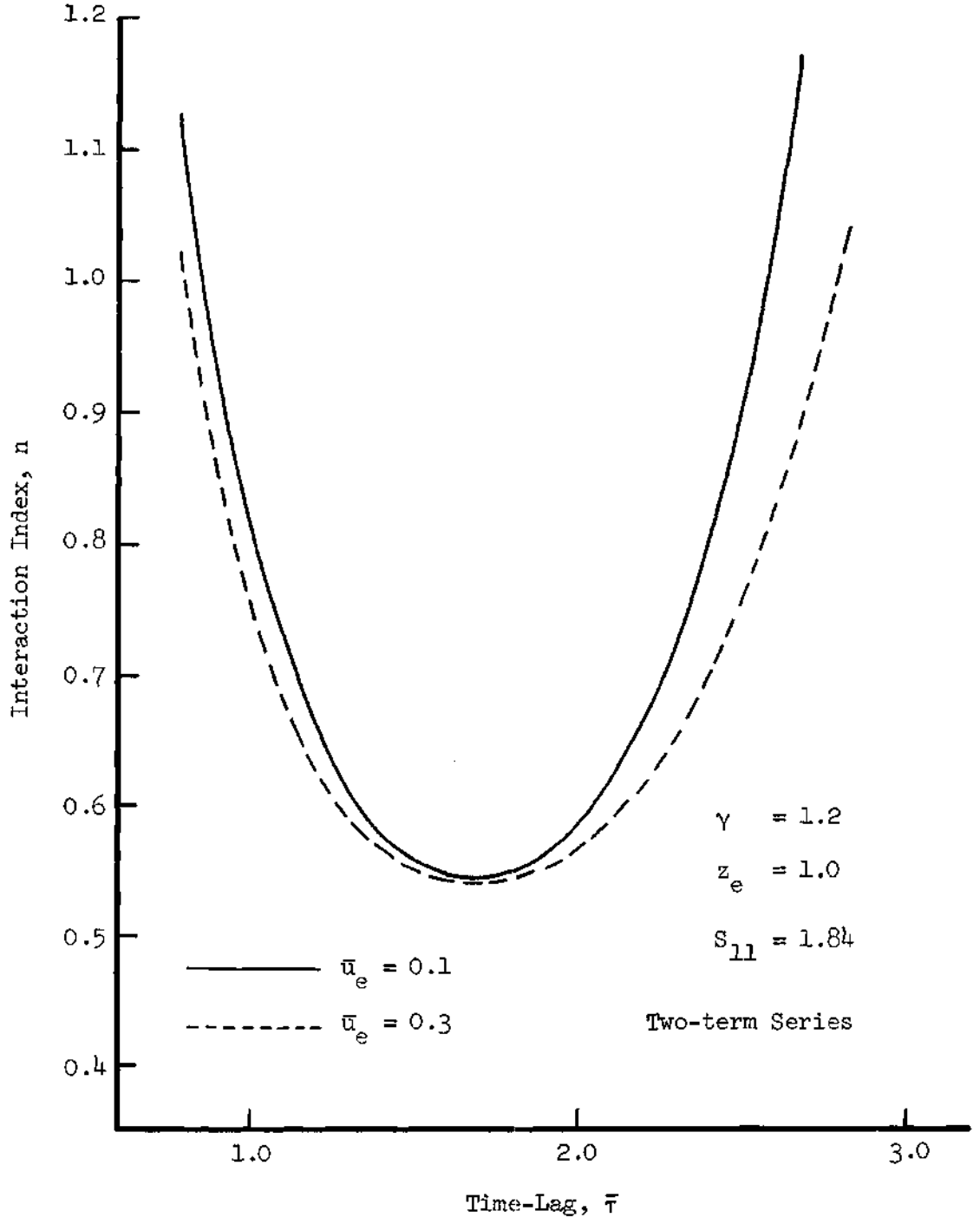

Figure 8. Effect of Steady State Velocity on the Stability Limits for the First Tangential Mode.

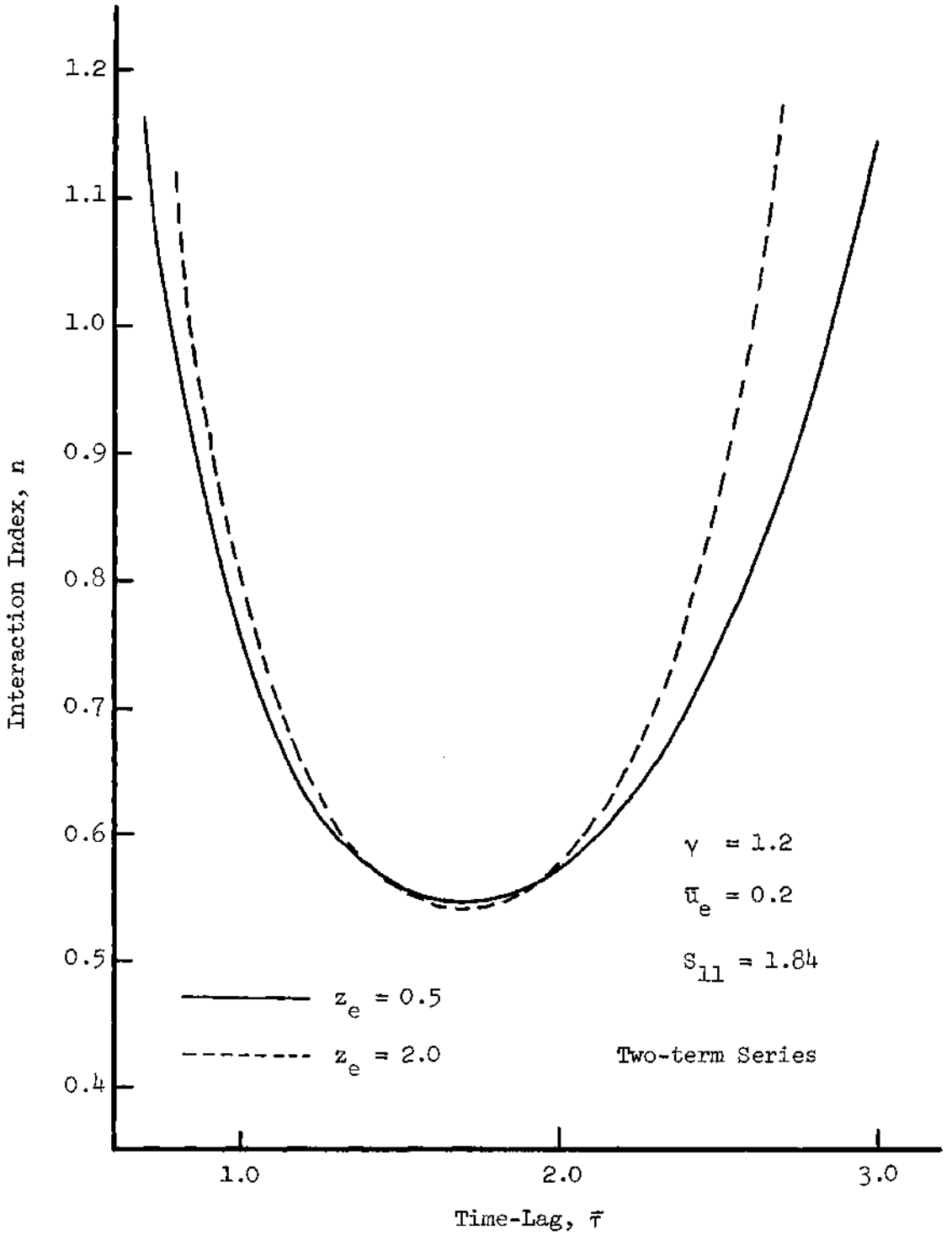

Figure 9. Effect of Chamber Length on the Stability Limits for the First Tangential Mode.

site effect.

Comparison of the approximate transverse stability limits with those obtained by other investigators is complicated by the fact that these researchers considered a more general nozzle configuration (not quasi-steady) than the one considered in the present investigation. Nevertheless the stability maps presented in these figures were found to be in qualitative agreement with the results obtained by Reardon[5], who treated a similar problem with the aid of more exact mathematical techniques.

Linear Stability Limits Consistent with the Third Order Theory

In order to derive linear stability limits compatible with the third order nonlinear solutions, the restrictions of irrotationality and uniform steady state properties will be relaxed. As a result the velocity can no longer be expressed as the gradient of a scalar potential, and the wave equations cannot be combined to yield a single governing equation. The unsteady flow, therefore, is described by the complete set of simplified wave equations given by Eqs. (46) through (48).

For reasons that will be explained in detail in Chapter VII it is convenient to represent the components of the velocity perturbation in terms of so-called quasi-potential functions. These are defined in a cylindrical coordinate system as follows:

$$u' = \frac{\partial \Phi}{\partial z} \quad ; \quad v' = \frac{\partial \eta}{\partial r} \quad ; \quad w' = \frac{1}{r} \frac{\partial \zeta}{\partial \theta}$$

where Φ, η, and ζ are respectively the axial, radial, and tangential quasi-potential functions. Since no relation between the velocity components is implied by these expressions the possibility of rotational flow is preserved.

Writing Eqs. (46) through (48) in cylindrical coordinates, introducing the quasi-potentials, and neglecting all products of perturbations yields the following linearized wave equations:

Continuity

$$E_\rho = \frac{\partial \rho'}{\partial t} + \bar{\rho}(z)\left[\eta_{rr} + \frac{1}{r}\eta_r + \frac{1}{r^2}\zeta_{\theta\theta} + \Phi_{zz}\right] \qquad (178)$$

$$+ \rho' \frac{d\bar{u}}{dz} + \bar{u}\rho'_z + \Phi_z \frac{d\bar{\rho}}{dz} - W'_m = 0$$

Radial momentum

$$E_\eta = \bar{\rho}(z)\eta_{rt} + \bar{\rho}\bar{u}\eta_{rz} + \frac{1}{\gamma} p'_r = 0 \qquad (179)$$

Tangential momentum

$$E_\zeta = \bar{\rho}(z)\zeta_{\theta t} + \bar{\rho}\bar{u}\zeta_{\theta z} + \frac{1}{\gamma} p'_\theta = 0 \qquad (180)$$

Axial momentum

$$E_\Phi = \bar{\rho}(z)\Phi_{zt} + \bar{\rho}\bar{u}\Phi_{zz} + \bar{\rho}\frac{d\bar{u}}{dz}\Phi_z + \rho'\bar{u}\frac{d\bar{u}}{dz} + \frac{1}{\gamma} p'_z = 0 \qquad (181)$$

Energy

$$E_h = \bar{\rho}(z)\,\frac{\partial h_s'}{\partial t} + \bar{\rho}\bar{u}\,\frac{\partial h_s'}{\partial z} + \frac{d}{dz}\,(\bar{\rho}\bar{u})h_s' - \frac{\gamma-1}{\gamma}\,\frac{\partial p'}{\partial t} = 0 \qquad (182)$$

Using Eq. (34b) the linearized equation of state becomes:

$$E_p = p' - \bar{\rho}h_s' - \bar{h}_s\rho' + (\gamma-1)\bar{\rho}\bar{u}\Phi_z + \frac{\gamma-1}{2}\,\bar{u}^2\rho' = 0 \qquad (183)$$

The corresponding burning rate function W_m' and quasi-steady nozzle condition Q_m' are easily determined by dropping the nonlinear terms in Eqs. (109) and (119) to obtain:

$$W_m' = n\,\frac{d\bar{u}}{dz}\left[p'(r,\theta,z,t) - p'(r,\theta,z,t-\bar{\tau})\right] \qquad (184)$$

$$Q_m' = -\frac{\gamma+1}{2}\,\bar{u}_e\rho' - \frac{3}{4}\,(\gamma+1)\bar{\rho}_e\left(\frac{\bar{u}_e}{\bar{c}_e}\right)^2\frac{\partial\Phi}{\partial z} \qquad (185)$$

where the nozzle boundary residual is given by

$$B_\rho = \left[Q_m' + \bar{\rho}\Phi_z + \bar{u}\rho'\right]_{z=z_e} \qquad (186)$$

The weighted residuals of the continuity equation and its boundary condition are combined in the manner indicated by Eq. (24),

that is:

$$\int_0^{\frac{2\pi}{\omega}} \left\{ \int_0^{z_e} \int_0^{2\pi} \int_0^1 E_\rho \Psi_n r dr d\theta dz - \int_0^{2\pi} \int_0^1 B_\rho \Psi_n r dr d\theta \right\} dt = 0 \qquad (187a)$$

Since Eqs. (179) through (181) are derived from the Euler form of the momentum equation, the Galerkin orthogonality conditions appropriate to these equations cannot be obtained directly from Eq. (24). Likewise the energy equation in the form given by Eq. (182) demands special treatment. It will be shown in Chapter VII that, in the absence of momentum and energy sources (due to combustion) at the nozzle entrance, the boundary residuals vanish and the following expressions are valid:

$$\int_0^{\frac{2\pi}{\omega}} \int_0^{z_e} \int_0^{2\pi} \int_0^1 E_m \Psi_n r dr d\theta dz dt = 0 \qquad (187b)$$

$$\int_0^{\frac{2\pi}{\omega}} \int_0^{z_e} \int_0^{2\pi} \int_0^1 E_h \Psi_n r dr d\theta dz dt = 0 \qquad (187c)$$

where E_m can represent any one of the components of the Euler residual. Lastly, applying the Galerkin method to the equation of state yields:

$$\int_0^{\frac{2\pi}{\omega}} \int_0^{z_e} \int_0^{2\pi} \int_0^1 E_p \Psi_n r dr d\theta dz dt = 0 \qquad (187d)$$

The dependent variables occurring in Eqs. (187) will now be expressed in terms of periodic functions of unknown frequency ω. The spatial dependence of the quasi-potentials as well as the pressure, density, and enthalpy is expected to be approximately that of the velocity potential Φ which is used in the second order theory. Thus each of the dependent variables will be expanded in terms of the transverse mode acoustic eigenfunctions $\Psi_{mn}(r,\theta)$ given by Eq. (163). For simplicity the variation of the unsteady properties in the axial direction will be neglected; that is, only two-dimensional pressure oscillations will be considered. Since this assumption implies that the velocity perturbation has no axial component, the axial quasi-potential Φ is not needed and can be assumed to be zero. The dependent variables will, therefore, be expressed in the following form:

$$\rho' = A_\rho \Psi_{mn}(r,\theta) e^{i\omega t} \tag{188}$$

$$\eta = A_\eta \Psi_{mn}(r,\theta) e^{i\omega t}$$

$$\zeta = A_\zeta \Psi_{mn}(r,\theta) e^{i\omega t}$$

$$p' = A_p \Psi_{mn}(r,\theta) e^{i\omega t}$$

$$h_s' = A_h \Psi_{mn}(r,\theta) e^{i\omega t}$$

where A_ρ, A_η, A_ζ, A_p, and A_h are complex constants to be determined by the Galerkin method. Since the eigenfunctions are mutually orthogonal

and the differential equations are linear, a single-mode expansion is adequate to obtain the neutral stability limits for that particular mode.

The assumed solutions given by Eqs. (188) are substituted into the differential equations to obtain the following residuals:

Continuity

$$E_\rho = \left\{\left[i\omega + \frac{d\bar{u}}{dz}\right]A_\rho + \bar{\rho}(z)\left[\frac{m^2}{r^2} - S_{mn}^2\right]A_\eta - \bar{\rho}(z)\,\frac{m^2}{r^2}\,A_\zeta \right. \tag{189}$$

$$\left. - n\,\frac{d\bar{u}}{dz}\left(1-e^{-i\omega\bar{\tau}}\right)A_p\right\}e^{i\omega t}\cos m\theta J_m\left(S_{mn}r\right)$$

Radial Momentum

$$E_\eta = \left[\bar{\rho}(z)\,i\omega A_\eta + \frac{1}{\gamma}\,A_p\right]S_{mn}e^{i\omega t}\cos m\theta J_m'\left(S_{mn}r\right) \tag{190}$$

Tangential Momentum

$$E_\zeta = -\left[\bar{\rho}(z)\,i\omega A_\zeta + \frac{1}{\gamma}\,A_p\right]me^{i\omega t}\sin m\theta J_m\left(S_{mn}r\right) \tag{191}$$

Energy

$$E_h = \left\{\left[i\omega\bar{\rho}(z) + \frac{d}{dz}\,(\bar{\rho}\bar{u})\right]A_h - \frac{\gamma-1}{\gamma}\,i\omega A_p\right\}e^{i\omega t}\cos m\theta J_m\left(S_{mn}r\right) \tag{192}$$

State

$$E_p = \left\{A_p - \bar{\rho}(z)A_h - \left[\bar{h}_s - \frac{\gamma-1}{2}\bar{u}^2\right]A_\rho\right\}e^{i\omega t}\cos m\theta J_m\left(S_{mn}r\right) \qquad (193)$$

where the residual of the axial momentum equation has been omitted because the unsteady flow has been assumed to be two dimensional.

Introducing the approximate solutions into the nozzle boundary condition yields the appropriate boundary residual:

$$B_\rho = -\frac{\gamma-1}{2}\bar{u}_e A_\rho e^{i\omega t}\cos m\theta J_m\left(S_{mn}r\right) \qquad (194)$$

These residuals are then substituted into the Galerkin orthogonality conditions (i.e. Eqs. (187)) where the weighting function is the complex conjugate given by

$$\Psi_1^* = e^{-i\omega t}\cos m\theta J_m\left(S_{mn}r\right) \qquad (195a)$$

and the integrations are performed to obtain a system of algebraic equations. This procedure must be modified however in order to accommodate the tangential momentum equation. In this case the volume integral of the expression $E_\zeta\Psi_1^*$ contains as a multiplying factor the azimuthal integral

$$\int_0^{2\pi} \sin m\theta \cos m\theta \, d\theta$$

which vanishes for any positive integer m. Thus the orthogonality condition imposed upon the residual of the tangential momentum equation is identically satisfied for all values of A_ζ and A_p, and no information is obtained from this equation. A relation between A_ζ and A_p can be extracted from the tangential momentum equation by weighting the corresponding residual with the function Ψ_2^* defined by

$$\Psi_2^* = e^{-i\omega t} \sin m\theta J_m(S_{mn} r) \tag{195b}$$

As this procedure may appear to be somewhat arbitrary, it will be rigorously justified in Chapter VII when the full nonlinear equations are considered.

Applying the Galerkin method in the manner described above yields the following system of five linear homogenous algebraic equations relating the five unknown constants.

$$\left[i\omega + \frac{\gamma+1}{2} \frac{\bar{u}_e}{z_e}\right] A_\rho + I_\rho \left[m^2 K_J - S_{mn}^2\right] A_\eta \tag{196}$$

$$- m^2 K_J I_\rho A_\zeta - \frac{n\bar{u}_e}{z_e} \left(1 - e^{-i\omega\bar{\tau}}\right) A_p = 0$$

$$i\omega I_\rho A_\eta + \frac{1}{\gamma} A_p = 0 \tag{197}$$

$$i\omega I_\rho A_\zeta + \frac{1}{\gamma} A_p = 0 \tag{198}$$

$$\left[i\omega I_\rho + \frac{\bar{\rho}_e \bar{u}_e}{z_e}\right] A_h - \frac{\gamma-1}{\gamma} i\omega A_p = 0 \tag{199}$$

$$A_p - I_\rho A_h - \left[1 - \frac{\gamma-1}{2} I_u\right] A_\rho = 0 \tag{200}$$

where

$$K_J = \frac{\int_o^1 \left[J_m\left(S_{mn} r\right)\right]^2 r^{-1} dr}{\int_o^1 \left[J_m\left(S_{mn} r\right)\right]^2 r dr}$$

$$I_\rho = \frac{1}{z_e} \int_o^{z_e} \bar{\rho}(z)\, dz$$

$$I_u = \frac{1}{z_e} \int_o^{z_e} \bar{u}^2 dz$$

In deriving the above equations, the steady state result, $\tilde{h}_s = \text{const.} = 1$, has been used (see Eqs. (40) and (44)).

To avoid the cumbersome task of expanding a fifth order determinant, the condition for the existence of nontrivial solutions to Eqs. (196) through (200) will be applied to a simpler equivalent system

obtained by eliminating unknowns. Solving Eqs. (197) and (198) for the quasi-potentials yields:

$$A_\eta = A_\zeta \simeq \frac{i}{\gamma\omega\bar{I}_\rho} A_p \qquad m \neq 0$$

$$A_\zeta = 0 \qquad m = 0$$

where the tangential quasi-potential is zero for radial modes. The above expressions are then substituted into Eq. (196) to eliminate the quasi-potentials giving the following equation which involves only two unknowns:

$$\left[i\omega + \frac{\gamma+1}{2}\frac{\bar{u}_e}{z_e}\right]A_\rho - \left[\frac{i}{\gamma\omega} S_{mn}^2 + \frac{n\bar{u}_e}{z_e}\left(1-e^{-i\omega\bar{\tau}}\right)\right]A_p = 0 \qquad (201)$$

To obtain a second equation relating A_ρ and A_p, the equation of state (i.e. Eq. (200)) is first solved for A_h to obtain:

$$A_h = \frac{1}{\bar{I}_\rho}\left[A_p - \left(1 - \frac{\gamma-1}{2} I_u\right)A_\rho\right]$$

which is subsequently introduced into the energy equation (i.e. Eq. (199)) to eliminate A_h, which gives:

$$\left[\frac{i\omega}{\gamma} + \frac{1}{I_\rho}\frac{\bar{\rho}_e\bar{u}_e}{z_e}\right]A_p - B\left[i\omega + \frac{1}{I_\rho}\frac{\bar{\rho}_e\bar{u}_e}{z_e}\right]A_\rho = 0 \tag{202}$$

where $$B = 1 - \frac{\gamma-1}{2} I_u$$

The requirement for neutral stability is then determined from the pair of homogeneous equations given by Eqs. (201) and (202). Equating the determinant of this system to zero yields the following complex equation:

$$\left[i\omega + \frac{\gamma+1}{2}\frac{\bar{u}_e}{z_e}\right]\left[\frac{i\omega}{\gamma} + \frac{1}{I_\rho}\frac{\bar{\rho}_e\bar{u}_e}{z_e}\right] \tag{203}$$

$$- B\left[i\omega + \frac{1}{I_\rho}\frac{\bar{\rho}_e\bar{u}_e}{z_e}\right]\left[\frac{i}{\gamma\omega} S_{mn}^2 + \frac{n\bar{u}_e}{z_e}\left(1-\cos\omega\bar{\tau} + i\sin\omega\bar{\tau}\right)\right] = 0$$

which separates (after considerable algebraic rearrangement) into the following expressions:

$$BS_{mn}^2 - \omega^2 + \gamma n \frac{\bar{u}_e}{z_e} B\omega\sin\omega\bar{\tau} \tag{204}$$

$$+ \gamma\left(\frac{\bar{u}_e}{z_e}\right)^2 \frac{\bar{\rho}_e}{I_\rho}\left[\frac{\gamma+1}{2} - Bn(1-\cos\omega\bar{\tau})\right] = 0$$

$$\frac{\gamma-B}{\gamma}\frac{\bar{\rho}_e}{I_\rho}+\frac{\gamma+1}{2\gamma}-Bn(1-\cos\omega\bar{\tau})-\frac{\gamma-1}{2}B\frac{I_u}{I_\rho}\frac{\bar{\rho}_e\bar{u}_e}{z_e}\frac{n}{\omega}\sin\omega\bar{\tau} \qquad (205)$$

$$+B\left(\frac{1}{I_\rho}\frac{\bar{\rho}_e\bar{u}_e}{z_e}\right)^2\frac{1}{\omega^2}\left[\frac{\gamma+1}{2}-Bn(1-\cos\omega\bar{\tau})\right]-\frac{\gamma-1}{2\gamma}BI_u\frac{\bar{\rho}_e}{I_\rho}\frac{S_{mn}^2}{\omega^2}=0$$

It should be pointed out that no terms involving the steady state velocity were neglected in the derivation of Eqs. (204) and (205); also these equations are valid for combustion chambers with arbitrary axial distributions of steady state velocity and density. Due to the presence of terms of $O(\bar{u}^2)$ neutral stability limits calculated from Eqs. (204) and (205) are expected to differ slightly from those predicted by the two-dimensional irrotational theory (i.e. from Eqs. (166) and (167)). It can be easily shown, however, that the predictions of these theories are in exact agreement in the small Mach number limit ($\bar{u} \to 0$). The quantities B, I_ρ, and $\bar{\rho}_e$ are all of the form $1 + O(\bar{u}^2)$. Introducing these expressions into Eqs. (204) and (205) and neglecting all terms of order $\bar{u}^2$ or higher yields equations identical to Eqs. (166) and (167).

Assuming a uniformly distributed combustion process (i.e. $\bar{u}(z) = \bar{u}_e(z/z_e)$) linear stability limits will be computed from Eqs. (204) and (205) with the aid of an iteration technique. In order to evaluate the influence of axial variations in steady state properties upon the linear stability characteristics of the combustor, two cases will be considered; (1) a fictitious case in which the steady state density is uniform (i.e. $\bar{\rho}_e = I_\rho = 1$) and (2) the mean flow density $\bar{\rho}(z)$ is determined by

a simple but crude model. In the latter case $\bar{\rho}(z)$ will be approximated by assuming that the burned gases exert no drag force upon the liquid droplets, which implies that the liquid velocity $\bar{u}_L$ is a constant.

In his formulation for systems with distributed combustion, Crocco[3] showed that the mean flow density can be expressed in terms of the velocities of the gas and liquid as follows:

$$\bar{\rho}(z) = \frac{1 - \gamma w_i\left(\bar{u}_L(z) - \bar{u}_{L_o}\right)}{1 + \frac{\gamma+1}{2}\bar{u}^2(z) - \gamma\bar{u}(z)\bar{u}_L(z)} \tag{206}$$

where $\bar{u}_{L_o}$ is the injection velocity and w_i is the dimensionless injection rate. In the absence of drag, $\bar{u}_L(z) = \bar{u}_{L_o}$ and Eq. (206) becomes

$$\bar{\rho} = \left[1 + \frac{\gamma+1}{2}\bar{u}^2 - \gamma\bar{u}_{L_o}\bar{u}\right]^{-1} \tag{207}$$

Assuming that the liquid and gas velocities are both small, Eq. (207) is expanded in a binomial series to give

$$\bar{\rho}(z) = 1 + \gamma\bar{u}_{L_o}\bar{u}(z) - \frac{\gamma+1}{2}\bar{u}^2(z) \tag{208}$$

where terms of higher order than $\bar{u}^2$ have been neglected. For uniformly distributed combustion Eq. (208) is introduced into the definitions of $\bar{\rho}_e$ and I_ρ to obtain the following expressions:

$$\bar{\rho}_e = 1 - \frac{\gamma+1}{2}\bar{u}_e^2 + \gamma\bar{u}_{L_o}\bar{u}_e \tag{209}$$

$$I_\rho = 1 - \frac{\gamma+1}{6}\bar{u}_e^2 + \frac{\gamma}{2}\bar{u}_{L_o}\bar{u}_e$$

For representative values of the velocities ($\bar{u}_e = 0.2$, $\bar{u}_L = 0.1$) the density at the nozzle entrance is 0.98 while the average density I_ρ is 0.997, which suggests that the effect of a non-uniform steady state density upon the stability limits will be small.

The effect of a non-uniform steady state density upon the first tangential mode stability limits calculated from Eqs. (204) and (205) is shown in Fig. (10). Under the approximations of the zero drag model, it is seen that axial gradients in the mean flow density are destabilizing. For most values of the time-lag the decrease in the threshold of instability amounts to only 0.3 percent. Therefore if the liquid and gas velocities are small, the variation of the steady state density will be neglected in the nonlinear analyses of Chapters VI and VII.

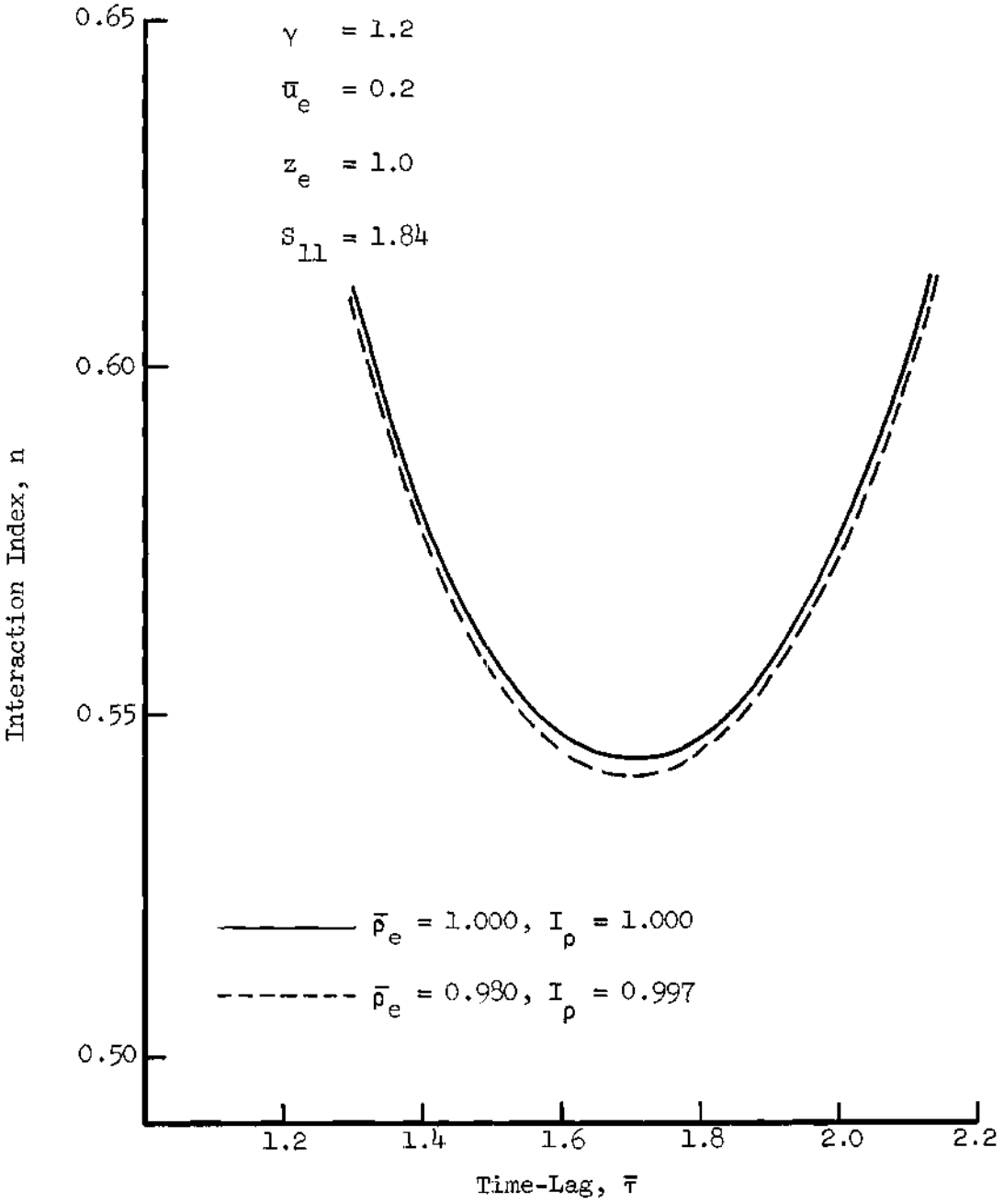

Figure 10. Effect of Non-Uniform Steady State Density Upon the First Tangential Mode Stability Limits.

CHAPTER VI

SECOND ORDER NONLINEAR THEORY

In this chapter the modified form of the Galerkin method will be used to study the effect of nonlinearities on the stability of a liquid-propellant rocket engine in which the distributed combustion process is described by Crocco's time-lag hypothesis. Both transverse and three-dimensional instabilities will be considered for a cylindrical combustor geometry with uniformly distributed injection at one end and a quasi-steady nozzle at the other (see Fig. 2). It has been shown in Chapter III that if, in addition to the assumptions involved in the derivation of the simplified wave equations (i.e. Eqs. (46) through (48)), the mean flow Mach number is small; the unsteady flow in the combustor can be described to second order by a single partial differential equation which contains the important mathematical and physical aspects of the problem. Applying the Galerkin method to this equation yields a set of nonlinear ordinary differential equations that describes the behavior of the amplitudes of the various acoustic modes of the chamber.

These approximate solutions obtained by the numerical integration of the above-mentioned differential equations can be used to determine the nonlinear stability characteristics of the rocket engine. According to linear theory the stability map is divided into stable and unstable regions by the curve of neutral stability. In the stable

domain all small-amplitude disturbances decay to zero, whereas in the unstable region all small-amplitude disturbances grow to infinite amplitudes. The theoretical analysis to be performed in this chapter is concerned with two experimentally observed nonlinear phenomena. In the linearly unstable region small disturbances cannot grow indefinitely but must reach a limiting amplitude; that is, a limit cycle. It is also known that in certain regions of the linearly stable domain sufficiently large disturbances can trigger combustion instability. The approximate solutions will be used to determine the limit cycle amplitudes and the triggering limits as a function of the appropriate system parameters. This information is of value to the rocket designer, who must know under what conditions destructively large pressure amplitudes will develop. Also finite amplitude pressure waveforms, which can be compared with those obtained experimentally, will be calculated.

Analysis

Proceeding with the analysis, the Galerkin orthogonality condition to be satisfied by the residual of Eq. (80) can be written in cylindrical coordinates in the following form:

$$\int_o^{t^*}\left\{\int_o^{z_e}\int_o^{2\pi}\int_o^{1}\left[R_{ac} - 2R_{N_1} - (\gamma-1)R_{N_2} - R_u - R_c\right]\Psi_n r dr d\theta dz \right. \tag{210}$$

$$\left. - \int_o^{2\pi}\int_o^{1}\left[B_o\Psi_n(r,\theta,0,t) + B_e\Psi_n\left(r,\theta,z_e,t\right)\right]r dr d\theta\right\}dt = 0$$

where the various linear and nonlinear components of the residuals are given by:

$$R_{ac} = \tilde{\Phi}_{rr} + \frac{1}{r}\tilde{\Phi}_{r} + \frac{1}{r^2}\tilde{\Phi}_{\theta\theta} + \tilde{\Phi}_{zz} - \tilde{\Phi}_{tt} \tag{211a}$$

$$R_{N_1} = \tilde{\Phi}_{r}\tilde{\Phi}_{rt} + \frac{1}{r^2}\tilde{\Phi}_{\theta}\tilde{\Phi}_{\theta t} + \tilde{\Phi}_{z}\tilde{\Phi}_{zt} \tag{211b}$$

$$R_{N_2} = \left[\tilde{\Phi}_{rr} + \frac{1}{r}\tilde{\Phi}_{r} + \frac{1}{r^2}\tilde{\Phi}_{\theta\theta} + \tilde{\Phi}_{zz}\right]\tilde{\Phi}_{t} \tag{211c}$$

$$R_{u} = 2\bar{u}(z)\tilde{\Phi}_{zt} + \gamma\frac{d\bar{u}}{dz}\tilde{\Phi}_{t} \tag{211d}$$

$$R_{c} = W_{m}'(\tilde{\Phi}) \tag{211e}$$

$$B_{o} = -\left[\tilde{\Phi}_{z} - \bar{u}\tilde{\Phi}_{t} - \tilde{\Phi}_{t}\tilde{\Phi}_{z}\right]_{z=0} \tag{212a}$$

$$B_{e} = \left[Q_{m}' + \tilde{\Phi}_{z} - \bar{u}\tilde{\Phi}_{t} - \tilde{\Phi}_{t}\tilde{\Phi}_{z}\right]_{z=z_e} \tag{212b}$$

In Eqs. (212) B_o is the boundary residual at the injector plate ($z = 0$) and is determined from the boundary term of Eq. (84) by setting the mass source Q_m' equal to zero. This residual is included in Eq. (210) to allow for the possibility that the assumed approximate solutions may not

satisfy the rigid wall boundary condition at the injector. Of course if the assumed solution satisfies this boundary condition the residual B_o vanishes.

In order to obtain approximate solutions to Eq. (210) the mass sources W_m' and Q_m' must be expressed as functions of the velocity potential. Since the investigations carried out in this thesis are confined to rocket engines with a distributed combustion process described by Crocco's time-lag model and having a multi-orifice (quasi-steady) nozzle, Eqs. (109) and (119) which were derived in Chapter IV are applicable. According to the order of magnitude scheme described in Chapter III the nonlinear terms in the expressions for W_m' and Q_m' are of third order and are assumed to be negligible. Likewise the linear term in Eq. (119) which is multiplied by a factor of order $\bar{u}^2$ can be neglected. In Chapter III it was shown that to first order the pressure and density perturbations are related to the velocity potential by the following expressions:

$$p' = -\gamma \Phi_t \quad ; \quad \rho' = -\Phi_t$$

With the knowledge that the resulting error is of third order, these relations are substituted into the remaining second order terms of Eqs. (109) and (119) to obtain the following second order burning rate function and quasi-steady nozzle condition:

$$W_m' = -\gamma n \frac{d\bar{u}}{dz} \left[\Phi_t(r,\theta,z,t) - \Phi_t(r,\theta,z,t-\bar{\tau}) \right] \qquad (213)$$

$$Q'_m = \frac{\gamma+1}{2} \bar{u}_e \Phi_t \tag{214}$$

The above expressions are seen to be identical to Eqs. (159) and (160) of the corresponding linear theory. Thus according to the second order theory the response of the combustion process and the nozzle to pressure oscillations is linear; the only nonlinearities described by this theory are those arising from the gasdynamics of the unsteady flow. A similar situation was encountered by Mitchell[11] who treated the problem of finite amplitude longitudinal mode instability subject to linear boundary conditions corresponding to a concentrated combustion zone at the injector and a quasi-steady nozzle. His results indicate that such nonlinear phenomena as limit cycles, triggering limits, and nonlinear pressure waveforms can be predicted in the absence of a nonlinear driving mechanism.

Expansion of the Velocity Potential

It is now necessary to select a set of "trial" functions Ψ_n in terms of which the approximate solution for the velocity potential will be expanded. Two possibilities will be considered: (1) these functions depend on both space and time, as in the case of linear stability treated in Chapter V (unknown constant method), and (2) the trial functions depend only upon the space coordinates, in which case the coefficients are unknown functions of time rather than constants (unknown function method). It will now be shown that in the study of nonlinear phenomena there are distinct advantages to be obtained by using the unknown function method. In the first place application of

the Galerkin method to an expansion in terms of $\Psi_n(\underline{x},t)$ results in a system of nonlinear algebraic equations, whereas nonlinear ordinary differential equations are obtained when the functions are only spatially dependent. Such a system of nonlinear algebraic equations is usually considerably more difficult to solve numerically than the corresponding differential equations for which standard numerical integration techniques are available. Furthermore if limit cycles and triggering limits are to be determined by the unknown constant method, $\Psi_n(\underline{x},t)$ must be periodic in time with frequency ω_n. This poses a difficulty since the frequency of the nonlinear oscillation depends not only on n and $\bar{\tau}$ but also on the amplitude of the oscillation (i.e. the unknown constants to be determined). By using the unknown function method the frequency is readily obtained from the numerical solutions of the governing differential equations. An additional advantage of the unknown function method is its ability to provide a time history of the various modes and thus enable one to easily distinguish between stable and unstable limit cycles. In view of the above remarks the dependent variable $\tilde{\Phi}$ will be expanded in terms of the spatially dependent functions $\Psi_n(\underline{x})$ which are multiplied by the unknown functions of time.

It is known from experimental observation that, in the absence of discontinuities, finite amplitude combustion instability resembles the acoustic modes that can be excited in a cylindrical cavity which is closed at both ends. Thus the velocity potential will be expanded in terms of products of the acoustic eigenfunctions and time dependent mode-amplitudes as follows:

$$\tilde{\Phi} = \sum_{\ell=0}^{L} \sum_{m=0}^{M} \sum_{n=n_o}^{N} \left[A_{\ell mn}(t) \sin m\theta + B_{\ell mn}(t) \cos m\theta \right] \cos \frac{\ell \pi z}{z_e} J_m\left(S_{mn} r\right) \quad (215)$$

In Eq. (215) S_{mn} is the n^{th} nonzero root of the equation $J_m'(x) = 0$ and $n_o = 0$ only if $m = 0$, otherwise the n-summation begins with $n = 1$. This series is seen to contain all of the acoustic modes as follows: (1) pure axial modes ($m = n = 0$; $\ell = 1, 2, \ldots$), (2) pure radial modes ($m = \ell = 0$; $n = 1, 2, \ldots$), (3) tangential and mixed tangential-radial modes ($\ell = 0$; $m = 1, 2, \ldots$; $n = 1, 2, \ldots$), and (4) mixed longitudinal-transverse modes (ℓ and n are nonzero). The special case $\ell = m = n = 0$ corresponds to a mode in which the pressure is uniform throughout the combustor but varies with time; that is, the low frequency or chugging mode. The inclusion of both azimuthal eigenfunctions with different coefficients admits the possibility of either standing or spinning waves or a combination of both. For example if either $A_{\ell mn}$ or $B_{\ell mn}$ is always zero the oscillation is standing. On the other hand a spinning wave is produced when $A_{\ell mn}(t)$ and $B_{\ell mn}(t)$ are sinusoidal functions of time with equal amplitudes but differing in phase by 90°.

It is a known property of the linear wave equation that the acoustic eigenfunctions used in Eq. (215) form a complete orthogonal set. As pointed out in Chapter II the completeness property is necessary to give reasonable assurance that the approximate solutions approach the exact solutions as the number of modes is increased; however for nonlinear systems convergence cannot be guaranteed. Although not necessary for convergence, the orthogonality property greatly

simplifies the numerical calculations by eliminating the linear coupling between the various modes.

The expansion given by Eq. (215) is seen to satisfy the solid wall boundary conditions at the chamber wall (r = 1) and at the injector face (z = 0). Unfortunately the axial velocity also vanishes at the nozzle entrance, therefore this particular expansion cannot account for energy transfer across the nozzle boundary by means of "pumping" work. Various attempts to modify this expansion to account for axial velocity components at the nozzle entrance resulted in the loss of desirable orthogonality properties or violation of the boundary condition at the injector. In order to avoid these mathematical difficulties specific numerical solutions will be obtained only for pure transverse modes ($\ell = 0$). This is permissible because the axial velocity components are of lesser importance when the nozzle is quasi-steady.

Formation of the Residuals

The expansion given by Eq. (215) is now substituted into Eqs. (211) and (212) to form the various residuals. To simplify the acoustic part R_{ac} of the residual of Eq. (80), the following expression is used:

$$S_{mn}^2 J_m''\left(S_{mn}r\right) + \frac{1}{r} S_{mn} J_m'\left(S_{mn}r\right) - \frac{m^2}{r^2} J_m\left(S_{mn}r\right) = - S_{mn}^2 J_m\left(S_{mn}r\right) \quad (216)$$

which was obtained from Bessel's differential equation. The resulting expressions are shown below:

$$R_{ac} = -\sum_{\ell}\sum_{m}\sum_{n}\left\{\left[\frac{d^2A_{\ell mn}}{dt^2} + \left(S_{mn}^2 + \frac{\ell^2\pi^2}{z_e^2}\right)A_{\ell mn}\right]\sin m\theta \right. \tag{217a}$$

$$\left. + \left[\frac{d^2B_{\ell mn}}{dt^2} + \left(S_{mn}^2 + \frac{\ell^2\pi^2}{z_e^2}\right)B_{\ell mn}\right]\cos m\theta\right\} \cos\frac{\ell\pi z}{z_e} J_m\left(S_{mn}r\right)$$

$$R_{N_1} = \sum_{\ell,m,n}\sum_{\lambda,\mu,\nu}\left\{\left[A_{\ell mn}\frac{dA_{\lambda\mu\nu}}{dt}\sin m\theta\sin\mu\theta + B_{\ell mn}\frac{dB_{\lambda\mu\nu}}{dt}\cos m\theta\cos\mu\theta\right.\right. \tag{217b}$$

$$\left. + A_{\ell mn}\frac{dB_{\lambda\mu\nu}}{dt}\sin m\theta\cos\mu\theta + B_{\ell mn}\frac{dA_{\lambda\mu\nu}}{dt}\cos m\theta\sin\mu\theta\right] \times$$

$$\times S_{mn}S_{\mu\nu}\cos\frac{\ell\pi z}{z_e}\cos\frac{\lambda\pi z}{z_e} J_m'\left(S_{mn}r\right)J_\mu'\left(S_{\mu\nu}r\right)$$

$$+ \left[A_{\ell mn}\frac{dA_{\lambda\mu\nu}}{dt}\cos m\theta\cos\mu\theta + B_{\ell mn}\frac{dB_{\lambda\mu\nu}}{dt}\sin m\theta\sin\mu\theta\right.$$

$$\left. - A_{\ell mn}\frac{dB_{\lambda\mu\nu}}{dt}\cos m\theta\sin\mu\theta - B_{\ell mn}\frac{dA_{\lambda\mu\nu}}{dt}\sin m\theta\cos\mu\theta\right] \times$$

$$\times \frac{m\mu}{r^2}\cos\frac{\ell\pi z}{z_e}\cos\frac{\lambda\pi z}{z_e} J_m\left(S_{mn}r\right)J_\mu\left(S_{\mu\nu}r\right)$$

$$+ \left[A_{\ell mn}\frac{dA_{\lambda\mu\nu}}{dt}\sin m\theta\sin\mu\theta + B_{\ell mn}\frac{dB_{\lambda\mu\nu}}{dt}\cos m\theta\cos\mu\theta\right.$$

$$\left. + A_{\ell mn}\frac{dB_{\lambda\mu\nu}}{dt}\sin m\theta\cos\mu\theta + B_{\ell mn}\frac{dA_{\lambda\mu\nu}}{dt}\cos m\theta\sin\mu\theta\right] \times$$

$$\times\ \ell\lambda\left(\frac{\pi}{z_e}\right)^2 \sin\frac{\ell\pi z}{z_e}\sin\frac{\lambda\pi z}{z_e}\,J_m\left(S_{mn}r\right)J_\mu\left(S_{\mu\nu}r\right)\Big\}$$

$$R_{N_2} = -\sum_{\ell,m,n}\sum_{\lambda,\mu,\nu}\Big[A_{\ell mn}\frac{dA_{\lambda\mu\nu}}{dt}\sin m\theta\sin\mu\theta + B_{\ell mn}\frac{dB_{\lambda\mu\nu}}{dt}\cos m\theta\cos\mu\theta \quad (217c)$$

$$+ A_{\ell mn}\frac{dB_{\lambda\mu\nu}}{dt}\sin m\theta\cos\mu\theta + B_{\ell mn}\frac{dA_{\lambda\mu\nu}}{dt}\cos m\theta\sin\mu\theta\Big]\times$$

$$\times\left[S_{mn}^2 + \frac{\ell^2\pi^2}{z_e^2}\right]\cos\frac{\ell\pi z}{z_e}\cos\frac{\lambda\pi z}{z_e}\,J_m\left(S_{mn}r\right)J_\mu\left(S_{\mu\nu}r\right)$$

$$R_u = \sum_\ell\sum_m\sum_n\left[\gamma\frac{d\bar{u}}{dz}\cos\frac{\ell\pi z}{z_e} - \frac{2\ell\pi\bar{u}}{z_e}\sin\frac{\ell\pi z}{z_e}\right]\times \quad (217d)$$

$$\times\left[\frac{dA_{\ell mn}}{dt}\sin m\theta + \frac{dB_{\ell mn}}{dt}\cos m\theta\right]J_m\left(S_{mn}r\right)$$

$$R_c = -\gamma n\frac{d\bar{u}}{dz}\sum_\ell\sum_m\sum_n\Big\{\Big[\frac{dA_{\ell mn}}{dt} - \frac{dA_{\ell mn}}{dt}(t-\bar{\tau})\Big]\sin m\theta \quad (217e)$$

$$+\left[\frac{dB_{\ell mn}}{dt} - \frac{dB_{\ell mn}}{dt}(t-\bar{\tau})\right]\cos m\theta\Big\}\cos\frac{\ell\pi z}{z_e}\,J_m\left(S_{mn}r\right)$$

$$B_o = 0 \quad (218a)$$

$$B_e = \frac{\gamma-1}{2}\bar{u}_e\sum_\ell\sum_m\sum_n\left[\frac{dA_{\ell mn}}{dt}\sin m\theta + \frac{dB_{\ell mn}}{dt}\cos m\theta\right](-1)^\ell J_m\left(S_{mn}r\right) \quad (218b)$$

Since the axial component of the velocity perturbation (i.e. Φ_z) is zero at both ends of the combustor, the residual at the injector B_o and the nonlinear part of the nozzle residual B_e both vanish.

Differential Equations Governing the Mode-Amplitudes

The residuals given by Eqs. (217) and (218) are introduced into the Galerkin orthogonality condition and the volume integrals are evaluated for each of the weighting functions given by

$$\Psi_{A_{hjk}} = \cos \frac{h\pi z}{z_e} \sin j\theta J_j\left(S_{jk} r\right) \tag{219}$$

$$\Psi_{B_{hjk}} = \cos \frac{h\pi z}{z_e} \cos j\theta J_j\left(S_{jk} r\right)$$

Since the unknown mode-amplitudes are functions of time, the time integration occurring in Eq. (210) is not performed. The resulting system of nonlinear ordinary differential equations that controls the behavior of the mode-amplitudes can be written in the following general form:

$$\frac{d^2 A_{hjk}}{dt^2} + \left(S_{jk}^2 + \frac{h^2\pi^2}{z_e^2}\right) A_{hjk} + \sum_{\ell}\left\{K(\ell,h) \frac{dA_{\ell jk}}{dt} + K_\tau(\ell,h) \frac{dA_{\ell jk}}{dt}(t-\tau)\right\} \tag{220}$$

$$+ \sum_{\ell,m,n} \sum_{\lambda,\mu,\nu} \left\{C_1(\ell,m,n;\ \lambda,\mu,\nu;\ h,j,k) A_{\ell mn} \frac{dB_{\lambda\mu\nu}}{dt}\right.$$

$$\left. + C_2(\ell,m,n;\ \lambda,\mu,\nu;\ h,j,k) B_{\ell mn} \frac{dA_{\lambda\mu\nu}}{dt}\right\} = 0$$

$$\frac{d^2B_{hjk}}{dt^2} + \left(S_{jk}^2 + \frac{h^2\pi^2}{z_e^2}\right)B_{hjk} + \sum_{\ell}\left\{K(\ell,h)\ \frac{dB_{\ell jk}}{dt} + K_{\tau}(\ell,h)\ \frac{dB_{\ell jk}}{dt}\ (t-\tau)\right\} \quad (221)$$

$$+ \sum_{\ell,m,n}\ \sum_{\lambda,\mu,\nu}\left\{C_3(\ell,m,n;\ \lambda,\mu,\nu;\ h,j,k)A_{\ell mn}\ \frac{dA_{\lambda\mu\nu}}{dt}\right.$$

$$\left. + C_4(\ell,m,n;\ \lambda,\mu,\nu;\ h,j,k)B_{\ell mn}\ \frac{dB_{\lambda\mu\nu}}{dt}\right\} = 0$$

where Eqs. (220) were obtained with the aid of the weighting functions $\Psi_{A_{hjk}}$ and Eqs. (221) were derived by using $\Psi_{B_{hjk}}$.

Each of these differential equations consists of three parts: (1) the acoustic part which describes a harmonic oscillator with natural frequency $\omega_{hjk} = \left(S_{jk}^2 + \frac{h^2\pi^2}{z_e^2}\right)^{1/2}$, (2) the terms involving the first derivatives of the mode-amplitudes which represent the combined damping or amplifying effect of the steady state flow, the nozzle, and the combustion process, and (3) the nonlinear coupling terms which are responsible for the energy transfer between modes. Due to the orthogonality property of the acoustic eigenfunctions, only one mode is involved in the acoustic part of a given equation. This mode corresponds to the weighting function used to derive that particular equation. Thus it may be inferred that each of Eqs. (220) and (221) governs the behavior of a single mode in the expansion for Φ; the coupling between modes in the damping and nonlinear terms serves to modify the harmonic oscillation described by the acoustic terms.

The coefficients of the first derivatives depend on various

weighted integrals of the steady state velocity distribution and are expressed as follows:

$$K(\ell,h) = \left\{\frac{\gamma-1}{2}\,\bar{u}_e(-1)^{\ell+h} + \gamma(1-n)\int_o^{z_e}\frac{d\bar{u}}{dz}\cos\frac{\ell\pi z}{z_e}\cos\frac{h\pi z}{z_e}\,dz \right. \quad (222)$$

$$\left. - \frac{2\ell\pi}{z_e}\int_o^{z_e}\bar{u}(z)\sin\frac{\ell\pi z}{z_e}\cos\frac{h\pi z}{z_e}\,dz\right\}\left[\int_o^{z_e}\cos^2\frac{h\pi z}{z_e}\,dz\right]^{-1}$$

$$K_\tau(\ell,h) = \left\{\gamma n\int_o^{z_e}\frac{d\bar{u}}{dz}\cos\frac{\ell\pi z}{z_e}\cos\frac{h\pi z}{z_e}\,dz\right\}\left[\int_o^{z_e}\cos^2\frac{h\pi z}{z_e}\,dz\right]^{-1}$$

The detailed derivation of these coefficients is presented in Appendix A. It is seen that these coefficients depend only upon the longitudinal mode numbers ℓ and h; they are the same for all pure transverse modes. If all of the modes contained in the assumed series expansion have the same longitudinal mode number, the ℓ-summation reduces to one term and the linear coupling between modes disappears.

Expressions for the coefficients of the nonlinear terms occurring in Eqs. (220) and (221) are derived in Appendix A. These coefficients are found to be independent of the operating parameters (i.e. n and $\bar{\tau}$) and are functions of the various integrals which result from applying the Galerkin method. These integrals, which involve products of three trigonometric or Bessel functions with different arguments, are evaluated in Appendix B. From Eqs. (220) and (221) it would appear that the number of nonlinear coupling terms could become quite large for expan-

sions containing only a moderate number of terms. For example, if the series contained ten terms (five A's and five B's) each of the ten differential equations would contain 50 nonlinear terms making a total of 500 terms. Fortunately, however, the great majority of the nonlinear coefficients are zero which reduces the number of nonlinear coupling terms considerably.

Differential Equations For Transverse Modes

For reasons to be given below, the remaining chapters of this thesis will be devoted to the study of the nonlinear behavior of purely transverse mode instability in liquid propellant rocket motors. To date the case of finite amplitude longitudinal instability has been adequately treated by Sirignano[10] and Mitchell[11], while relatively little has been accomplished in the field of nonlinear transverse instability. In addition the investigation of longitudinal or combined longitudinal-transverse modes with the aid of the Galerkin method and the eigenfunction expansion given by Eq. (215) is fraught with difficulties. It is a well known fact that finite amplitude waves involving longitudinal modes frequently develop into shock waves (see Mitchell[11]). To treat shock wave instability would require extensive modification of the Galerkin method or the series expansion. On the other hand the analysis of Maslen and Moore[8] and experimental observation[2] indicate that shock-free transverse oscillations can exist in cylindrical rocket combustion chambers. Finally it has been previously mentioned that according to Eq. (215) there is no axial velocity perturbation at the nozzle entrance, which is admittedly a poor approximation for longitudinal or mixed modes. Since the resolution of these difficulties is beyond the scope

of this investigation, only purely transverse instability will be considered in this work.

The differential equations which control the behavior of the transverse modes are obtained from Eqs. (220) and (221) by setting $\ell = \lambda = h = 0$. In writing these equations the superfluous longitudinal mode numbers are omitted from the subscripts of the mode-amplitudes. The resulting equations, which are no longer coupled in the linear terms, are given by:

$$\frac{d^2A_{jk}}{dt^2} + S_{jk}^2 A_{jk} + K\frac{dA_{jk}}{dt} + K_\tau \frac{dA_{jk}}{dt}(t-\tau) \tag{223}$$

$$+ \sum_{m,n}\sum_{\mu,\nu}\left\{C_1(m,n;\,\mu,\nu;\,j,k)A_{mn}\frac{dB_{\mu\nu}}{dt} + C_2(m,n;\,\mu,\nu;\,j,k)B_{mn}\frac{dA_{\mu\nu}}{dt}\right\} = 0$$

$$\frac{d^2B_{jk}}{dt^2} + S_{jk}^2 B_{jk} + K\frac{dB_{jk}}{dt} + K_\tau \frac{dB_{jk}}{dt}(t-\tau) \tag{224}$$

$$+ \sum_{m,n}\sum_{\mu,\nu}\left\{C_3(m,n;\,\mu,\nu;\,j,k)A_{mn}\frac{dA_{\mu\nu}}{dt} + C_4(m,n;\,\mu,\nu;\,j,k)B_{mn}\frac{dB_{\mu\nu}}{dt}\right\} = 0$$

where the summation over μ and ν covers the same range of indices as the summation over m and n corresponding to the modes included in the series expansion for the velocity potential. The coefficients K and K_τ are the same for all modes and are given by:

$$K = \frac{\gamma \bar{u}_e}{z_e}\left[1 + \frac{\gamma-1}{2\gamma} - n\right] \tag{225}$$

$$K_\tau = \frac{\gamma n \bar{u}_e}{z_e}$$

which were acquired from Eqs. (222) by introducing $\ell = h = 0$ and using the results of Appendix B that $Ui_{cc}(0, 0) = \bar{u}_e$ and $Ui_{sc}(0, 0) = 0$. These coefficients are seen to depend on the value of the steady state velocity at the nozzle entrance (i.e. $\bar{u}_e$) but not upon the actual velocity distribution $\bar{u}(z)$. For this reason it is not necessary to calculate $\bar{u}(z)$, a fact that saves considerable computation time.

The coefficients of the nonlinear terms occurring in Eqs. (223) and (224) are obtained by substituting $\ell = \lambda = h = 0$ into Eqs. (A11), (A12), (A14) and (A15) and using the expressions $Zi_c(0, 0, 0) = z_e$ and $Zi_s(0, 0, 0) = 0$ which are shown in Appendix B. It is found that the effect of the length z_e cancels and the coefficients of the nonlinear terms are given by:

$$C_1(m,n;\ \mu,\nu;\ j,k) = \frac{1}{\pi}\frac{2S_{jk}^2}{\left[S_{jk}^2 - j^2\right]J_j^2(S_{jk})} \times \tag{226a}$$

$$\times \left\{2\left[S_{mn}S_{\mu\nu}I_{css}(\mu,m,j)Ji_3(m,n;\ \mu,\nu;\ j,k) - \right.\right.$$

$$\left.\left. - m\mu I_{css}(m,\mu,j)Ji_2(m,n;\ \mu,\nu;\ j,k)\right] \right. -$$

$$- (\gamma-1) S_{mn}^2 I_{css}(\mu,m,j)\, Ji_1(m,n;\ \mu,\nu;\ j,k)\Big\}$$

$$C_2(m,n;\ \mu,\nu;\ j,k) = \frac{1}{\pi}\frac{2S_{jk}^2}{\left[S_{jk}^2 - j^2\right]J_j^2(S_{jk})} \times \qquad (226b)$$

$$\times \Big\{2\Big[S_{mn}S_{\mu\nu} I_{css}(m,\mu,j)\, Ji_3(m,n;\ \mu,\nu;\ j,k) -$$

$$- m\mu I_{css}(\mu,m,j)\, Ji_2(m,n;\ \mu,\nu;\ j,k)\Big] -$$

$$- (\gamma-1) S_{mn}^2 I_{css}(m,\mu,j)\, Ji_1(m,n;\ \mu,\nu;\ j,k)\Big\}$$

$$C_3(m,n;\ \mu,\nu;\ j,k) = \frac{1}{N_j\pi}\frac{2S_{jk}^2}{\left[S_{jk}^2 - j^2\right]J_j^2(S_{jk})} \times \qquad (226c)$$

$$\times \Big\{2\Big[S_{mn}S_{\mu\nu} I_{css}(j,m,\mu)\, Ji_3(m,n;\ \mu,\nu;\ j,k) +$$

$$+ m\mu I_{ccc}(m,\mu,j)\, Ji_2(m,n;\ \mu,\nu;\ j,k)\Big] -$$

$$- (\gamma-1) S_{mn}^2 I_{css}(j,m,\mu)\, Ji_1(m,n;\ \mu,\nu;\ j,k)\Big\}$$

$$C_4(m,n;\ \mu,\nu;\ j,k) = \frac{1}{N_j\pi}\frac{2S_{jk}^2}{\left[S_{jk}^2 - j^2\right]J_j^2(S_{jk})} \times \qquad (226d)$$

$$\times \Big\{2\Big[S_{mn}S_{\mu\nu} I_{ccc}(m,\mu,j)\, Ji_3(m,n;\ \mu,\nu;\ j,k) +$$

$$+ m\mu I_{css}(j,m,\mu)\,Ji_2(m,n;\ \mu,\nu;\ j,k)\Big] -$$

$$- (\gamma-1)S_{mn}^2 I_{ccc}(m,\mu,j)\,Ji_1(m,n;\ \mu,\nu;\ j,k)\Big\}$$

The number N_j occurring in the above expressions is defined as follows:

$$N_j = 1 \qquad \text{for } j \text{ nonzero}$$

$$N_j = 2 \qquad \text{for } j = 0$$

According to Eqs. (226) the coefficients of the nonlinear terms depend only on the integrals of trigonometric and Bessel functions which are defined in Appendix B; these coefficients do not depend upon either the combustion parameters (i.e. n and $\bar{\tau}$) or the steady state flow or combustor length. This result is a direct consequence of the fact that in the derivation of the partial differential equation describing the behavior of the velocity potential all nonlinear terms involving the steady state velocity (including those arising from the combustion process) were neglected as being of higher order. This property of the coefficients of the nonlinear terms saves considerable computer time since it is not necessary to compute new values of these coefficients each time a change is made in the system parameters.

Before proceeding with a discussion of the differential equations given by Eqs. (223) and (224) it should be stressed that care must be exercised in the application of these equations if radial modes are

included in the expansion of the velocity potential. Serious error can be avoided by observing that although both mode-amplitudes $A_{jk}(t)$ and $B_{jk}(t)$ are used to completely describe a tangential mode ($j \neq 0$) only one mode-amplitude $B_{ok}(t)$ is needed to describe a radial mode ($j = 0$). There is no corresponding function $A_{ok}(t)$ because such a function would be multiplied by $\sin j\theta$ which vanishes for $j = 0$. Thus $j = 0$ is not used in Eqs. (223) and although terms of the form $A_{on}dB_{\mu\nu}/dt$ and $A_{mn}dA_{o\nu}/dt$ are indicated by the summations in the nonlinear parts of Eqs. (223) and (224) such terms are omitted.

Linear Behavior. The small amplitude behavior of the mode-amplitudes is easily investigated by dropping the nonlinear terms in Eqs. (223) and (224). The resulting linear equations are no longer coupled; that is, each equation describes the behavior of only one mode and can be solved independently of the remaining equations. Each of these equations is of the following form:

$$\frac{d^2B_{jk}}{dt^2} + S_{jk}^2 B_{jk} + K\frac{dB_{jk}}{dt} + K_\tau \frac{dB_{jk}}{dt}(t-\bar{\tau}) = 0 \qquad (227)$$

which, except for the additional term involving a time delay, is analogous to the differential equation governing the motion of a mass-spring-dashpot system. The first two terms in Eqs. (227) describe an undamped oscillator with natural frequency S_{jk}; the remaining terms determine whether the oscillations will grow or decay.

Tracing the origin of the various terms that appear in the

expressions for the coefficients K and K_τ it can be shown that they are all related to the steady state flow (first term in K), the nozzle boundary condition (second term), and the unsteady combustion process (last term). From a physical point of view the nozzle and the mean flow (by means of convection) are expected to act as energy sinks with regard to the wave motion, while the combustion process should act as an energy source. That this is indeed the case can be shown by examining the expression for K, which can be considered to be an "effective resistance" or "damping coefficient". Here the term that resulted from the presence of an unsteady combustion process (i.e. the last term) and the terms that resulted from the mean flow and the nozzle boundary condition have opposite signs.

The linear stability characteristics of the system are not determined solely by the value of K, because the retarded term contributes an additional damping or amplifying effect. This fact is easily shown by rearranging Eq. (227) in the following form:

$$\frac{d^2B_{jk}}{dt^2} + S_{jk}^2 B_{jk} + K' \frac{dB_{jk}}{dt} + K_\tau \left[\frac{dB_{jk}}{dt}(t-\bar{\tau}) - \frac{dB_{jk}}{dt} \right] = 0 \qquad (228)$$

where

$$K' = \frac{\gamma \bar{u}_e}{z_e} \left[1 + \frac{\gamma - 1}{2\gamma} \right]$$

and K_τ is given in Eqs. (225). In Eq. (228) the effect of the mean flow and the nozzle have been separated from that of the combustion process.

The coefficient K' is always positive, thus it is seen that the mean flow and the nozzle are always stabilizing. It is also observed that for values of γ which are usually assumed for the hot combustion chamber gases the second term in K' is an order of magnitude smaller than the first term which implies that the quasi-steady nozzle has a relatively minor influence upon the stability of transverse mode oscillations.

Since it involves a time delay, the combustion term is more complicated than the terms arising from the steady state flow and the nozzle. Depending upon the relation between the time-lag and the period of oscillation the effect of the combustion process can be either damping or amplification of the waves. In order to obtain a better understanding of the effect of the combustion process, consider the case of neutrally stable oscillations for which the time-lag is one half of the period of oscillation. Under these conditions $B_{jk}(t)$ will be a sinusoidal function of time and the following relation is valid:

$$\frac{dB_{jk}}{dt}(t-\bar{\tau}) = -\frac{dB_{jk}}{dt}(t) \tag{229}$$

Substituting Eq. (229) into Eq. (228) reveals that the contribution of the combustion process is described by the term $-2K_{\tau}\frac{dB_{jk}}{dt}$ which is seen to be destabilizing. The combined effects of the mean flow, nozzle, and the combustion process is then described by the total damping coefficient K_d which is given by:

$$K_d = \frac{\gamma \bar{u}_e}{z_e}\left[1 + \frac{\gamma-1}{2\gamma} - 2n\right] \tag{230}$$

For neutral stability the total damping coefficient must vanish implying that

$$n_o = \frac{1}{2}\left(1 + \frac{\gamma-1}{2\gamma}\right)$$

which is the minimum interaction index for neutral stability as determined in Chapter V (see Eq. (170)). The oscillations are neutrally stable for this particular choice of n and $\bar{\tau}$ because the energy contributed to the pressure oscillations by the combustion process is equal to the energy extracted by the steady state flow and the nozzle. Assuming that Eq. (229) still holds when the oscillations are no longer neutrally stable, Eq. (230) indicates that if $n > n_o$ the damping coefficient K_d is negative and the oscillations are amplified; that is, more energy is provided by the combustion process than is necessary to sustain neutral oscillations. On the other hand if $n < n_o$ positive damping results, the energy input is insufficient to maintain the oscillations, and the pressure disturbances decay. In reality for $n \neq n_o$ the solutions for $B_{jk}(t)$ are not strictly periodic and Eq. (229) is only an approximation. However this effect is not sufficiently strong to change the qualitative behavior as outlined above.

When the time-lag $\bar{\tau}$ is equal to half of the period of oscillation, the engine is said to be resonant, for the frequency of the

combustion oscillations is equal to the frequency of the corresponding natural acoustic mode that can be excited in the given combustor geometry. For other values of the time-lag the engine is off-resonant, the frequency of the pressure oscillations differs from the acoustic frequency, and Eq. (229) is no longer true. Assuming neutral stability it is readily seen that if $\bar{\tau}$ is greater or less than the half-period the ability of the combustion process to amplify the oscillations is less than at resonant conditions. For off-resonant values of $\bar{\tau}$, therefore, a larger value of the interaction index is necessary to balance the damping terms and give neutral stability. For sufficiently large departures from resonant conditions the combustion process will not contribute a sufficient amount of energy to the wave motion and the engine will be stable for all values of the interaction index. It is thus seen that the off-resonant conditions are more stable in complete agreement with the results of Chapter V.

The linear stability limits which were determined in Chapter V are easily derived from the differential equations given by Eq. (227) to provide a check on the analysis. Since periodic solutions are being sought the mode-amplitude $B_{jk}(t)$ is assumed to be given by:

$$B_{jk}(t) = a_o e^{i\omega t}$$

which is substituted into the linearized differential equation. The resulting expression is identical to Eq. (165) of Chapter V, and the condition that a_o is nonzero yields Eqs. (168) and (169). Thus the

linear behavior of the mode-amplitudes agrees with the results of Chapter V.

Nonlinear Behavior. Each of the nonlinear terms occurring in Eqs. (223) and (224) consists of the product of a mode-amplitude and the time derivative of the same or a different mode-amplitude. In order to more easily discuss the influence of these terms some definitions must be made. Let the mode whose behavior is described by the differential equation under consideration (the mode occurring in the linear terms) be called the major mode. All other modes present in the nonlinear terms of this equation will be referred to as minor modes; they serve to modify the behavior of the major mode. It should be emphasized that the major mode is not the dominant mode of the assumed series expansion, but is the mode whose behavior is controlled by the given differential equation. In applying these definitions it should be noted that $A_{jk}(t)$ and $B_{jk}(t)$ refer to the same mode.

According to the above definitions one can distinguish between three types of nonlinear coupling terms present in Eqs. (223) and (224): (1) the product of a major mode and its derivative (self-coupling), (2) products of major and minor modes (cross-coupling), and (3) the products of minor modes (minor mode coupling). Examples of these terms are given below for the equations governing $A_{11}(t)$ and $B_{11}(t)$:

Self-coupling: $$A_{11}\frac{dA_{11}}{dt}\ ,\quad B_{11}\frac{dB_{11}}{dt}\ ,\quad A_{11}\frac{dB_{11}}{dt}$$

Cross-coupling: $A_{11}\frac{dA_{21}}{dt}$, $B_{11}\frac{dB_{21}}{dt}$

Minor mode coupling: $A_{21}\frac{dA_{21}}{dt}$, $A_{21}\frac{dA_{31}}{dt}$

From the definition of major modes it is seen that the term $A_{11}\frac{dA_{11}}{dt}$ represents self-coupling only in the equations describing $A_{11}(t)$ and $B_{11}(t)$ and is minor mode coupling in all of the other equations.

Due to the nature of the coefficients of these nonlinear terms (see Eqs. (226)) all three types of nonlinear coupling terms do not appear in any given equation. Suppose that the series expansion for the velocity potential does not contain radial modes (i.e. m, μ, and j are nonzero). From the properties of the azimuthal integrals I_{ccc} and I_{css} (see Appendix B) the coefficients of the nonlinear terms vanish unless one of the indices m, μ, or j is the sum of the other two. For example consider a truncated series which includes only the first and second tangential modes. In the equations describing the first tangential mode (i.e. the major mode) the following nonlinear terms occur:

$$A_{11}\frac{dB_{21}}{dt} \quad , \quad B_{11}\frac{dA_{21}}{dt} \quad , \quad A_{11}\frac{dA_{21}}{dt} \quad , \quad B_{11}\frac{dB_{21}}{dt} \qquad (m + j \approx \mu)$$

$$A_{21}\frac{dB_{11}}{dt} \quad , \quad B_{21}\frac{dA_{11}}{dt} \quad , \quad A_{21}\frac{dA_{11}}{dt} \quad , \quad B_{21}\frac{dB_{11}}{dt} \qquad (\mu + j \approx m)$$

which are all seen to be cross-coupling terms. In the equations govern-

ing the second tangential mode the only nonlinear terms are of the form $A_{11} \frac{dA_{11}}{dt}$ (corresponding to $m + \mu = j$) which is minor mode coupling since the second tangential mode is the major mode in these equations. More generally it is found that if the series expansion for Φ contains only tangential and combined tangential-radial modes ($m = 1, 2, 3, \ldots$; $n = 1, 2, 3, \ldots$) only cross-coupling and minor mode coupling terms occur in the differential equations resulting from application of the Galerkin method. Since no self-coupling terms appear it is obvious that if the series expansion for Φ consists of only a single mode ($m \neq 0$) the resulting differential equation will contain no nonlinear terms. Thus it is impossible to describe the nonlinear behavior of a tangential mode from the equations of the second order theory by means of the Galerkin method and a one-mode series. At least two modes are necessary because the second order nonlinear mechanism appears to be the interaction between different transverse modes whereby energy is transferred from one mode to another.

When radial modes ($m = 0$) are included in the series expansion of Φ the results described above must be modified. Self-coupling terms appear in the equations which describe the behavior of $B_{ok}(t)$ because the azimuthal integral $I_{ccc}(0, 0, 0)$ is nonzero. If the expansion of Φ consists of only a single radial mode application of the Galerkin method yields a nonlinear equation which contains the self-coupling term $B_{ok} \frac{dB_{ok}}{dt}$. Thus it is possible to study the nonlinear behavior of radial modes with the aid of a one-mode series.

On the basis of the preceding discussion it is expected that the nonlinear behavior of a single radial mode will be qualitatively differ-

ent from that of a transverse mode (using a multi-mode expansion). For this reason both types of expansion will be investigated in this thesis. From the results of the numerical calculations it will be shown that the self-coupling terms are necessary to obtain unstable limit cycles; that is, triggering limits.

Calculation of the Pressure Perturbation. Solution of the system of nonlinear differential equations given by Eqs. (223) and (224) yields the time dependence of the unknown mode-amplitude functions, which are combined according to the assumed series expansion to obtain the velocity potential. However the mode-amplitudes and the velocity potential are of little physical interest and are not directly measurable. The pressure perturbation, on the other hand, is easily measured by means of pressure transducers, consequently it is the quantity of greatest interest to engineers engaged in the design and testing of stable rocket motors. Therefore the solutions of Eqs. (223) and (224) will be used primarily to compute the time and space dependence of the pressure perturbation.

The pressure perturbation is related to the time and space derivatives of the velocity potential by the second order momentum equation (see Eq. (74) of Chapter III). Restricting attention to two-dimensional oscillations (i.e. $\Phi_z \approx 0$) and introducing a cylindrical coordinate system Eq. (74) becomes:

$$p'(r,\theta,t) = -\gamma\left[\Phi_t + \frac{1}{2}\left(\Phi_r^2 + \frac{1}{r^2}\Phi_\theta^2 - \Phi_t^2\right)\right] \qquad (231)$$

The derivatives of the velocity potential are obtained by differentiating the assumed series expansion to obtain:

$$\Phi_t = \sum_{m=0}^{M} \sum_{n=1}^{N} \left[\frac{dA_{mn}}{dt} \sin m\theta + \frac{dB_{mn}}{dt} \cos m\theta\right] J_m\left(S_{mn} r\right) \tag{232}$$

$$\Phi_r = \sum_{m=0}^{M} \sum_{n=1}^{N} S_{mn} \left[A_{mn}(t) \sin m\theta + B_{mn}(t) \cos m\theta\right] J_m'\left(S_{mn} r\right) \tag{233}$$

$$\Phi_\theta = \sum_{m=1}^{M} \sum_{n=1}^{N} m \left[A_{mn}(t) \cos m\theta - B_{mn}(t) \sin m\theta\right] J_m\left(S_{mn} r\right) \tag{234}$$

It is thus seen that the pressure perturbation is a function of both the mode-amplitudes and their derivatives.

The calculation of the pressure perturbation for most locations within the combustor is straightforward, however the behavior of the pressure at points along the combustor's axis (r = 0) must receive special consideration. At these points Φ_θ vanishes and the term Φ_θ^2/r^2 which appears in Eq. (231) becomes indeterminate. The limit of this term as r approaches zero can be found by introducing Eq. (234) and applying L'Hospital's Rule as follows:

$$L = \left\{ \sum_{m=1}^{M} \sum_{n=1}^{N} m \left[A_{mn} \cos m\theta - B_{mn} \sin m\theta\right] \left[\lim_{r \to 0} \frac{J_m(S_{mn} r)}{r}\right] \right\}^2$$

where $$\lim_{r\to 0} \frac{J_m(S_{mn}r)}{r} = S_{mn}J'_m(0)$$

Using the results $J'_m(0) = 0$ for $m \neq 1$ and $J'_1(0) = 1/2$ the desired limit can be expressed in the following form:

$$\lim_{r\to 0} \Phi_\theta^2/r^2 = \left\{ \sum_{n=1}^{N} \left[A_{1n}\cos\theta - B_{1n}\sin\theta \right] \frac{S_{1n}}{2} \right\}^2 \qquad (235)$$

It would appear from Eq. (235) that the pressure perturbation along the axis of the chamber would exhibit a multiplicity of values depending upon which value of θ was chosen. It can be shown, however, that when Eq. (235) is combined with the other terms in Eq. (231) the resulting expression for the pressure perturbation is independent of θ and thus single-valued.

Truncated Series Expansions

One of the major advantages of the Galerkin method is the fact that in most applications the majority of the desired information can be obtained by using a truncated series expansion that contains two or three terms. In these cases the solution for the first term describes the most important physical aspects of the problem while the solutions for the other terms present in the series expansion provide additional minor corrections.

Series Containing the First Tangential Mode. Available experimental data (e.g. see Ref. 2) indicates that in the majority of cases

unstable oscillations inside liquid-propellant rocket motors have a frequency and space dependence close to that of the first tangential mode. Instabilities that behave like the second tangential or first radial modes have also been observed on occasion. Based on this information a truncated three-mode series expansion is used to describe the unknown velocity potential. This series contains the lowest frequency pure transverse modes (i.e. n = 1) which are the first tangential (1T; m = 1, $S_{11} = 1.84118$), the second tangential (2T; m = 2, $S_{21} = 3.05424$), and the first radial (1R; m = 0, $S_{01} = 3.83171$) modes. Accordingly $\tilde{\Phi}$ can be expressed in the following form:

$$\tilde{\Phi} = B_{01}(t) J_0\left(S_{01} r\right) + \left[A_{11}(t) \sin\theta + B_{11}(t) \cos\theta\right] J_1\left(S_{11} r\right) \qquad (236)$$

$$+ \left[A_{21}(t) \sin 2\theta + B_{21}(t) \cos 2\theta\right] J_2\left(S_{21} r\right)$$

which involves five unknown mode-amplitude functions.

A system of five differential equations which controls the behavior of the mode-amplitudes is readily obtained from Eqs. (223) and (224) by letting j = 0, 1, 2; k = 1 and omitting the equation describing the non-existent function $A_{01}(t)$. In the nonlinear terms, of course, all terms involving A_{01} are disregarded. Proceeding in this manner yields the following nonlinear system of equations:

$$\frac{d^2 B_{01}}{dt^2} + S_{01}^2 B_{01} + K \frac{dB_{01}}{dt} + K_\tau \frac{dB_{01}}{dt}(t-\bar{\tau}) + C_1 B_{01} \frac{dB_{01}}{dt} \qquad (237a)$$

$$+ C_2\left(A_{11}\frac{dA_{11}}{dt} + B_{11}\frac{dB_{11}}{dt}\right) + C_3\left(A_{21}\frac{dA_{21}}{dt} + B_{21}\frac{dB_{21}}{dt}\right) = 0$$

$$\frac{d^2A_{11}}{dt^2} + S_{11}^2A_{11} + K\frac{dA_{11}}{dt} + K_\tau\frac{dA_{11}}{dt}(t-\bar{\tau}) + C_4B_{01}\frac{dA_{11}}{dt} + C_5A_{11}\frac{dB_{01}}{dt} \quad (237b)$$

$$+ C_6\left(B_{11}\frac{dA_{21}}{dt} - A_{11}\frac{dB_{21}}{dt}\right) + C_7\left(A_{21}\frac{dB_{11}}{dt} - B_{21}\frac{dA_{11}}{dt}\right) = 0$$

$$\frac{d^2B_{11}}{dt^2} + S_{11}^2B_{11} + K\frac{dB_{11}}{dt} + K_\tau\frac{dB_{11}}{dt}(t-\bar{\tau}) + C_4B_{01}\frac{dB_{11}}{dt} + C_5B_{11}\frac{dB_{01}}{dt} \quad (237c)$$

$$+ C_6\left(A_{11}\frac{dA_{21}}{dt} + B_{11}\frac{dB_{21}}{dt}\right) + C_7\left(A_{21}\frac{dA_{11}}{dt} + B_{21}\frac{dB_{11}}{dt}\right) = 0$$

$$\frac{d^2A_{21}}{dt^2} + S_{21}^2A_{21} + K\frac{dA_{21}}{dt} + K_\tau\frac{dA_{21}}{dt}(t-\bar{\tau}) \quad (237d)$$

$$+ C_8B_{01}\frac{dA_{21}}{dt} + C_9A_{21}\frac{dB_{01}}{dt} - C_{10}\left(A_{11}\frac{dB_{11}}{dt} + B_{11}\frac{dA_{11}}{dt}\right) = 0$$

$$\frac{d^2B_{21}}{dt^2} + S_{21}^2B_{21} + K\frac{dB_{21}}{dt} + K_\tau\frac{dB_{21}}{dt}(t-\bar{\tau}) \quad (237e)$$

$$+ C_8B_{01}\frac{dB_{21}}{dt} + C_9B_{21}\frac{dB_{01}}{dt} + C_{10}\left(A_{11}\frac{dA_{11}}{dt} - B_{11}\frac{dB_{11}}{dt}\right) = 0$$

where the coefficients K and K_τ are given by Eqs. (225). Out of the 63

nonlinear coefficients computed from Eqs. (226) only 25 are nonzero; many of these occur in pairs which are equal or differ only in sign and can be combined to yield the coefficients C_1, C_2, ... C_{10} which appear in Eqs. (237). These coefficients are all of order unity and their values are given below:

$$\begin{aligned} C_1 &= 4.1373 & C_6 &= 1.7187 \\ C_2 &= 1.0423 & C_7 &= 1.4828 \\ C_3 &= -0.2084 & C_8 &= -2.7850 \\ C_4 &= -1.9394 & C_9 &= -3.0388 \\ C_5 &= -2.3123 & C_{10} &= 1.1318 \end{aligned} \tag{238}$$

As can be seen from Eqs. (237) self-coupling terms occur only in the equation which governs the first radial mode, while the nonlinear behavior of the first tangential mode is controlled by cross-coupling with both the 1R and 2T modes. The equations describing the 2T mode contain both cross-coupling terms with the 1R mode and minor mode coupling involving only the 1T mode. Due to the nature of these nonlinear coupling terms it is possible to ascertain much qualitative information concerning the nonlinear behavior of the mode-amplitudes by analysis of the differential equations without obtaining a numerical solution. Analyses of this type will also be used to interpret the numerical data to be presented later in this chapter.

To gain insight into this nonlinear coupling mechanism, suppose

that at the instant t = 0 all of the mode-amplitudes and their derivatives are zero with the exception of $B_{11}(t)$ and dB_{11}/dt. In other words only first tangential standing oscillations are initially present in the combustor. From the differential equations governing the 1R and 2T modes it is found that:

$$\frac{d^2B_{01}}{dt^2} = - C_2B_{11}(0) \frac{dB_{11}}{dt}(0) \neq 0$$

$$\frac{d^2B_{21}}{dt^2} = C_{10}B_{11}(0) \frac{dB_{11}}{dt}(0) \neq 0$$

which indicates that the 1R and 2T modes will begin to grow. Thus it is seen that an initial 1T disturbance can excite the higher frequency modes by means of nonlinear coupling. This fact reveals that energy is transferred from the 1T mode to the 1R and 2T modes. On the other hand if the initial disturbance has the form of the 2T mode, it can be shown that the 1R mode will be excited but the 1T mode will never appear because all of the nonlinear terms in the equations which govern the 1T mode involve the 1T mode and will always remain zero. Similarly it is observed that an initial disturbance of the 1R mode does not excite either of the other two modes. These results indicate that, although the 1T mode can transfer energy to the other modes, the reverse energy exchange is either impossible or it occurs to a lesser extent after the 1R and 2T modes have been previously excited by the 1T mode.

From the differential equations governing the mode-amplitudes it can be shown that the mechanism of nonlinear coupling between modes can limit the amplitude of an unstable mode. Consider a rocket motor whose operating parameters n and τ are such that the 1T mode is linearly unstable while the other modes present in the truncated series expansion are stable. According to linear theory the 2T and 1R modes could not be excited and the 1T mode would grow indefinitely. The nonlinear coupling of the 1T mode with the stable modes, however, provides an additional energy sink for the 1T mode; a portion of the energy supplied to the 1T mode by the unsteady combustion process is transferred to the 2T and 1R modes. This energy loss increases with increasing amplitude of the 1T mode until a certain amplitude is reached at which the energy lost to the stable modes is equal to the excess energy received by the 1T mode from the combustion process. Thereafter the amplitude of the 1T mode remains constant; that is, a stable limit cycle has been reached. The amplitudes of the 2T and 1R modes are also constant and such that the energy received by these stable modes from coupling with the 1T mode is equal to that extracted by the damping processes. Thus such a stable limit cycle is characterized by a continuous flow of energy from the combustion process to the unstable mode, then to the stable modes by the mechanism of nonlinear coupling, and finally leaving the system by damping processes acting upon the stable modes.

Series Containing the Radial Mode Only. In previous discussions it has been shown that only radial modes exhibit self-coupling in the differential equations that result from applying the Galerkin method.

Therefore the nonlinear behavior of the first radial mode may be investigated by using a one-mode series expansion. The velocity potential is assumed to be given by the following expression:

$$\tilde{\Phi} = B_{01}(t) J_0\left(S_{01} r\right) \tag{239}$$

The differential equation which controls the behavior of $B_{01}(t)$ is:

$$\frac{d^2 B_{01}}{dt^2} + S_{01}^2 B_{01} + K \frac{dB_{01}}{dt} + K_\tau \frac{dB_{01}}{dt}(t-\bar{\tau}) + C_1 B_{01} \frac{dB_{01}}{dt} = 0 \tag{240}$$

which is obtained from Eq. (224) by taking $j = 0$ and $k = 1$ and omitting the nonlinear term involving A_{01}. This equation is particularly simple in form since it contains only a single nonlinear term. Due to the presence of this self-coupling term, the nonlinear behavior of the 1R mode is expected to be qualitatively different from that of the 1T mode. For this reason the results of a separate investigation of the 1R mode will be presented in addition to the results obtained by using the three-mode series.

Method of Numerical Solution and Initial Conditions

The differential equations which govern the behavior of the mode-amplitudes will be solved numerically by means of the fourth order Runge-Kutta method. This widely used method was chosen because of its ease of application, its inherent accuracy, and its favorable stability characteristics. Since this method is not used normally to solve equa-

tions which involve a time delay, it must be slightly modified. The treatment of this problem and other aspects of the numerical solution of the equations is presented in Appendix C.

In order to start the numerical integration initial conditions must be specified, thus the values of the mode-amplitude functions and their time derivatives at the time t = 0 must be assumed. Because of the presence of first derivative terms involving the time delay the derivatives of the mode-amplitudes must be specified as functions of time in the interval $-\bar{\tau} \leq t \leq 0$. The simplest possibility is that these derivatives are zero for $-\bar{\tau} \leq t \leq 0$ and jump suddenly to finite values at t = 0; this corresponds to the sudden introduction of a disturbance or pulse into a quiescent medium. An alternative is that these derivatives are sinusoidal functions of time prior to t = 0; that is, a neutrally stable acoustic oscillation is initially present and at t = 0 the effects of the combustion process, mean flow, and nonlinear coupling between modes is suddenly turned on. The exact functional form of these "pre-initial conditions" is of little consequence, however, as the final solution is expected to be independent of the initial conditions if a true limit cycle exists.

Standing Wave Solution. The differential equation which controls the behavior of the velocity potential cannot predict whether the final solution will be a standing or a spinning wave. A mechanism that selects, for example, a spinning wave in preference to a standing wave can be obtained by assuming that the combustion process is sensitive to transverse velocity components and displacements. Such a model is postulated by Reardon[5] who introduces the velocity indices ℓ_r and ℓ_θ in

addition to the pressure interaction index n. In this analysis, however, it has been assumed that the combustion process is sensitive only to properties which can be directly correlated to the pressure, therefore the type of wave predicted (i.e. standing or spinning) is expected to depend upon the initial conditions.

In order to study the nonlinear behavior of standing waves the initial disturbance is assumed to be a standing wave. To describe an oscillation of the standing form both $A_{mn}(t)$ and $B_{mn}(t)$ must be periodic functions which oscillate in phase, therefore the "pre-initial conditions" can be expressed as follows:

$$A_{mn}(t) = A\cos S_{mn}t \quad ; \quad \frac{dA_{mn}}{dt} = - S_{mn}A\sin S_{mn}t \tag{241}$$

$$B_{mn}(t) = B\cos S_{mn}t \quad ; \quad \frac{dB_{mn}}{dt} = - S_{mn}B\sin S_{mn}t$$

for $-\tau \leq t \leq 0$. The orientation of the standing wave pattern is determined by the relative values of the amplitudes A and B. If $A \neq 0$ and $B = 0$ the pressure nodes occur at angles θ which are even multiples of $\pi/2m$, while if $B \neq 0$ and $A = 0$ the nodes occur at odd multiples of $\pi/2m$. For other values of A and B the pressure nodes occur at intermediate angles. Since the equation governing the behavior of the velocity potential does not indicate any preferred orientation, the orientation of the wave pattern corresponding to a stable limit cycle will depend upon the orientation of the initial disturbance. For simplicity in the study of standing waves, therefore, it will be

assumed that the initial disturbance has a pressure node at $\theta = 0$ which corresponds to $B = 0$ in Eqs. (241).

If it is assumed that the initial disturbance has the form of a radial mode, the pressure does not depend on angular position and the initial condition is given by:

$$B_{on}(t) = B\cos S_{on}t \quad ; \quad \frac{dB_{on}}{dt} = - S_{on}B\sin S_{on}t \tag{242}$$

Initial conditions of the form given by Eq. (242) will be used in the study of radial mode instability with the aid of the one-mode series and Eq. (240).

Spinning Wave Solution. In the investigation of the nonlinear aspects of spinning tangential instability the initial disturbance will be assumed to be a single spinning acoustic mode. The velocity potential describing a wave travelling in the direction of increasing θ is given by:

$$\Phi = A\cos\left(m\theta - S_{m1}t\right)J_m\left(S_{m1}r\right) \tag{243a}$$

which can be written in the equivalent form:

$$\Phi = \left[\left(A\cos S_{m1}t\right)\cos m\theta + \left(A\sin S_{m1}t\right)\sin m\theta\right]J_m\left(S_{m1}r\right) \tag{243b}$$

Comparing the coefficients of $\sin m\theta$ and $\cos m\theta$ in Eq. (243b) with those

occurring in the assumed series expansion for $\tilde{\Phi}$ yields:

$$A_{ml}(t) = A\sin S_{ml}t \quad ; \quad \frac{dA_{ml}}{dt} = S_{ml}A\cos S_{ml}t \tag{244}$$

$$B_{ml}(t) = A\cos S_{ml}t \quad ; \quad \frac{dB_{ml}}{dt} = -S_{ml}A\sin S_{ml}t$$

for $-\bar{\tau} \leq t \leq 0$. Thus it is seen that the spinning initial disturbance is obtained when $A_{ml}(t)$ and $B_{ml}(t)$ have equal amplitudes and are in quadrature.

Results and Discussion

In order to investigate all aspects of the nonlinear stability problem a considerable amount of numerical calculations were performed. Only the most important conclusions and some typical results will be reported in the remainder of this chapter. These results are presented with the following objectives in mind:

(a) The prediction of stable limit cycles and triggering limits for transverse mode instability.

(b) The determination of the waveform and frequency of the nonlinear solutions.

(c) The determination of the dependence of the amplitudes of the stable and unstable limit cycles upon the combustion parameters n and $\bar{\tau}$, the steady state velocity, and the length to diameter ratio.

(d) The investigation of the convergence of the assumed expansion for the velocity potential; that is, how many modes are needed to obtain

an accurate approximation.

Numerical calculations were obtained using the following series expansions: (1) the three-mode series (1T, 2T, and 1R), (2) a one-mode series involving only the 1R mode, and (3) expansions containing higher tangential modes and combined tangential-radial modes. From the results of these calculations the effect of various modes upon the nonlinear stability characteristics of the rocket engine can be evaluated.

Three-Mode Series Expansion

Nonlinear solutions were obtained using the three-mode expansion for Φ (i.e. Eq. (236)) by integrating Eqs. (237) numerically on a Univac 1108 computer. As expected stable limit cycles were found if the engine's combustion parameters (i.e. n and $\bar{\tau}$) were such that the 1T mode was linearly unstable and the 2T and 1R modes were linearly stable. These stable limit cycles were computed by specifying an initial disturbance of the form of a 1T standing or spinning wave and continuing the step-by-step integration until a periodic solution was obtained; that is, the amplitude of the mode-amplitude functions remained essentially constant. That the limit cycles were indeed stable was easily verified by observing the time history of initial disturbances with amplitudes slightly smaller and slightly larger than the limit cycle. In both cases the amplitude of the oscillations approached the limit cycle, thus the stability of the limit cycle was demonstrated. To obtain the amplitude of the limit cycle to a sufficient degree of accuracy required an integration over a time interval of about one hundred cycles of the 1T mode, which corresponds to about 30 seconds

of actual computation time. The accuracy of numerical calculations over such a large number of integration steps is discussed in Appendix C.

These numerical calculations also predicted the possibility of triggering combustion oscillations by the introduction of very large disturbances in linearly stable engines. Since the second order theory upon which these results are based is limited to considerations of moderate amplitude oscillations, the accuracy of the predicted triggering limits is open to question. It appears that a third order theory is needed to predict such limits accurately. Such a theory has been developed and is presented in Chapter VII.

Initial Conditions and Transient Solutions. Many preliminary calculations were made to investigate the behavior of the limit cycles in the region of the $(n, \bar{\tau})$ plane where the first tangential mode is unstable. The major objective of this preliminary study was to determine to what extent the final solutions are dependent upon the initial conditions. Various combinations of the three modes included in the series expansion for Φ were assumed to be initially present in the combustor. The subsequent time evolution of these modes is shown on an amplitude-time plot. On these plots the ordinate is the maximum value of the mode-amplitude function or the pressure perturbation (which occurs once per cycle) and the time scale is expressed in terms of cycles of the 1T mode. Such amplitude plots are presented in Figs. (11) through (15) which were computed for the point $n = 0.60167$, $\bar{\tau} = 1.70629$ (where the 1T mode is unstable and the 1R and 2T modes are

stable) and show that in each case the final amplitude of each of the modes is independent of the initial conditions.

The simplest case is shown in Figs. (11) and (12) where the initial disturbance was of the form of the 1T mode while the other modes were absent. In Fig. (11) the initial amplitude of $A_{11}(t)$ (the 1T mode) is smaller than its final value. It is seen that immediately following the disturbance the 2T and 1R modes are excited and the amplitudes of all modes approach their limiting values asymptotically. For initial amplitudes of the 1T mode considerably larger than the value at the limit cycle (see Fig. 12) it is seen that the amplitudes of the 2T and 1R modes overshoot their final values and approach the limit cycle from above. In both cases the final amplitude was the same, but the large disturbance approached the limit cycle faster. During the first 15 cycles considerable modulation of the amplitudes occurs, particularly for the 2T mode. It is during this transient period that the waveform and frequency of the oscillations must adjust from their initial to final values. As shown in Figs. (13) and (14) similar results are obtained when two or more modes are initially present as long as one of these is the 1T mode. In all cases the solutions were close to the limit cycle after about 50 cycles.

The initial disturbances considered in Figs. (11) through (14) contained a large 1T component, therefore it is not surprising that a 1T oscillation developed. However Fig. (15) shows that a 1T oscillation can arise from an initial disturbance dominated by the 2T mode. In this case the initial amplitude of the 2T mode is large and that of the 1T mode is very small. Initially the 2T mode decays rapidly because

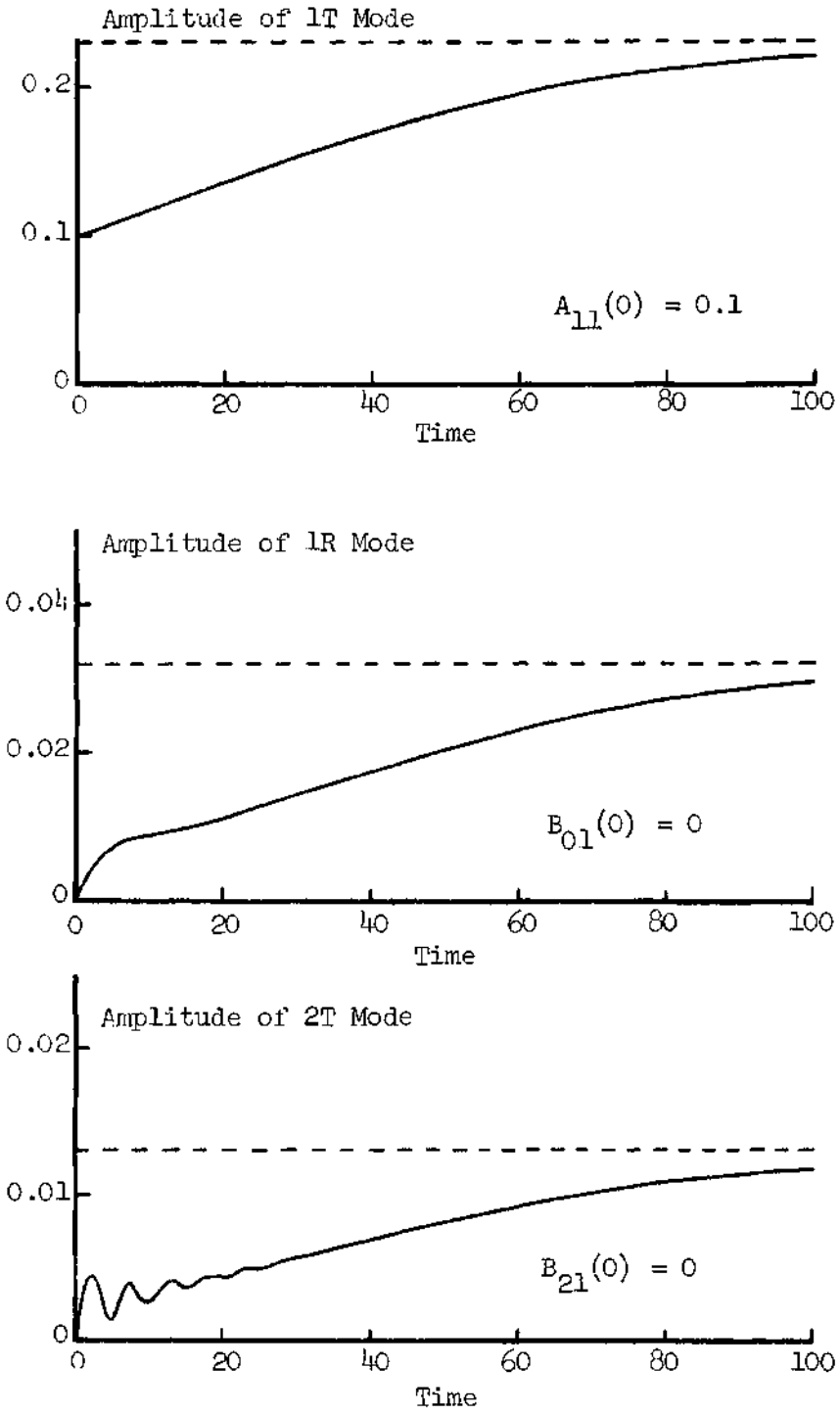

$\bar{\tau} = 1.70629$; $n = 0.60167$; $\gamma = 1.2$; $\bar{u}_e = 0.2$; $z_e = 1.0$

Figure 11. Time History of a Small Amplitude 1T Mode Disturbance.

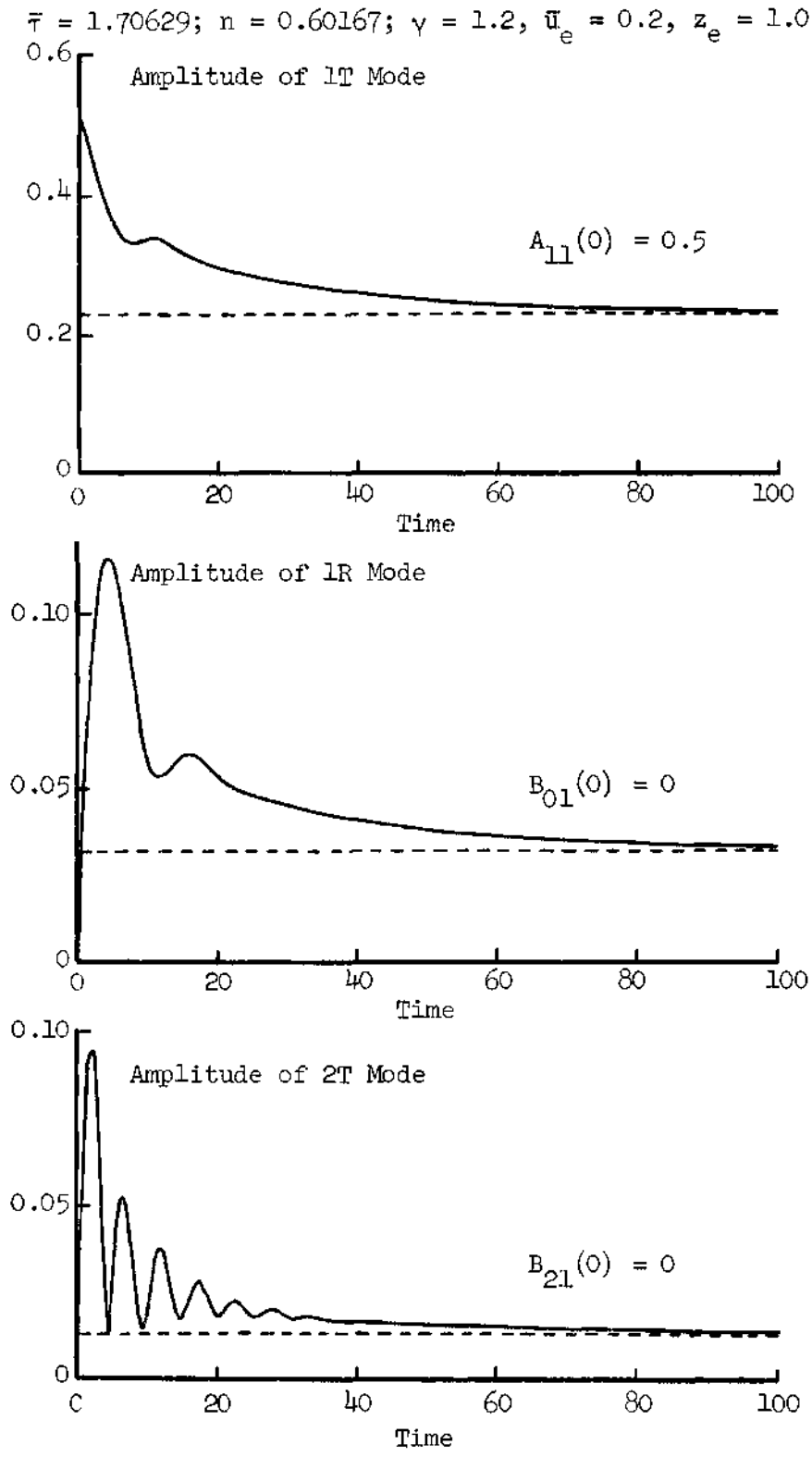

Figure 12. Time History of a Large Amplitude 1T Mode Disturbance.

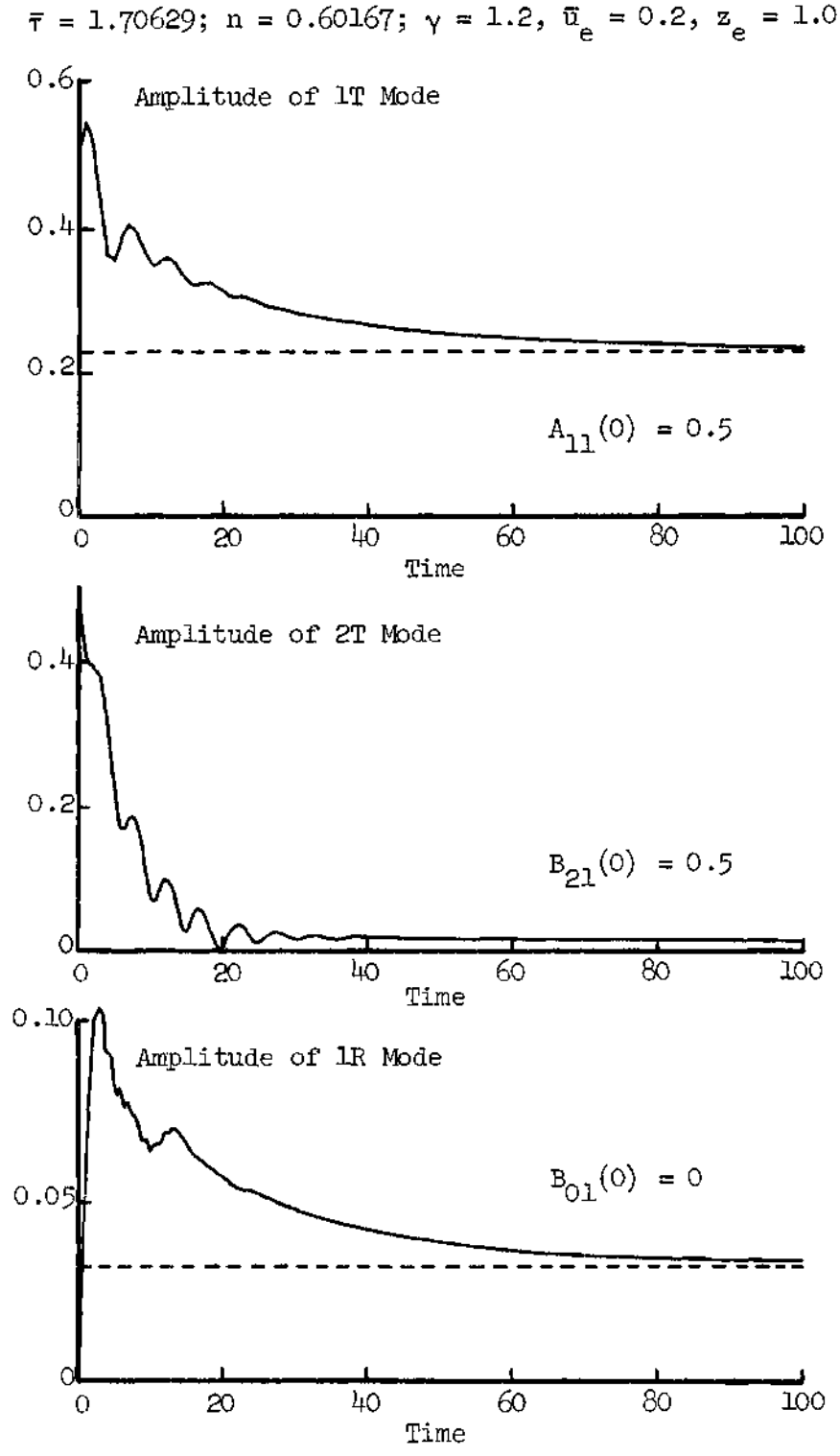

Figure 13. Time History of a Disturbance Involving the 1T and 2T Modes.

$\bar{\tau} = 1.70629$; $n = 0.60167$; $\gamma = 1.2$; $\bar{u}_e = 0.2$, $z_e = 1.0$

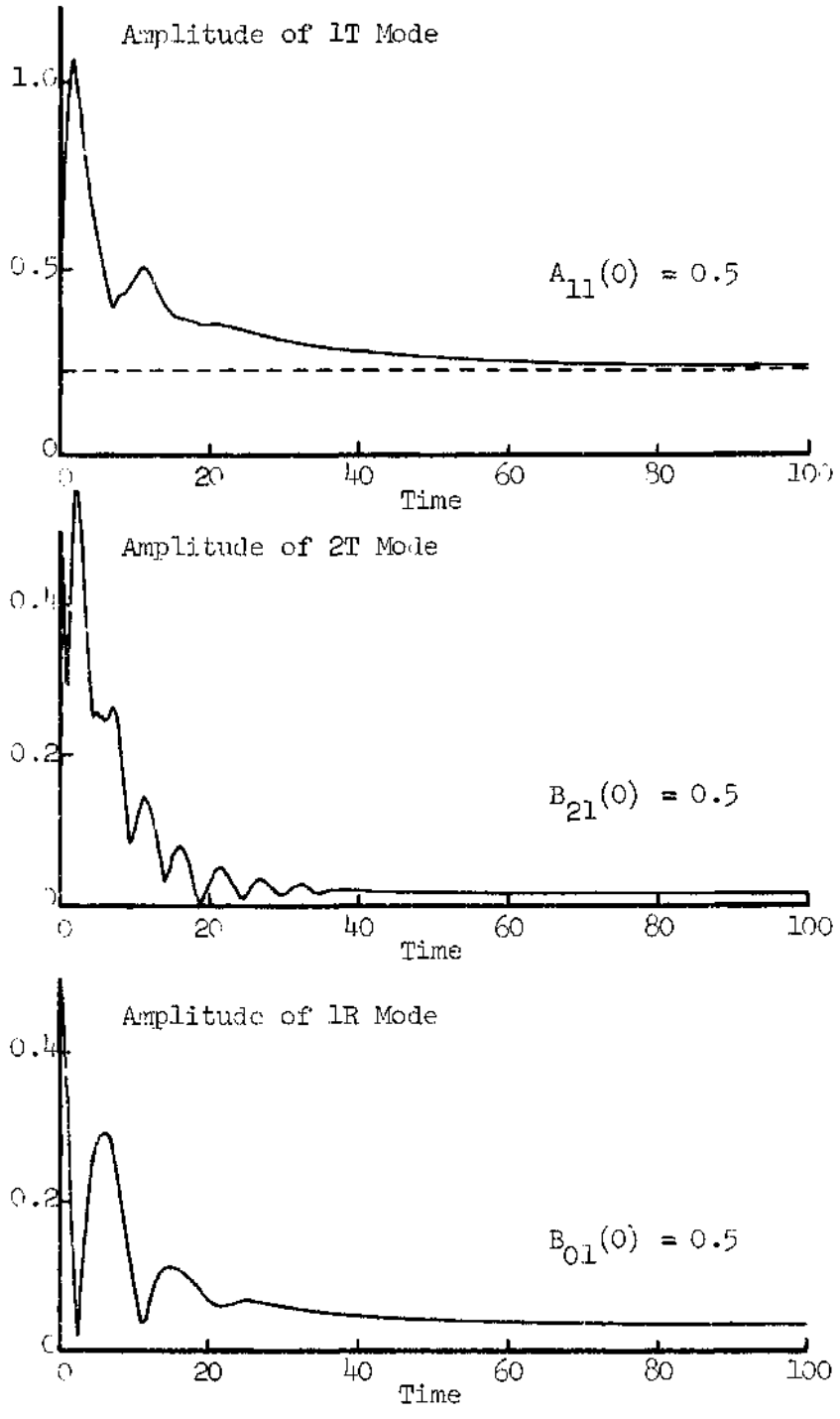

Figure 14. Time History of a Disturbance Involving the 1T, 2T, and 1R Modes.

it is linearly stable in this region of the $(n, \bar{\tau})$ plane, and the 1T mode grows slowly in an exponential fashion in accord with linear theory. During the first 50 cycles of the 1T mode the coupling between modes is weak and the behavior is very close to that predicted by linear theory. As the amplitude of the 1T mode increases the nonlinear coupling with the 2T mode becomes sufficiently strong that the 2T mode also begins to grow. Growth of all modes does not continue indefinitely but levels off to a stable limit cycle.

In all of the cases considered above the initial waveform contained a 1T component. If the 1T mode is not initially present the numerical calculations using the three-mode series predict entirely different behavior from that described above. An initial 1R or 2T disturbance does not excite the 1T mode, consequently if the 1R and 2T modes are stable the oscillations will decay. If one of these modes is unstable, however, a limit cycle is obtained which differs from that found when the 1T mode is excited. Neither of these cases have been investigated in detail with the aid of the three-mode series because if an arbitrary initial pressure waveform is expanded in terms of the acoustic eigenfunctions it is most likely that a 1T component will be present. Therefore in the study of the nonlinear aspects of 1T mode instability it will be assumed that the initial disturbances consists only of the 1T acoustic mode.

General Characteristics of the Nonlinear Solutions. The general characteristics of the stable limit cycles will now be described. In the region of the $(n, \bar{\tau})$ plane for which the 1T mode is the only linearly unstable mode two points are selected along the line $\bar{\tau} = 1.70629$

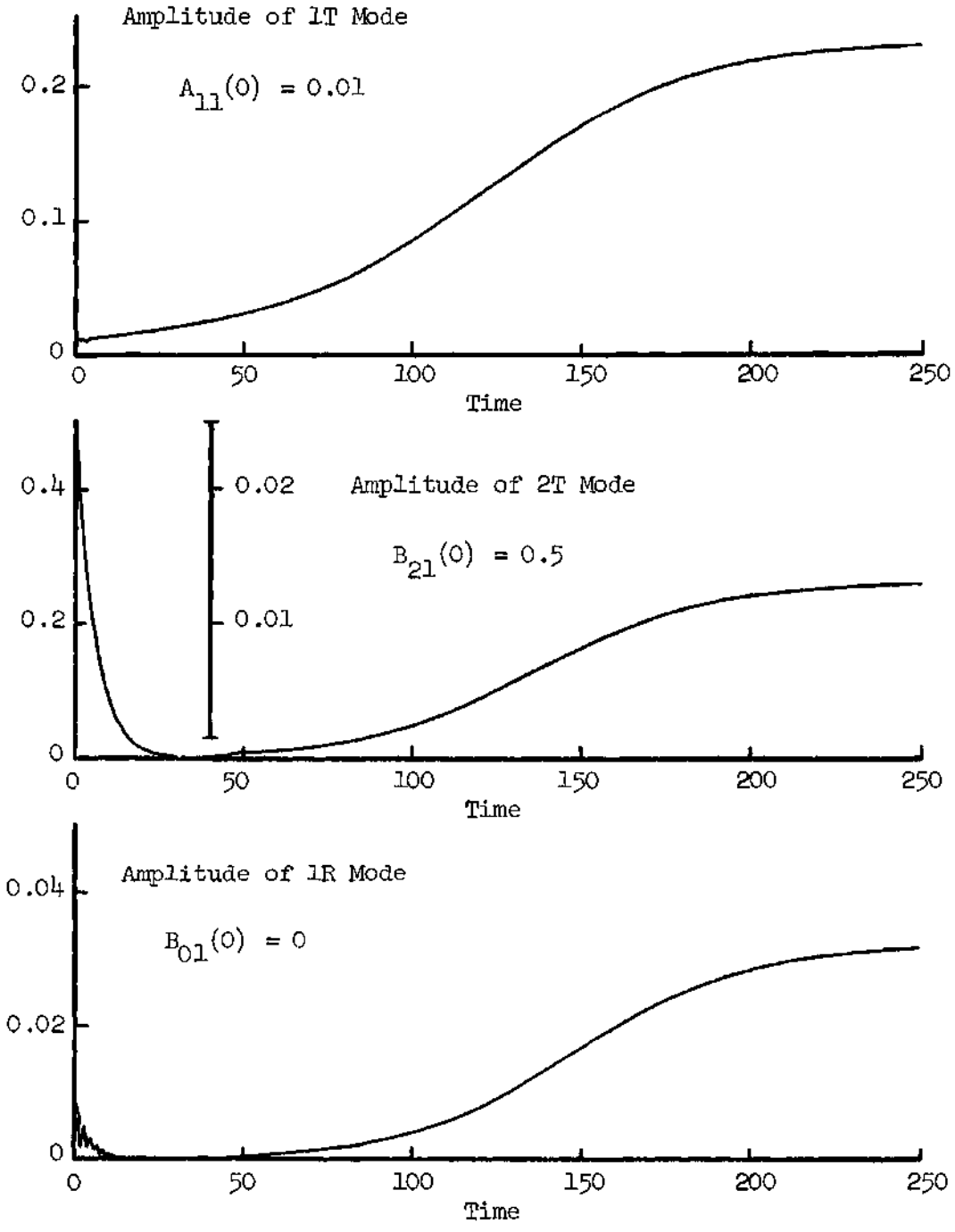

$\bar{\tau} = 1.70629$; $n = 0.60167$; $\gamma = 1.2$; $\bar{u}_e = 0.2$; $z_e = 1.0$

Figure 15. Time History of an Initial Disturbance Dominated by the 2T Mode.

(e.g. see points A and B of Fig. 16). Pressure waveforms and the mode-amplitude functions were calculated at these points and the results are presented in Figs. (17) through (25). In all cases the numerical calculations were started by specifying the initial conditions in the form:

$$\text{(Standing form)}\quad A_{11}(t) = A\cos S_{11}t\ ;\ \frac{dA_{11}}{dt} = -S_{11}A\sin S_{11}t \tag{248a}$$

$$\text{(Spinning form)}\quad A_{11}(t) = A\sin S_{11}t\ ;\ \frac{dA_{11}}{dt} = AS_{11}\cos S_{11}t \qquad (-\bar{\tau}\leq t\leq 0)$$

$$B_{11}(t) = A\cos S_{11}t\ ;\ \frac{dB_{11}}{dt} = -AS_{11}\sin S_{11}t \tag{248b}$$

that is, it is assumed that only 1T mode oscillations are initially present. Since the final solution (limit cycle) has been shown to be independent of the initial conditions, specifying the initial conditions in the above manner is simply a matter of convenience. In the case of standing waves only the functions $A_{11}(t)$, $B_{01}(t)$, and $B_{21}(t)$ appear in the calculations for when the initial disturbance is described by Eq. (248a) the functions $B_{11}(t)$ and $A_{21}(t)$ always remain zero. This implies that the orientation of the standing wave pattern does not change as the wave develops.

As shown in Fig. (17) the mode-amplitude functions characteristic of the stable limit cycle strongly resemble sine waves from which the frequencies of the various modes are readily determined. It was found

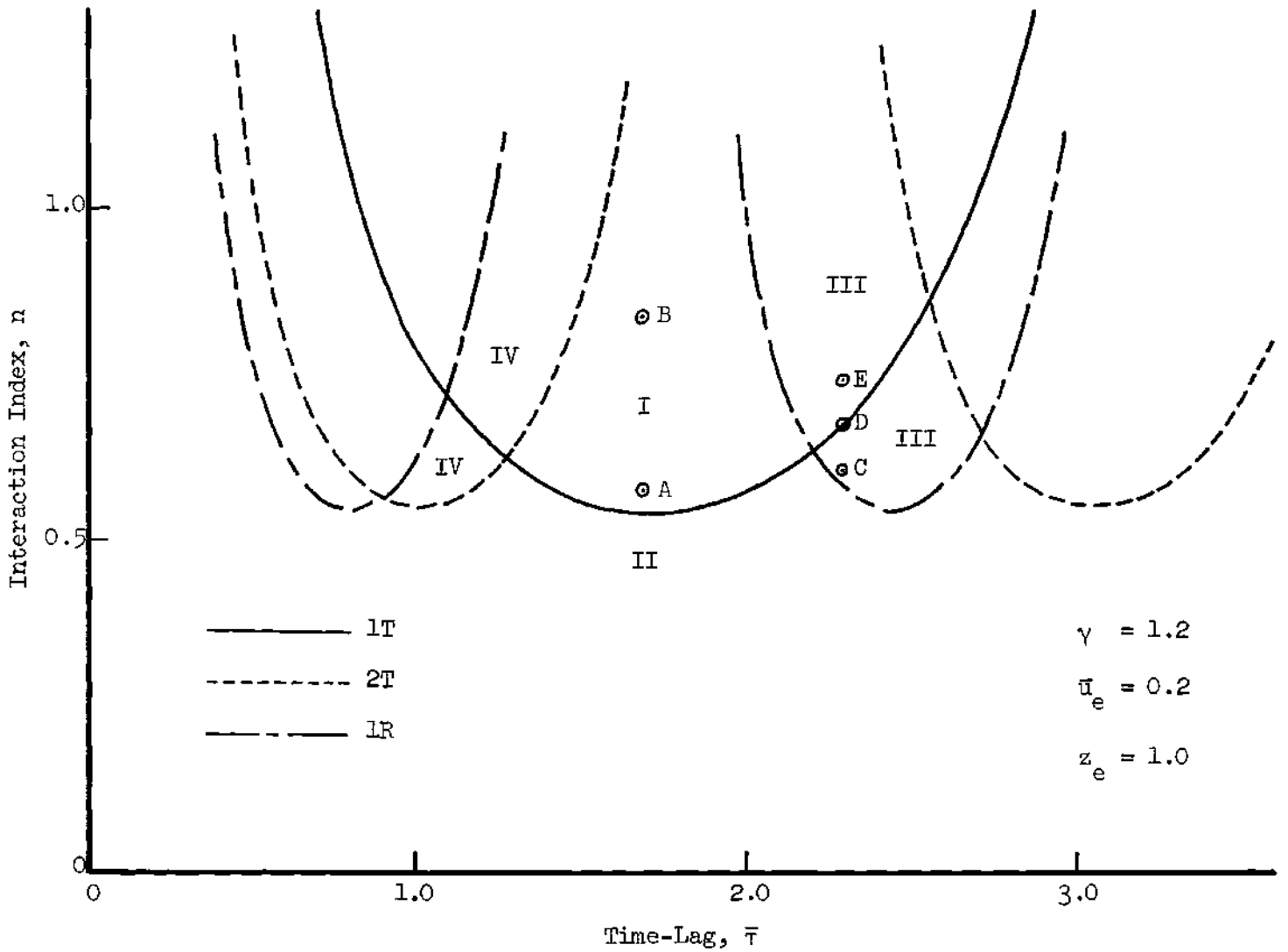

Figure 16. Regions of Interest in the Stability Plane.

that the frequency of the 1T mode (i.e. $A_{11}(t)$) differed only by a few percent from the frequency predicted by linear theory, and it was found to decrease slightly with increasing amplitude of the 1T mode. This result is in agreement with the predictions of Sirignano[10], Zinn[7], and Maslen and Moore[8] as well as available experimental data. The first radial and second tangential modes (i.e. $B_{01}(t)$ and $B_{21}(t)$) were found to oscillate at twice the frequency of the first tangential mode. This nonlinear result is in strong contrast to the results of acoustic theory since the natural frequencies of the various transverse modes are not integral multiples of the frequency of the fundamental (i.e. 1T) mode. Such a result is hardly surprising since in this case the behavior of the 1R and 2T modes is controlled primarily by the nonlinear coupling with the 1T mode.

An examination of the differential equations which govern the 1R and 2T modes reveals why these modes are driven at double the fundamental frequency. Both Eqs. (237a) and (237e) contain nonlinear terms of the form $A_{11}\frac{dA_{11}}{dt}$. Due to the similarity of the mode-amplitudes to sinusoids it may be assumed that the 1T mode is described by:

$$A_{11}(t) = A\cos\omega t \quad ; \quad \frac{dA_{11}}{dt} = -\omega A\sin\omega t$$

and the appropriate nonlinear term becomes:

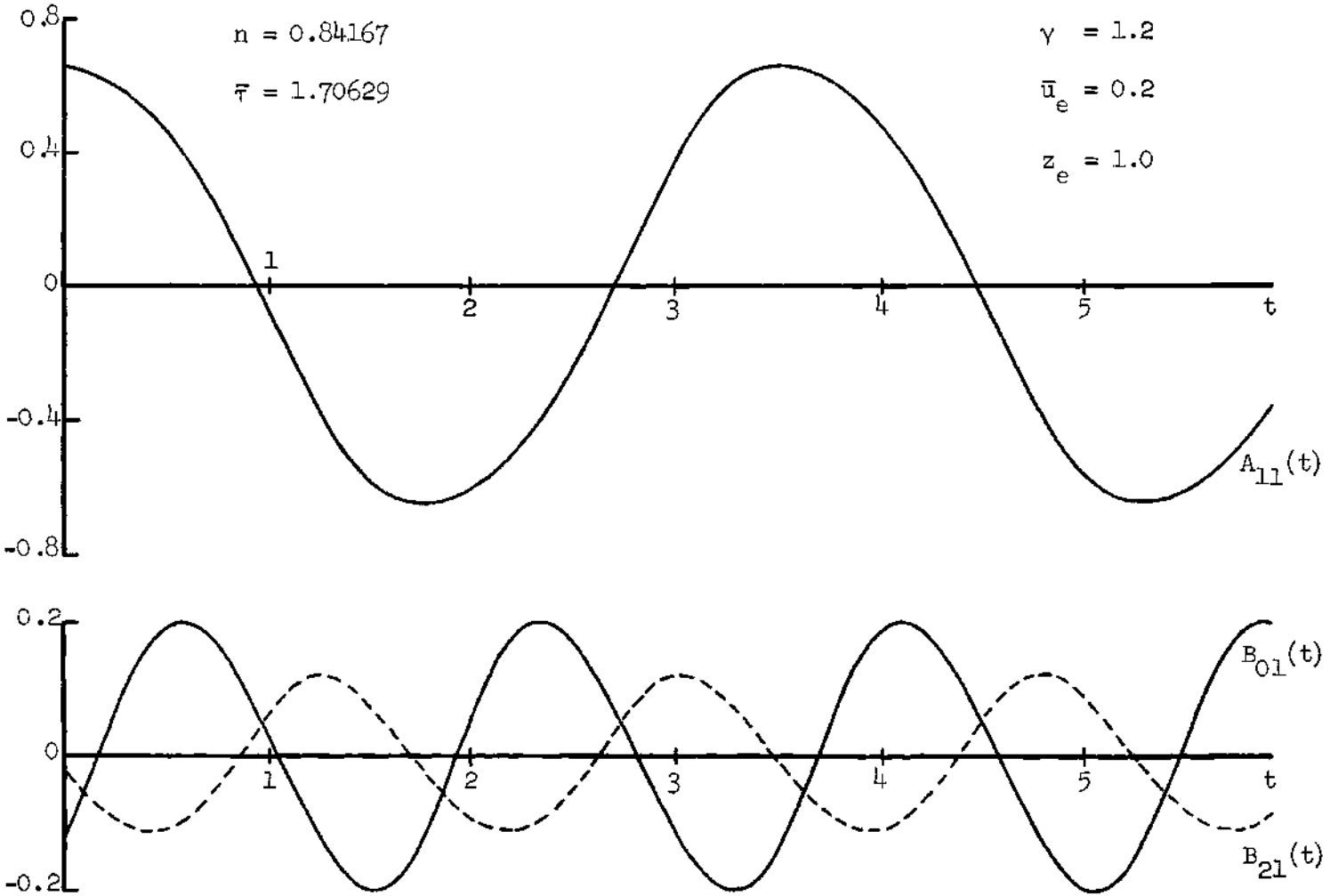

Figure 17. Time Dependence of the Mode-Amplitude Functions at a Stable Limit Cycle.

$$A_{11}\frac{dA_{11}}{dt} = -\omega A^2 \sin\omega t\cos\omega t = -\frac{\omega A^2}{2}\sin 2\omega t \qquad (249)$$

If these terms are transferred to the right hand sides of Eqs. (237a) and (237e) it is seen that the 1R and 2T modes are controlled by inhomogeneous equations which are analogous to those describing forced oscillations of a mass-spring-dashpot system. The frequency of the functions $B_{01}(t)$ and $B_{21}(t)$ will be equal to the frequency of the driving force which is twice the frequency of $A_{11}(t)$.

The pressure perturbation is a function of both space and time and is readily computed with the aid of Eq. (231) once the mode-amplitude functions are known. From the form of this expression and the calculated behavior of the mode-amplitudes it is anticipated that the pressure waveforms will exhibit a strong second harmonic distortion. This distortion arises from two sources: (1) the contribution of the double frequency functions $B_{01}(t)$ and $B_{21}(t)$ to the velocity potential and (2) the effect of the quadratically nonlinear terms in Eq. (231) upon $A_{11}(t)$ which introduces an additional double frequency component. These effects have been verified by numerical calculation.

Calculated pressure waveforms are presented in Figs. (18) through (25) for points A and B of Fig. (16). Figures (18) and (19) show the time dependence of the pressure perturbation corresponding to standing mode oscillations for the following stations on the wall of the combustor: (1) a pressure anti-node ($\theta = \pi/2$), (2) the pressure node of the acoustic mode ($\theta = 0$), and (3) a point midway between the node and antinode ($\theta = \pi/4$). The angular dependence of the wall pressure wave-

forms for various instants during a cycle of oscillation are presented in Figs. (20) and (21). These wall pressure waveforms are of particular interest since pressure measurements are most easily made at this boundary. For completeness, the radial dependence is given in Figs. (22) and (23). In all cases the axial station is arbitrary because the assumed form of the approximate solutions does not depend upon the axial coordinate. The corresponding waveforms for spinning waves are shown in Figs. (24) and (25).

As seen from Figs. (18) through (21) the nonlinear distortion of the pressure waveforms increases dramatically with increasing amplitude. For point A which lies relatively close to the neutral stability limit the limiting pressure amplitude is moderate and the waveforms depart only slightly from sinusoids (see Figs. 18 and 20). For the large amplitude oscillations corresponding to point B the nonlinear distortion of the waveforms is very pronounced (see Figs. (19) and (21)); in many cases these curves are characterized by sharp peaks and shallow minima. In this particular case the peak height at an anti-node is about twice the depth of the corresponding minimum. Although the maximum pressure perturbation may exceed unity, it appears that the minimum value will not drop below -1, thus the absolute pressure (i.e. $1 + p'$) will always be positive.

Another nonlinear effect predicted by the second order theory is the presence of pressure oscillations at the positions (nodes) where acoustic theory predicts that the oscillations vanish. As seen in Figs. (18) and (19) for $\theta = 0$ the pressure perturbation is not zero, instead a small amplitude oscillation of twice the fundamental frequency appears.

This waveform is very nearly sinusoidal, and for point B has an amplitude about half of that at the anti-node. In regard to the θ-dependence of the waveforms an effect similar to that noted above is observed. In Figs. (20) and (21) it is seen that at no time does the pressure perturbation become zero throughout the chamber as predicted by acoustic theory. At the times when the pressure is small two peaks occur between $\theta = 0$ and $\theta = 2\pi$ as a result of the presence of the 2T mode. The θ-waveforms are also seen to be symmetric about the anti-nodes ($\theta = \pi/2$ and $3\pi/2$).

In Fig. (22) the radial dependence of the pressure perturbation at the anti-node is given for different instants of time as calculated for point A. These curves are complicated combinations of the Bessel functions $J_0(S_{01}r)$, $J_1(S_{11}r)$ and $J_2(S_{21}r)$. It is seen that the pressure does not vanish at the axis of the chamber ($r = 0$) due to the presence of the 1R mode, and the greatest pressure fluctuation (i.e. $|p'|$) does not always occur at the wall. Figure (23) shows the radial dependence at the time of maximum amplitude (i.e. $t = t_4$) for the same angular stations given in Figs. (18) and (19). At the anti-node ($\theta = \pi/2$) and $\theta = \pi/4$ these curves resemble the function $J_1(S_{11}r)$ while at the node the radial mode predominates and the curve resembles $J_0(S_{01}r)$. It should be noted that at $r = 0$ the pressure is the same for all angles, which must be true if the pressure is to be single-valued.

Beginning with an initial spinning disturbance of the form given by Eq. (248b) spinning waveforms were calculated for a point close to the neutral stability limit. The time dependence of the wall pressure is shown in Fig. (24), while the dependence upon angular position is

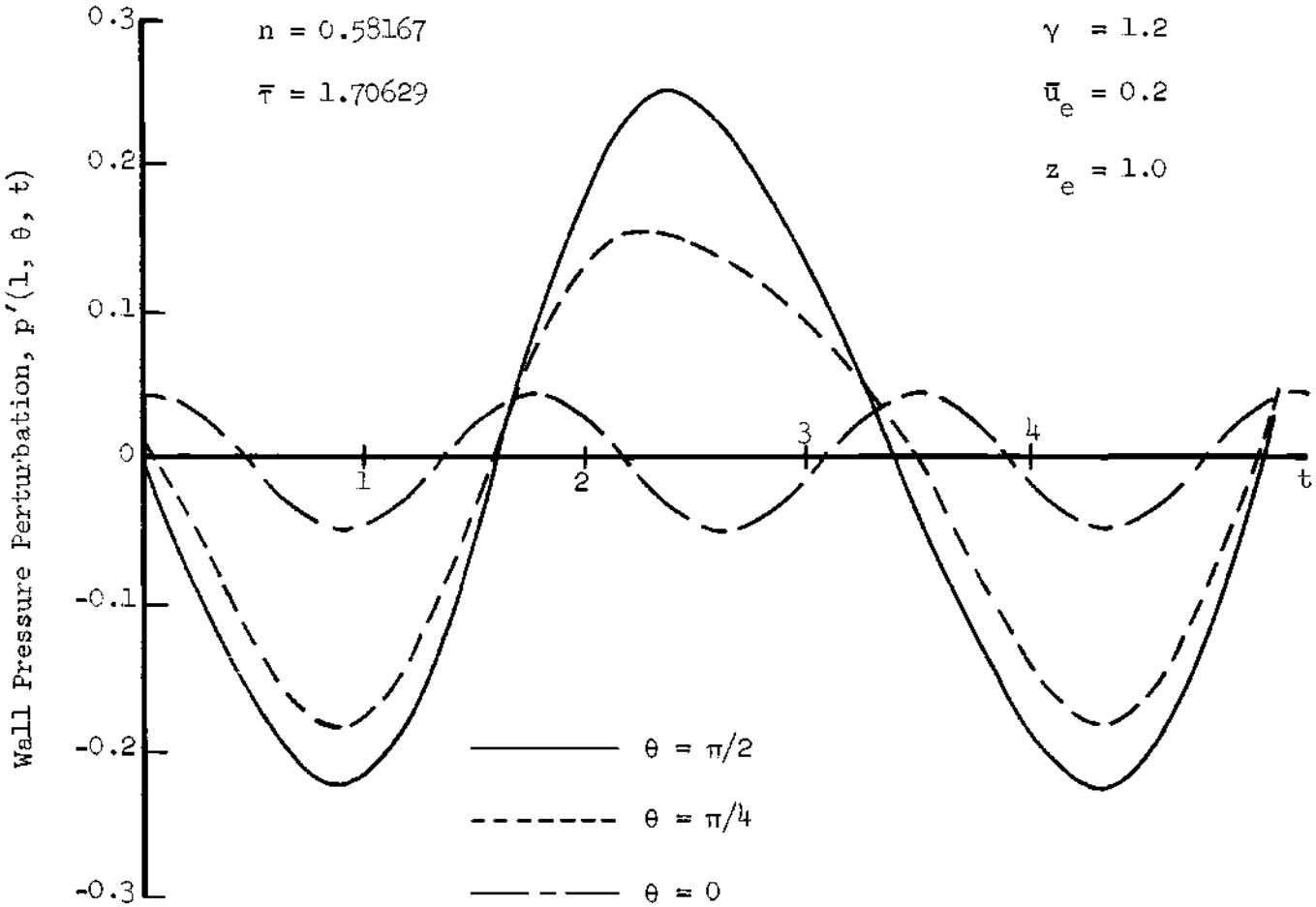

Figure 18. Time Dependence of the Wall Pressure Waveforms for a Small Amplitude Standing 1T Oscillation.

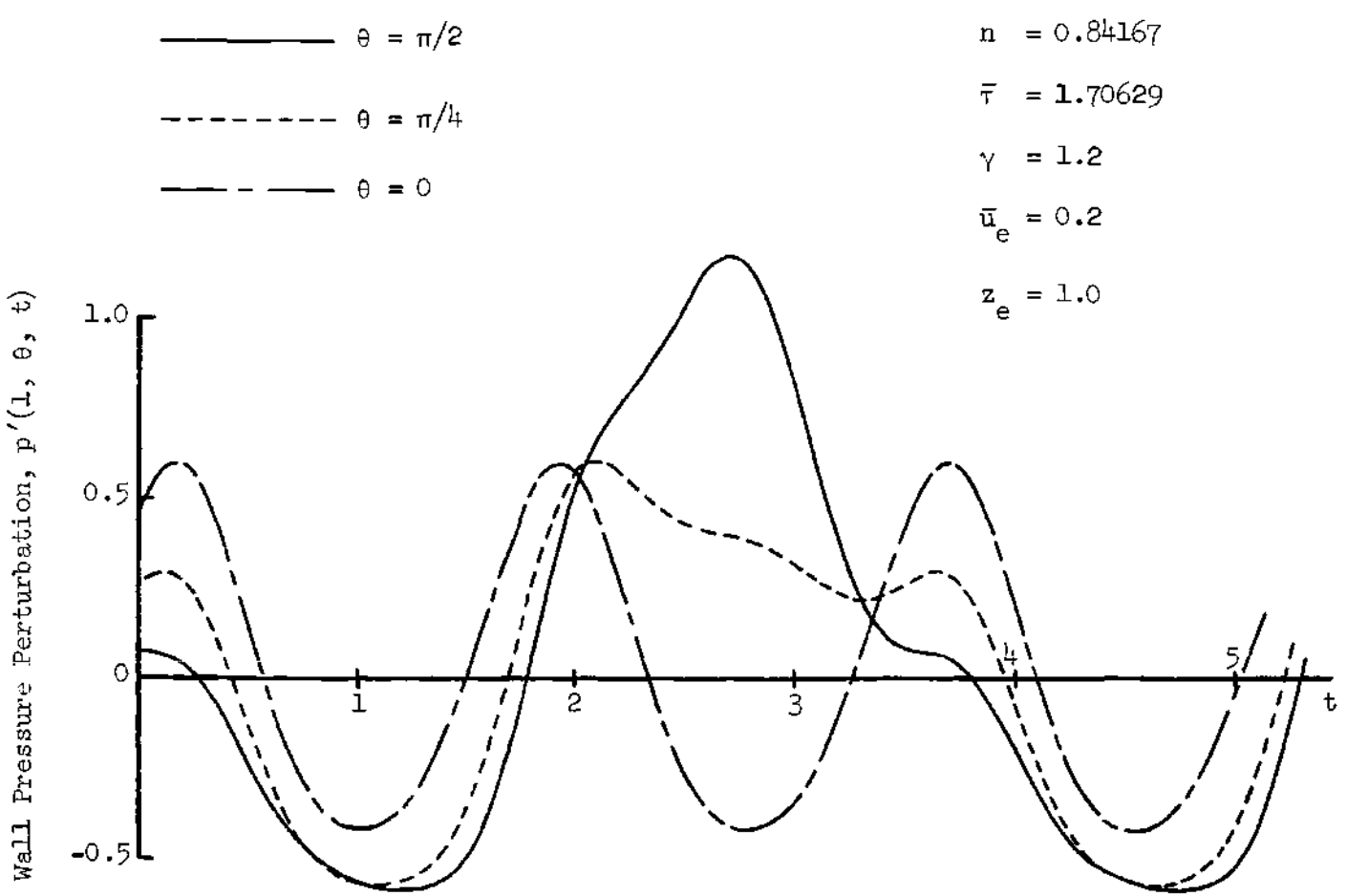

Figure 19. Time Dependence of the Wall Pressure Waveforms for a Large Amplitude Standing 1T Oscillation.

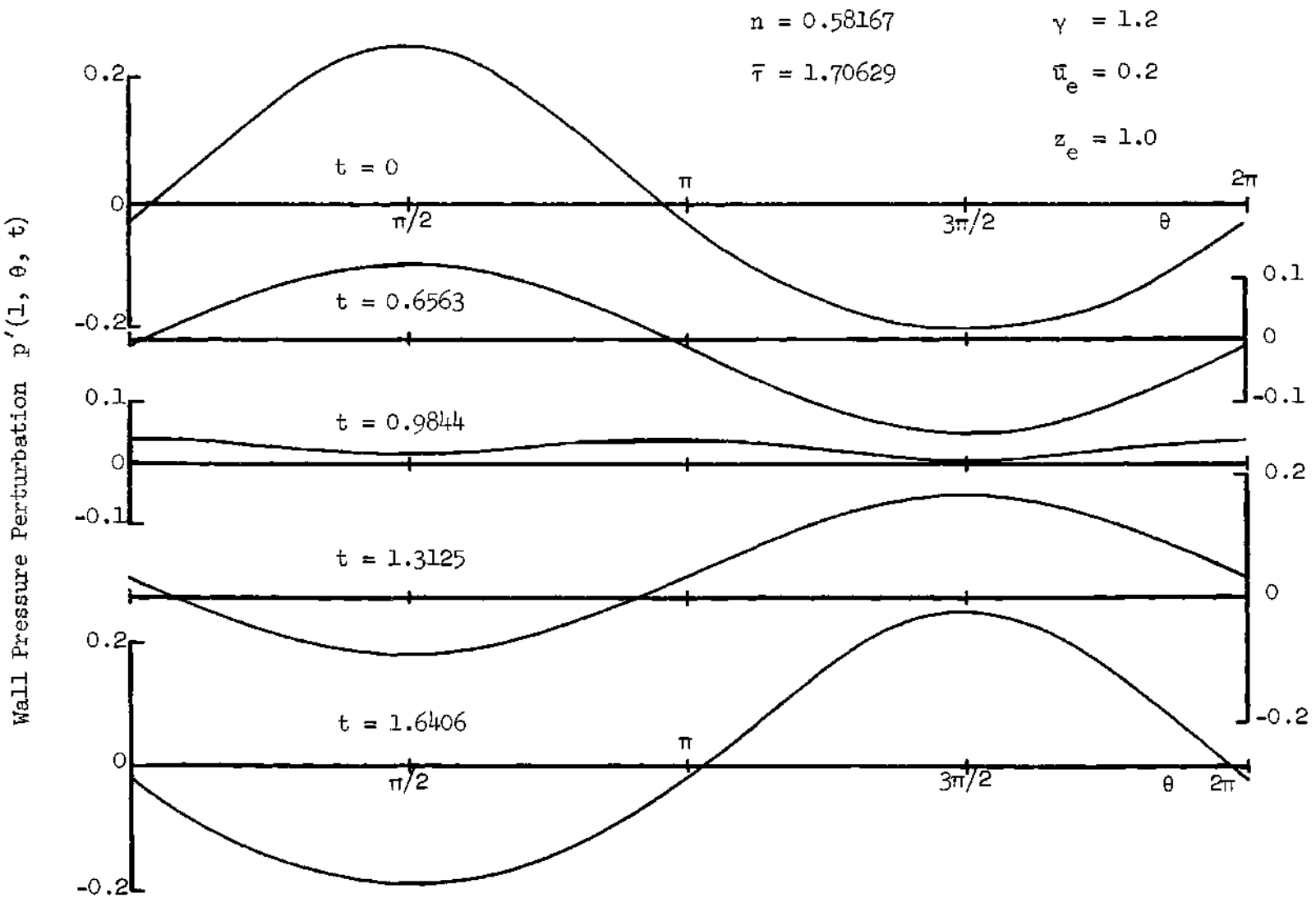

Figure 20. Angular Dependence of the Wall Pressure Waveforms for a Small Amplitude Standing 1T Oscillation.

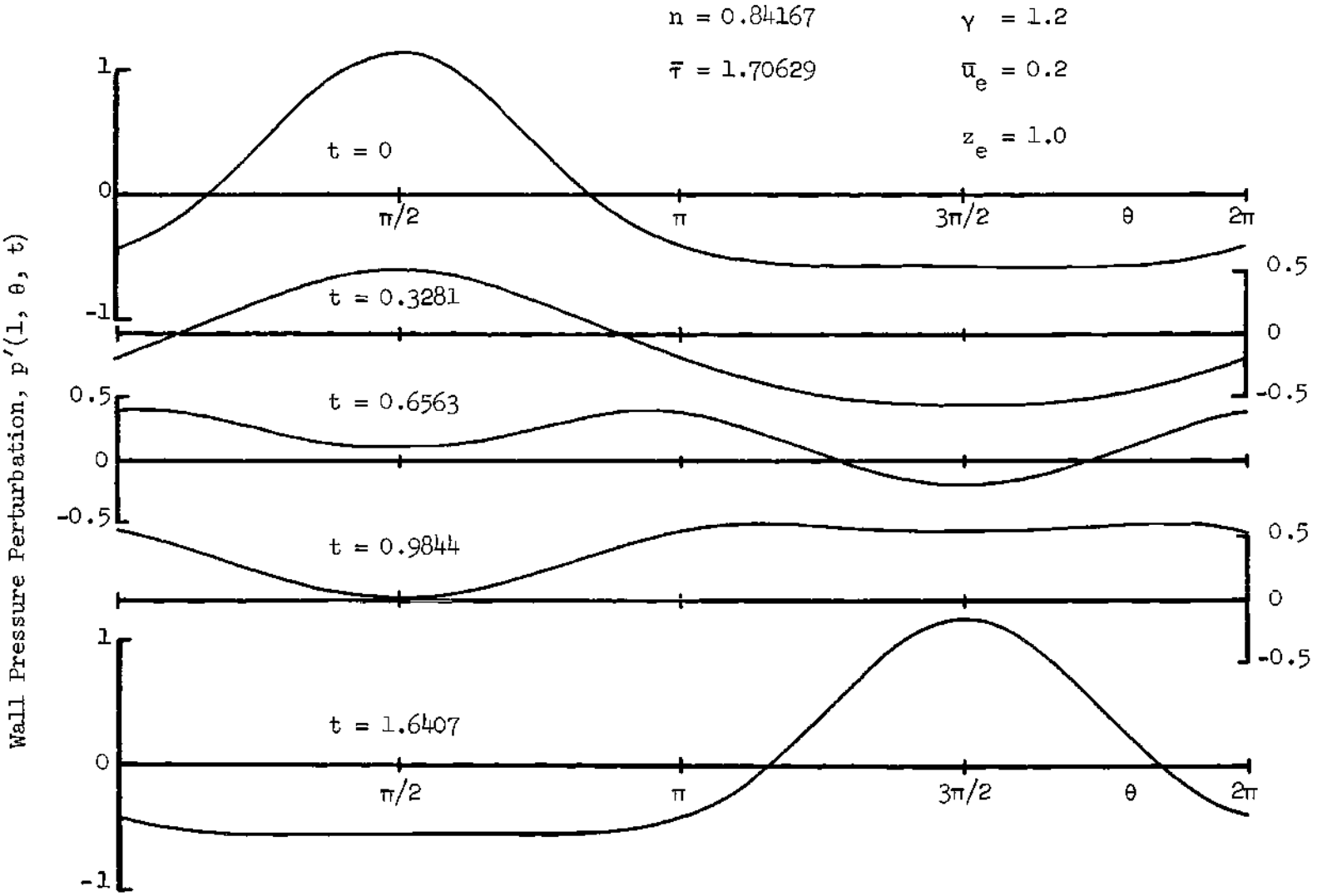

Figure 21. Angular Dependence of the Wall Pressure Waveforms for a Large Amplitude Standing 1T Oscillation.

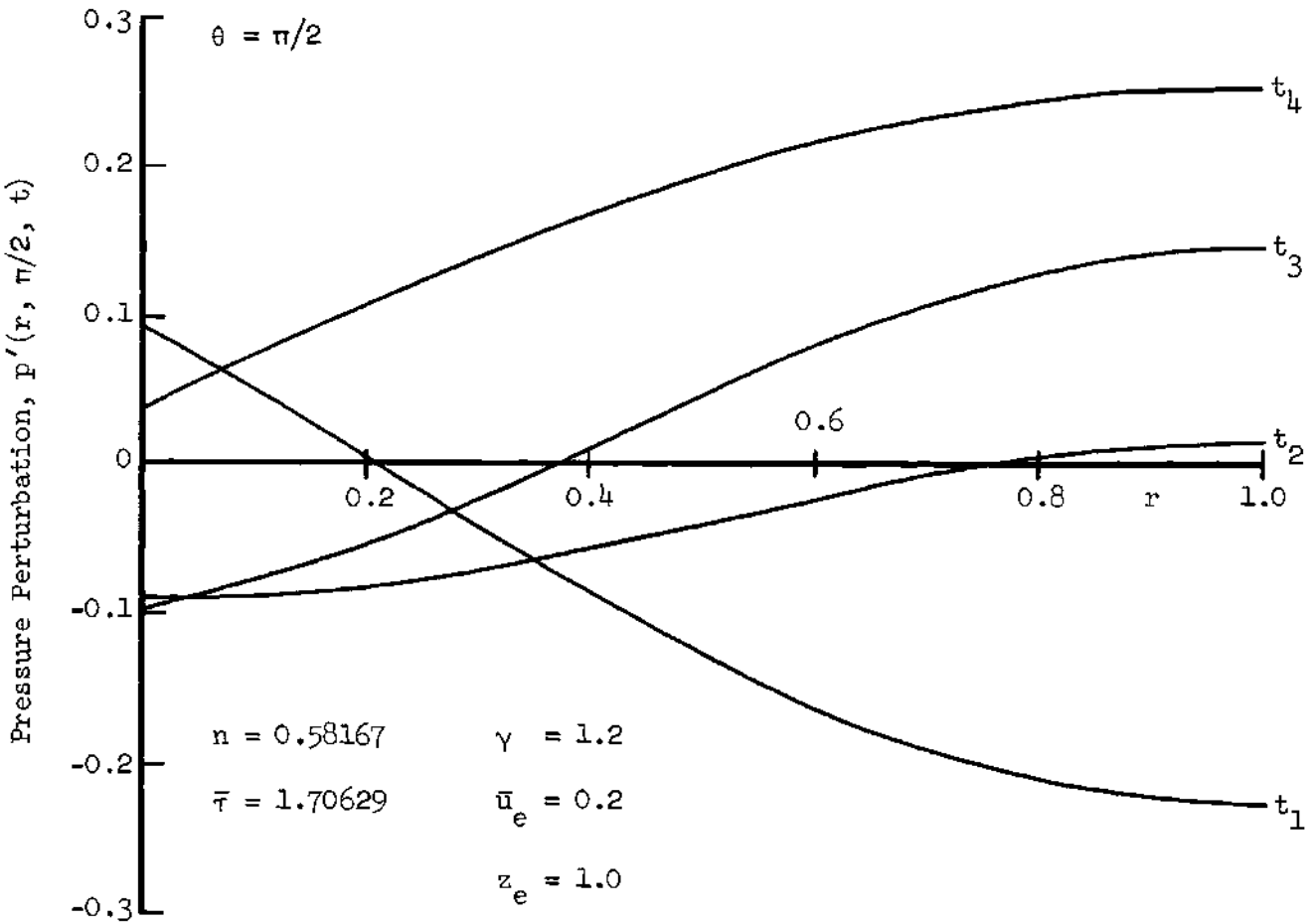

Figure 22. Radial Dependence of the Pressure Waveforms at an Anti-node for a 1T Standing Oscillation.

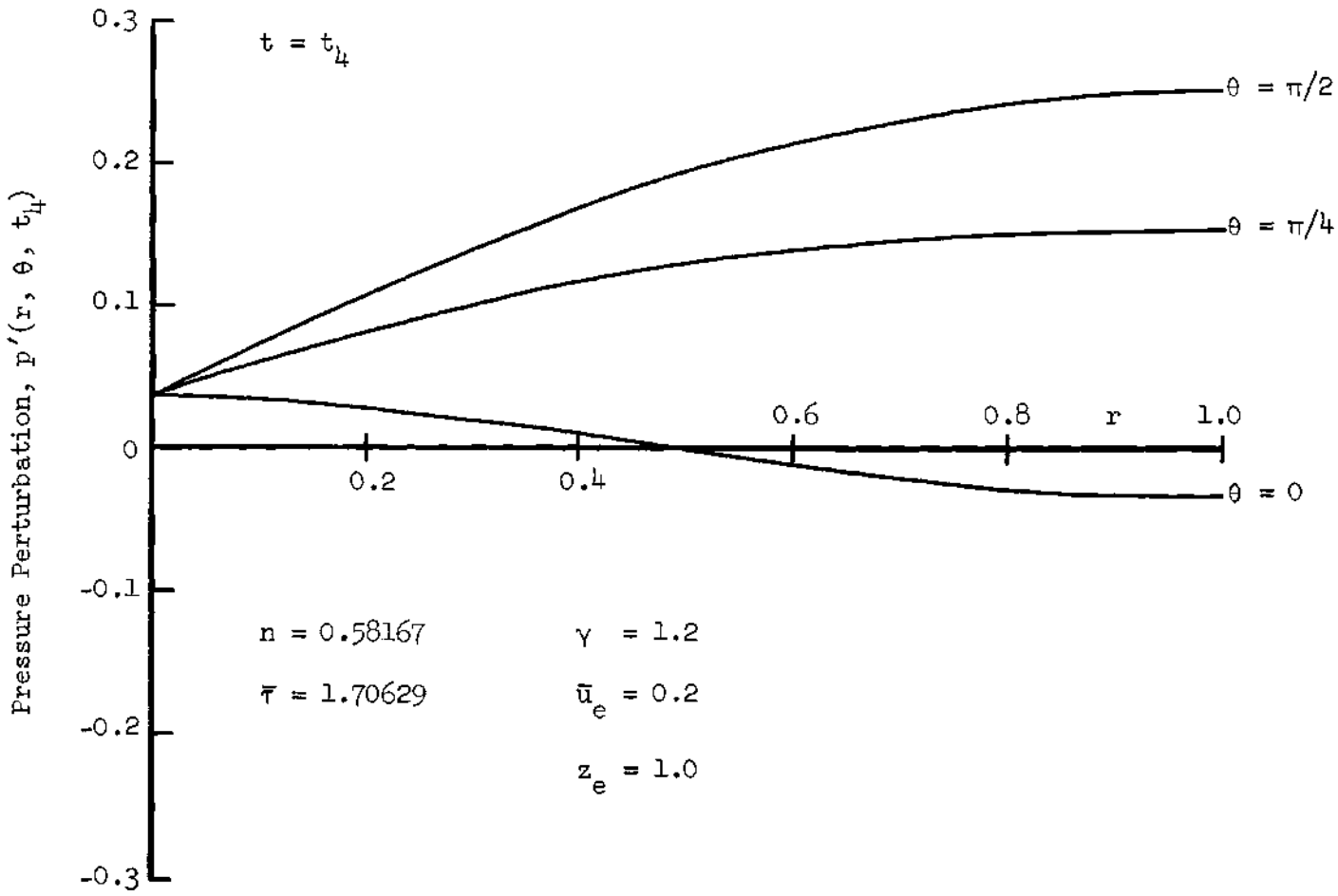

Figure 23. Radial Dependence of the Pressure Waveforms at Three Angular Stations.

given in Fig. (25). These waveforms appear similar to those at $\theta = \pi/2$ for standing waves, exhibiting sharp peaks and flat minima. Inspection of these curves shows that the wave is travelling in the direction of increasing θ while maintaining the same shape. A wave travelling in the opposite direction can be obtained by choosing an initial disturbance of this form.

Nonlinear Behavior as a Function of Combustion Parameters. The determination of the nonlinear behavior of unstable engines in various regions of the $(n, \bar{\tau})$ plane is one of the major objectives of this investigation. In order to define the regions of interest it is necessary to obtain the linear stability limits of the engine under consideration with respect to each of the modes present in the series expansion. These linear stability limits were calculated with the aid of the Galerkin method in Chapter V and the results are shown in Fig. (16). According to the linear stability characteristics of the modes considered in the three-mode series the $(n, \bar{\tau})$ plane can be divided into several subdomains. In Region I the 1T mode is linearly unstable while the remaining modes (i.e. 1R and 2T) are linearly stable. In this region the existence of stable limit cycles of the 1T mode has already been discussed. If triggering limits exist they should be found in Region II where all modes present in the series expansion for $\tilde{\Phi}$ are linearly stable. Other regions of interest are: Region III where the 1R mode is unstable, the 1T mode is either stable or unstable, and the 2T mode is stable and Region IV where the 2T mode is unstable, the 1T mode is either stable or unstable, and the 1R mode is stable. Other possible regions, for example, where all three modes are unstable will

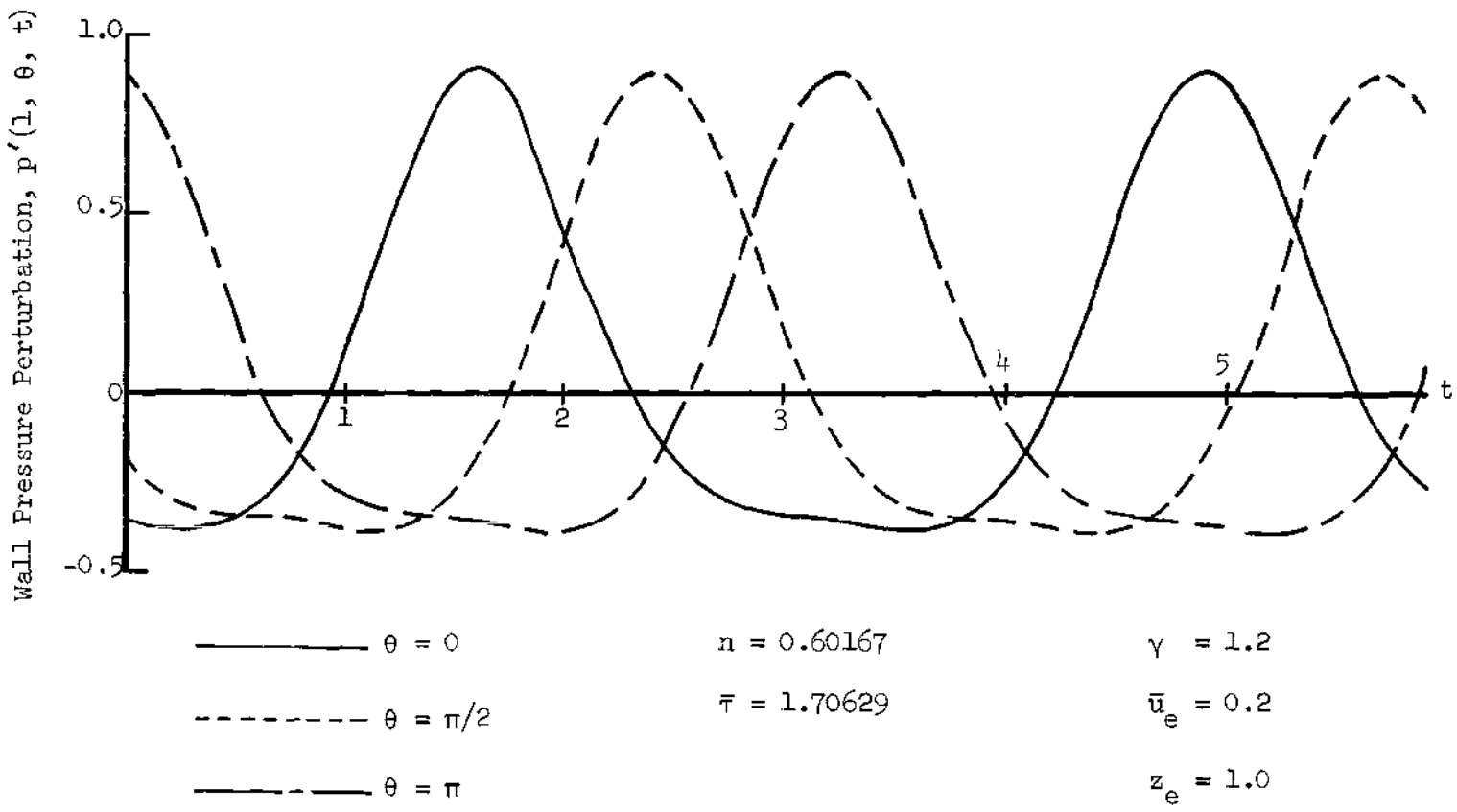

Figure 24. Time Dependence of the Wall Pressure Waveforms for Spinning 1T Oscillations.

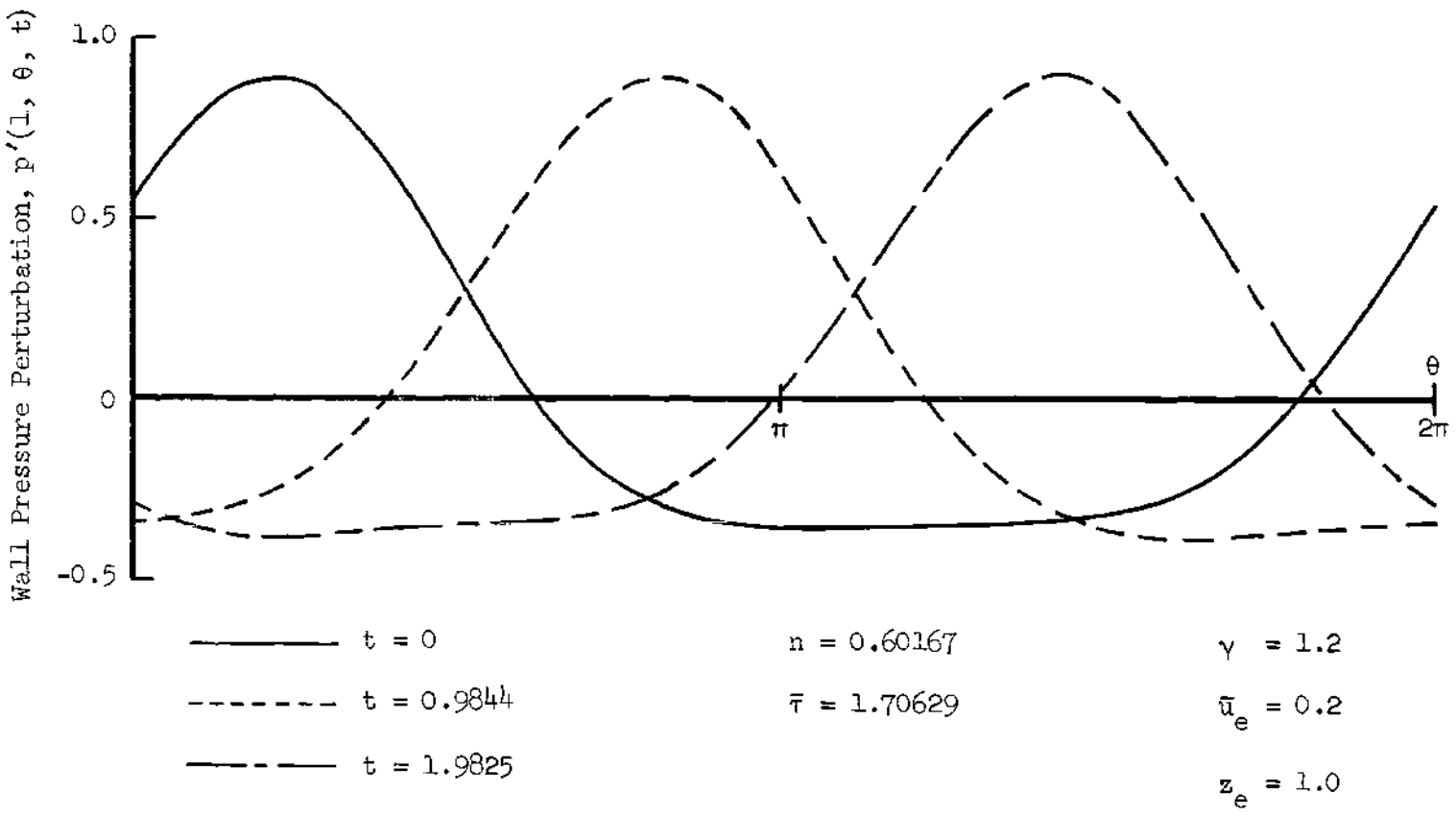

Figure 25. Angular Dependence of the Wall Pressure Waveforms for Spinning 1T Oscillations.

not be considered in this study.

Nonlinear Behavior in Region I: Stable Limit Cycles. Most of the results presented in this chapter are for engines whose operating parameters n and $\bar{\tau}$ fall within Region I of Fig. (16) for which stable limit cycles exist. For a number of points in this region an initial standing or spinning 1T disturbance was assumed and the computations were continued until a stable limit cycle was obtained. In contrast to the work of Mitchell[11] and Zinn[7], who considered points along a line normal to the neutral stability limit, these points were taken along lines of constant time-lag $\bar{\tau}$. The location of a point along such a line is specified by the vertical distance $\delta = n - n_o(\bar{\tau})$ from the neutral stability limit for the 1T mode. From this definition it is seen that positive values of δ indicate displacements into the linearly unstable region for the 1T mode.

For each of the points considered in this study several quantities of interest were calculated that characterize the limiting solution: (1) the amplitudes of all of the mode-amplitude functions, (2) the maximum and minimum pressure perturbation occurring in the chamber, and (3) the frequency of the pressure oscillation. Knowledge of the relative amplitudes of $A_{11}(t)$, $B_{01}(t)$, and $B_{21}(t)$ is useful in determining the importance of the various modes included in the series expansion. The maximum and minimum pressure perturbation occurring during a cycle are found at the chamber's outer wall ($r = 1$) and occur at a pressure anti-node for standing waves and at any angular position for spinning waves. The peak pressure perturbation provides a convenient measure of the amplitude of the final pressure oscillation. The frequency of the

pressure oscillation is equal to that of the fundamental mode (i.e. $A_{11}(t)$) and is easily determined from the numerical solution.

The dependence of the limit cycle pressure amplitude upon the combustion parameters n and $\bar{\tau}$ for standing wave oscillations is presented in Fig. (26) in the form of curves of peak pressure plotted against vertical displacement δ along lines of constant $\bar{\tau}$. For each of the values of $\bar{\tau}$ shown the limit cycle amplitude is zero at the neutral stability limit (i.e. $\delta = 0$) and increases as the operating point moves away from the neutral stability curve. In the range of $\bar{\tau}$ considered here larger amplitudes occurred (for equal displacement δ) for the larger values of $\bar{\tau}$.

The curves shown in Fig. (26) may be interpreted as neutral stability limits in an amplitude-displacement plane; one such plane exists for each value of $\bar{\tau}$. These curves separate initial disturbances which decay from those which grow, while along the curves the solutions are periodic (neutrally stable). All initial disturbances corresponding to points lying below and to the right of the curve are found to grow while in the region above and to the left of the curve all disturbances decay. The final amplitude attained by the disturbance is the value indicated by the curve for $\delta > 0$. If $\delta \leq 0$ the disturbances decay to zero amplitude. These results show therefore that it is impossible to trigger the 1T mode (at least according to results obtained by using the three mode expansion) in the range of $\bar{\tau}$ shown.

Alternate methods of presenting the results shown in Fig. (26) are given in Figs. (27) and (28). Figure (27) shows the dependence of the limit cycle peak pressure on $\bar{\tau}$ for points which lie along lines of

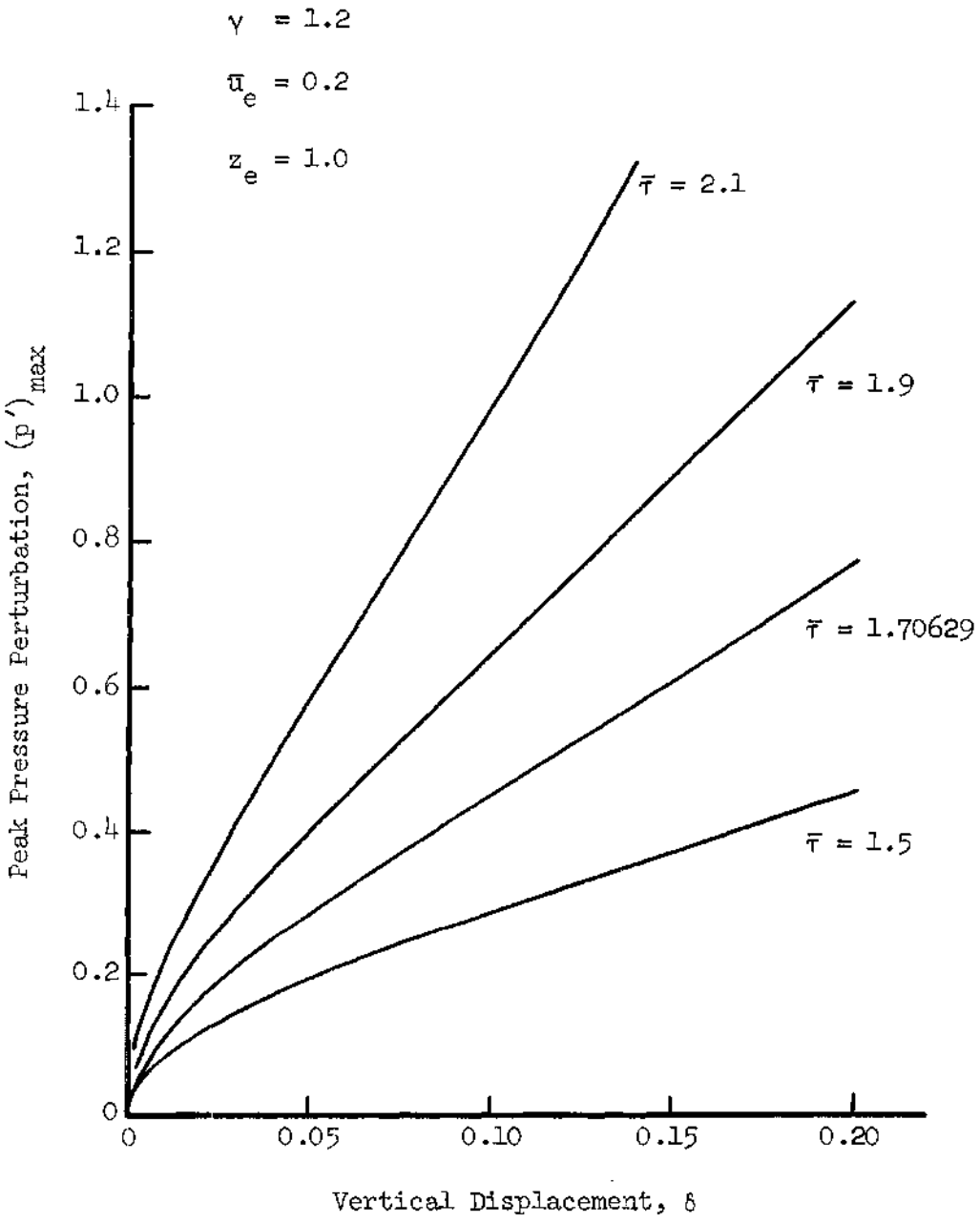

Figure 26. Dependence of the Limiting Pressure Amplitude Upon Combustion Parameters.

constant displacement δ from the neutral stability limit. These curves show clearly that the peak pressure increases with increasing $\bar{\tau}$ and δ. Curves of constant pressure amplitude are shown in Fig. (28) plotted on an $(n, \bar{\tau})$ coordinate system. The curve corresponding to zero amplitude is identical to the neutral stability curve calculated by linear theory. According to nonlinear theory the points of neutral stability (stable limit cycles) form a surface in a space formed by considering pressure amplitude as a third coordinate normal to the $(n, \bar{\tau})$ plane. The curves corresponding to finite values of the pressure amplitude are simply the level curves of this surface; they resemble the neutral stability curve and are shifted upward and to the right. It is easily seen from these curves that the limit cycle amplitude increases faster with increasing δ for large values of $\bar{\tau}$ than for small.

Curves similar to those of Fig. (26) can also be plotted for 1T spinning instability. These are shown in Figs. (29) and (30) where the limit cycle amplitude corresponding to standing and spinning type instabilities are compared. These curves reveal the interesting fact that in nearly all cases the spinning wave had the larger amplitude. This observation is in agreement with the well known result that spinning transverse modes are the most detrimental. It is interesting to note that for changes in the operating parameters along a curve of constant δ the amplitude of the spinning 1T mode decreases with increasing $\bar{\tau}$; exactly the opposite trend is observed for standing modes. For this reason the amplitudes of the standing and spinning forms differ less for the larger values of $\bar{\tau}$.

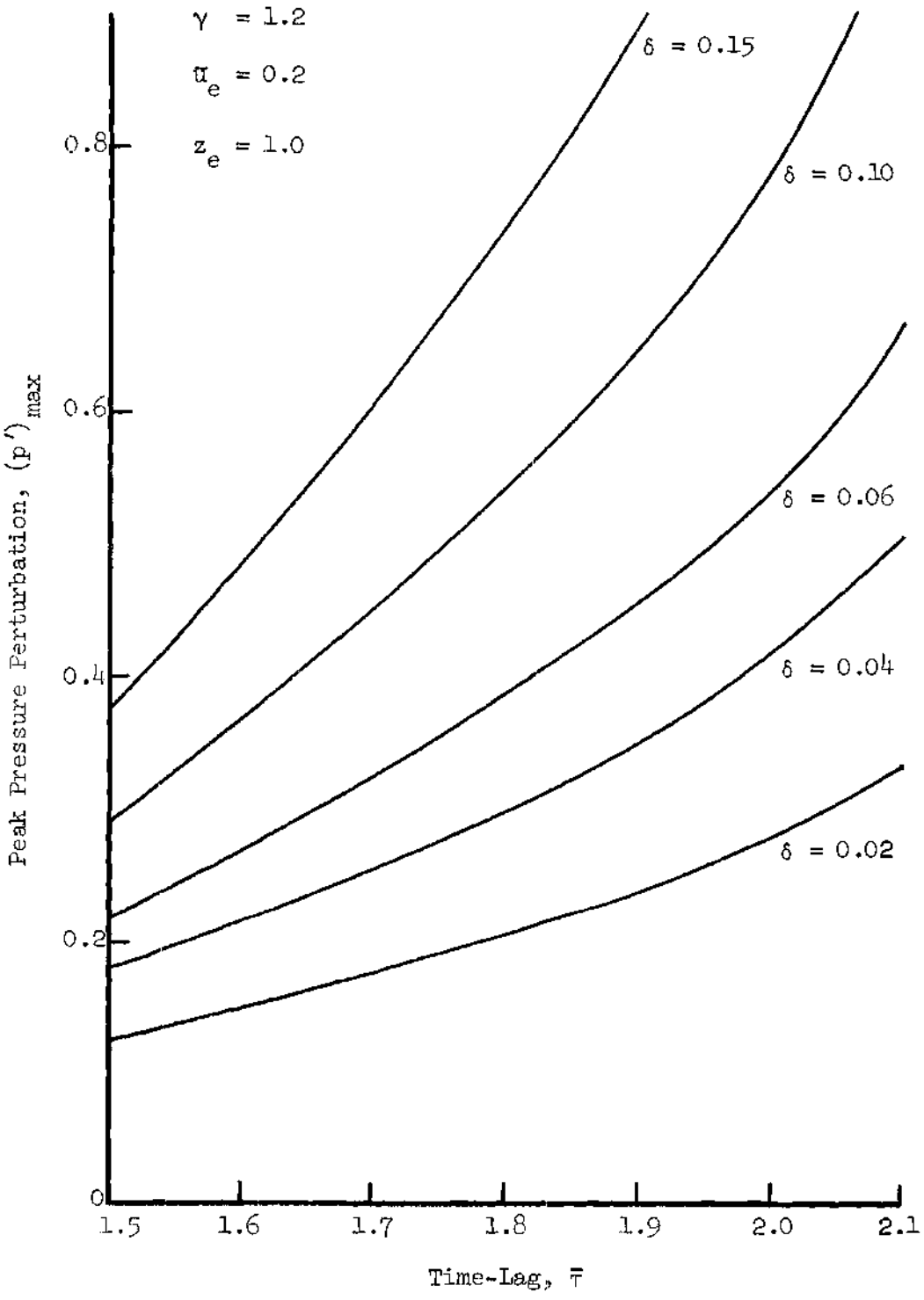

Figure 27. Dependence of Pressure Amplitude Upon Time-Lag along Lines of Constant Displacement.

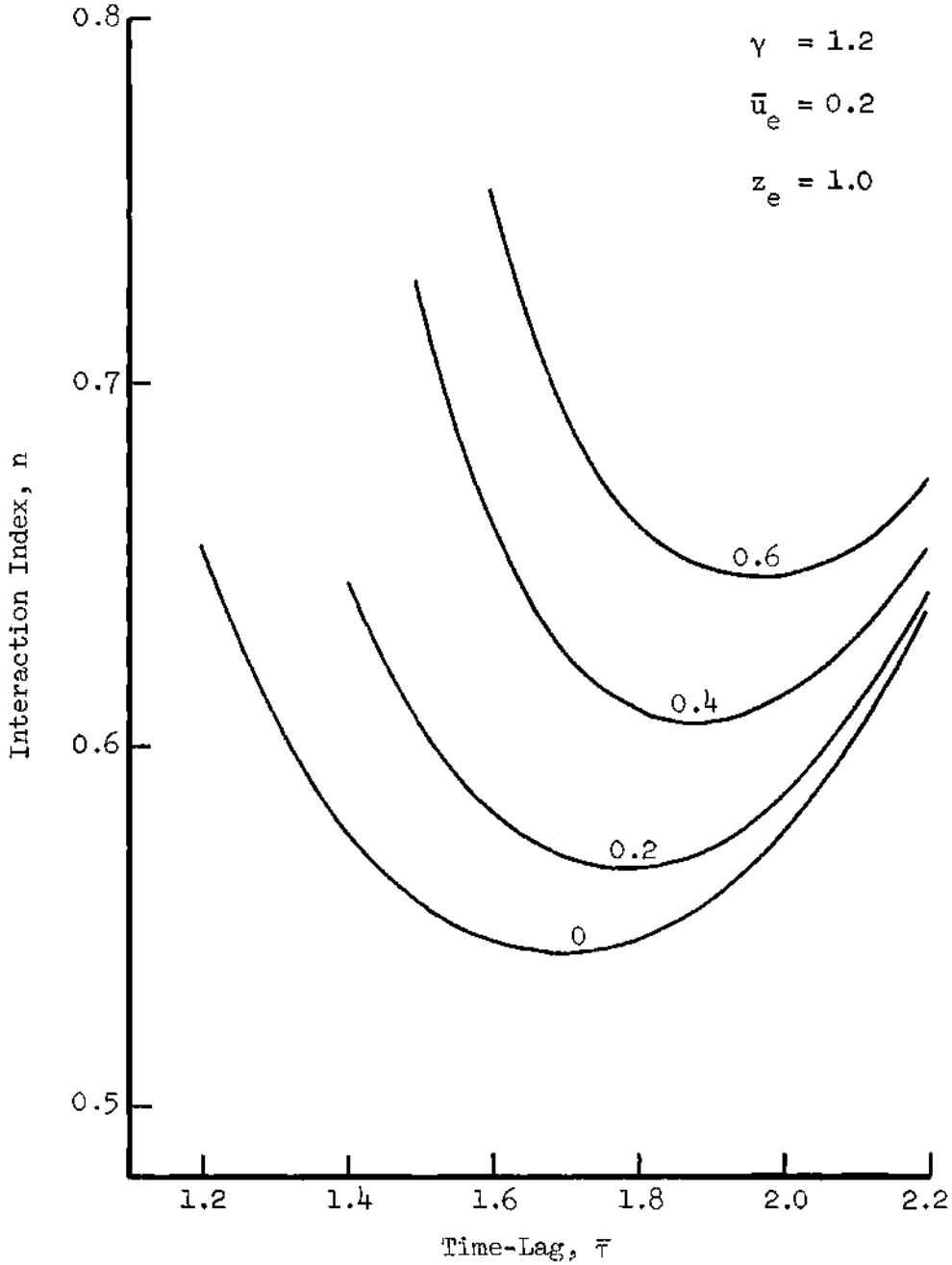

Figure 28. Stability Map with Curves of Constant Pressure Amplitude.

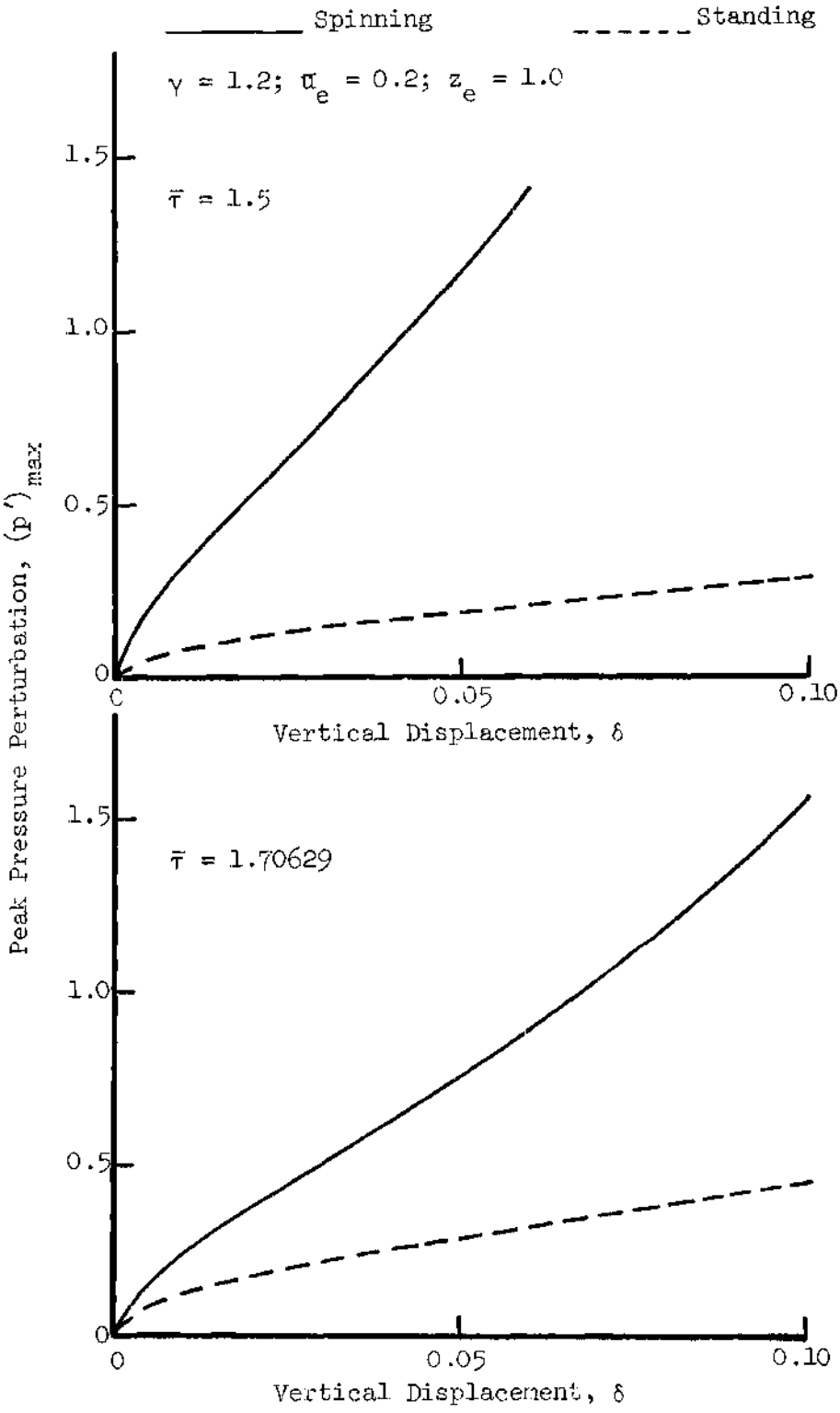

Figure 29. Comparison of the Limiting Pressure Amplitude for Spinning and Standing Type Instabilities.

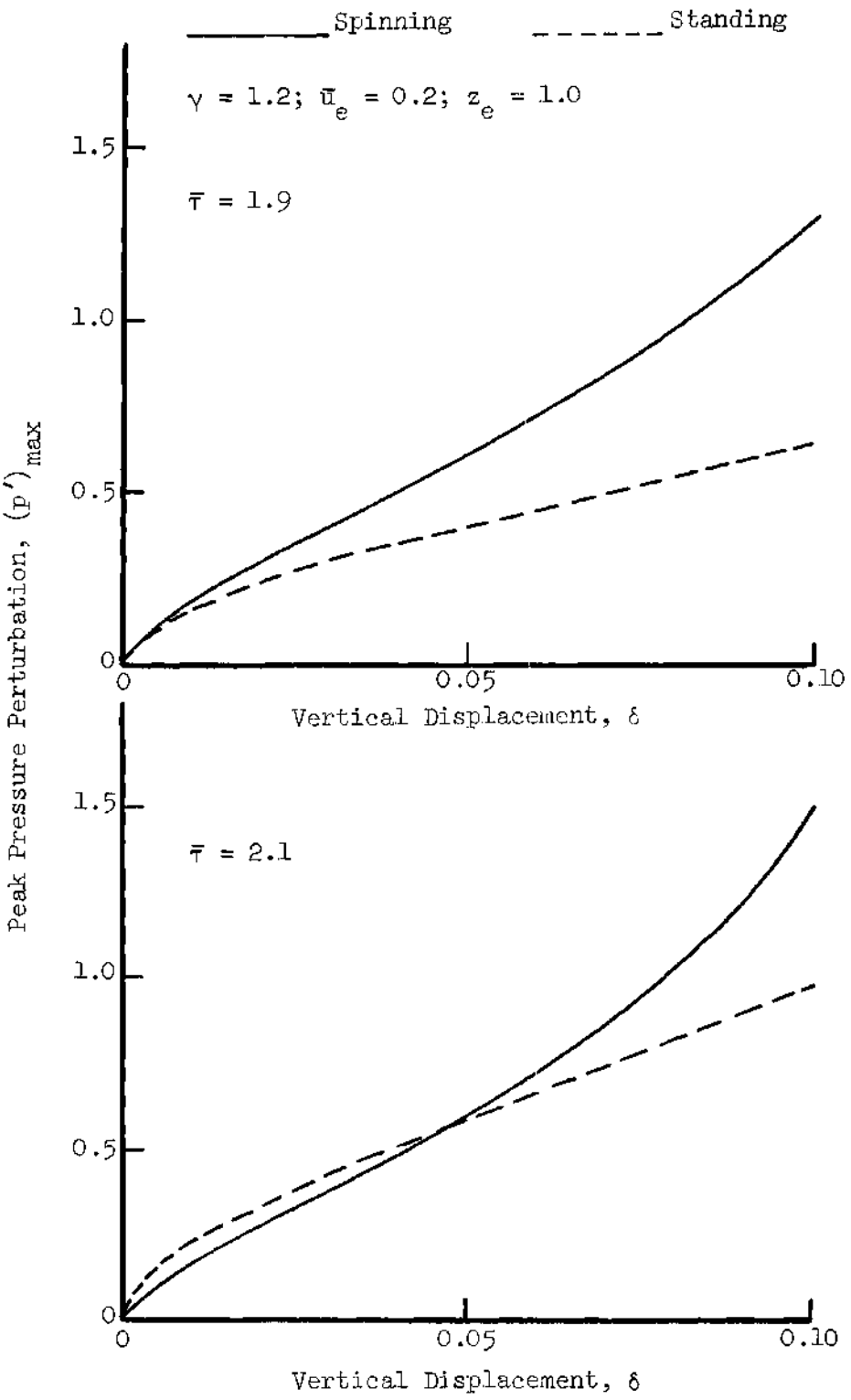

Figure 30. Comparison of the Limiting Pressure Amplitude for Spinning and Standing Type Instabilities.

Curves similar to those of Fig. (26) can be plotted for each of the mode amplitude functions occurring in the series expansion of $\tilde{\Phi}$. These are presented in Fig. (31) and reveal that, although the amplitude of the 1T standing mode varies with δ in the same parabolic manner as the peak pressure, the amplitudes of the 1R and 2T modes vary nearly linearly with δ. It is also observed that for moderate amplitudes of the 1T mode the amplitudes of the corresponding 1R and 2T modes are an order of magnitude smaller than that of the 1T mode. This indicates that in Region I of the $(n, \bar{\tau})$ plane the 1T mode dominates the behavior of the solution while the higher frequency modes limit the final amplitude attained and provide corrections to the shape of the pressure waveform. Also shown (see Fig. (32) are cross-plots of the amplitude of the higher frequency modes as a function of the amplitude of the fundamental mode. From these plots it is observed that the amplitudes of the 1R and 2T modes increase roughly as the square of the amplitude of the 1T mode, a behavior which is expected from the quadratic form of the nonlinear coupling terms in the governing differential equations. Similar curves are obtained for oscillations of the spinning form, however, in this case the 1R mode is not excited (values of $B_{01}(t)$ were less than 10^{-6}). It thus appears that a spinning mode cannot couple effectively with a mode which does not exhibit the spinning form (i.e. radial modes). This fact may provide a clue to the reason the spinning modes attain a higher amplitude, for if the radial mode does not appear one of the energy sinks for the 1T mode is missing.

The frequency of the pressure oscillation is found to be not only a function of n and $\bar{\tau}$ but also of the amplitude of the oscillation.

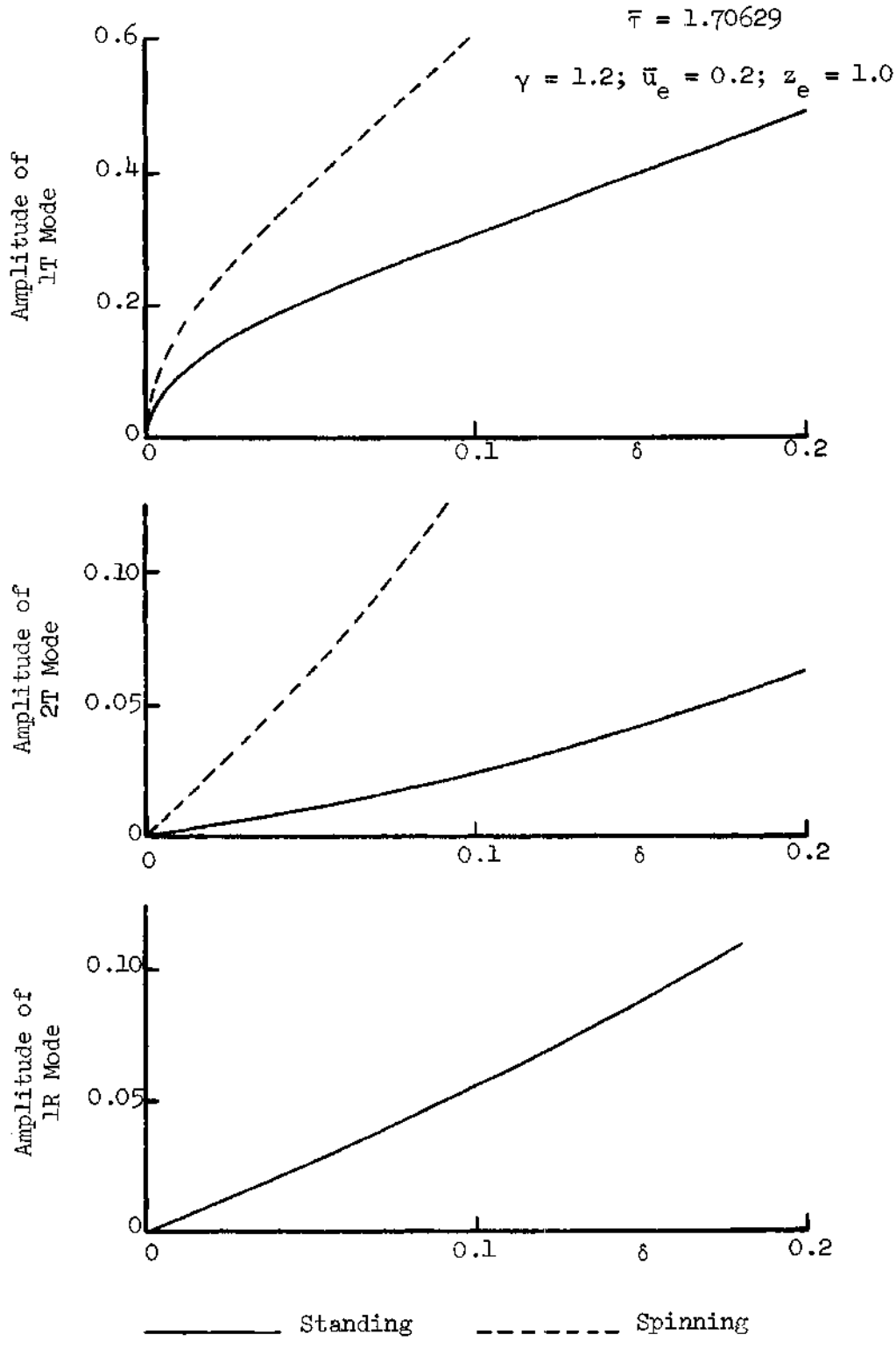

Figure 31. Dependence of the Amplitudes of the 1T, 2T, and 1R Modes Upon δ.

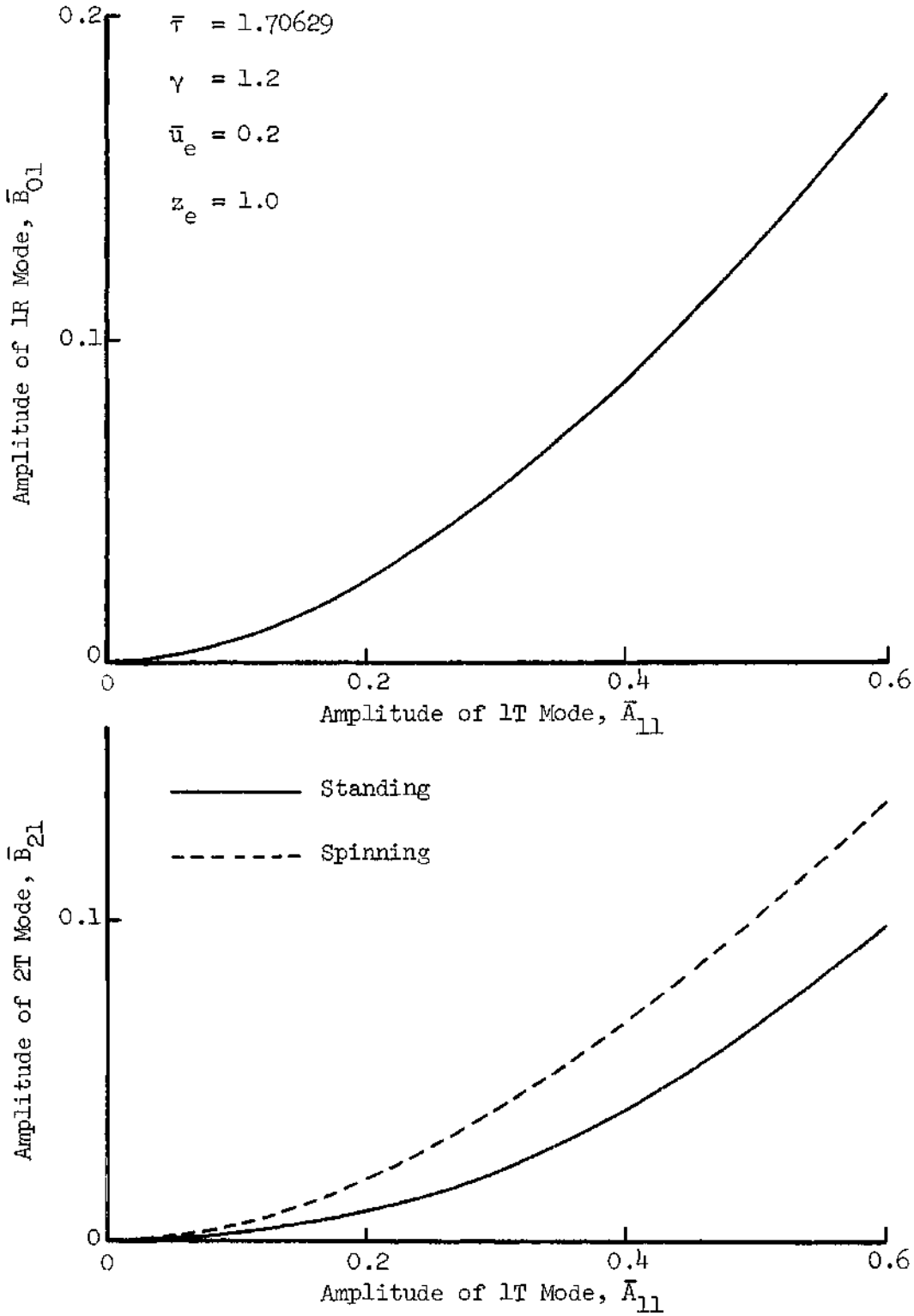

Figure 32. Dependence of the Amplitudes of the 2T and 1R Modes upon the Amplitude of the 1T Mode.

This dependence of the frequency upon the amplitude is characteristic of many nonlinear systems; one of the most familiar being the simple pendulum. In the fields of nonlinear acoustics and combustion instability such effects are predicted by Maslen and Moore[8], Mitchell[11], Zinn[7], and others. In Figs. (33) and (34) the dependence of the frequency upon the amplitude is shown for both standing and spinning instability along lines of constant $\bar{\tau}$. The displacement δ, of course, is not constant for one of these curves, because it increases as the amplitude increases. It is therefore meaningless to speak of the amplitude dependence of the frequency for fixed values of n and $\bar{\tau}$ since only one amplitude corresponds to a given point. These curves show that the frequency decreases with increasing amplitude for standing waves while the opposite behavior is observed for spinning instability. In both cases the limiting value of the calculated frequency as the amplitude approaches zero ($\delta \to 0$) is in agreement with that computed by linear theory. The largest observed departure of the frequency from the acoustic value $S_{11} = 1.84118$ amounted to only about six percent of S_{11} in agreement with experimental observation[2].

Effects of Length and Mach Number. In the studies which have just been discussed the effect of the combustion parameters n and $\bar{\tau}$ has been explored by computing the nonlinear solutions for various points in the $(n, \bar{\tau})$ plane while holding the other parameters fixed. It is now desired to evaluate the effect of the steady state velocity $\bar{u}_e$ (at the nozzle entrance) and the length to diameter ratio z_e upon the nonlinear stability characteristics of the combustor. For a few selected points in Region I of the $(n, \bar{\tau})$ plane periodic solutions were

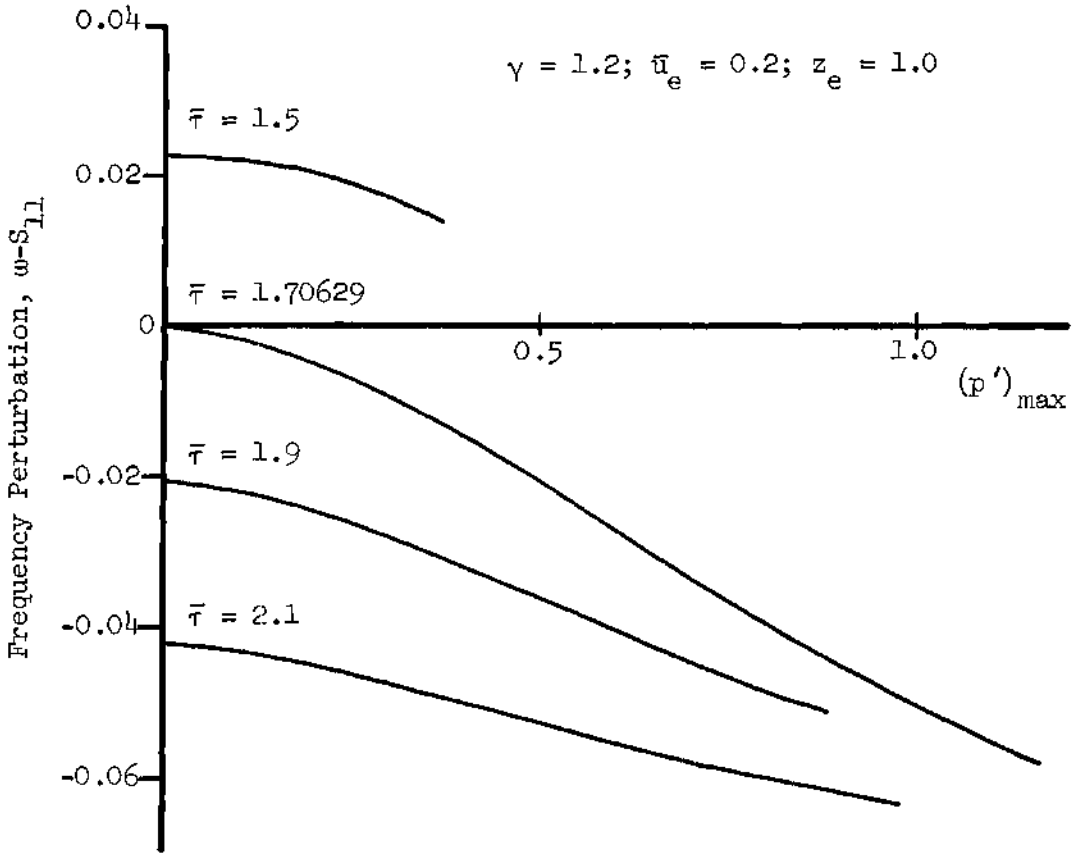

Figure 33. Dependence of the Frequency upon the Amplitude for Standing Type Instabilities.

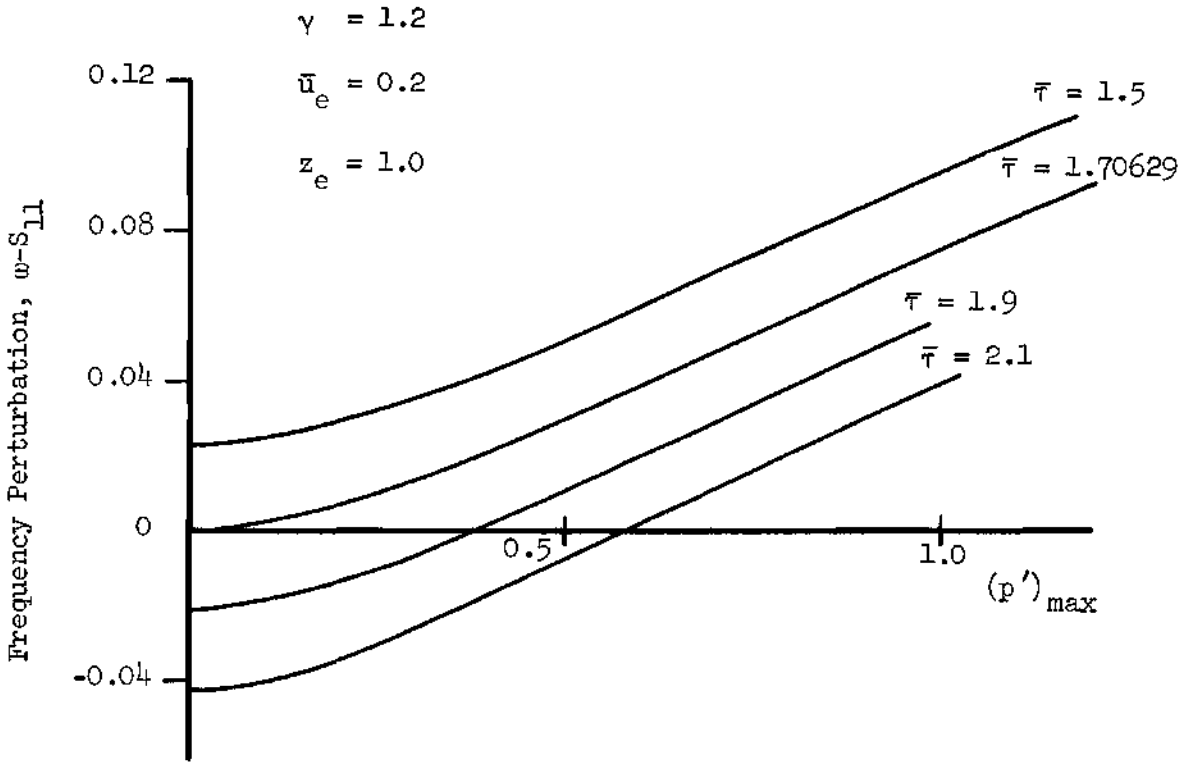

Figure 34. Dependence of the Frequency upon the Amplitude for Spinning Type Instabilities.

computed for various values of $\bar{u}_e$ and z_e. These parameters appear in the governing differential equations as the ratio $\bar{u}_e/z_e$ which is an average steady state velocity gradient. Considerable computation time was saved by varying only this ratio, for once curves of pressure amplitude as a function of $\bar{u}_e/z_e$ are obtained the individual effects of changes in length or Mach number are easily determined.

The effect of the parameter $\bar{u}_e/z_e$ upon the final amplitude of standing 1T oscillations is presented in Fig. (35) where the displacement δ from the neutral stability limit is held constant. The value of n therefore varies along each of these curves as n_o is a function of $\bar{u}_e/z_e$. It is seen from these curves that for most values of the time-lag $\bar{\tau}$ an increase in the ratio $\bar{u}_e/z_e$ resulted in an increase in the final magnitude of the pressure amplitude. An exception to this trend occurs for the smaller values of $\bar{\tau}$ (see curve for $\bar{\tau} = 1.5$) where for low values of $\bar{u}_e/z_e$ the pressure amplitude decreased slightly with increasing values of this ratio and after reaching a minimum value it increased thereafter. The effect of varying the Mach number with the length held constant is described by curves very similar to those of Fig. (35). On the other hand the effect of changes in length for fixed exit Mach number are given by curves which are the inverse of those given in Fig. (35). Thus the limiting pressure amplitude decreases with increasing length as shown in Fig. (36). These results show that in most cases the nonlinear stability characteristics of the engine with respect to the 1T mode can be improved by decreasing the Mach number at the nozzle entrance or by increasing the length to diameter ratio. The latter effect is in agreement with the well known result

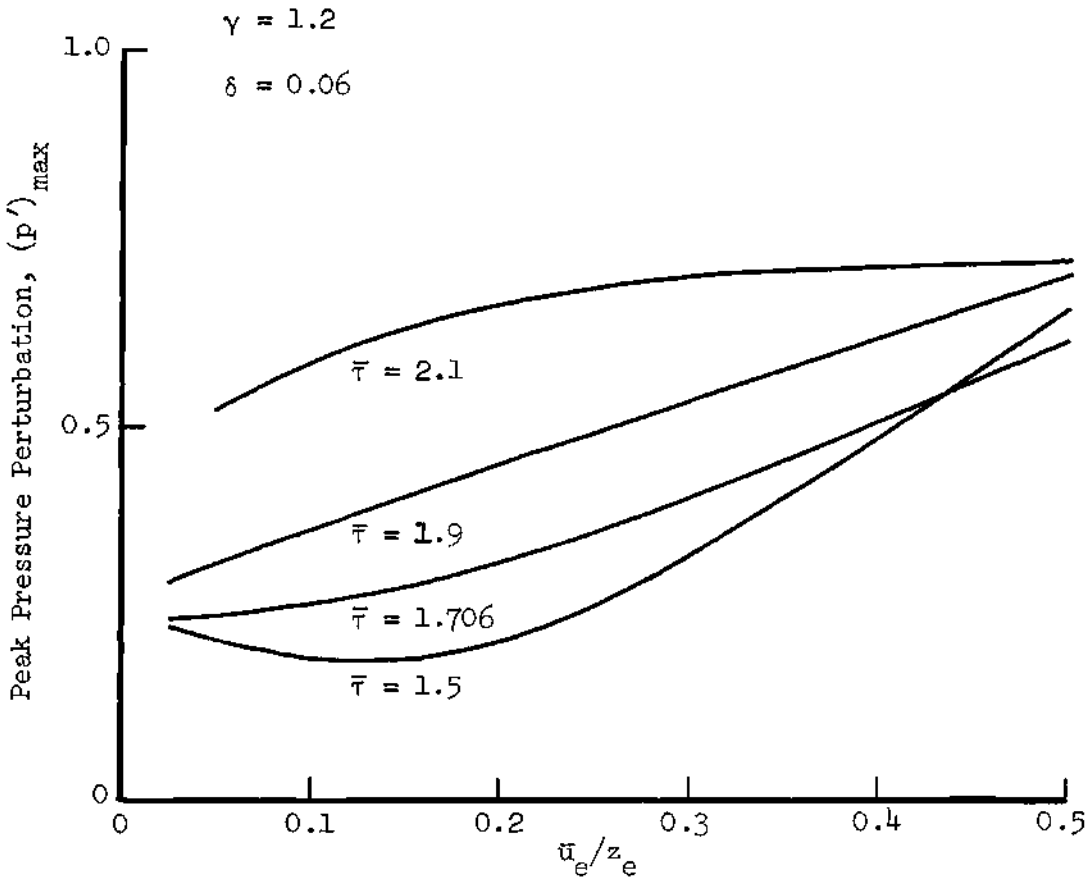

Figure 35. Dependence of the Limiting Pressure Amplitude upon the Ratio $\bar{u}_e/z_e$.

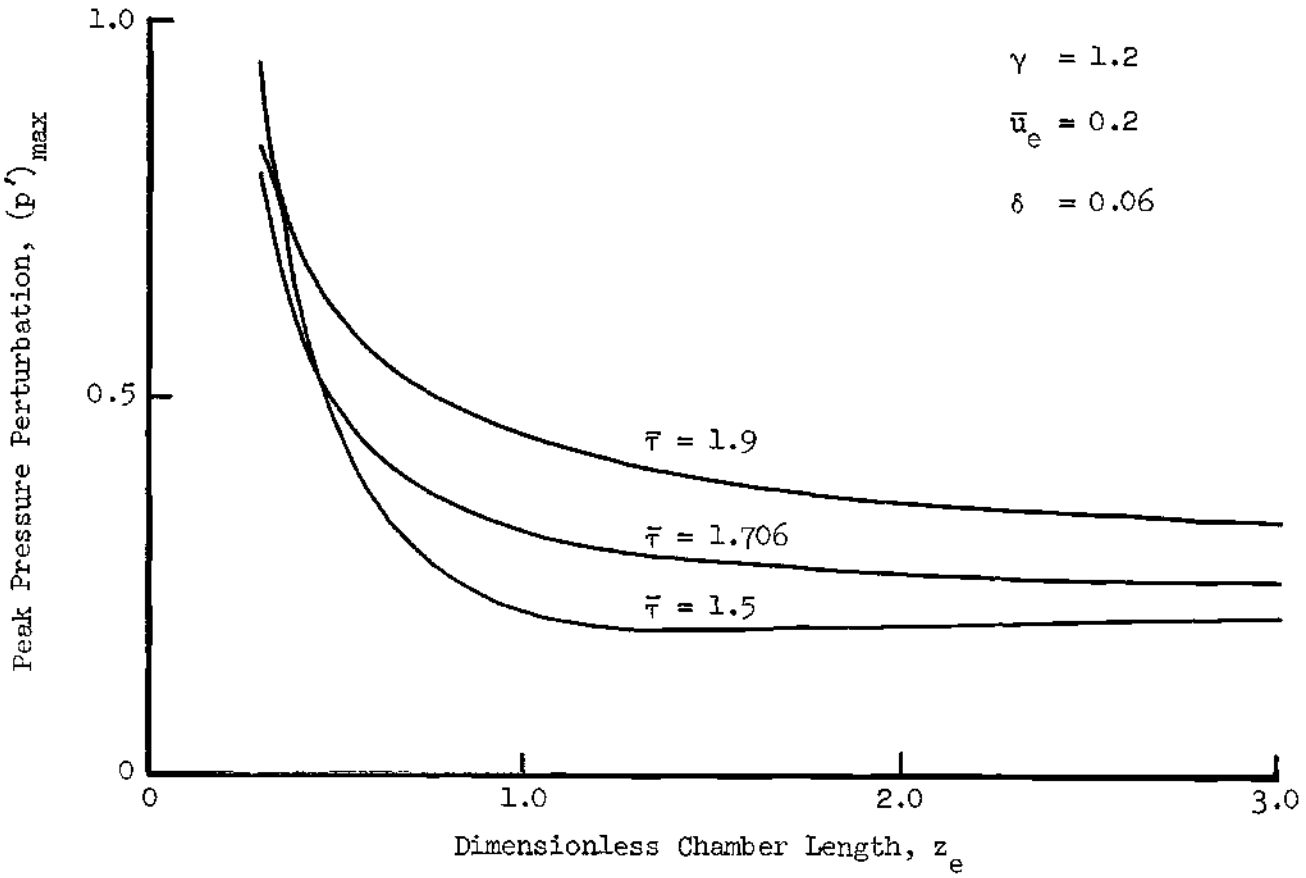

Figure 36. Effect of Chamber Length upon the Limiting Pressure Amplitude.

that short chambers are more prone to transverse mode instability.

An interesting special case occurs in the limit of zero Mach number. As can be seen from the differential equations and deduced from physical considerations the effects of the combustion process, mean flow, and the nozzle disappear when the steady state velocity vanishes. The differential equations then reduce to those governing finite amplitude transverse waves in a circular cylinder without flow, which is the case treated by Maslen and Moore[8]. Since there is no driving or damping mechanism the limit cycle behavior is lost; the amplitude and waveform of the solution depends upon the initial conditions. This behavior is verified by the numerical solutions for $\bar{u}_e = 0$, however, the solutions are not strictly periodic even though they are neutrally stable. The amplitudes of the various modes included in the assumed series expansion are found to vary slowly in amplitude due to nonlinear coupling between these neutrally stable modes. This amplitude modulation is negligible however for small amplitude oscillations.

Behavior in Region II. In Region II of the $(n, \bar{\tau})$ plane all of the modes included in the approximate solution are linearly stable. For a number of points in this region initial disturbances of various amplitudes were assumed and the subsequent behavior of the various modes was computed. In all cases initial 1T disturbances of moderate amplitude were found to decay; however, if the initial amplitude was very large the waves would grow rapidly and apparently without limit. While it is believed that the behavior predicted for moderate amplitude oscillations is correct there exist valid reasons that cast doubts about

the applicability of this "triggering limit". For instance the amplitude for triggering is so large that the moderate amplitude assumption of the second order theory is violated; the third order terms that were omitted from this analysis are no longer negligible. It is hardly surprising that these "triggering limits" exhibit characteristics that are contrary to those expected from physical intuition. For example this triggering behavior was observed for the special cases of $n = 0$ and $\bar{u}_e = 0$; in both cases the unsteady combustion mass sources vanish and no amplification of the pressure oscillations should occur. These "triggering limits" also occur for points in Region I at an amplitude much greater than that of the stable limit cycle. Such behavior has not been observed experimentally. It appears, therefore, that these "triggering limits" are either a characteristic of the approximate differential equations or they are a result of numerical instability and should be disregarded.

Regions III and IV. In the next phase of the investigation the same three-mode expansion was used to investigate the behavior of the engine for ranges of n and $\bar{\tau}$ where either the 1R or 2T modes were linearly unstable but the 1T mode could be either stable, neutral, or unstable. The results of this study can be best described by considering points C, D, and E in Region III of Fig. (16). Calculations for point C, where the 1R mode is linearly unstable and the 1T and 2T modes are stable, showed that an initial 1T disturbance develops into a pressure wave that has a modulated amplitude and oscillates with a frequency close to that of the 1R mode (see Fig. (37a)). As one moves to points D and E the waveform and the frequency of the resulting

oscillation change as shown in Figs. (37b) and (37c). At point D the 1T mode is neutrally stable; its interaction with the 1R mode produces a highly modulated waveform which has some of the characteristics of both modes. In contrast to points C and D the oscillation corresponding to point E where both 1R and 1T modes are unstable is very regular with a frequency close to that of the 1T mode, and the waveforms are similar to those computed in Region I. Pressure amplitudes in these regions are generally larger than those in regions where only the 1T mode is unstable.

The importance of nonlinear coupling becomes increasingly evident when the unstable behavior at point C is analyzed. At this point the 1T mode is linearly stable; nevertheless the introduction of an initial 1T disturbance resulted in a finite amplitude instability. The reasons for this behavior become clear as one carefully observes the development with time of the unknown amplitudes. The calculations show that initially the 1T mode starts decaying and at the same time, through nonlinear coupling, it transfers energy to the other modes present in the series solution. This energy transfer initiates oscillations and growth of the 1R mode which is linearly unstable for the given values of n and $\bar{\tau}$. Once the 1R mode attains a sufficient amount of energy it starts transferring energy back to the 1T and 2T modes. This "back-and-forth" mode-energy transfer results in growth of the amplitude of the 1T mode and it also explains the observed modulation of the wave amplitude. This behavior also emphasizes the need to use nonlinear theories in engine design.

The behavior characteristic of point C should not be confused

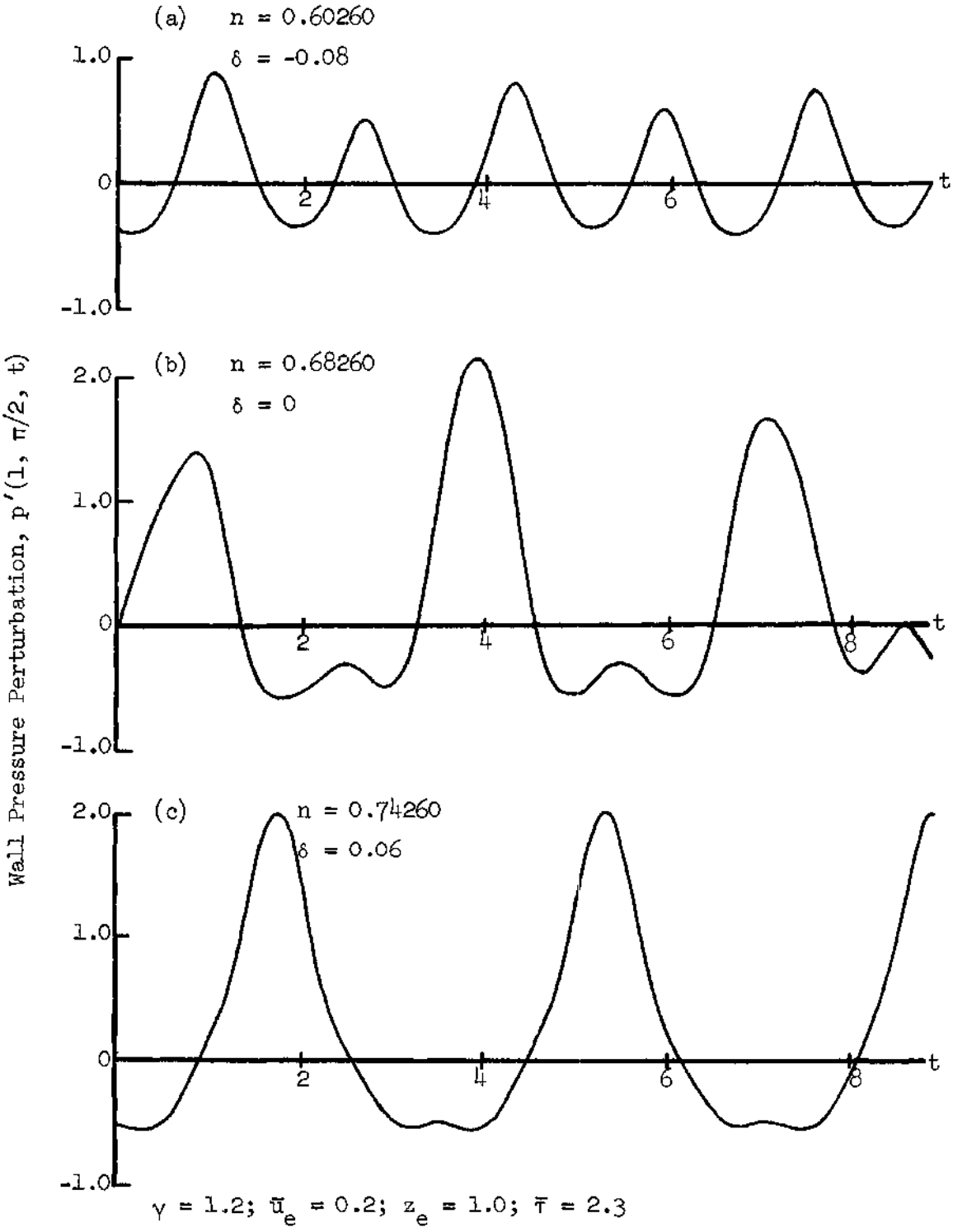

Figure 37. Representative Wall Pressure Waveforms for an Engine Operating in Region III.

with the triggering phenomenon. Triggering occurs only if the amplitude of the initial disturbance is greater than a certain threshold amplitude, otherwise all disturbances decay. At point C, however, instability develops no matter how small the initial amplitude of the 1T mode, because the unstable 1R mode is excited. Even if the amplitude of the 1T mode is so small that coupling with the unstable mode is too weak to drive the 1T mode, a stable limit cycle of the 1R mode will eventually result. These results seem to indicate that a true triggering behavior does not occur in a region of the $(n, \bar{\tau})$ plane where one or more of the modes present in the assumed series expansion are linearly unstable.

The dependence of the final amplitudes of the pressure and mode-amplitudes upon the displacement from the 1T neutral stability limit along a line of constant $\bar{\tau}$ in Region III is shown in Figs. (38) and (39). Since the pressure peaks vary greatly in height, a measure of the pressure amplitude is taken to be the arithmetic average of a large number of pressure peaks. Similar averages are used to describe the amplitudes of $A_{11}(t)$, $B_{01}(t)$, and $B_{21}(t)$. Also shown is the maximum pressure peak of the modulation pattern which recurs at intervals of several cycles. When the pressure peaks are of constant height as at point E, the average and maximum pressures agree.

When the point under consideration is just above the 1R neutral stability limit (indicated in Figs. (38) and (39) by the vertical dashed line) the amplitude of $B_{01}(t)$ is an order of magnitude greater than that of the other modes and the pressure oscillations resemble the 1R mode. As the displacement into the region of 1R instability increases the 1R and 1T modes become of equal importance and the pressure

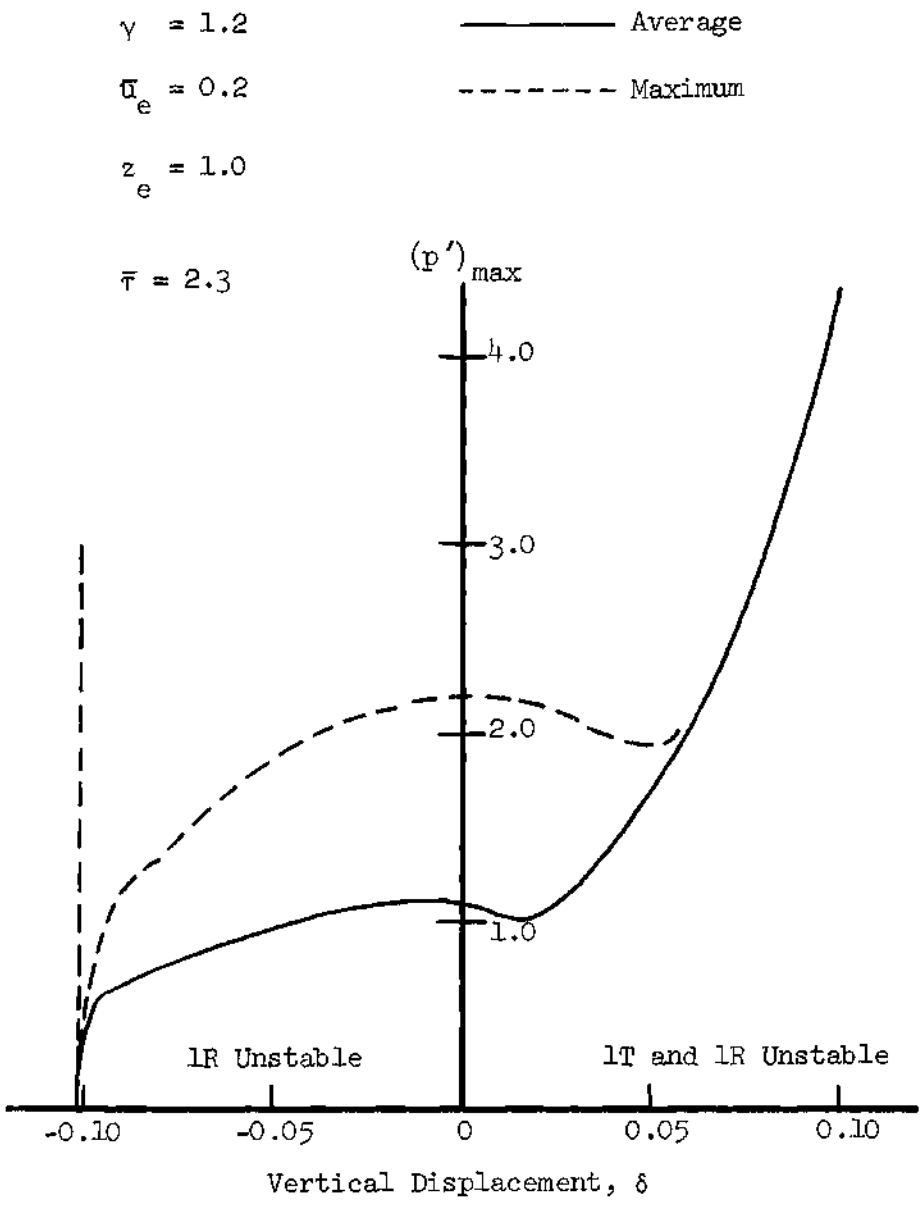

Figure 38. Dependence of the Pressure Amplitude upon δ along a Line of Constant $\bar{\tau}$ in Region III.

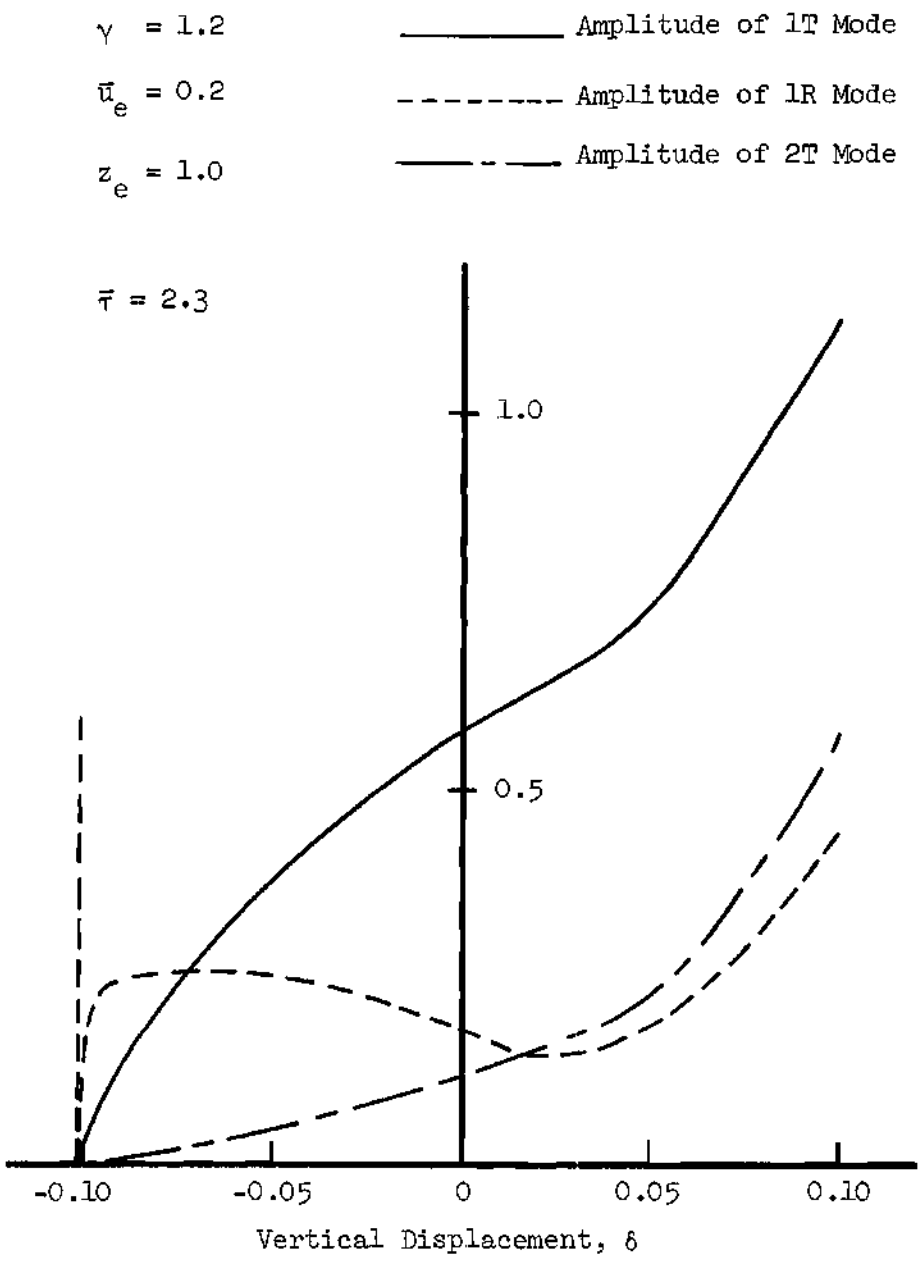

Figure 39. Dependence of the Amplitudes of the 1T, 2T, and 1R Modes upon δ along a Line of Constant $\bar{\tau}$ in Region III.

peaks exceed unity. Further increases in pressure amplitude with increasing δ are slight until the 1T mode becomes unstable ($\delta > 0$). For $\delta > 0.06$ the pressure waveforms are very regular but the amplitude is more than twice the steady state chamber pressure. For such large amplitudes the moderate amplitude assumption inherent in the second order theory is violated, therefore the accuracy of these solutions is open to question.

Results similar to those predicted for Region III were obtained for Region IV where the 2T mode is linearly unstable, the 1T mode is either stable or unstable, and the 1R mode is stable. Stable limit cycles of modulated waveform were also calculated in this region, but their amplitude was generally larger than that observed in Region III.

One-Mode Series Expansion (Radial Mode)

The results obtained with the aid of the three mode series expansion indicate that the second order theory cannot predict triggering of the 1T mode, at least for amplitudes within the realm of applicability of the theory. Based on available numerical data and from the works of Sirignano[10] and Zinn[7], it may be concluded that this limitation of the second order theory is due to the lack of self-coupling terms involving the 1T mode in the approximate differential equations which govern the behavior of the amplitudes of the modes. It appears that the controlling second order nonlinear mechanism is the transfer of energy between modes which can limit the amplitude of 1T oscillations in the linearly unstable region of the $(n, \bar{\tau})$ plane but cannot cause triggering in the linearly stable region. A self-coupling term does appear in the equation governing the 1R mode, but when the 1T

mode is present the effect of this term is overpowered by coupling with the 1T mode.

To isolate the effects of self-coupling from those of coupling with other modes an expansion consisting only of the 1R mode was considered. This expansion and the resulting differential equation are given by Eqs. (239) and (240) respectively. As seen from Eq. (240) only a single nonlinear term of the self-coupling form is present. To determine if self-coupling can play a role in the development of triggered instability numerical calculations were made for values of n and $\bar{\tau}$ in the neighborhood of the 1R mode neutral stability limit (see Fig. (40)). The results of this investigation were encouraging, for indeed triggering limits were obtained for the 1R mode.

Characteristics of the Stable and Unstable Limit Cycles. The nonlinear behavior of the 1R mode is best illustrated by considering the growth or decay of initial 1R disturbances of various sizes for a fixed point in the $(n, \bar{\tau})$ plane. In each case the form of the initial disturbance is given by Eqs. (242). The results of this study are shown in Fig. (41) for point A of Fig. (40) which is in the linearly stable region. The time evolution of the 1R mode is presented on an amplitude-time plot in which the ordinate $\bar{B}_{01}$ is the amplitude of $B_{01}(t)$ and the time is measured in units of the oscillation period. In this case an unstable limit cycle or triggering limit was found with an amplitude $\bar{B}_{01} = 0.55$ as shown by the broken horizontal line. An initial disturbance of slightly smaller amplitude ($\bar{B}_{01} = 0.53$) was found to decay as shown by the lower curve of Fig. (41). An initial disturbance of amplitude slightly larger than the critical value ($\bar{B}_{01} = 0.57$) will

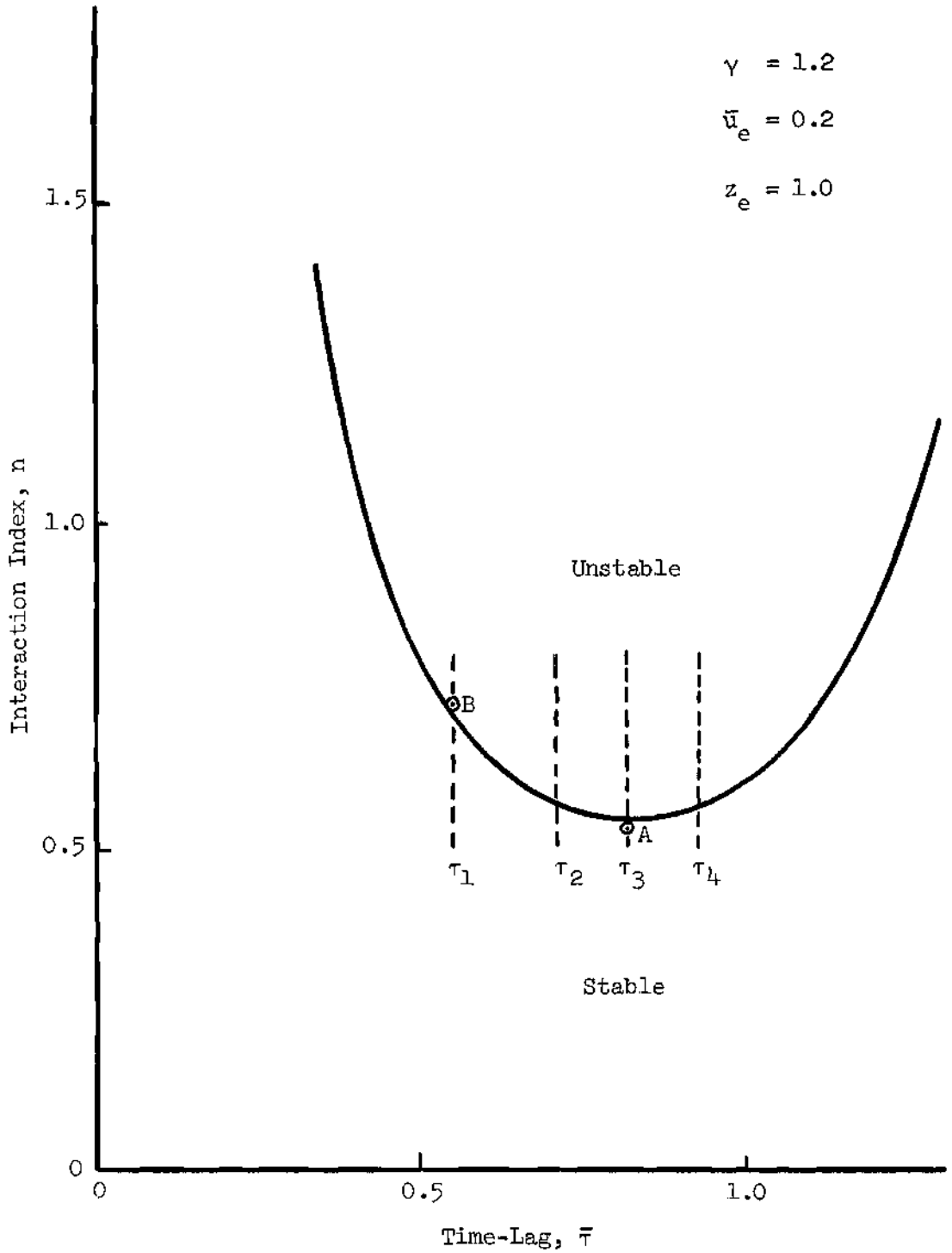

Figure 40. Linear Stability Limit for the First Radial Mode.

grow and eventually attain a stable limit cycle of very large amplitude. If the initial wave shape, frequency, and amplitude are exactly those corresponding to the unstable limit cycle the oscillation should remain neutral, however the slightest error in specifying the initial conditions will result in oscillations which either decay or grow. The triggering amplitude is calculated numerically by an iterative process in which the initial amplitude is varied until a solution is obtained which does not grow or decay during an initial time interval (of about 100 cycles).

Wall pressure waveforms and the time dependence of the mode-amplitude function $B_{01}(t)$ are shown for both stable and unstable limit cycles in Figs. (42) and (43). Only within very narrow regions in the $(n, \bar{\tau})$ plane were the calculated amplitudes within the limits imposed by the second order theory, therefore the waveforms for an unstable limit cycle are shown in Fig. (42) for a point between point A of Fig. (40) and the neutral stability limit. The waveforms for the stable limit cycle are given for point B in the linearly unstable region. In both cases the mode-amplitude function is nearly sinusoidal and the pressure perturbation exhibits peaked waveforms similar to those obtained for the 1T mode. It should be noted that for radial modes the pressure is independent of angular position and the maximum pressure occurs at the axis of the chamber rather than at the wall. For both stable and unstable limit cycles the frequency of the oscillation was found to be somewhat smaller than that of the acoustic 1R mode and decreased with increasing amplitude.

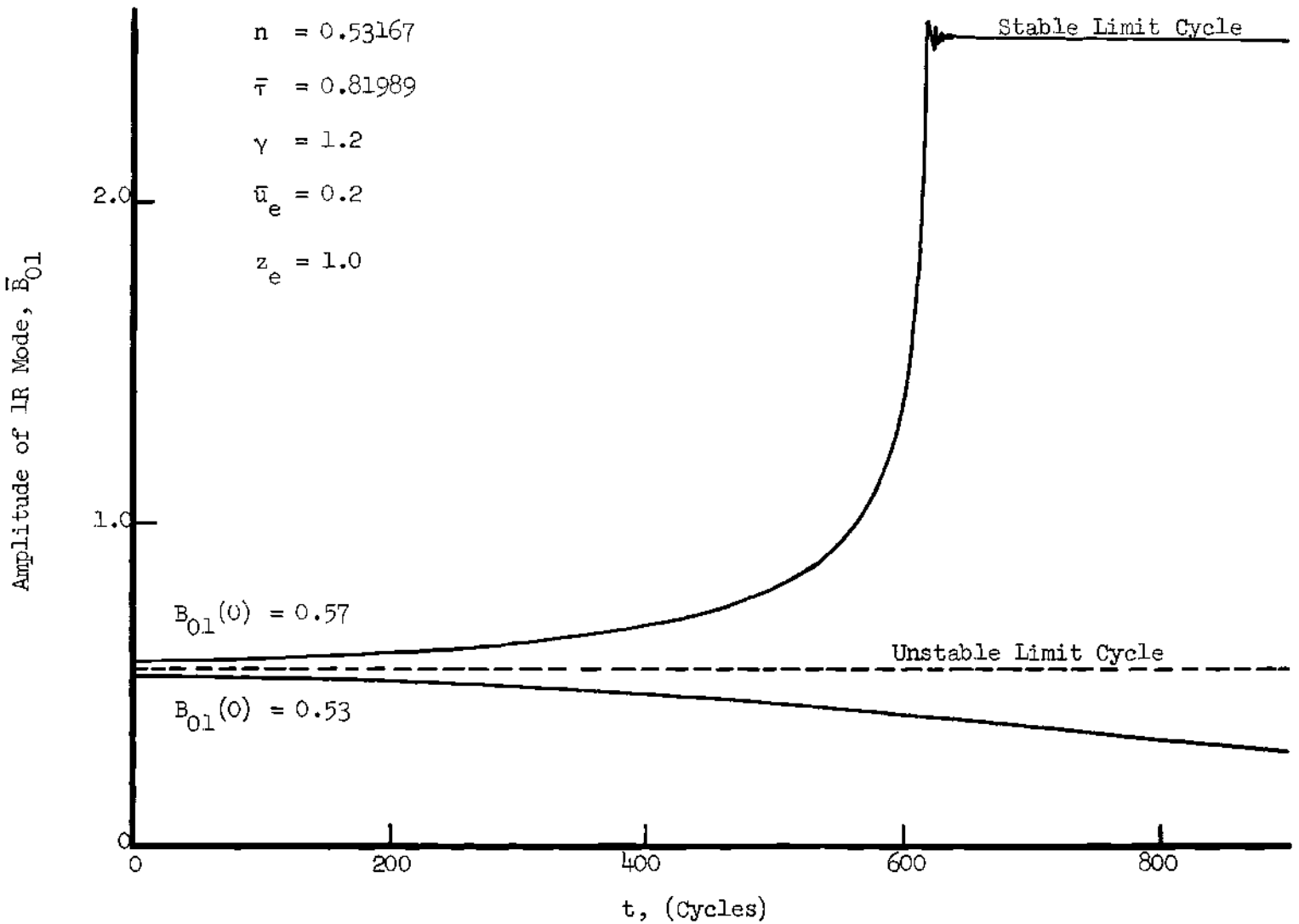

Figure 41. Time Histories of Initial 1R Disturbances in the Neighborhood of an Unstable Limit Cycle.

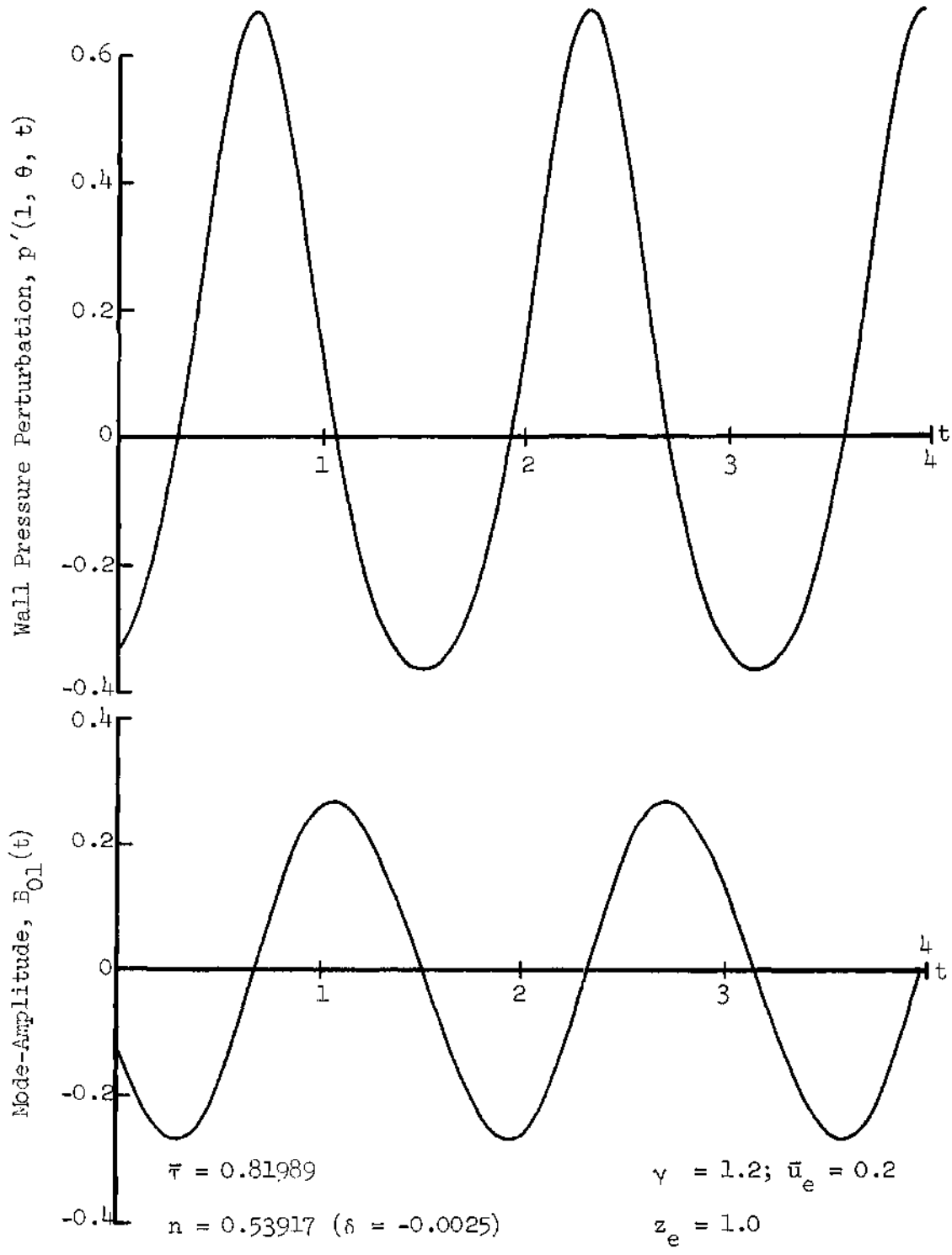

Figure 42. Wall Pressure Waveform and Mode-Amplitude Function for the 1R Mode at an Unstable Limit Cycle.

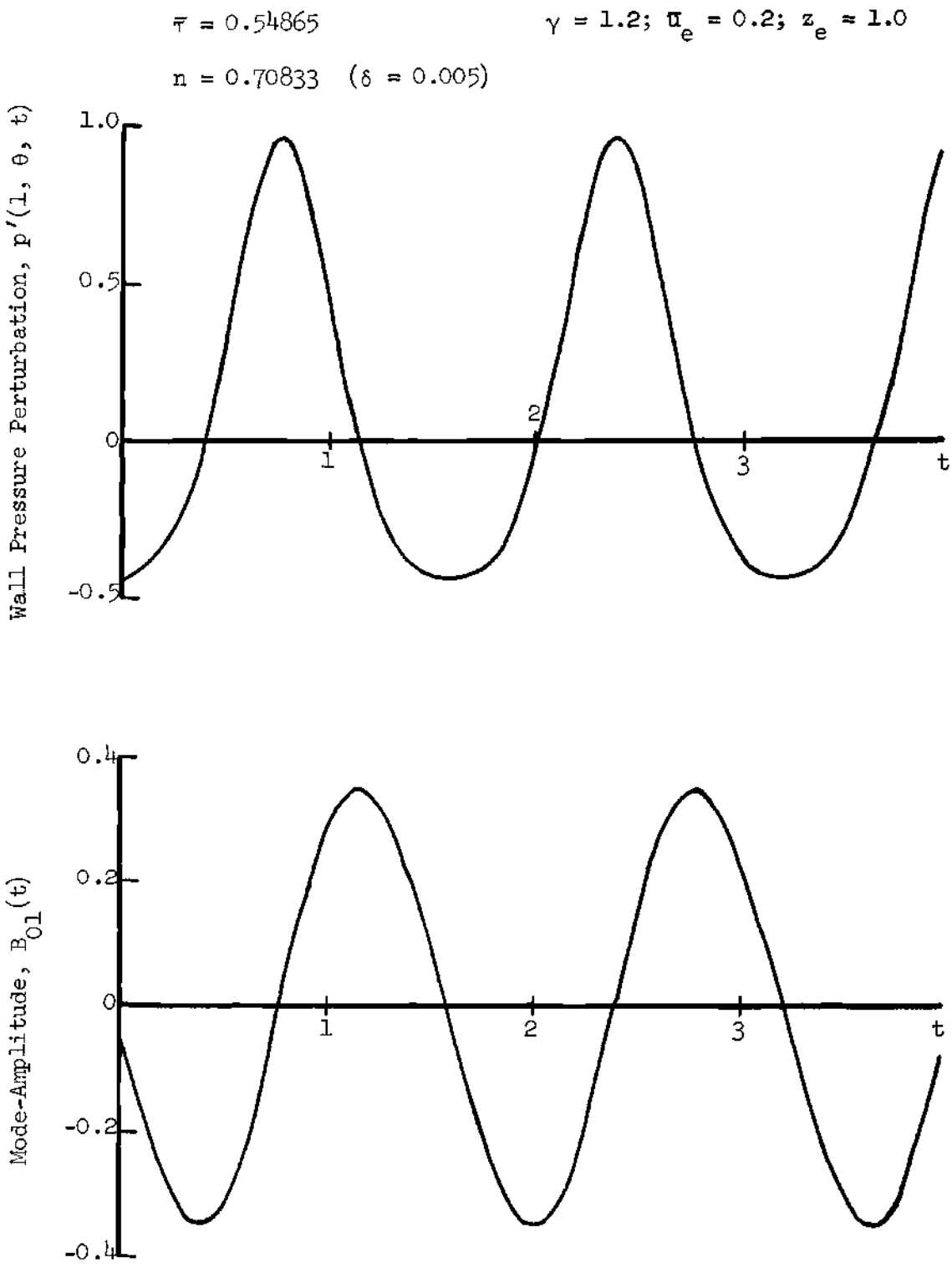

Figure 43. Wall Pressure Waveform and Mode-Amplitude Function for the 1R Mode at a Stable Limit Cycle.

Dependence Upon Combustion Parameters. In order to determine the influence of the engine parameters n and $\bar{\tau}$ upon the nonlinear behavior of the 1R mode, numerical calculations were performed for selected points lying along lines of constant $\bar{\tau}$. The results of this study are presented in Figs. (44) through (46) as curves on an amplitude-displacement plane. For a given value of $\bar{\tau}$ each point in this plane represents an oscillation of given amplitude (measured by $\bar{B}_{01}$) occurring at a given displacement δ from the neutral stability limit. The curves divide the amplitude-displacement plane into two regions. All points to the right of the curve represent disturbances which grow, while points to the left represent oscillations which decay. Along the curves the oscillations are neutral, but these solutions may be either stable or unstable with respect to small changes in amplitude. In these figures stable limit cycles are represented by solid curves and the unstable limit cycles are depicted as dashed curves.

In Fig. (44) is shown the behavior along the line $\tau = \tau_1$ (see Fig. (40)) for which no triggering is observed. In this case finite amplitude periodic oscillations were observed only in the linearly stable region. The limiting amplitude is seen to vary with increasing δ in a manner very similar to that obtained for the 1T mode. For larger values of $\bar{\tau}$ (i.e. $\bar{\tau} = \tau_2$ and $\bar{\tau} = \tau_3$) the shape of the curves is quite different as shown in Fig. (45); here finite amplitude periodic oscillations are obtained in the linearly stable region. These curves exhibit vertical tangents at the neutral stability limit $\delta = 0$ and at a point in the linearly stable region $\delta = \delta_t$. For $\delta \leq \delta_t$ there are no periodic solutions, all oscillations decay, and the engine is said to

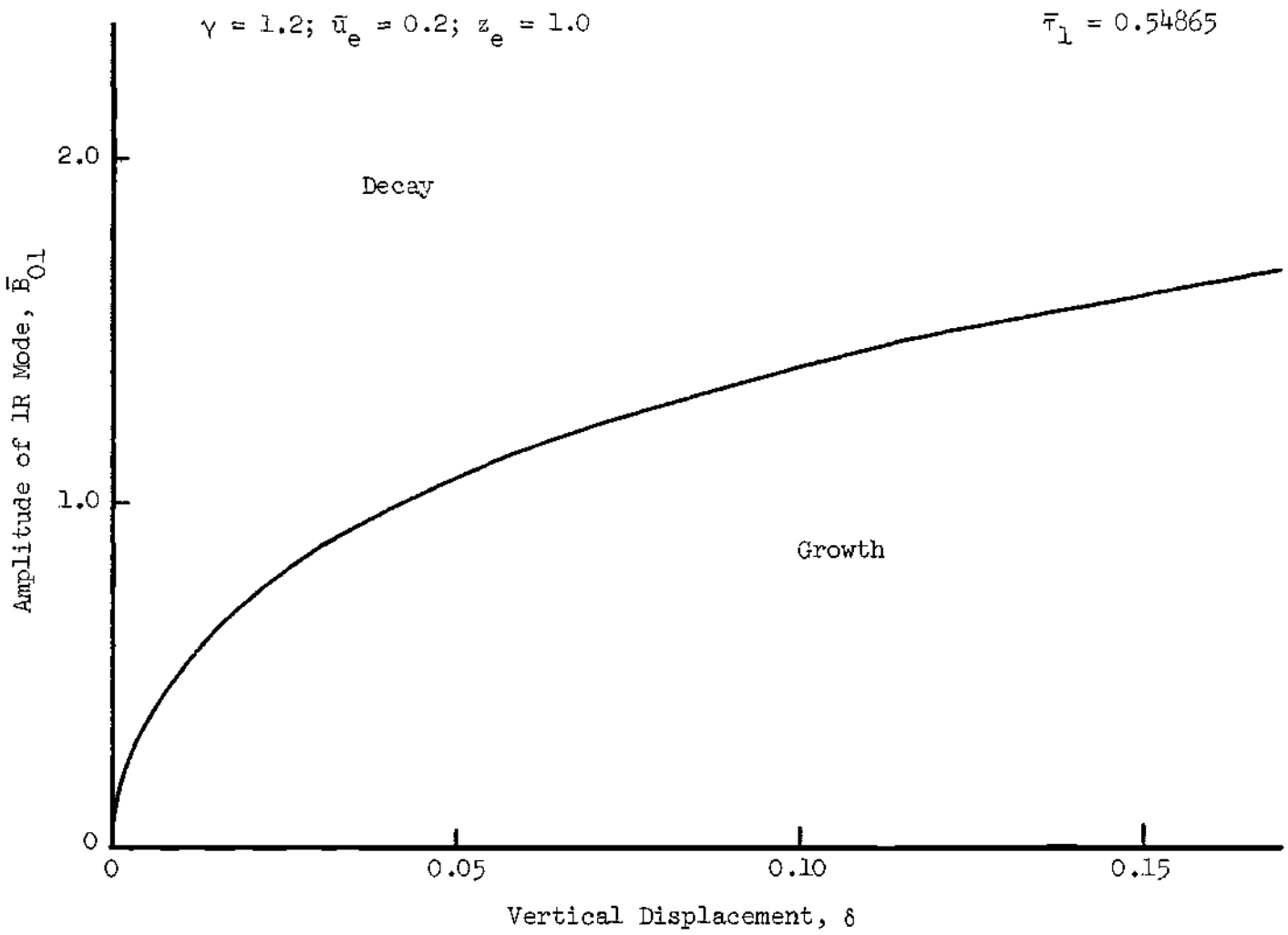

Figure 44. Stable Limit Cycles for 1R Mode Oscillations at a Small Value of the Time-Lag.

be unconditionally stable. In the region $\delta_t < \delta \leq 0$ there are two periodic solutions: the lower one is unstable while the upper one is stable. Triggering of combustion instability by the introduction of sufficiently large disturbances occurs in this region. The critical amplitude for triggering is seen to decrease to zero at the neutral stability limit and attain its maximum value at the "nonlinear stability limit" $\delta = \delta_t$. For $\delta > 0$ only one periodic solution is predicted corresponding to the case of spontaneously generated combustion instability. Figure (46) shows the nonlinear behavior along the line $\bar{\tau} = \tau_4$. In this case only the unstable periodic solution is obtained, oscillations of sufficiently large amplitude continue to grow indefinitely. Since this is not physically possible it must be inferred that the amplitudes in this case are too large to be described by the second order theory.

Comparison of the results shown in Figs. (45) and (46) reveal that as $\bar{\tau}$ increases the range of n for nonlinear instability increases and for a fixed displacement δ the critical amplitude for triggering decreases. Thus it is seen that increasing $\bar{\tau}$ may result in a more unstable engine.

In Fig. (47) the various stability regions are shown on an $(n, \bar{\tau})$ coordinate system. Above the uppermost solid curve (the neutral stability limit) the engine is linearly unstable and stable limit cycles were found. The lower solid curve is the nonlinear stability limit; below this curve all disturbances decayed. Between these curves is the region of nonlinear instability where small amplitude disturbances decay and large ones grow. In this nonlinearly unstable region curves

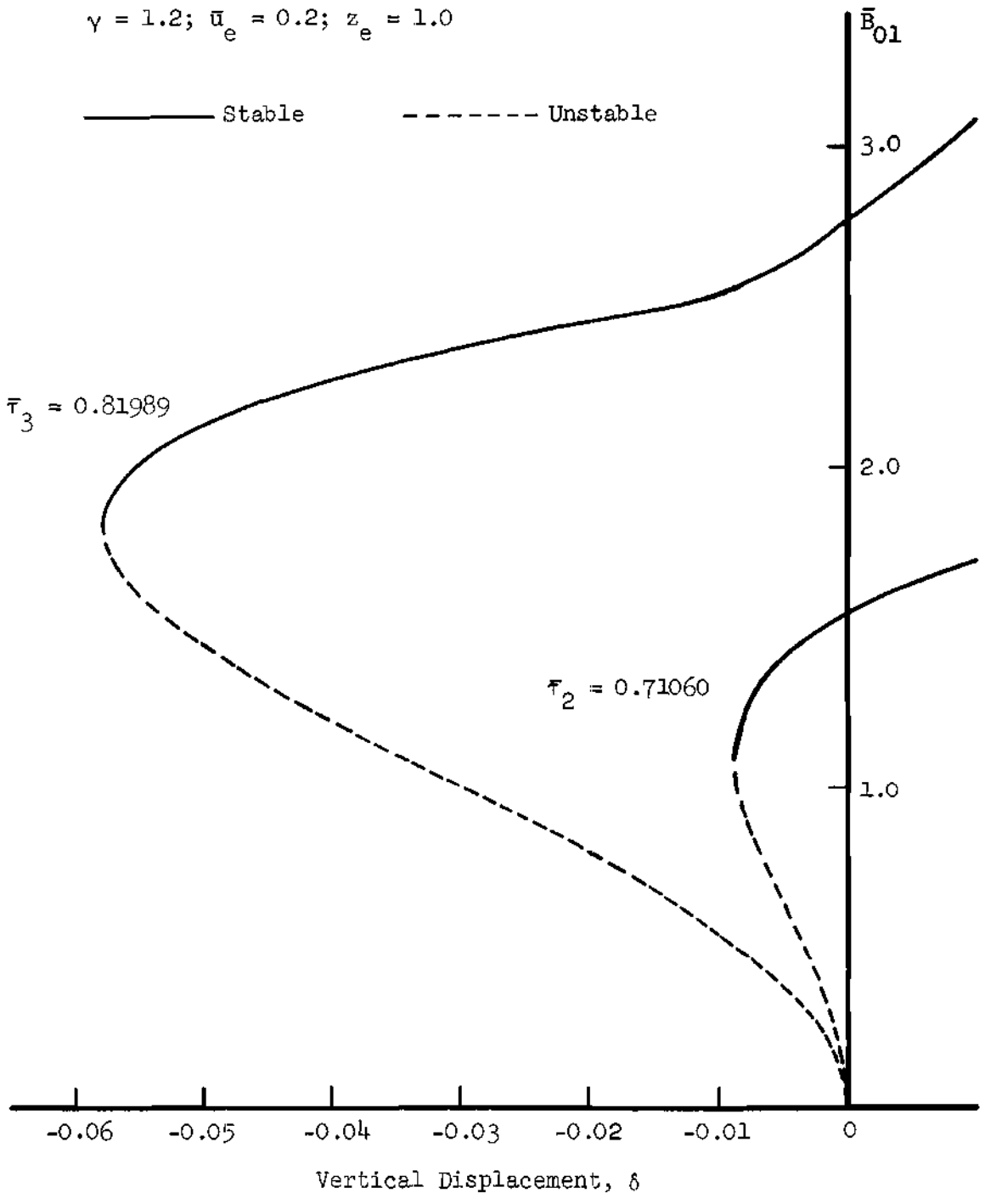

Figure 45. Stable Limit Cycles and Triggering Limits for 1R Mode Oscillations.

$\gamma = 1.2$; $\bar{u}_e = 0.2$; $z_e = 1.0$ $\qquad\qquad$ $\bar{\tau}_4 = 0.93066$

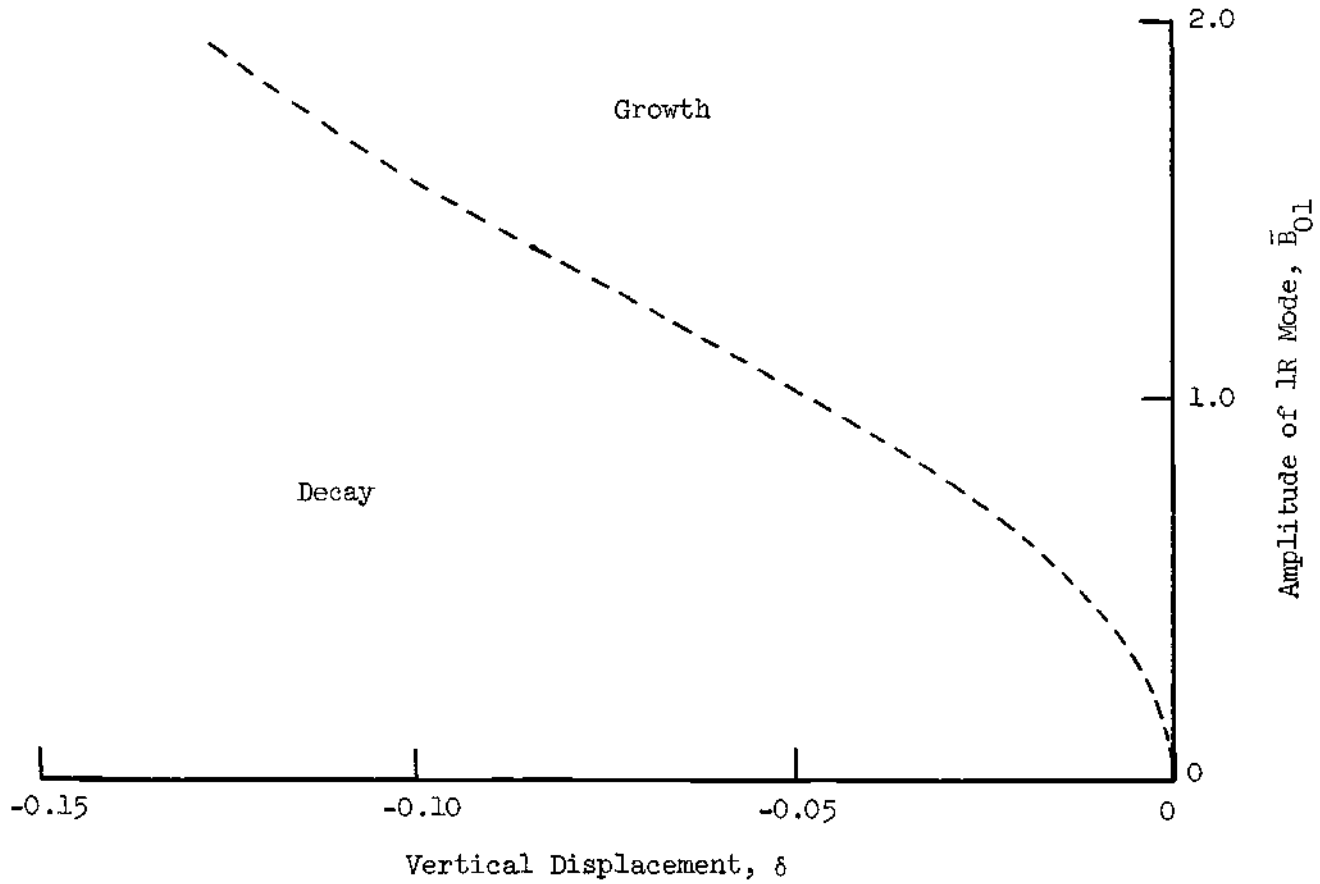

Figure 46. Unstable Limit Cycles for 1R Mode Oscillations at a Large Value of the Time-Lag.

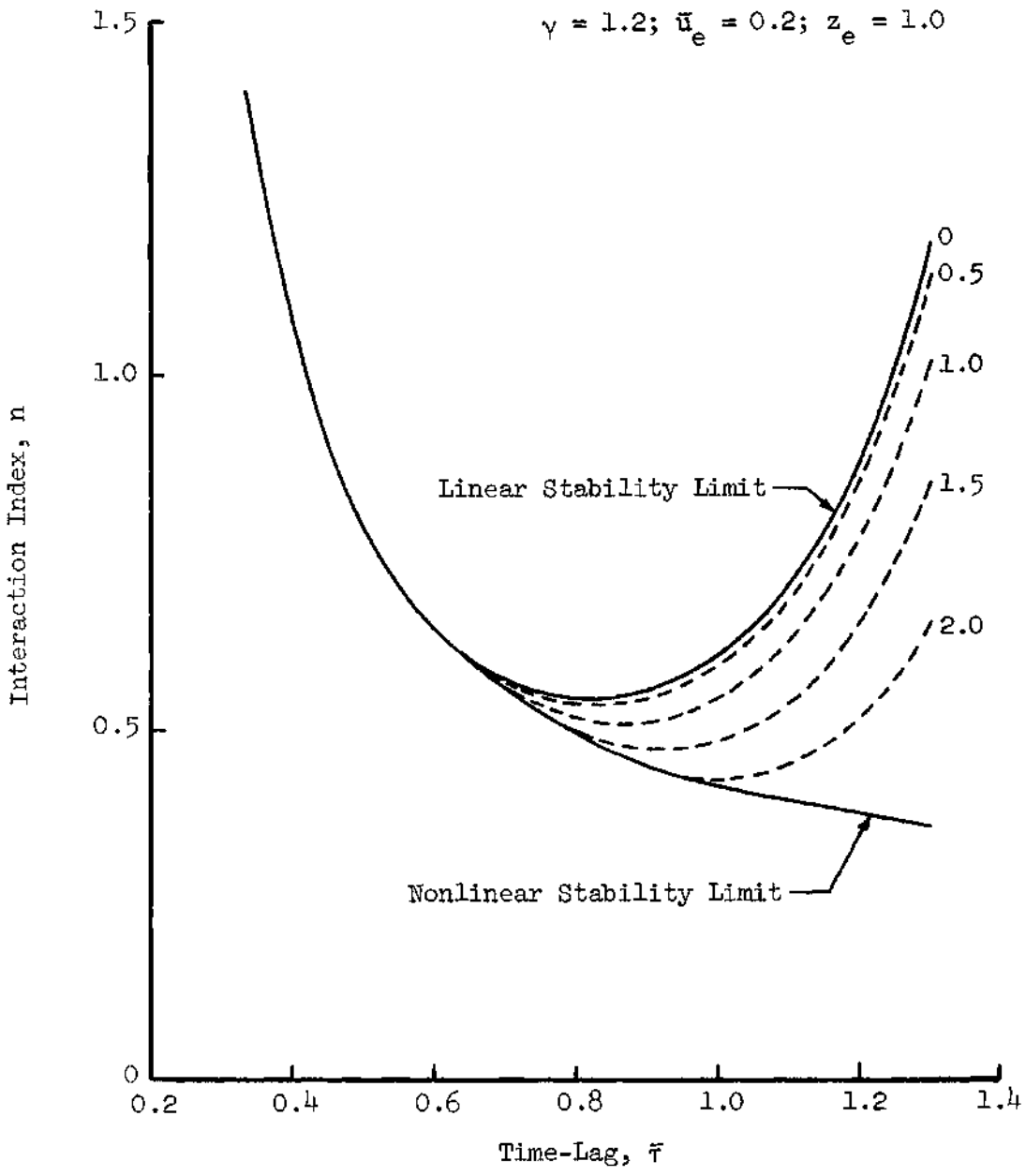

Figure 47. Linear and Nonlinear Stability Limits for 1R Mode Instability.

of constant triggering amplitude as measured by $\bar{E}_{01}$ are shown. Only in the extremely narrow region between the curve $\bar{E}_{01} = 0.5$ and the neutral stability limit is the triggering amplitude sufficiently small that the second order theory is valid.

Effect of $\bar{u}_e$ and z_e. For a few selected points in the linearly stable region the influence of the length to diameter ratio and the Mach number at the nozzle entrance upon the nonlinear stability characteristics of the engine was calculated. These results are shown in Fig. (48) where it is seen that the triggering amplitude is nearly independent of $\bar{u}_e/z_e$ until a very small value (about 0.005) is reached. The triggering amplitude increases rapidly with further decreases in $\bar{u}_e/z_e$. In this case the pressure amplitude is much greater than unity, thus this result is open to question. Nevertheless, this result is consistent with the fact that as the strength of the unsteady combustion mass source (proportional to $\bar{u}_e/z_e$) diminishes it should become increasingly more difficult to trigger instability. In the limiting case of $\bar{u}_e = 0$ the triggering behavior vanishes and the numerical calculations predict neutrally stable oscillations whose amplitude depends only upon the initial conditions.

Convergence Study

The number of terms that should be included in the approximate series solution is one of the important questions that faces those who attempt to solve nonlinear problems by using the method of weighted residuals[14]. Although convergence theorems exist for rather specialized types of linear equations (see Ref. 30), there are no general mathematical theorems applicable to nonlinear equations that can be used to

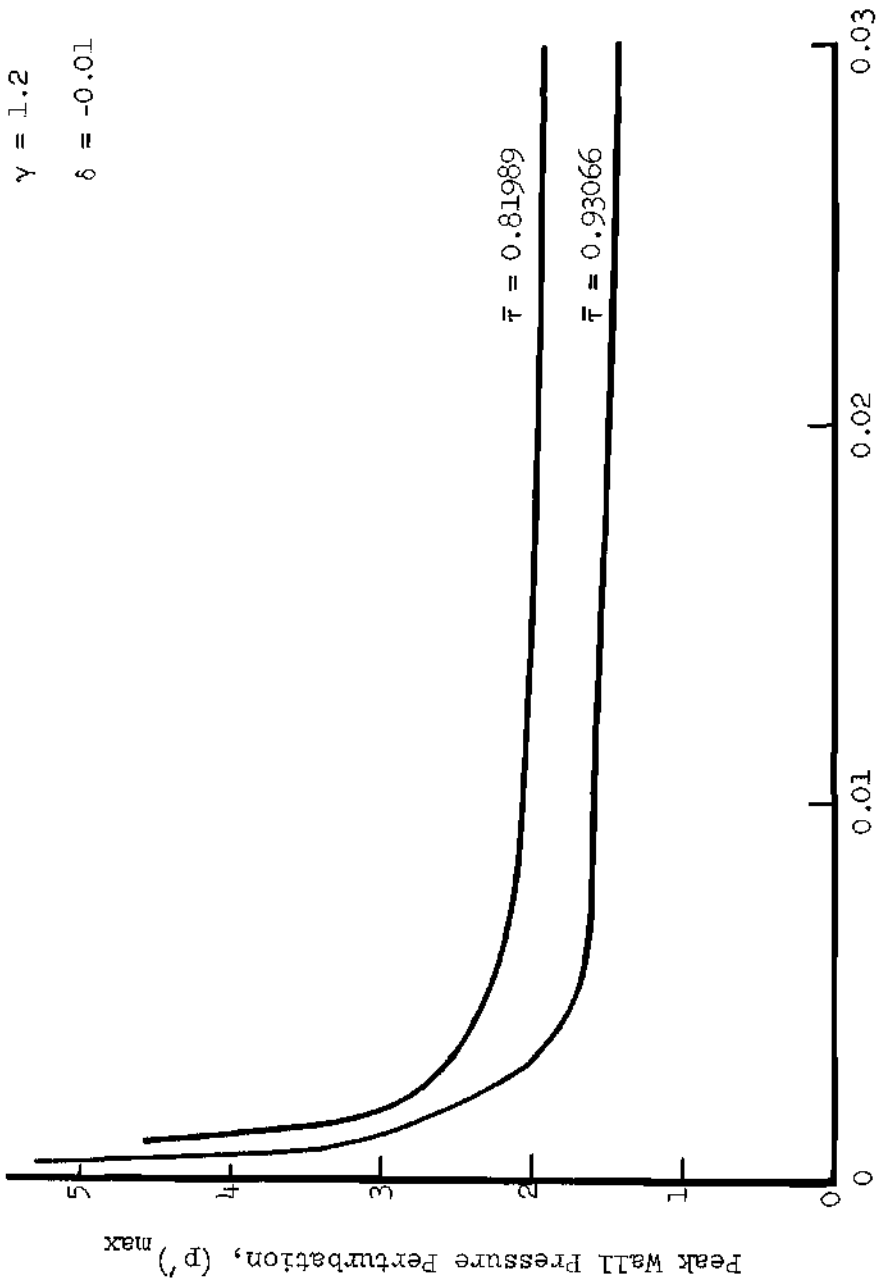

Figure 48. Dependence of the 1R Mode Triggering Amplitude upon the Ratio $\bar{u}_e/z_e$.

obtain answers to the above question. As a result intuition and numerical experimentation must be used to obtain a satisfactory answer. Observed qualitative agreement between the results presented in this chapter with available experimental data and the theoretical results of Maslen and Moore[8], Zinn[7], and Burstein[12] suggests that the assumed series solution was properly constructed. To further investigate this point solutions were obtained by adding or deleting terms from the assumed series expansion for Φ.

In these studies the effect of tangential modes was determined with the aid of the following series expansion:

$$\tilde{\Phi} = B_{01}(t) J_0\left(S_{01} r\right) + \sum_{m=1}^{M} \left[A_{m1}(t) \sin m\theta + B_{m1}(t) \cos m\theta\right] J_m\left(S_{m1} r\right) \quad (250)$$

where the 1R mode may be omitted. The simplest possible expansion which can be used to investigate the nonlinear behavior of the 1T mode consists of only two modes. The most logical choice appears to be the two lowest frequency modes; that is, the 1T and 2T modes. Numerical calculations obtained with this two-mode series were compared with those obtained when the 1R mode was included as well as additional higher order tangential modes. In each case stable limit cycles for standing oscillations were computed in the region of the $(n, \bar{\tau})$ plane where the 1T mode was linearly unstable, the 1R and 2T modes were stable, but other higher order modes were possibly unstable.

Effect of the 1R Mode. In order to evaluate the importance of the 1R mode in determining the final amplitude of the pressure oscilla-

tion, results obtained with the aid of the two-mode (1T, 2T) expansion described above were compared with similar results obtained by adding the 1R mode (1T, 2T, 1R). The results of this study are shown in Fig. (49) as plots of peak pressure and amplitude of the 1T mode as a function of δ for a constant value of $\bar{\tau}$. It is seen that for a given value of n and $\bar{\tau}$ the final pressure amplitude is considerably smaller for a series containing the 1R mode than for one without it. Comparison of wall pressure waveforms (see Fig. (50)) for solutions of comparable amplitude (but not for the same value of δ) show that the 1R mode has a marked influence upon the wave shape. For oscillations of smaller amplitude, however, the wave shapes computed with the two expansions are more alike. The dependence of the frequency upon amplitude is influenced strongly by the presence of the 1R mode as seen from Fig. (51). With the two-mode series the frequency is observed to increase with increasing amplitude, while the opposite behavior is obtained if the 1R mode is included. Due to this strong influence of the 1R mode it was therefore decided to retain it in the series expansion. The remainder of this convergence study then will aim to determine whether the addition of higher frequency modes to the three mode series will significantly alter the predicted results.

Effect of Higher Tangential Modes. Four and five mode series expansions were constructed by adding the third (3T) and fourth (4T) tangential modes to the basic three-mode series. Numerical solutions were obtained for a broad range of $\bar{\tau}$ in order to include regions where one or more of the higher order modes were linearly unstable. For example if $\delta = 0.06$ the 3T mode is unstable for $\bar{\tau} > 2.1$ and the 4T mode

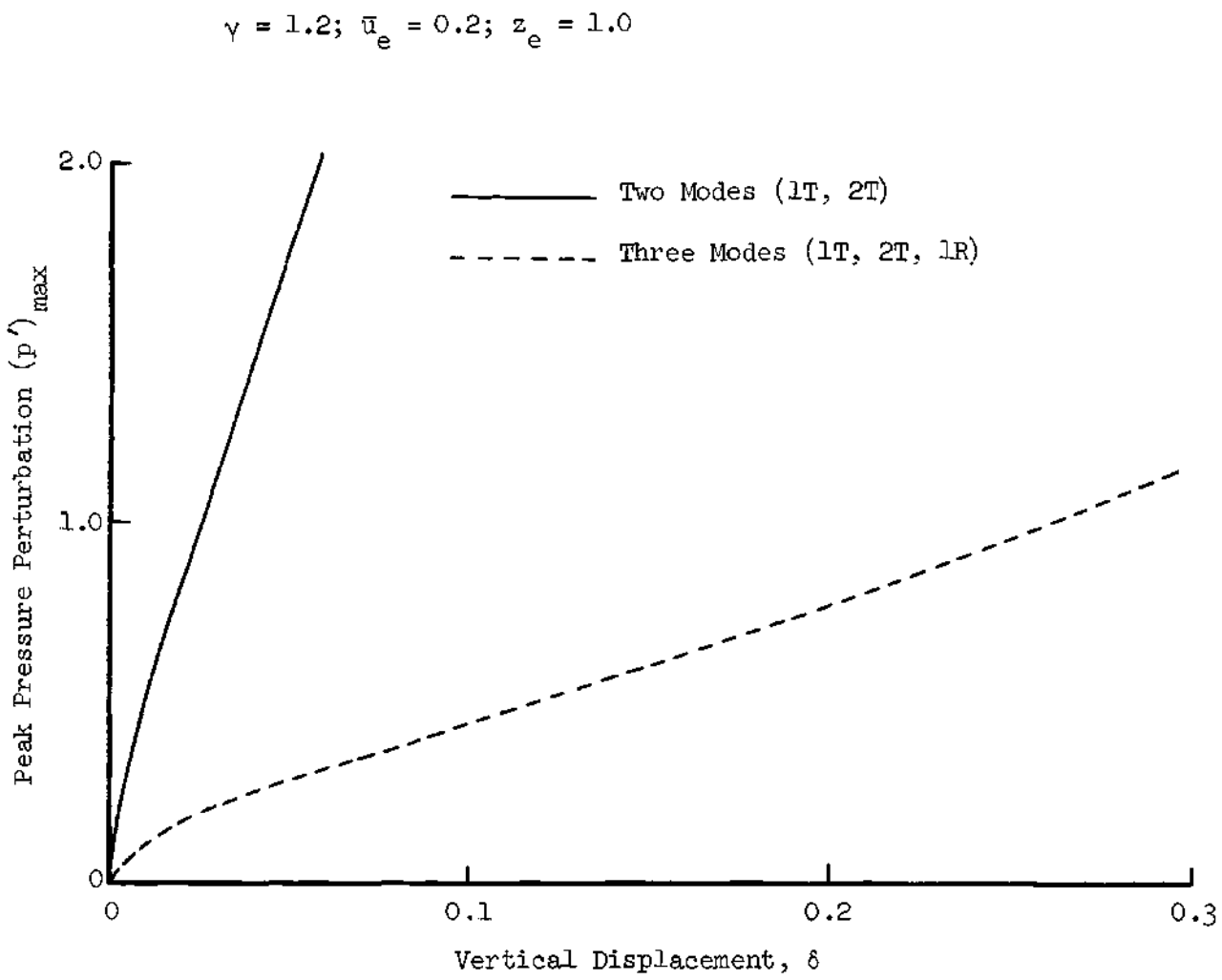

Figure 49. Effect of the First Radial Mode upon the Limiting Pressure Amplitude.

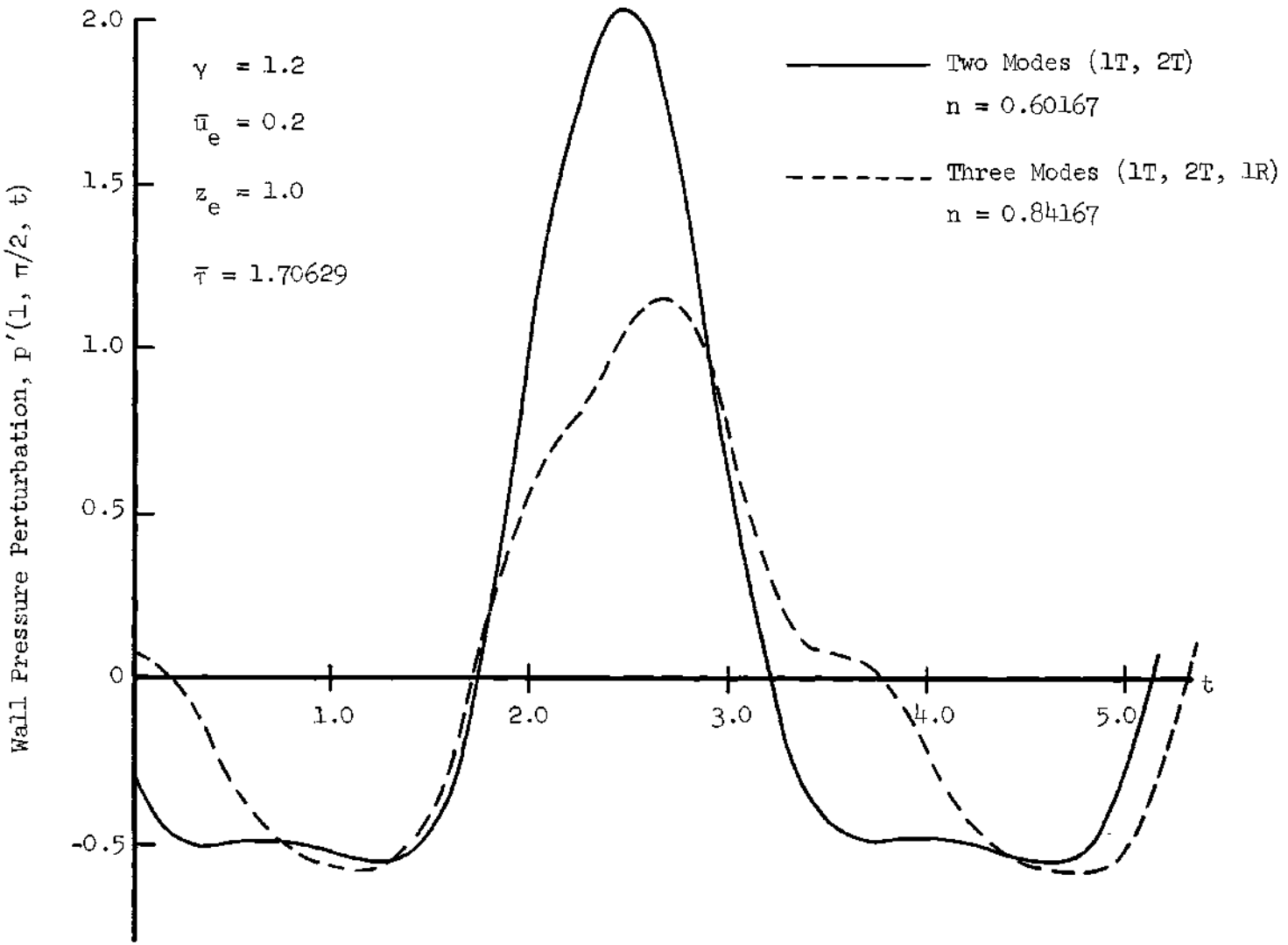

Figure 50. Effect of the First Radial Mode upon the Wall Pressure Waveforms.

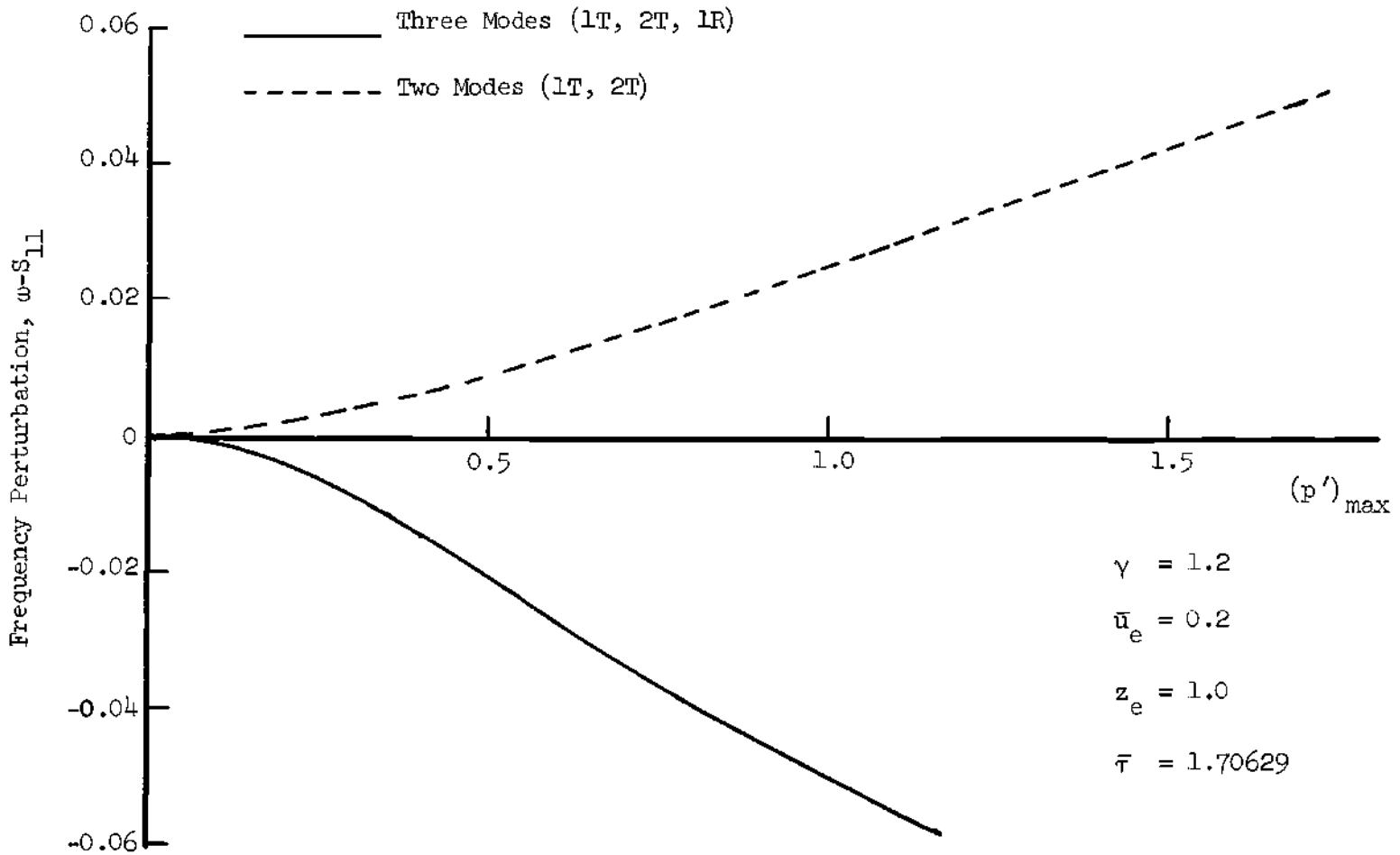

Figure 51. Effect of the First Radial Mode upon the Dependence of the Frequency upon Amplitude.

is unstable in a narrow range centered on $\bar{\tau} = 1.8$. Results of this study are summarized in the following table in which pressure amplitudes computed with the three, four, and five mode expansions are compared. The asterisk indicates that one of the higher modes was unstable.

Table 1. Effect of Higher Tangential Modes

$\bar{\tau}$	$n(\delta = 0.06)$	Peak Pressure		
		3 Modes	4 Modes	5 Modes
1.4	0.63931	0.187	0.187	0.187
1.5	0.61817	0.216	0.216	0.217
1.6	0.60594	0.263	0.265	0.266
1.706	0.60167	0.322	0.326	0.335*
1.8	0.60491	0.381	0.386	0.398*
1.9	0.61554	0.451	0.459	0.460*
2.0	0.63382	0.538	0.546	0.551
2.1	0.66037	0.666	0.717*	0.671*

From this data it is seen that the influence of the higher tangential modes upon the calculated amplitude was very slight; in most cases the values differ only in the third decimal place. Pressure waveforms computed with the three and four mode expansions are shown in Fig. (52). For the upper curves ($\bar{\tau} = 2.1$) the 3T mode was unstable, while this mode was stable for $\bar{\tau} = 1.9$. Inspection of the pressure waveforms and the data presented in the table reveal that the effect of adding a higher order mode is appreciably greater if that mode is linearly

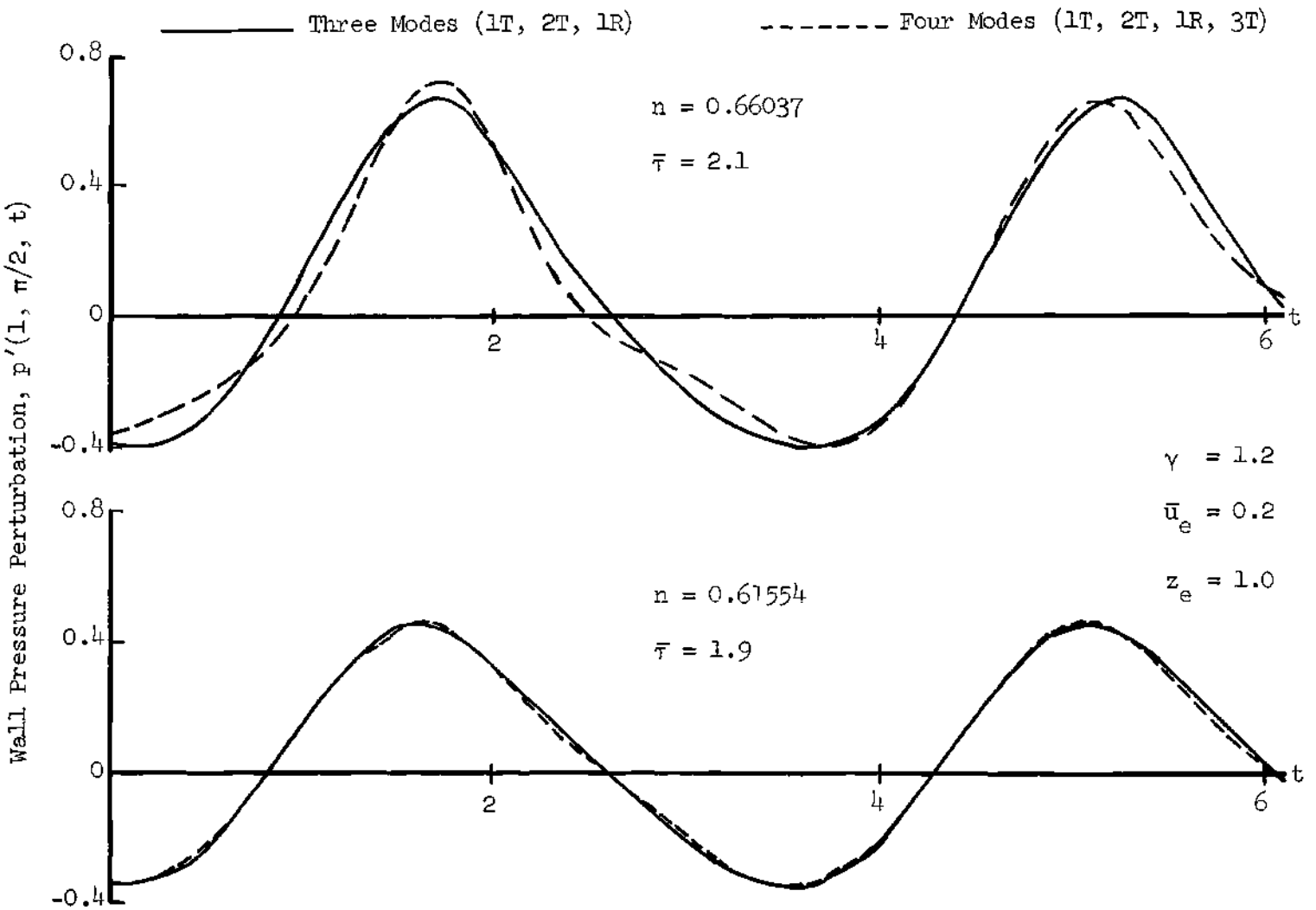

Figure 52. Effect of Higher Tangential Modes upon the Wall Pressure Waveforms.

unstable. These results indicate that in the region of the $(n, \bar{\tau})$ plane considered the assumed series expansion is rapidly convergent with respect to tangential modes.

A further manifestation of the convergence properties of the series expansion is observed in the amplitudes of the various modes. For a five-mode series for which only the 1T mode is unstable the modes can be arranged in a sequence of decreasing amplitude as follows: 1T, 1R, 2T, 3T, 4T. Each mode in the sequence was found to be approximately one order of magnitude smaller than its predecessor. Thus the contribution of the 3T and 4T modes to the sum of the series (which determines the pressure) is negligible compared to that of the first three modes.

Effect of Higher Radial and Combined Radial-Tangential Modes. In the previous studies only modes with $n = 1$ were included in the assumed series expansion as shown in Eq. (250). It is now desired to determine the importance of terms with $n > 1$ which are the higher radial and combined radial-tangential modes. Such modes have occasionally been observed experimentally and may have an effect upon the numerical solutions. This study has been limited to the consideration of a six-mode series formed by adding to the three mode series ($m = 0, 1, 2$; $n = 1$) the corresponding modes for $n = 2$. These are the 2R ($m = 0$, $n = 2$), the 1T-1R ($m = 1$, $n = 2$), and the 2T-1R ($m = 2$, $n = 2$) modes. The results computed with the three and six mode expansions are shown in Figs. (53) and (54). For $\bar{\tau} = 1.70629$ the pressure amplitude computed with the six mode series was about 50 per cent larger than that obtained with the three mode series for small δ; the discrepancy

became larger as δ increased. In this case the 1T-1R mode was linearly unstable and its effect is easily seen as the double peak in the pressure waveform (see Fig. (54)). For other values of $\bar{\tau}$ pressure waveforms were observed which were very similar to those computed with the three-mode series. These calculations indicate that the series expansion for Φ converges much more slowly as terms of higher radial mode number n are added than was observed when additional tangential modes (m increasing) were included. It would be desirable to add three more modes (corresponding to $n = 3$) to the six mode series to determine if the solution is converging, however the required computer time was found to be excessive.

In conclusion it should be remembered that in the second order analysis the dissipative effects of viscosity, heat conductivity, and droplet drag were neglected. For chambers which are not too large, it is expected that due to the large gradients and velocities involved the damping of the higher order modes due to these processes should be greater than that of the lowest frequency modes. Such behavior was predicted by Maslen and Moore[8]. Thus the omission of modes with $n > 2$ from the expansion of Φ could be justified if these modes are too heavily damped to have a significant influence upon the stability of the combustor.

Concluding Remarks

It should be emphasized that the nonlinear solutions presented in this chapter were calculated subject to several assumptions and restrictions. In this case a rather specialized combustor configuration was considered, i.e. one in which the propellants are injected uniformly

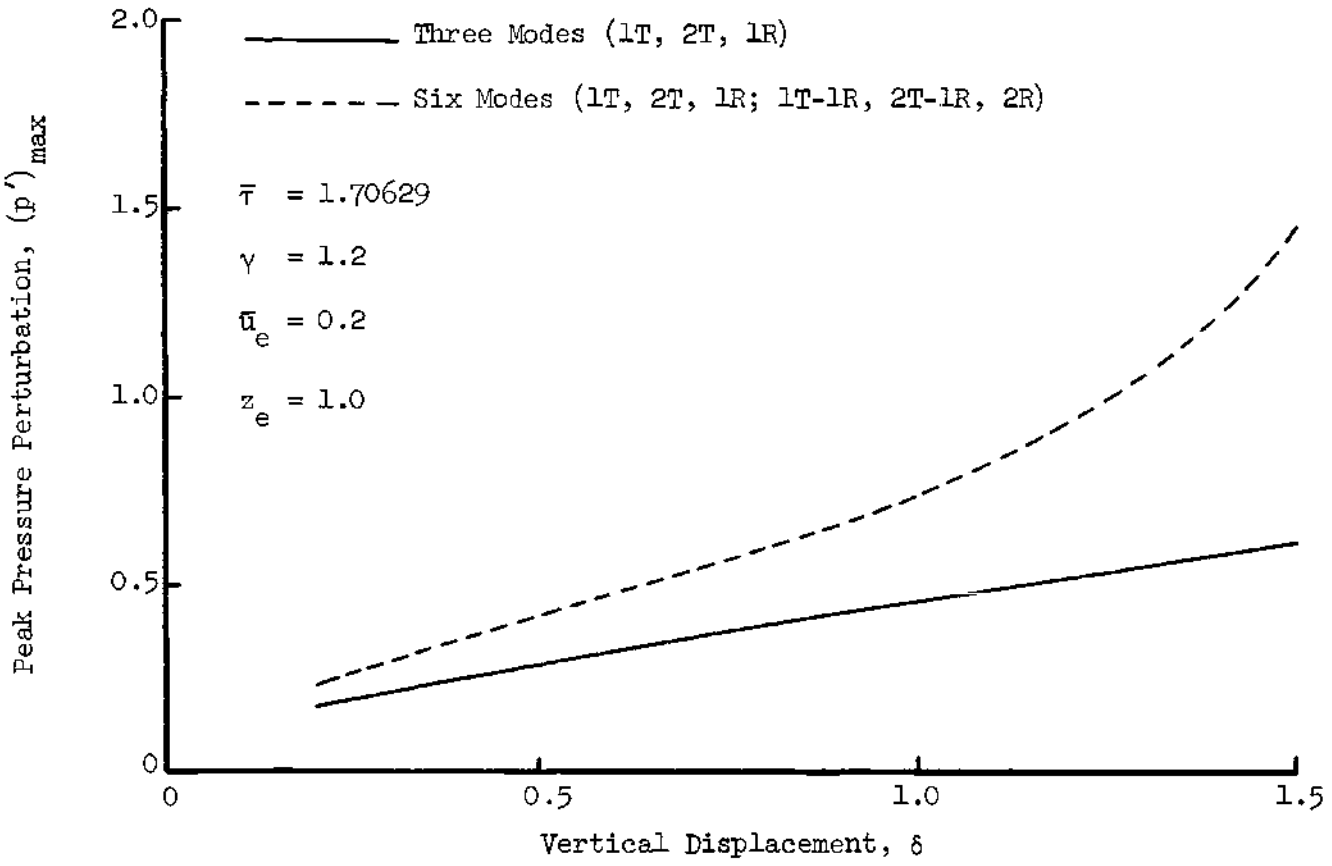

Figure 53. Effect of Combined Tangential-Radial Modes upon the Limiting Pressure Amplitude.

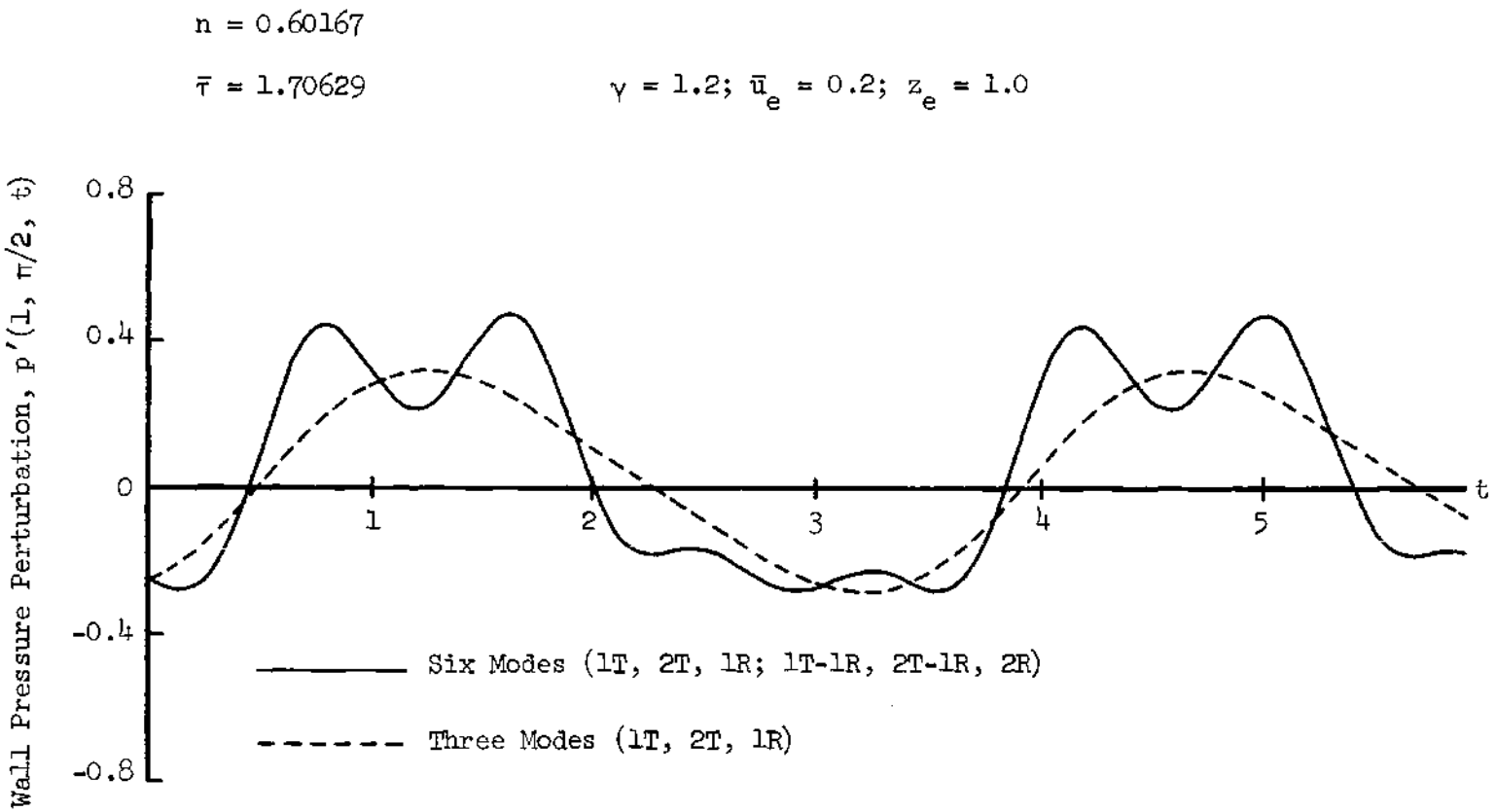

Figure 54. Effect of Combined Tangential-Radial Modes upon the Wall Pressure Waveforms.

and the nozzle behaves in a quasi-steady manner. Also a specific combustion model (n-$\bar{\tau}$ model) was assumed. These restrictions were made in order to simplify the analysis but are by no means necessary. It is believed that the second order theory and the Galerkin method can be used to analyze combustors for which the injection distribution, combustion process, and nozzle admittance functions are specified in a more general form.

In addition to the above remarks the results presented in this chapter are of limited applicability due to the assumptions of moderate amplitude and small steady state Mach number. These assumptions have been shown to result in a linear combustion and nozzle response. The only nonlinearities present are those related to the gasdynamics of the unsteady flow in the combustor; these have been shown to result in energy transfer between modes. Thus only one of several possible nonlinear mechanisms has been considered in this chapter. In order to relax some of the restrictions inherent in the second order theory and obtain a nonlinear combustion driving mechanism a third order analysis will be performed in the next chapter.

CHAPTER VII

THIRD ORDER NONLINEAR ANALYSIS

In the development of the second order theory several restrictions were imposed upon the flow in the rocket's combustor. The most important of these were the assumptions of small steady state Mach number and the presence of waves whose amplitudes are not too large. It has been shown in Chapter III that to second order these conditions imply that the wave motion is irrotational and the effect of variations in steady state thermodynamic properties with axial position can be neglected. As a result the conservation equations could be reduced to a single partial differential equation governing the behavior of the velocity potential.

A more accurate theory to describe the unsteady flow in the combustor is highly desirable. For instance the trend in modern rocket design has been the development of engines of small contraction ratio which implies that the mean flow Mach number is large and variations in steady state properties can no longer be safely neglected. Also the results of Chapter VI as well as experimental data indicate that the final pressure amplitude in an unstable rocket engine often becomes so large that products of three perturbation quantities which occur in the conservation equations are no longer negligible. It is believed that the omission of such third order terms is at least partly responsible for the failure of the second order theory to predict

triggering of the first tangential mode. Application of the Galerkin method to the second order equations resulted in equations which lacked self-coupling terms involving the 1T mode, while similar studies for radial modes demonstrated the importance of such self-coupling terms in the prediction of triggering limits. Examination of terms omitted in the second order analysis indicate that self-coupling terms involving the 1T mode will be obtained in equations correct to third order. Thus a third order analysis is expected to yield triggering limits for the 1T mode. This result is in agreement with Zinn[7] who showed that a third order approximation was necessary to predict triggering.

The analysis to follow represents an attempt to relax some of the restrictions imposed on the second order theory. In this analysis no terms will be neglected in the conservation equations; the only approximations used are those related to the absence of droplet drag and the constancy of droplet temperature. Both of the latter assumptions were used in the second order theory. Thus the following terms which were previously neglected will now be retained: (1) products of three perturbation quantities, and (2) products of two perturbation quantities and the steady state velocity (or its gradient). As a result the unsteady flow can no longer be assumed to be irrotational (see Chapter III) and the conservation equations cannot be combined to obtain a single governing equation. Instead a system of partial differential equations must be solved. This system has already been derived in Chapter III and is given by Eqs. (46) through (48) and Eq. (34b).

To complete the third order theory it was necessary to derive

higher order expressions for the burning rate and the nozzle admittance relation. Unlike the equations describing the gas dynamics of the problem these expressions contained terms of all orders and had to be truncated to include terms up to third order only. As in the second order analysis it was assumed that the burning rate was described by Crocco's time-lag hypothesis and the nozzle was quasi-steady (multi-orifice nozzle). The appropriate higher order expressions have been derived in Chapter IV where it was necessary to assume that the combustor's mean flow Mach number was small.

Analysis

Galerkin Orthogonality Conditions

In Chapter II the classical Galerkin method was modified to accommodate the complicated boundary conditions which are so often encountered in the solution of combustion instability problems. At that time the proper Galerkin orthogonality conditions were derived for the "natural" form of the conservation equations; that is, the form which results directly from the application of conservation of mass, momentum, and energy. The simplified wave equations of Chapter III, which form the basis for the third order theory, are of a somewhat different form. For example the continuity and momentum equations have been combined to obtain the Euler equation which expresses Newton's law of motion for a fluid particle. The boundary residuals appropriate to the Euler equation will therefore differ from those corresponding to the momentum equation. The appropriate Galerkin orthogonality conditions for the momentum and energy equations in the form given in

Chapter III will now be derived.

Momentum Equation. The dimensionless momentum equation which describes the flow of the burned gases in the presence of liquid droplets is given by (see Eq. (26) of Chapter III):

$$E_2(\rho, \underset{\rightarrow}{V}, p) = \frac{\partial}{\partial t}(\rho \underset{\rightarrow}{V}) + \nabla\cdot(\rho \underset{\rightarrow}{V}\underset{\rightarrow}{V}) + \frac{1}{\gamma}\nabla p \tag{251}$$

$$+ \left\{\frac{\partial}{\partial t}\left(\rho_L \underset{L}{\underset{\rightarrow}{V}}\right) + \nabla\cdot\left(\rho_L \underset{L}{\underset{\rightarrow}{V}}\underset{L}{\underset{\rightarrow}{V}}\right)\right\} = 0$$

In Eq. (251) the expression involving the liquid quantities corresponds to $-F_{mom}$ in Eq. (8) of Chapter II. The boundary conditions imposed upon Eq. (251) are easily obtained from Eq. (6b) of Chapter II. If Eq. (6b) represents a concentrated combustion zone at the injector, $\underset{\rightarrow}{V}_1 = 0$ because there is no gas flow into the zone. The same result holds in the nozzle formulation because the boundary zone "swallows" the entire mass flow entering the nozzle, hence there is no flow out of the zone. In both cases the pressure will be allowed to change across the boundary zone, thus $p_2 \neq p_1$. Introducing these results into Eq. (6b) yields the following expression:

$$B_2(\rho, \underset{\rightarrow}{V}, p) = \underset{\rightarrow}{Q}_{mom} + [\underset{\rightarrow}{V}(\rho \underset{\rightarrow}{V}\cdot\underset{\rightarrow}{n})] + (p-p_1)\underset{\rightarrow}{n} = 0 \tag{252}$$

where p_1 is the pressure on the "outside" side of the boundary zone.

By using the vector identity $\nabla\cdot(a\underset{\rightarrow}{A}\underset{\rightarrow}{A}) = a\underset{\rightarrow}{A}\cdot\nabla\underset{\rightarrow}{A} + \underset{\rightarrow}{A}\nabla\cdot a\underset{\rightarrow}{A}$ and adding and subtracting the term $W_m \underset{m}{\underset{\rightarrow}{V}}$ Eq. (251) can be written in the following

form:

$$E_2 = \rho \frac{\partial \underset{\rightarrow}{V}}{\partial t} + \rho \underset{\rightarrow}{V} \cdot \nabla \underset{\rightarrow}{V} + \frac{1}{\gamma} \nabla p + \rho_L \frac{\partial \underset{\rightarrow}{V}_L}{\partial t} + \rho_L \underset{\rightarrow}{V}_L \cdot \nabla \underset{\rightarrow}{V}_L$$

$$+ \left[\frac{\partial \rho}{\partial t} + \nabla \cdot (\rho \underset{\rightarrow}{V}) - W_m\right] \underset{\rightarrow}{V} + \left[\frac{\partial \rho_L}{\partial t} + \nabla \cdot \left(\rho_L \underset{\rightarrow}{V}_L\right)\right] \underset{\rightarrow}{V}_L + W_m \underset{\rightarrow}{V} = 0$$

From the continuity equation (i.e. Eq. (25)) it is seen that $\partial \rho_L / \partial t + \nabla \cdot \left(\rho_L \underset{\rightarrow}{V}_L\right) = - W_m$; substituting this result into the above equation yields:

$$E_2 = \left\{\rho \frac{\partial \underset{\rightarrow}{V}}{\partial t} + \rho \underset{\rightarrow}{V} \cdot \nabla \underset{\rightarrow}{V} + \frac{1}{\gamma} \nabla p + W_m \left(\underset{\rightarrow}{V} - \underset{\rightarrow}{V}_L\right) + \rho_L \frac{\partial \underset{\rightarrow}{V}_L}{\partial t} + \rho_L \underset{\rightarrow}{V}_L \cdot \nabla \underset{\rightarrow}{V}_L\right\} \quad (253)$$

$$+ \left[\frac{\partial \rho}{\partial t} + \nabla \cdot (\rho \underset{\rightarrow}{V}) - W_m\right] \underset{\rightarrow}{V} = 0$$

Equation (253) consists of two parts: the terms in brackets represent the Euler equation (see Eq. (28)) while the remaining terms are the continuity equation multiplied by $\underset{\rightarrow}{V}$. For solutions satisfying the continuity equation the latter terms vanish, however in this analysis only approximate solutions will be considered.

The boundary momentum source $\underset{\rightarrow}{Q}_{mom}$ which appears in Eq. (252) can be expressed as

$$\underset{\rightarrow}{Q}_{mom} = \underset{\rightarrow}{V} Q_{mass} + \underset{\rightarrow}{M} \quad (254)$$

where $\underset{\rightarrow}{V}Q_{mass}$ is the momentum associated with the gases generated within the boundary zone and $\underset{\rightarrow}{M}$ represents a momentum source resulting from interactions between the liquid droplets and the gas in the boundary zone. The boundary condition can now be written as:

$$B_2(\rho, \underset{\rightarrow}{V}, p) = \underset{\rightarrow}{V}Q_{mass} + \underset{\rightarrow}{M} + [\underset{\rightarrow}{V}(\rho \underset{\rightarrow}{V}\cdot \underset{\rightarrow}{n})] + (p-p_1)\underset{\rightarrow}{n} = 0 \qquad (255)$$

Residuals are formed from Eqs. (253) and (255) by introducing the approximate solutions $\tilde{\rho}$, $\underset{\rightarrow}{\tilde{V}}$, and $\tilde{p}$. The corresponding Galerkin orthogonality condition is obtained directly from Eq. (24) of Chapter II and is given by

$$\int_0^{t^*} \left\{ \int_V \left[\tilde{\rho} \frac{\partial \underset{\rightarrow}{\tilde{V}}}{\partial t} + \tilde{\rho} \underset{\rightarrow}{\tilde{V}} \cdot \nabla \underset{\rightarrow}{\tilde{V}} + \frac{1}{\gamma} \nabla \tilde{p} + \tilde{W}_m \left(\underset{\rightarrow}{\tilde{V}} - \underset{\rightarrow}{\tilde{V}}_L \right) + \tilde{\rho}_L \frac{\partial \underset{\rightarrow}{\tilde{V}}_L}{\partial t} + \tilde{\rho}_L \underset{\rightarrow}{\tilde{V}}_L \cdot \nabla \underset{\rightarrow}{\tilde{V}}_L \right] \varphi_n dv \right. \qquad (256)$$

$$\left. - \int_s \left[\underset{\rightarrow}{\tilde{M}} + \left(p-p_1 \right) \underset{\rightarrow}{n} \right] \varphi_n ds \right\} dt$$

$$+ \int_0^{t^*} \left\{ \int_V \left[\frac{\partial \tilde{\rho}}{\partial t} + \nabla \cdot (\tilde{\rho} \underset{\rightarrow}{\tilde{V}}) - \tilde{W}_m \right] \underset{\rightarrow}{\tilde{V}} \varphi_n dv - \int_s \left[\tilde{Q}_{mass} + \tilde{\rho} \underset{\rightarrow}{\tilde{V}} \cdot \underset{\rightarrow}{n} \right] \underset{\rightarrow}{\tilde{V}} \varphi_n ds \right\} dt = 0$$

The last pair of integrals are seen to be the residuals of the continuity equation and its boundary condition weighted with $\underset{\rightarrow}{\tilde{V}}\varphi_n$ rather than φ_n. It will now be shown that if the expansions of the dependent variables are properly constructed these terms will vanish.

Using the expansions presented in Eq. (10) with $N = \infty$ the

product $\varphi_n \underset{\rightarrow}{\tilde{V}}$ can be written in the following form:

$$\varphi_n \underset{\rightarrow}{\tilde{V}} = \varphi_n \sum_{k=0}^{\infty} A_{k_i} \varphi_k(\underset{\rightarrow}{x}, t) \underset{\rightarrow}{e}_i \tag{257}$$

$$= \underset{\rightarrow}{e}_i \sum_{k=0}^{\infty} A_{k_i} \varphi_k(\underset{\rightarrow}{x}, t) \varphi_n(\underset{\rightarrow}{x}, t) \qquad i = 1, 2, 3$$

where $\underset{\rightarrow}{e}_i$ is a unit vector in the ith direction. It is now required that the functions $\varphi_n(\underset{\rightarrow}{x}, t)$ form a complete set, but it is not necessary that they be mutually orthogonal. Under these conditions the product $\varphi_n \varphi_k$ can be expanded in terms of the functions φ_j as follows:

$$\varphi_n \varphi_k = \sum_{j=0}^{\infty} a_j^{nk} \varphi_j(\underset{\rightarrow}{x}, t) \tag{258}$$

which is substituted into Eq. (257) to obtain:

$$\varphi_n \underset{\rightarrow}{\tilde{V}} = \underset{\rightarrow}{e}_i \sum_{k=0}^{\infty} A_{k_i} \sum_{j=0}^{\infty} a_j^{nk} \varphi_j(\underset{\rightarrow}{x}, t) \tag{259}$$

$$= \underset{\rightarrow}{e}_i \sum_{k=0}^{\infty} \sum_{j=0}^{\infty} A_{k_i} a_j^{nk} \varphi_j(\underset{\rightarrow}{x}, t)$$

Thus $\varphi_n \underset{\rightarrow}{\tilde{V}}$ has been expanded in terms of the complete set of functions

φ_n. Substituting Eq. (259) into the last volume integral and the last surface integral of Eq. (256) yields:

$$\int_o^{t^*} \left\{ \int_v \left[\frac{\partial \tilde{\rho}}{\partial t} + \nabla \cdot (\tilde{\rho} \underset{\rightarrow}{\tilde{V}}) - \tilde{W}_m \right] \underset{\rightarrow}{\tilde{V}} \varphi_n dv - \int_s \left[\tilde{Q}_{mass} + \tilde{\rho} \underset{\rightarrow}{\tilde{V}} \cdot \underset{\rightarrow}{n} \right] \underset{\rightarrow}{\tilde{V}} \varphi_n ds \right\} dt \qquad (260)$$

$$= \underset{\rightarrow}{e}_i \sum_{k=0}^{\infty} \sum_{j=0}^{\infty} A_{k_i} a_j^{nk} \int_o^{t^*} \left\{ \int_v E_1(\tilde{\rho}, \underset{\rightarrow}{\tilde{V}}) \varphi_j dv - \int_s B_1(\tilde{\rho}, \underset{\rightarrow}{\tilde{V}}, \tilde{p}) \varphi_j ds \right\} dt$$

where it has been assumed that the series can be integrated term by term. Each of the terms in the series expansion of Eq. (260) vanishes according to the orthogonality conditions imposed on the continuity equation residual and its boundary residual (i.e. Eq. (24) with i = 1). Introducing this result into Eq. (256) yields the following expression:

$$\int_o^{t^*} \left\{ \int_v \left[\tilde{\rho} \frac{\partial \underset{\rightarrow}{\tilde{V}}}{\partial t} + \tilde{\rho} \underset{\rightarrow}{\tilde{V}} \cdot \nabla \underset{\rightarrow}{\tilde{V}} + \frac{1}{\gamma} \nabla \tilde{p} + \tilde{W}_m \left(\underset{\rightarrow}{\tilde{V}} - \underset{\rightarrow}{\tilde{V}}_L \right) + \tilde{\rho}_L \frac{\partial \underset{\rightarrow}{\tilde{V}}_L}{\partial t} + \tilde{\rho}_L \underset{\rightarrow}{\tilde{V}}_L \cdot \nabla \underset{\rightarrow}{\tilde{V}}_L \right] \varphi_n dv \qquad (261)$$

$$- \int_s \left[\underset{\rightarrow}{\tilde{M}} + (p - p_1) \underset{\rightarrow}{n} \right] \varphi_n ds \Big\} \, dt = 0$$

which is the Galerkin orthogonality condition applicable to the Euler equation for two phase flow.

Energy Equation. A similar analysis will now be applied to the energy equation. The natural form of the energy equation for the combustor flow as given by Eq. (27) can be expressed in terms of the stagnation

enthalpies as follows:

$$E_3 = \frac{\partial}{\partial t}\left[\rho h_s - \frac{\gamma-1}{\gamma} p\right] + \nabla\cdot\left(\rho \underrightarrow{V} h_s\right) \tag{262}$$

$$+ \left\{\frac{\partial}{\partial t}\left(\rho_L h_{L_s}\right) + \nabla\cdot\left(\rho_L \underrightarrow{V}_L h_{L_s}\right)\right\} = 0$$

The corresponding boundary residual is obtained from Eq. (6c) of Chapter II as:

$$B_3 = \frac{Q_E}{\gamma} + \rho \underrightarrow{V}\left\{\frac{1}{\gamma}\left[e + (\gamma-1)\frac{p}{\rho}\right] + \frac{\gamma-1}{2}\rho V^2\right\}\cdot \underrightarrow{n} = 0 \tag{263}$$

where again $\underrightarrow{V}_1 = 0$. In deriving Eq. (262) the original energy equation was divided by γ, thus the same operation has been performed on the boundary conditions as shown by Eq. (263). The expression in brackets in Eq. (263) is seen to be the dimensionless stagnation enthalpy, thus Eq. (263) can be written in the more convenient form:

$$B_3 = \frac{Q_E}{\gamma} + \rho \underrightarrow{V} h_s \cdot \underrightarrow{n} = 0 \tag{264}$$

The boundary energy source Q_E will be expressed in a form analogous to Eq. (254), that is:

$$Q_E = \gamma H + Q_{mass}\left[e + (\gamma-1)\frac{p}{\rho} + \frac{\gamma(\gamma-1)}{2} V^2\right] \tag{265}$$

where γH is an energy source (or sink) not associated with the generation of mass in the boundary zone. For example γH may represent the effects of droplet heating. Introducing Eq. (265) into Eq. (264) yields the desired form of the boundary condition:

$$B_3 = H + \left[Q_{mass} + \rho \underset{\rightarrow}{V}\cdot\underset{\rightarrow}{n}\right]h_s = 0 \tag{266}$$

The Galerkin orthogonality conditions appropriate to the form of the energy equation given by Eq. (33) of Chapter III can now be derived. Adding and subtracting the term $W_m h_s$ and expanding and rearranging terms, Eq. (262) becomes:

$$\rho\left[\frac{\partial h_s}{\partial t} + \underset{\rightarrow}{V}\cdot\nabla h_s\right] - \frac{\gamma-1}{\gamma}\frac{\partial p}{\partial t} + \rho_L\left[\frac{\partial h_{L_s}}{\partial t} + \underset{\rightarrow}{V}_L\cdot\nabla h_{L_s}\right] + W_m h_s$$

$$+ h_{L_s}\left[\frac{\partial \rho_L}{\partial t} + \nabla\cdot\left(\rho_L \underset{\rightarrow}{V}_L\right)\right] + \left[\frac{\partial \rho}{\partial t} + \nabla\cdot\left(\rho \underset{\rightarrow}{V}\right) - W_m\right]h_s = E_3$$

Introducing the continuity equation $\partial\rho_L/\partial t + \nabla\cdot\left(\rho_L \underset{\rightarrow}{V}_L\right) = - W_m$ and the approximate solutions $\tilde{\rho}$, $\tilde{p}$, $\underset{\rightarrow}{\tilde{V}}$, $\tilde{h}_s$ the above equation simplifies to:

$$\tilde{\rho}\left[\frac{\partial \tilde{h}_s}{\partial t} + \underset{\rightarrow}{\tilde{V}}\cdot\nabla\tilde{h}_s\right] - \frac{\gamma-1}{\gamma}\frac{\partial \tilde{p}}{\partial t} + \tilde{\rho}_L\left[\frac{\partial \tilde{h}_{L_s}}{\partial t} + \underset{\rightarrow}{\tilde{V}}_L\cdot\nabla\tilde{h}_{L_s}\right] + \tilde{W}_m\left(\tilde{h}_s - \tilde{h}_{L_s}\right) \tag{267}$$

$$+ \left[\frac{\partial \tilde{\rho}}{\partial t} + \nabla\cdot\left(\tilde{\rho}\underset{\rightarrow}{\tilde{V}}\right) - \tilde{W}_m\right]\tilde{h}_s = E_3$$

Equation (267) consists of two parts: the residual of Eq. (33) and the residual of the continuity equation multiplied by $\tilde{h}_s$. The appropriate orthogonality condition which must be satisfied by E_3 and B_3 is obtained directly from Eq. (24) with i = 3, thus:

$$\int_o^{t^*} \left\{ \int_v \left[\tilde{\rho} \left(\frac{\partial \tilde{h}_s}{\partial t} + \tilde{\vec{V}} \cdot \nabla \tilde{h}_s \right) - \frac{\gamma - 1}{\gamma} \frac{\partial \tilde{p}}{\partial t} + \tilde{\rho}_L \left(\frac{\partial \tilde{h}_{L_s}}{\partial t} + \tilde{\vec{V}}_L \cdot \nabla \tilde{h}_{L_s} \right) \right. \right. \tag{268}$$

$$\left. \left. + \tilde{W}_m \left(\tilde{h}_s - \tilde{h}_{L_s} \right) \right] \varphi_n dv - \int_s \tilde{H} \varphi_n ds \right\} dt$$

$$+ \int_o^{t^*} \left\{ \int_v \left[\frac{\partial \tilde{\rho}}{\partial t} + \nabla \cdot \left(\tilde{\rho} \tilde{\vec{V}} \right) - \tilde{W}_m \right] \tilde{h}_s \varphi_n dv - \int_s \left[\tilde{Q}_{mass} + \tilde{\rho} \tilde{\vec{V}} \cdot \vec{n} \right] \tilde{h}_s \varphi_n ds \right\} dt = 0$$

This result is very similar to Eq. (256) which was derived from the momentum equation; in this case the last volume and surface integrals represent the continuity equation and its boundary condition weighted by $\tilde{h}_s \varphi_n$. The product $\tilde{h}_s \varphi_n$ can also be expanded in terms of the complete set of functions φ_j. Introducing this expansion into Eq. (268) and imposing the orthogonality conditions which must be satisfied by the continuity equation and its boundary residual the last integrals in Eq. (268) vanish and the desired orthogonality condition becomes:

$$\int_o^{t^*} \left\{ \int_v \left[\tilde{\rho} \left(\frac{\partial \tilde{h}_s}{\partial t} + \tilde{\vec{V}} \cdot \nabla \tilde{h}_s \right) - \frac{\gamma - 1}{\gamma} \frac{\partial \tilde{p}}{\partial t} + \tilde{\rho}_L \left(\frac{\partial \tilde{h}_{L_s}}{\partial t} + \tilde{\vec{V}}_L \cdot \nabla \tilde{h}_{L_s} \right) \right. \right. \tag{269}$$

$$+ \tilde{W}_m\left(\tilde{h}_s - \tilde{h}_{L_s}\right)\Big]\varphi_n dv - \int_s \tilde{H}\varphi_n ds\Big\}dt = 0$$

Application to the Simplified Wave Equations. The Galerkin orthogonality conditions given by Eqs. (261) and (269) are applicable to more general problems than will be treated in this chapter. Since the third order analysis will be restricted to combustors with a distributed combustion process it is only necessary to consider boundary residuals at the nozzle entrance. In this case the pressure does not change across the boundary zone, thus $p = p_1$ in Eq. (261). Furthermore it is assumed that the combustion is complete before the nozzle is reached, therefore the boundary momentum and energy sources $\underrightarrow{M}$ and H vanish. Under these assumptions the Galerkin orthogonality conditions are particularly simple because the boundary residuals disappear. In deriving the simplified wave equations (i.e. Eqs. (46) through (48)) the momentum source due to the liquid phase was neglected, thus Eq. (261) becomes

$$\int_o^{t^*}\left\{\int_v\left[\tilde{\rho}\frac{\partial\tilde{\underrightarrow{V}}}{\partial t} + \tilde{\rho}\tilde{\underrightarrow{V}}\cdot\nabla\tilde{\underrightarrow{V}} + \frac{1}{\gamma}\nabla\tilde{p}\right]\varphi_n dv\right\}dt = 0 \qquad (270)$$

by using $p = p_1$, $\underrightarrow{M} = 0$, and dropping the liquid terms. It was also assumed (see Chapter III) that the stagnation enthalpy of the liquid is constant, which applied to the approximate liquid quantities gives:

$$\frac{\partial \tilde{h}_{L_s}}{\partial t} + \tilde{\vec{V}}_L \cdot \nabla \tilde{h}_{L_s} = 0 \tag{271}$$

Introducing Eq. (271) into Eq. (269) with H = 0 gives the following expression:

$$\int_0^{t^*} \left\{ \int_V \left[\tilde{\rho} \left(\frac{\partial \tilde{h}_s}{\partial t} + \tilde{\vec{V}} \cdot \nabla \tilde{h}_s \right) - \frac{\gamma - 1}{\gamma} \frac{\partial \tilde{p}}{\partial t} + \tilde{W}_m \left(\tilde{h}_s - \tilde{h}_{L_s} \right) \right] \varphi_n \, dv \right\} dt = 0 \tag{272}$$

Equations (270) and (272) can also be applied to the perturbed equations and will be used to obtain approximate solutions of the wave equations given by Eqs. (46) through (48) in Chapter III.

Equations Governing the Perturbations

The unsteady flow in the combustor is described by a system of five nonlinear partial differential equations and the equation of state. These are as follows: (1) the continuity equation (Eq. 46), (2), (3), (4) the three components of the Euler equation (Eq. 47), (5) the energy equation (Eq. 48), and (6) the equation of state (Eq. 34b). These equations must be solved for the six unknowns: ρ', the three velocity components, p', and h_s'. These equations were derived in vector form in Chapter III and must now be written in terms of a cylindrical coordinate system. This is easily accomplished for the continuity, energy, and state equations, but for the Euler equation it simplifies the algebra if one separates the unperturbed vector equation into its three scalar components before introducing perturbations. The resulting equations

are shown below:

Continuity:

$$\frac{\partial \rho'}{\partial t} + (\bar{\rho}(z) + \rho')\left[v_r' + \frac{1}{r} v' + \frac{1}{r} w_\theta' + u_z'\right] \tag{273}$$

$$+ v'\rho_r' + \frac{1}{r} w'\rho_\theta' + u'\rho_z' + \rho' \frac{d\bar{u}}{dz} + \bar{u}\rho_z' + u' \frac{d\bar{\rho}}{dz} - \dot{W}_m' = 0$$

Radial momentum:

$$(\bar{\rho}+\rho')v_t' + (\bar{\rho}+\rho')\left[v'v_r' + \frac{1}{r} w'v_\theta' - \frac{1}{r} (w')^2 + (\bar{u}+u')v_z'\right] = - \frac{1}{\gamma} p_r' \tag{274}$$

Tangential momentum:

$$(\bar{\rho}+\rho')\left[w_t' + v'w_r' + \frac{w'}{r} w_\theta' + \frac{v'w'}{r} + (\bar{u}+u')w_z'\right] = - \frac{1}{\gamma r} p_\theta' \tag{275}$$

Axial momentum:

$$(\bar{\rho}+\rho')\left[u_t' + v'u_r' + \frac{1}{r} w'u_\theta' + u'u_z' + u' \frac{d\bar{u}}{dz} + \bar{u}u_z'\right] + \rho'\bar{u} \frac{d\bar{u}}{dz} = - \frac{1}{\gamma} p_z' \tag{276}$$

Energy:

$$(\bar{\rho}+\rho')\left[\frac{\partial h_s'}{\partial t} + v' \frac{\partial h_s'}{\partial r} + \frac{1}{r} w' \frac{\partial h_s'}{\partial \theta} + u' \frac{\partial h_s'}{\partial z} + \bar{u} \frac{\partial h_s'}{\partial z}\right] \tag{277}$$

$$- \frac{\gamma-1}{\gamma} \frac{\partial p'}{\partial t} + \frac{d}{dz} (\bar{\rho}\bar{u}) h_s' + W_m' h_s' = 0$$

State:

$$p' = \bar{\rho} h_s' + \rho' \bar{h}_s + \rho' h_s' \tag{278}$$

$$- \frac{\gamma-1}{2} \left[(\bar{\rho}+\rho') \left(v'^2 + w'^2 + u'^2 \right) + 2(\bar{\rho}+\rho') \bar{u} u' + \rho' \bar{u}^2 \right]$$

In the above equations the steady state density is a function of the distance from the injector; the reference quantities used in the non-dimensionalization of these equations correspond to stagnation conditions at the injector end of the chamber. The quantities v', w', and u' respectively represent the radial, tangential, and axial components of the velocity perturbation.

The solutions to Eqs. (273) through (278) must satisfy rigid wall boundary conditions at the injector face and the outer wall, while the nozzle admittance condition must be satisfied at the nozzle entrance. These boundary conditions are expressed in cylindrical coordinates as follows:

$$v' = 0 \quad \text{at} \quad r = 1 \tag{279}$$

$$u' = 0 \quad \text{at} \quad z = 0$$

$$B_1 = Q_m' + \bar{\rho} u' + \rho' \bar{u} + \rho' u' = 0 \quad \text{at} \quad z = z_e$$

Introduction of Quasi-Potentials

In order to obtain an approximate solution using the Galerkin method the six dependent variables must be expanded in terms of a complete set of functions φ_n. In the second order analysis the φ_n were chosen to be the acoustic eigenfunctions, and the single dependent variable Φ was expanded in terms of these functions. Since the form of combustion instability often resembles the natural acoustic modes it is also desirable in the third order theory to expand the dependent variables in terms of the acoustic eigenfunctions. The variables ρ', p', and h_s' can be adequately represented in this manner because the space dependence of these thermodynamic properties is similar to that of the velocity potential Φ. On the other hand the components of the velocity perturbation resemble those obtained from potential flow; that is $v' \sim \Phi_r$, $w' \sim \frac{1}{r}\Phi_\theta$, $u' \sim \Phi_z$. In order to obtain a good approximation, therefore, the velocity components must be expanded in terms of the appropriate derivatives of φ_n. Thus it appears that an adequate solution cannot be obtained by expanding the velocity components and the thermodynamic properties in terms of the same set of eigenfunctions φ_n. It is possible to introduce additional sets of functions, but this procedure greatly complicates the analysis and the boundary conditions at the wall can no longer be easily satisfied.

The above mentioned difficulties can be circumvented by expressing the velocity components in terms of "quasi-potentials". These functions were used by Zinn[7] and are defined by:

$$\eta = \int_o^r v'dr + g(\theta, z, t) \tag{280}$$

$$\zeta = \int_o^\theta rw'd\theta + h(r, z, t)$$

$$\Phi = \int_o^z u'dz + f(r, \theta, t)$$

where g, h, and f are arbitrary functions of their arguments. Differentiating these expressions with respect to the variable of integration yields particularly simple relations for the velocity components:

$$v' = \eta_r(r, \theta, z, t) \tag{281}$$

$$w' = \frac{1}{r}\zeta_\theta(r, \theta, z, t)$$

$$u' = \Phi_z(r, \theta, z, t)$$

The use of the quasi-potentials has the same advantages as the velocity potential without restricting the flow to be irrotational. Irrotationality only occurs when η, ζ, and Φ differ only as a result of the functions g, h, and f, in which case Eqs. (281) reduce to $\underrightarrow{V}' = \nabla\Phi$. The functions η, ζ, and Φ can be expanded in terms of the acoustic eigenfunctions φ_n with the result that the velocity perturbations will be expressed in terms of the derivatives of φ_n as desired.

The governing differential equations (i.e. Eqs. (273) through (278)) are easily written in terms of the quasi-potentials as follows:

Continuity:

$$\frac{\partial \rho'}{\partial t} + \left[\bar{\rho}(z) + \rho'\right]\left[\eta_{rr} + \frac{1}{r}\eta_r + \frac{1}{r^2}\zeta_{\theta\theta} + \Phi_{zz}\right] \tag{282}$$

$$+ \eta_r \rho_r' + \frac{1}{r^2}\zeta_\theta \rho_\theta' + \Phi_z \rho_z' + \rho' \frac{d\bar{u}}{dz} + \bar{u}\rho_z' + \Phi_z \frac{d\bar{\rho}}{dz} - W_m' = 0$$

Radial momentum:

$$(\bar{\rho}+\rho')\left[\eta_{rt} + \eta_r \eta_{rr} + \frac{1}{r^2}\zeta_\theta \eta_{r\theta} - \frac{1}{r^3}\zeta_\theta^2 + \left(\bar{u}+\Phi_z\right)\eta_{rz}\right] + \frac{1}{\gamma} p_r' = 0 \tag{283}$$

Tangential momentum:

$$(\bar{\rho}+\rho')\left[\zeta_{\theta t} + \eta_r \zeta_{r\theta} + \frac{1}{r^2}\zeta_\theta \zeta_{\theta\theta} + \left(\bar{u}+\Phi_z\right)\zeta_{\theta z}\right] + \frac{1}{\gamma} p_\theta' = 0 \tag{284}$$

Axial momentum:

$$(\bar{\rho}+\rho')\left[\Phi_{zt} + \eta_r \Phi_{rz} + \frac{1}{r^2}\zeta_\theta \Phi_{\theta z} + \left(\bar{u}+\Phi_z\right)\Phi_{zz} + \Phi_z \frac{d\bar{u}}{dz}\right] \tag{285}$$

$$+ \rho' \bar{u} \frac{d\bar{u}}{dz} + \frac{1}{\gamma} p_z' = 0$$

Energy:

$$(\bar{\rho}+\rho')\left[\frac{\partial h_s'}{\partial t} + \eta_r \frac{\partial h_s'}{\partial r} + \frac{1}{r^2}\zeta_\theta \frac{\partial h_s'}{\partial \epsilon} + \left(\bar{u} + \Phi_z\right)\frac{\partial h_s'}{\partial z}\right] \tag{286}$$

$$- \frac{\gamma-1}{\gamma}\frac{\partial p'}{\partial t} + \frac{d}{dz}(\bar{\rho}\bar{u})h_s' + W_m' h_s' = 0$$

Equation of State:

$$p' = \bar{\rho}h_s' + \rho'\bar{h}_s + \rho' h_s' \tag{287}$$

$$- \frac{\gamma-1}{2}\left[(\bar{\rho}+\rho')\left(\eta_r^2 + \frac{1}{r^2}\zeta_\theta^2 + \Phi_z^2\right) + 2(\bar{\rho}+\rho')\bar{u}\Phi_z + \rho'\bar{u}^2\right]$$

The corresponding boundary conditions (i.e. Eq. (279)) become:

$$\eta_r = 0 \quad \text{at} \quad r = 1 \tag{288}$$

$$\Phi_z = 0 \quad \text{at} \quad z = 0$$

$$B_1 = Q_m' + \bar{\rho}\Phi_z + \rho'\bar{u} + \rho'\Phi_z = 0 \quad \text{at} \quad z = z_e$$

To complete the mathematical description of the problem the mass sources W_m' and Q_m' must be expressed as functions of the dependent variables. Such expressions correct to third order were derived in Chapter IV for a combustion process described by Crocco's time lag model and a quasi-steady nozzle. Equation (109) for W_m' will be repeated here for convenience:

$$W_m' = n \frac{d\bar{u}}{dz} \left\{ \left(p'-p_\tau'\right) + \frac{n-1}{2} (p')^2 - np'p_\tau' \right. \tag{289}$$

$$\left. + \frac{n+1}{2} \left(p_\tau'\right)^2 - n \frac{\partial p_\tau'}{\partial t} \int_{t-\bar{\tau}}^{t} p'(t')\,dt' \right\}$$

where $p_\tau' = p'(r, \theta, z, t-\bar{\tau})$. The expression for Q_m' (i.e. Eq. (119)) involves the velocity components and will be expressed in terms of the quasi-potentials as follows:

$$Q_m' = - \frac{\gamma+1}{2} \bar{u}_e \rho' - \frac{1}{8} (\gamma-1)(\gamma+1) \frac{\bar{u}_e}{\bar{\rho}_e} (\rho')^2 - \frac{\gamma+1}{4} \frac{\bar{\rho}_e}{\bar{c}_e^2} \left[3\bar{u}_e^2 \Phi_z + 3\bar{u}_e \Phi_z^2 \right. \tag{290}$$

$$\left. + \bar{u}_e \left(\eta_r^2 + \frac{1}{r^2} \zeta_\theta^2\right) + \Phi_z \left(\eta_r^2 + \frac{1}{r^2} \zeta_\theta^2 + \Phi_z^2\right) \right]$$

In order to obtain solutions of Eqs. (282) through (287) the steady state velocity $\bar{u}(z)$ and density $\bar{\rho}(z)$ must be known. By using a specific combustion model, as in the analysis of Priem and Heidmann[31], $\bar{u}(z)$ and $\bar{\rho}(z)$ could be determined by numerically solving the steady state conservation equations where the droplet-gas interaction has been taken into account. To avoid the necessity of making such lengthy calculations the velocity distribution $\bar{u}(z)$ will be assumed and $\bar{\rho}(z)$ computed so as to satisfy continuity requirements.

Expansion of the Dependent Variables

As discussed previously each of the dependent variables can be expanded in a series of acoustic eigenfunctions with time dependent

coefficients similar to those used in the expansion for $\tilde{\Phi}$ (see Eq. (215) Chapter VI). However the number of terms arising from the products of three perturbations (cubic nonlinearities) is very large even for series expansions of only a few terms. It was therefore decided to limit the discussion in this chapter to an expansion consisting of a single standing transverse mode whose spatial dependence is given by:

$$\Psi_{mn}(r, \theta) = \cos m\theta J_m\left(S_{mn} r\right) \tag{291}$$

Thus each of the dependent variables is expressed as the product of Ψ_{mn} and an unknown function of time to be determined by the Galerkin method. Since the assumed spatial dependence Ψ_{mn} is not a function of z, the axial quasi-potential Φ can be assumed to be zero. The dependent variables can then be expressed in the following form:

$$\tilde{\rho}' = A_\rho(t)\Psi_{mn}(r, \theta) \tag{292}$$

$$\tilde{\eta} = A_\eta(t)\Psi_{mn}(r, \theta)$$

$$\tilde{\zeta} = A_\zeta(t)\Psi_{mn}(r, \theta)$$

$$\tilde{p}' = A_p(t)\Psi_{mn}(r, \theta)$$

$$\tilde{h}_s' = A_h(t)\Psi_{mn}(r, \theta)$$

Formation of the Residuals

The assumed solutions given by Eq. (292) are now substituted into the differential equations to obtain the following residuals:

Continuity:

$$E_\rho = \left\{\frac{dA_\rho}{dt} + \bar{\rho}(z)\left[\left(\frac{m^2}{r^2} - S_{mn}^2\right)A_\eta - \frac{m^2}{r^2}A_\zeta\right] + \frac{d\bar{u}}{dz}A_\rho\right\}\cos m\theta J_m\left(S_{mn}r\right) \quad (293)$$

$$+ \left\{\left(\frac{m^2}{r^2} - S_{mn}^2\right)A_\rho A_\eta - \frac{m^2}{r^2}A_\rho A_\zeta\right\}\cos^2 m\theta J_m^2\left(S_{mn}r\right)$$

$$+ S_{mn}^2 A_\rho A_\eta \cos^2 m\theta\left[J_m'\left(S_{mn}r\right)\right]^2 + \frac{m^2}{r^2}A_\rho A_\zeta \sin^2 m\theta J_m^2\left(S_{mn}r\right) - \tilde{W}_m'$$

Radial Momentum:

$$E_\eta = \left[\bar{\rho}(z)\frac{dA_\eta}{dt} + \frac{1}{\gamma}A_p\right]S_{mn}\cos m\theta J_m'\left(S_{mn}r\right) \quad (294)$$

$$+ A_\rho \frac{dA_\eta}{dt} S_{mn}\cos^2 m\theta J_m J_m' + \bar{\rho}(z)A_\eta^2 S_{mn}^3 \cos^2 m\theta J_m' J_m''$$

$$+ \bar{\rho}(z)\frac{m^2}{r^2}A_\eta A_\zeta S_{mn}\sin^2 m\theta J_m J_m' - \bar{\rho}(z)\frac{m^2}{r^3}A_\zeta^2 \sin^2 m\theta J_m^2$$

$$+ A_\rho A_\eta^2 S_{mn}^3 \cos^3 m\theta J_m J_m' J_m'' + \frac{m^2}{r^2}A_\rho A_\eta A_\zeta S_{mn}\sin^2 m\theta \cos m\theta J_m^2 J_m'$$

$$- \frac{m^2}{r^3} A_\rho A_\zeta^2 \sin^2 m\theta \cos m\theta J_m^3\left(S_{mn} r\right)$$

Tangential Momentum:

$$E_\zeta = \left[\bar{\rho}(z) \frac{dA_\zeta}{dt} + \frac{1}{\gamma} A_p\right] m \sin m\theta J_m\left(S_{mn} r\right) \tag{295}$$

$$+ A_\rho \frac{dA_\zeta}{dt} m \sin m\theta \cos m\theta J_m^2 + \bar{\rho}(z) A_\eta A_\zeta m S_{mn}^2 \sin m\theta \cos m\theta \left(J_m'\right)^2$$

$$- \frac{1}{r^2} \bar{\rho}(z) A_\zeta^2 m^3 \sin m\theta \cos m\theta J_m^2$$

$$+ A_\rho A_\eta A_\zeta m S_{mn}^2 \sin m\theta \cos^2 m\theta J_m \left(J_m'\right)^2 - \frac{1}{r^2} A_\rho A_\zeta^2 m^3 \sin m\theta \cos^2 m\theta J_m^3$$

Energy:

$$E_h = \left[\bar{\rho}(z) \frac{dA_h}{dt} - \frac{\gamma - 1}{\gamma} \frac{dA_\rho}{dt} + \frac{d}{dz} (\bar{\rho} \bar{v}) A_h\right] \cos m\theta J_m\left(S_{mn} r\right) \tag{296}$$

$$+ A_\rho \frac{dA_h}{dt} \cos^2 m\theta J_m^2 + \bar{\rho}(z) A_\eta A_h S_{mn}^2 \cos^2 m\theta \left(J_m'\right)^2$$

$$+ \bar{\rho}(z) \frac{m^2}{r^2} A_\zeta A_h \sin^2 m\theta J_m^2 + \tilde{W}_m' A_h \cos m\theta J_m\left(S_{mn} r\right)$$

$$+ A_\rho A_\eta A_h S_{mn}^2 \cos^3 m\theta J_m \left(J_m'\right)^2 + \frac{m^2}{r^2} A_\rho A_\zeta A_h \cos m\theta \sin^2 m\theta J_m^3$$

Equation of State:

$$E_p = \left[A_p - \bar{\rho}(z)A_h - \bar{h}_s A_\rho + \frac{\gamma-1}{2}\bar{u}^2 A_\rho\right]\cos m\theta J_m\left(S_{mn}r\right) \qquad (297)$$

$$- A_\rho A_h \cos^2 m\theta J_m^2 + \frac{\gamma-1}{2}\bar{\rho}(z)A_\eta^2 S_{mn}^2 \cos^2 m\theta \left(J_m'\right)^2$$

$$+ \frac{\gamma-1}{2}\bar{\rho}(z)\frac{m^2}{r^2}A_\zeta^2 \sin^2 m\theta J_m^2 + \frac{\gamma-1}{2}A_\rho A_\eta^2 S_{mn}^2 \cos^3 m\theta J_m\left(J_m'\right)^2$$

$$+ \frac{\gamma-1}{2}\frac{m^2}{r^2}A_\rho A_\zeta^2 \cos m\theta \sin^2 m\theta J_m^3$$

where the residual of the axial momentum equation has been omitted in order to be consistent with the assumption of a two-dimensional solution. In the above expressions the function $J_m\left(S_{mn}r\right)$ has been expressed as J_m and the primes indicate differentiation of the Bessel function with respect to its argument. These residuals are valid for both radial ($m = 0$) and tangential ($m = 1, 2, \ldots$) modes. In the case of radial modes, however, the tangential velocity component is zero, consequently the residual E_ζ vanishes and the tangential quasi-potential A_ζ is not needed. It is seen that all of the terms involving A_ζ disappear when $m = 0$.

The nozzle boundary residual is obtained by substituting the assumed solutions into Eq. (228), which yields the following result:

$$B_\rho = \tilde{Q}' + \bar{u}_e A_\rho \cos m\theta J_m\left(S_{mn}r\right) \qquad (298)$$

Differential Equations Governing the Unknown Amplitudes

The unknown functions $A_\rho(t)$, $A_\eta(t)$, $A_\zeta(t)$, $A_p(t)$, and $A_h(t)$ are determined by requiring the residuals to satisfy the Galerkin orthogonality conditions. The conditions applied to the continuity equation residual E_ρ and its boundary residual B_ρ are the same as given in Chapter II except that the time integration is omitted, thus:

$$\int_o^{z_e}\int_o^{2\pi}\int_o^1 E_\rho \Psi_{mn}(r, \theta)\, r\,dr\,d\theta\,dz - \int_o^{2\pi}\int_o^1 B_\rho \Psi_{mn}(r, \theta)\, r\,dr\,d\theta = 0 \qquad (299)$$

From Eqs. (270) and (272) it is seen that no boundary residuals are needed for the Euler and energy equations thus the appropriate orthogonality conditions are simply:

$$\int_o^{z_e}\int_o^{2\pi}\int_o^1 E_\eta \Psi_{mn}(r, \theta)\, r\,dr\,d\theta\,dz = 0 \qquad (300)$$

$$\int_o^{z_e}\int_o^{2\pi}\int_o^1 E_\zeta \Psi_{mn}(r, \theta)\, r\,dr\,d\theta\,dz = 0 \qquad (301)$$

$$\int_o^{z_e}\int_o^{2\pi}\int_o^1 E_h \Psi_{mn}(r, \theta)\, r\,dr\,d\theta\,dz = 0 \qquad (302)$$

In the treatment of the equation of state it is possible to solve Eq. (287) for h_s' and substitute the result into the energy equation to eliminate h_s'. This procedure not only results in cumbersome equations

but also introduces higher order nonlinearities and is therefore undesirable. Instead the Galerkin method will also be applied to the residual of the equation of state as follows:

$$\int_o^{z_e}\int_o^{2\pi}\int_o^{1} E_p \Psi_{mn}(r, \theta)\, r\,dr\,d\theta\,dz = 0 \tag{303}$$

In each of the above expressions the weighting function is $\Psi_{mn}(r, \theta) = \cos m\theta J_m\left(S_{mn} r\right)$.

In performing the integrations indicated in Eqs. (299) through (303) several definite integrals involving products of trigonometric or Bessel functions arise. Those involving trigonometric functions are given below:

$$\int_o^{2\pi} \cos^2 m\theta\, d\theta = \begin{cases} 2\pi & \text{for } (m = 0) \\ \pi & (m \neq 0) \end{cases} \tag{304a}$$

$$\int_o^{2\pi} \sin m\theta \cos m\theta\, d\theta = 0 \tag{304b}$$

$$\int_o^{2\pi} \cos^3 m\theta\, d\theta = \begin{cases} 2\pi & (m = 0) \\ 0 & (m \neq 0) \end{cases} \tag{304c}$$

$$\int_o^{2\pi} \sin^2 m\theta \cos m\theta\, d\theta = 0 \tag{304d}$$

$$\int_0^{2\pi} \sin m\theta \cos^2 m\theta \, d\theta = 0 \tag{304e}$$

$$\int_0^{2\pi} \cos^4 m\theta \, d\theta = \begin{cases} 2\pi & (m = 0) \\ 3\pi/4 & (m \neq 0) \end{cases} \tag{304f}$$

$$\int_0^{2\pi} \sin^2 m\theta \cos^2 m\theta \, d\theta = \begin{cases} 0 & (m = 0) \\ \pi/4 & (m \neq 0) \end{cases} \tag{304g}$$

$$\int_0^{2\pi} \sin m\theta \cos^3 m\theta \, d\theta = 0 \tag{304h}$$

while those involving Bessel functions are defined in Appendix B. These latter integrals must be evaluated numerically. In the developments to follow these integrals will be designated by the symbol $J_i^{(k)}$ where the superscript refers to the number of Bessel functions in the integrand.

Introducing the residuals as given by Eqs. (293) through (297) into Eqs. (299) through (303) and performing the integrations is expected to yield a system of four ordinary differential equations and one algebraic equation to be solved for the five unknown A's. However a difficulty arises in regard to the tangential momentum equation. In this case each term in the volume integral of Eq. (301) contains as a multiplying factor an integral over θ which vanishes (see Eqs. 304). Thus the orthogonality condition imposed upon the residual of the tangential momentum equation is satisfied for all values of the unknown

A's and no information is obtained from this equation. This result is a direct consequence of the fact that each term in the tangential momentum equation contains a factor that is differentiated only once with respect to θ.

The above mentioned difficulty poses no problem in the case of radial modes ($m = 0$) since the function A_ζ is not needed. For $m > 0$, however, there will be fewer equations than unknowns, and unless another equation can be found no solution can be obtained. The necessary equation can be extracted from the tangential momentum equation by weighting its residual with the function $\Phi_{mn}(r, \theta) = \sin m\theta J_m\left(S_{mn} r\right)$. This procedure will be justified rigorously after the differential equations governing the behavior of the A's are derived.

Applying the Galerkin method in the manner described above yields the desired differential equations. Since the integrals given by Eqs. (304) for $m = 0$ differ from those for $m \neq 0$, the cases of radial and tangential modes will be treated separately.

Equations Governing Tangential Modes. The equations which describe the behavior of the unknown A's for $m \neq 0$ can be written in the following form:

Continuity:

$$\frac{dA_\rho}{dt} = -\frac{\gamma+1}{2}\frac{\bar{u}_e}{z_e} A_\rho + I_\rho\left(S_{mn}^2 - m^2 K_1\right)A_\eta + I_\rho m^2 K_1 A_\zeta \qquad (305)$$

$$+ \frac{n\bar{u}_e}{z_e}\left[A_p(t) - A_p(t-\bar{\tau})\right]$$

Radial Momentum:

$$\frac{dA_\eta}{dt} = -\frac{1}{\gamma I_\rho} A_p - \frac{3}{4}\frac{S_{mn}^2}{I_\rho} K_2 A_\rho A_\eta^2 - \frac{1}{4}\frac{m^2}{I_\rho} K_3 A_\rho A_\eta A_\zeta \tag{306}$$

$$+ \frac{1}{4}\frac{m^2}{S_{mn}}\frac{1}{I_\rho} K_4 A_\rho A_\zeta^2$$

Tangential Momentum:

$$\frac{dA_\zeta}{dt} = -\frac{1}{\gamma I_\rho} A_p - \frac{1}{4}\frac{S_{mn}^2}{I_\rho} K_5 A_\rho A_\eta A_\zeta + \frac{m^2}{4I_\rho} K_6 A_\rho A_\zeta^2 \tag{307}$$

Energy:

$$\frac{dA_h}{dt} - \frac{\gamma-1}{\gamma I_\rho}\frac{dA_p}{dt} = -\left\{\frac{\bar{\rho}_e \bar{u}_e}{z_e}\frac{1}{I_\rho} A_h + \frac{3}{4}\frac{S_{mn}^2}{I_\rho} K_5 A_\rho A_\eta A_h + \frac{1}{4}\frac{m^2}{I_\rho} K_6 A_\rho A_\zeta A_h\right\} \tag{308}$$

Equation of State:

$$A_h = \frac{1}{I_\rho}\left\{A_p - \left[1 - \frac{\gamma-1}{2} I_u\right] A_\rho + \frac{3(\gamma-1)}{8} S_{mn}^2 K_5 A_\rho A_\eta^2 \right. \tag{309}$$

$$\left. + \frac{\gamma-1}{8} m^2 K_6 A_\rho A_\zeta^2\right\}$$

The constants K_i which appear in the above equations are defined in

terms of the integrals of the Bessel functions as follows:

$$K_1 = \frac{J_3^{(2)}(m,n)}{J_1^{(2)}(m,n)} \quad ; \quad K_4 = \frac{J_2^{(4)}(m,n)}{J_2^{(2)}(m,n)} \tag{310}$$

$$K_2 = \frac{J_5^{(4)}(m,n)}{J_2^{(2)}(m,n)} \quad ; \quad K_5 = \frac{J_4^{(4)}(m,n)}{J_1^{(2)}(m,n)}$$

$$K_3 = \frac{J_3^{(4)}(m,n)}{J_2^{(2)}(m,n)} \quad ; \quad K_6 = \frac{J_1^{(4)}(m,n)}{J_1^{(2)}(m,n)}$$

These constants are evaluated in Appendix B. As a result of the integration over the length of the combustor the average quantities I_ρ and I_u appear and are defined by:

$$I_\rho = \frac{1}{z_e}\int_o^{z_e} \bar{\rho}(z)\,dz \qquad I_u = \frac{1}{z_e}\int_o^{z_e} \bar{u}^2 dz \tag{311}$$

From Eqs. (305) through (309) a number of interesting observations can be made. The θ-integrals associated with the quadratically nonlinear terms (see Eqs. 304c, d, and e) all vanish for $m \neq 0$, thus all of the nonlinear terms appearing in these equations consists of products of three dependent variables; that is, they are cubically nonlinear. This result is in harmony with the results of Chapter VI; that is, to second order no nonlinearities are obtained with a series

consisting of a single tangential mode. Under the assumption of small mean flow Mach number, cubic nonlinearities were neglected in the expressions for W_m' and Q_m'. As a result the response of the combustion process and the nozzle to pressure oscillations is linear in this case.

The nonlinear terms on the right hand side of Eq. (306) are seen to differ from those in Eq. (307). Consequently it is expected that the quasi-potential functions A_η and A_ζ will not be equal, which implies that the unsteady flow will be rotational. This is strictly a nonlinear effect because the linearized versions of Eqs. (306) and (307) indicate that A_η and A_ζ can differ at most only by a constant, which is equivalent to potential flow. This result is consistent with the analysis of Chapter III where it was shown that for low Mach number flows the generation of vorticity is a third order effect.

Equations Governing Radial Modes. The governing differential equations for radial modes (m = 0) are given below:

Continuity:

$$\frac{dA_\rho}{dt} = S_{On}^2 I_\rho A_\eta - S_{On}^2 \left(K_2' - K_1'\right) A_\rho A_\eta \tag{312}$$

$$- \frac{\gamma+1}{2} \frac{\bar{u}_e}{z_e} A_\rho - \frac{(\gamma-1)(\gamma+1)}{8} \frac{\bar{u}_e}{z_e} K_1' A_\rho^2 - \frac{\gamma+1}{4} \frac{\bar{u}_e}{z_e} S_{On}^2 K_2' A_\eta^2$$

$$+ \frac{n\bar{u}_e}{z_e} \left\{ \left[A_p(t) - A_p(t-\bar{\tau}) \right] + K_1' \left[\frac{n-1}{2} A_p^2(t) - n A_p(t) A_p(t-\bar{\tau}) \right.\right.$$

$$\left.\left. + \frac{n+1}{2} A_p^2(t-\bar{\tau}) - n \frac{dA_p}{dt} (t-\bar{\tau}) \int_{t-\bar{\tau}}^{t} A_p(t')\, dt' \right] \right\}$$

Radial Momentum:

$$\frac{dA_\eta}{dt} = - \frac{\frac{1}{\gamma I_\rho} A_p + S_{On}^2 \left[K_4' + \left(\frac{K_5'}{I_\rho} \right) A_\rho \right] A_\eta^2}{\left[1 + \frac{K_3'}{I_\rho} A_\rho \right]} \tag{313}$$

Energy Equation:

$$\left[1 + \left(\frac{K_1'}{I_\rho} \right) A_\rho \right] \frac{dA_h}{dt} - \frac{\gamma-1}{\gamma} \frac{1}{I_\rho} \frac{dA_p}{dt} = - \frac{\bar{\rho}_e \bar{u}_e}{z_e} \frac{1}{I_\rho} A_h - S_{On}^2 K_2' A_\eta A_h \tag{314}$$

$$- S_{On}^2 \frac{K_6'}{I_\rho} A_\rho A_\eta A_h - \frac{n\bar{u}_e}{z_e} \frac{K_1'}{I_\rho} \left[A_p(t) - A_p(t-\bar{\tau}) \right] A_h$$

Equation of State:

$$A_h = \left[1 + \left(\frac{K_1}{I_\rho} \right) A_\rho \right]^{-1} \left\{ \frac{A_p}{I_\rho} - \frac{1}{I_\rho} \left(1 - \frac{\gamma-1}{2} I_u \right) A_\rho \right. \tag{315}$$

$$\left. + \frac{\gamma-1}{2} S_{On}^2 K_2' A_\eta^2 + \frac{\gamma-1}{2} S_{On}^2 \frac{K_6'}{I_\rho} A_\rho A_\eta^2 \right\}$$

The constants K_i' differ from those corresponding to tangential modes; they are defined as follows:

$$K_1' = \frac{J_1^{(3)}(0,n)}{J_1^{(2)}(0,n)} \quad ; \quad K_4' = \frac{J_4^{(3)}(0,n)}{J_2^{(2)}(0,n)} \tag{316}$$

$$K_2' = \frac{J_2^{(3)}(0,n)}{J_1^{(2)}(0,n)} \quad ; \quad K_5' = \frac{J_5^{(4)}(0,n)}{J_2^{(2)}(0,n)}$$

$$K_3' = \frac{J_3^{(3)}(0,n)}{J_2^{(2)}(0,n)} \quad ; \quad K_6' = \frac{J_4^{(4)}(0,n)}{J_1^{(2)}(0,n)}$$

The case of radial mode instability is interesting because the governing differential equations contain both quadratic and cubic nonlinearities as well as a nonlinear combustion mass source. The nonlinear driving terms appear in the continuity equation (Eq. 312) and are of quadratic form. Additional quadratically nonlinear terms arise from the quasi-steady nozzle boundary condition; one of these terms accounts for the effect of transverse velocity components on the unsteady flow through the nozzle[27]. The remaining nonlinear terms arise from the chamber gasdynamics. The radial mode case therefore provides an opportunity to study the relative importance of nonlinearities associated with the various physical phenomena of combustion instability.

Numerical Solution and Initial Conditions

The differential equations which describe the unknown amplitudes can be solved numerically by the fourth order Runge-Kutta method as described in Appendix C. In order to start the integration of these equations the values of A_ρ, A_η, A_ζ, and A_p must be specified at the

initial time $t = 0$ (A_h is eliminated from the equations with the aid of the equation of state). Furthermore $A_p(t)$ must be given as a function of time for $-\bar{\tau} \leq t \leq 0$. Rather than consider an arbitrary choice of the initial conditions, it will be assumed that an acoustic oscillation is initially present in the combustor. Under these circumstances the initial values of A_ρ, A_η, and A_ζ can all be related to the pressure A_p from the acoustic solutions.

The acoustic solutions in terms of the quasi-potentials are easily obtained by solving the linearized equations for the case of no mean flow. These equations are obtained from Eqs. (305) through (309) by introducing $\bar{u}_e = 0$ and dropping all nonlinear terms and are shown below:

$$\frac{dA_\rho}{dt} = \left(S_{mn}^2 - m^2 K_1\right) A_\eta + m^2 K_1 A_\zeta \tag{317}$$

$$\frac{dA_\eta}{dt} = -\frac{1}{\gamma} A_p \tag{318}$$

$$\frac{dA_\zeta}{dt} = -\frac{1}{\gamma} A_p \tag{319}$$

$$\frac{dA_p}{dt} = \gamma \frac{dA_\rho}{dt} \tag{320}$$

The last of these was obtained by combining the energy equation and the equation of state to eliminate A_h. Differentiating Eq. (317) and intro-

ducing Eqs. (318) and (319) yields:

$$\gamma \frac{d^2 A_\rho}{dt^2} = - S_{mn}^2 A_p \tag{321}$$

while differentiating Eq. (320) and substituting the result into Eq. (321) produces a second order differential equation describing $A_p(t)$:

$$\frac{d^2 A_p}{dt^2} + S_{mn}^2 A_p = 0 \tag{322}$$

Equation (322) describes a simple harmonic oscillator of natural frequency S_{mn} as expected. Assuming that the pressure A_p attains its maximum value at $t = 0$; that is, $A_p(0) = P_M$, $A_p'(0) = 0$ the solution to Eq. (322) becomes:

$$A_p(t) = P_M \cos S_{mn} t \tag{323}$$

The quantities A_ρ, A_η, and A_ζ are related to $A_p(t)$ by introducing Eq. (323) into Eqs. (318) through (320) and performing the integrations. Since the acoustic quantities oscillate about the undisturbed condition all arbitrary constants that arise will be taken to be zero. Thus the following relations are obtained:

$$A_\rho(t) = \frac{P_M}{\gamma} \cos S_{mn} t \tag{324}$$

$$A_\eta(t) = A_\zeta(t) = \frac{-P_M}{\gamma S_{mn}} \sin S_{mn} t \tag{325}$$

The initial conditions will therefore be expressed in the following form:

$$A_p(0) = P_M \tag{326}$$

$$A_\rho(0) = 1/\gamma \, P_M$$

$$A_\eta(0) = A_\zeta(0) = 0$$

Although Eqs. (326) were derived for tangential modes, repeating the analysis with $m = 0$ yields the same results, except that $A_\zeta(0)$ does not appear.

Justification of the Treatment of the Tangential Momentum Equation

In deriving Eqs. (307) it was necessary to depart from the conventional Galerkin procedure and weight the residual of the tangential momentum equation with $\Phi_{mn}(r, \theta) = \sin m\theta J_m\left(S_{mn} r\right)$ which was not included in the assumed expansion of the dependent variables. This procedure can now be justified by expanding the dependent variables in terms of the two sets of functions:

$$\Psi_{mn}(r, \theta) = \cos m\theta J_m\left(S_{mn} r\right) \tag{327}$$

$$\Phi_{mn}(r, \theta) = \sin m\theta J_m\left(S_{mn} r\right) \tag{328}$$

This expansion is similar to that employed in the solution of the second order equation in order to account for the possibility of spinning waves. Retaining only one mode in the series the dependent variables are expressed in the following form:

$$\widetilde{\rho}' = A_\rho(t)\Psi_{mn}(r, \theta) + B_\rho(t)\Phi_{mn}(r, \theta) \tag{329}$$

$$\widetilde{\eta} = A_\eta(t)\Psi_{mn}(r, \theta) + B_\eta(t)\Phi_{mn}(r, \theta)$$

$$\widetilde{\zeta} = A_\zeta(t)\Psi_{mn}(r, \theta) + B_\zeta(t)\Phi_{mn}(r, \theta)$$

$$\widetilde{p}' = A_p(t)\Psi_{mn}(r, \theta) + B_p(t)\Phi_{mn}(r, \theta)$$

$$\widetilde{h}_s' = A_h(t)\Psi_{mn}(r, \theta) + B_h(t)\Phi_{mn}(r, \theta)$$

Applying the Galerkin orthogonality conditions to the residual of the tangential momentum equation (formed by introducing Eqs. (329) into Eq. (284)) yields the following pair of differential equations:

$$\frac{dA_\zeta}{dt} = -\frac{1}{\gamma I_\rho} A_p \tag{330}$$

$$+\frac{1}{4}\frac{S_{mn}^2}{I_\rho} K_5\left[A_\rho B_\eta B_\zeta - A_\rho A_\eta A_\zeta + B_\rho A_\eta B_\zeta - 3B_\rho B_\eta A_\zeta\right]$$

$$+\frac{m^2}{4I_\rho} K_6\left[A_\rho A_\zeta^2 - A_\rho B_\zeta^2 - B_\rho A_\zeta B_\zeta + 3B_\rho A_\zeta B_\zeta\right]$$

$$\frac{dB_\zeta}{dt} = -\frac{1}{\gamma I_\rho} B_p \tag{331}$$

$$+\frac{1}{4}\frac{S_{mn}^2}{I_\rho} K_5\left[B_\rho A_\eta A_\zeta - B_\rho B_\eta B_\zeta + A_\rho A_\zeta B_\eta - 3A_\rho A_\eta B_\zeta\right]$$

$$+\frac{m^2}{4I_\rho} K_6\left[B_\rho B_\zeta^2 - B_\rho A_\zeta^2 - A_\rho A_\zeta B_\zeta + 3A_\rho A_\zeta B_\zeta\right]$$

Equation (330), which describes the behavior of $A_\zeta(t)$, was obtained by weighting the residual of the tangential momentum equation with $\sin m\theta J_m\left(S_{mn} r\right)$. This equation differs from its counterpart, Eq. (307), by the presence of nonlinear coupling terms between the B's and the A's. Similarly Eq. (331) was obtained by weighting the residual of the tangential momentum equation with $\cos m\theta J_m\left(S_{mn} r\right)$.

Assume that $A_\rho(t)$, $A_\eta(t)$, $A_\zeta(t)$, and $A_p(t)$ are unspecified functions of time and the B's are the zero functions, that is

$$B_\rho(t) = B_\eta(t) = B_\zeta(t) = B_p(t) = 0 \tag{332}$$

In addition to Eq. (331) expressions for the derivatives $\frac{dB_\rho}{dt}$, $\frac{dB_\eta}{dt}$, and $\frac{dB_p}{dt}$ are obtained by weighting the appropriate residuals with $\sin m\theta J_m\left(S_{mn}r\right)$. In each of these expressions terms which involve only the A's are lacking, as the θ-integrals corresponding to these terms are found to vanish. Therefore, introducing Eq. (332) into these equations yields the result:

$$\frac{dB_\rho}{dt} = \frac{dB_\eta}{dt} = \frac{dB_\zeta}{dt} = \frac{dB_p}{dt} = 0 \tag{333}$$

which is independent of the values of the A's. It is thus seen that a solution involving only A's satisfies the more general differential equations obtained when the dependent variables are expanded in terms of both Φ_{mn} and Ψ_{mn}. In other words, if only the A's are initially present the B's will not be excited. Introducing Eq. (332) into Eq. (330) yields:

$$\frac{dA_\zeta}{dt} = -\frac{1}{\gamma I_\rho} A_p - \frac{1}{4}\frac{S_{mn}^2}{I_\rho} K_5 A_\rho A_\eta A_\zeta + \frac{m^2}{4I_\rho} K_6 A_\rho A_\zeta^2$$

which is identical to Eq. (307). Thus it is seen that when the dependent variables are expanded only in terms of $\Psi_{mn}(r, \theta)$, weighting the residual E_ζ with $\Phi_{mn} = \sin m\theta J_m\left(S_{mn}r\right)$ yields correct results.

Numerical Results and Discussion

Using the third order theory numerical solutions were obtained for the following two cases: (1) the approximate solutions consisted of the first tangential (1T) mode only, and (2) the approximate solutions consisted of the first radial mode (1R) only. The systems of differential equations governing these two cases differed in several respects. The equations controlling the behavior of the 1R mode contained both quadratic and cubic nonlinearities while the corresponding equations for the 1T mode involved only cubically nonlinear terms. The radial mode equations contained nonlinearities in the combustion mass source term whereas a nonlinear driving term was missing in the equations for the 1T mode. Although stable limit cycles and triggering limits were obtained in both cases, the numerical results show that the above-mentioned differences are important. The important characteristics of these solutions will now be summarized.

In order to obtain specific numerical solutions, the steady state velocity $\bar{u}(z)$ and density $\bar{\rho}(z)$ must be known. By using a specific combustion model, such as Priem's vaporization rate model[31], $\bar{u}(z)$ and $\bar{\rho}(z)$ could be determined by numerically integrating the steady state conservation equations where the droplet-gas interaction has been taken into account. To avoid the necessity of making such lengthy calculations the velocity distribution $\bar{u}(z)$ will be assumed to be linear. It can be shown[5] that under low Mach number conditions the linear velocity distribution corresponds to a uniformly distributed combustion process. Also it has been shown in Chapter V that the effect of a nonuniform steady state density is negligible for small Mach number mean flows, therefore

it will be assumed that $\bar{\rho}(z) = 1$ for these calculations. Under the above assumptions the appropriate integrals are given by:

$$I_u = 1/3\ \bar{u}_e^2 \quad ; \quad I_\rho = 1$$

First Tangential Mode

Numerical solutions of Eqs. (305) through (309) (for m = 1) were obtained for values of n and $\bar{\tau}$ in the immediate vicinity of the 1T mode neutral stability limit (the linear stability limits were obtained by applying the Galerkin method to the system of linearized perturbation equations as given in Chapter V). Stable limit cycles were found in the region above the neutral stability limit for $\bar{\tau} < 2.1$, while for larger values of $\bar{\tau}$ the possibility of triggering combustion oscillations exists in the region below the neutral stability curve. This latter result is in contrast to the predictions of the second order theory for which no triggering of the 1T mode was obtained.

Characteristics of the Solutions. Pressure and velocity waveforms at the outer wall (r = 1) are shown for both stable and unstable limit cycles in Figs. (55) and (56). These curves were computed from the values of $A_p(t)$ and $A_\zeta(t)$ by using Eq. (292), thus at the pressure anti-node $\theta = 0$ the wall pressure is given by:

$$p'(1, 0, t) = J_1(S_{11})A_p(t) = 0.58187\ A_p(t) \qquad (334)$$

At the wall only the tangential velocity component is present; its value

is given by $w' = \frac{1}{r}\zeta_\theta = -\sin\theta J_1(S_{11}r)A_\zeta(t)$ which at the velocity antinode $\theta = \pi/2$ becomes:

$$w'(1, \pi/2, t) = -0.58187\, A_\zeta(t) \tag{335}$$

As seen from Figs. (55) and (56) the pressure and velocity waveforms are nearly sinusoidal in shape, thus they are nearly symmetric about the time axis. This result does not agree with the results of the second order theory, where pressure waveforms characterized by sharp peaks and shallow troughs were obtained. The inability of the third order theory to predict nonlinear waveforms can be traced to differences in the manner in which the approximate solutions were constructed. In the second order analysis only the velocity potential Φ was expanded in terms of the acoustic eigenfunctions, and the pressure was computed from the momentum equation, an expression containing quadratic nonlinearities. Furthermore higher frequency modes were retained in the series. Both of these effects introduce a strong second harmonic distortion to the pressure waveform. In the present case, however, the pressure perturbation itself was expanded in terms of the acoustic eigenfunctions and only one term was retained. As a result the sources of second harmonic distortion are lost. A small third harmonic component of the pressure waveform is expected to arise from the cubic nonlinearities in the governing differential equations, but this effect does not result in a peaked waveform.

Another effect of retaining only one mode in the series expansion

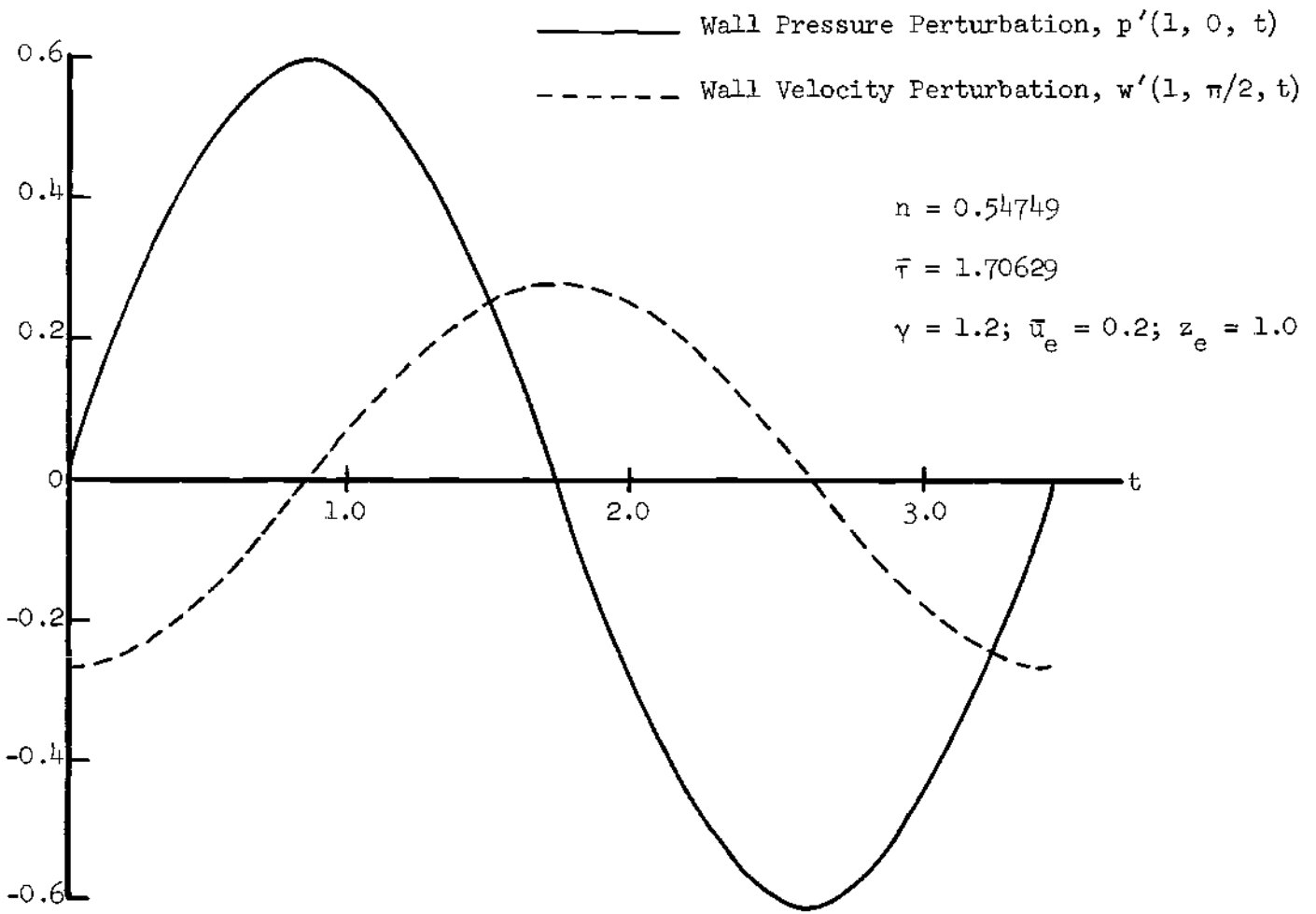

Figure 55. Third Order Wall Pressure and Velocity Waveforms for the 1T Mode at a Stable Limit Cycle.

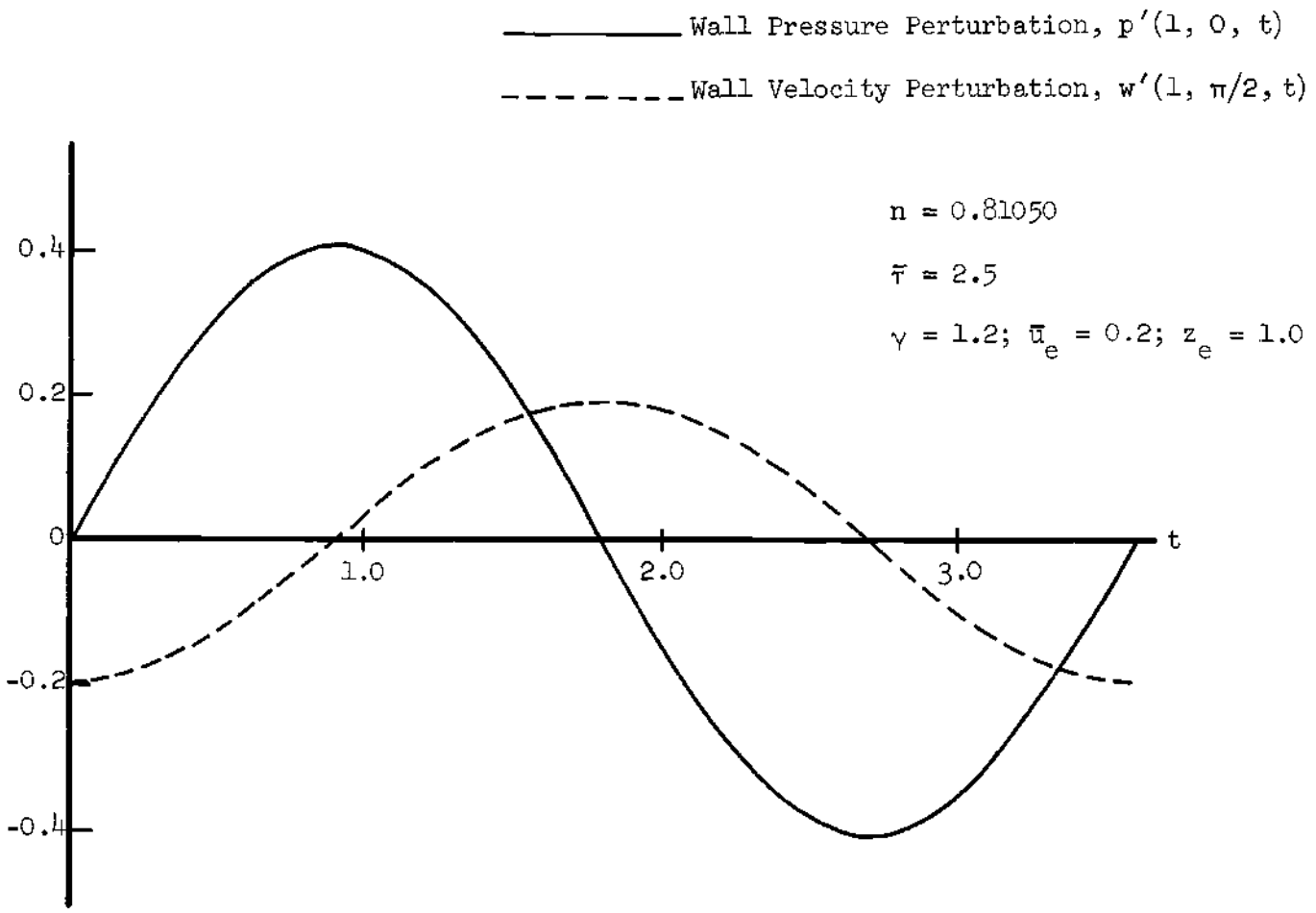

Figure 56. Third Order Wall Pressure and Velocity Waveforms for the 1T Mode at an Unstable Limit Cycle.

for $\tilde{p}'$ is the lack of higher harmonics in the angular dependence of the pressure waveforms; that is, at any instant $p' \sim \cos\theta$. Suppose that at time $t = t_0$ and at $\theta = 0$ the pressure attains a maximum value at the wall which exceeds unity, say $p'_{max} > 1$. According to the assumed spatial variation of p', the pressure perturbation at that instant on the opposite side of the chamber ($\theta = \pi$) will be $p' = -p'_{max} < -1$. This corresponds to a negative pressure* $(1 + p')$ which is physically impossible. Thus it is seen that a region of negative pressure is predicted if the pressure amplitude exceeds unity at the wall. Negative pressures will also occur as a result of the symmetry of the pressure-time waveform, thus if $p' > 1$ at a certain instant, one-half period later $p' < -1$. It follows from the above discussion that the applicability of the third order theory using a one-mode series must be restricted to regions of the $(n, \bar{\tau})$ plane for which the computed pressure amplitude does not exceed unity. It is expected that this limitation can be removed by adding more modes to the series expansion at the cost of increased computation time.

Examination of the computed values of $A_\eta(t)$ and $A_\zeta(t)$ reveal that these functions are nearly equal; the agreement was found to three significant digits. Thus the numerical calculations confirm the results of Chapter III that the vorticity of the unsteady flow is small.

Dependence of Solutions Upon Combustion Parameters. A survey of

---

* For the numerical solutions presented in this chapter it was assumed that the variation of steady state properties was negligible; that is, $\bar{p}(z) = 1$. Otherwise the proper criterion for physically meaningful solutions is $p' > -\bar{p}(z)$.

the $(n, \bar{\tau})$ plane was conducted by computing the limiting periodic solutions for various values of n along lines of constant $\bar{\tau}$. The results of this study are presented in Figs. (57) and (58) as plots of pressure amplitude as a function of the vertical distance δ from the neutral stability limit. These curves exhibit the familiar parabolic shape which was obtained with the second order theory.

Figure (57) shows the behavior at smaller values of $\bar{\tau}$ ($\bar{\tau} < 2.1$). In this case stable limit cycles are obtained in the linearly unstable region; the pressure amplitude is zero at the neutral stability limit and increases as δ increases. Thus it is impossible to trigger the 1T mode (in the linearly stable region) for these values of $\bar{\tau}$. It can also be seen from these figures that for a given value of δ the pressure amplitude increases as $\bar{\tau}$ increases.

The above results are in qualitative agreement with those obtained from the second order theory, however, for a given value of δ the third order analysis predicts a much larger amplitude. This difference in the magnitude of the final amplitude predicted by the two theories can be attributed to differences in the nonlinear mechanisms which limit the amplitude. In the second order analysis the only nonlinear mechanism obtained was the coupling between modes in which energy is transferred to the stable modes. These cross-coupling terms are not obtained in the present analysis because only one mode is included in the series expansion. In this case the amplitude is limited by the cubically nonlinear self-coupling terms, an effect which was neglected in the second order theory.

Figure (58) shows that for sufficiently large values of $\bar{\tau}$ it is

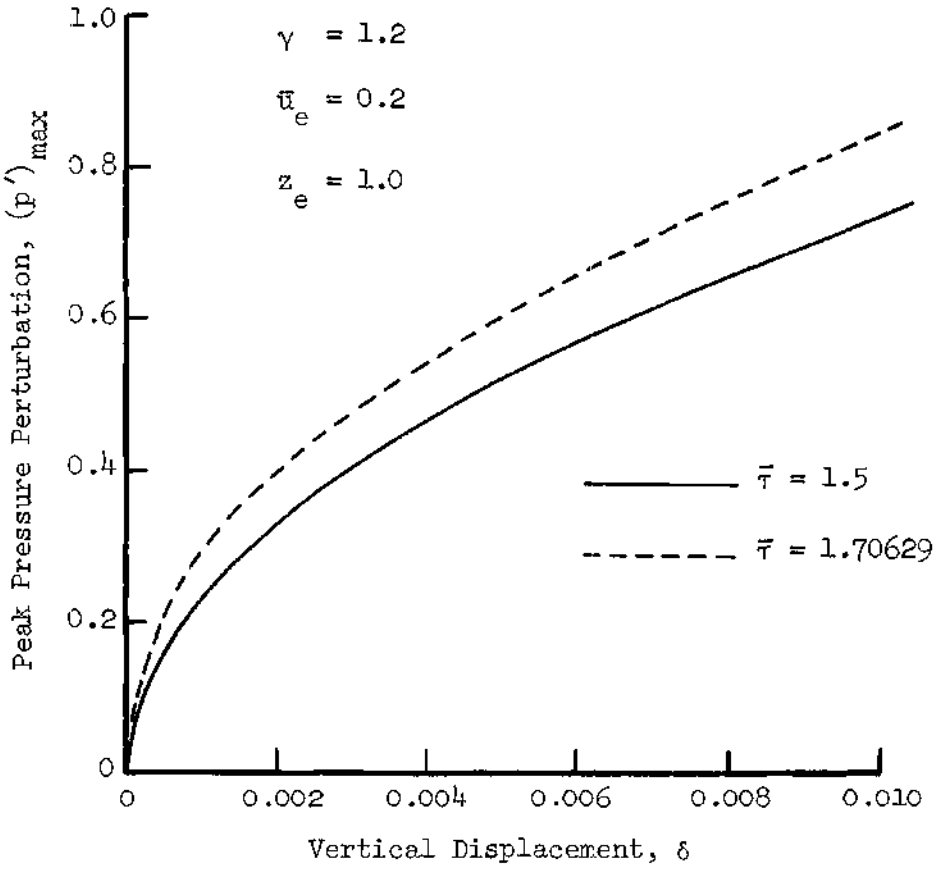

Figure 57. Third Order Stable Limit Cycles for the First Tangential Mode.

possible to trigger combustion oscillations, a result not obtained with the second order theory (for the 1T mode). For given values of δ and $\bar{\tau}$ the point on the corresponding curve is a measure of the size of the initial disturbance necessary to trigger combustion instability. A disturbance slightly larger than this threshold value was found to grow without limit, thus no stable limit cycles were found in this region. As the curves indicate, the triggering amplitude increases as one moves away from the neutral stability limit (decreasing n) until the pressure at the wall becomes negative. Thus this analysis was unable to predict the minimum value of n below which it is impossible to trigger the 1T mode. It is also observed from Fig. (58) that for a constant displacement δ a smaller disturbance is required to trigger instability as $\bar{\tau}$ increases.

For both stable and unstable limit cycles the frequency of oscillation was found to be close to that of the acoustic 1T mode and was found to decrease slightly with increasing amplitude. This behavior is in qualitative agreement with the results obtained with the second order theory when the 1R mode was included in the expansion of Φ.

First Radial Mode

The nonlinear behavior of the 1R mode was investigated by solving Eqs. (312) through (315) numerically for different values of n and $\bar{\tau}$. Unlike the 1T mode, stable limit cycles for 1R mode instability were found in the vicinity of the neutral stability limit for both linearly stable and unstable values of n and $\bar{\tau}$. For values of n and $\bar{\tau}$ in the linearly stable region an unstable limit cycle (i.e. a triggering limit) was found with an amplitude below that of the stable limit cycle. These

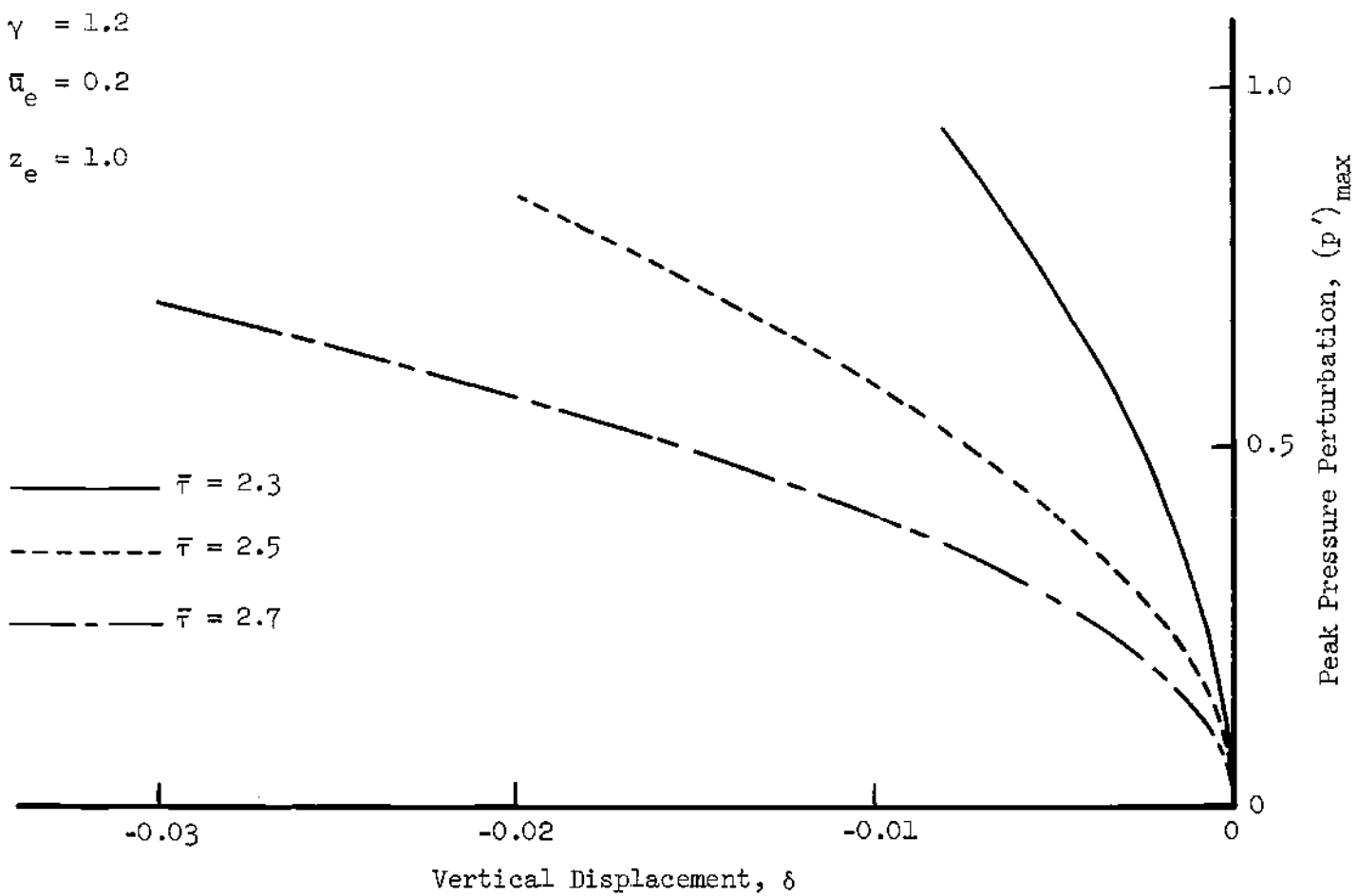

Figure 58. Third Order Triggering Limits for the First Tangential Mode.

solutions are qualitatively similar to those obtained for the 1R mode with the aid of the second order theory and a one-mode expansion (see Chapter VI).

Characteristics of the Solutions. Typical pressure and velocity waveforms are shown in Fig. (59) for an unstable limit cycle and in Fig. (60) for a stable limit cycle. The pressure was calculated from the value of $A_p(t)$ according to Eq. (292) as follows:

$$p'(r, \theta, t) = A_p(t) J_0\left(S_{01} r\right) \tag{336}$$

which shows that the pressure perturbation is independent of θ. Since the Bessel function J_0 has its maximum value when the argument is zero (i.e. $J_0(0) = 1$) the amplitude of the pressure oscillation is greatest at the chamber axis ($r = 0$). There is a pressure node at an intermediate radial position and at the wall the pressure is 180° out of phase with respect to the pressure at the axis. The pressure waveforms at the axis ($r = 0$) and the wall ($r = 1$) are presented in Figs. (59) and (60) and are given by:

$$p'(0, \theta, t) = A_p(t) \tag{337}$$

$$p'(1, \theta, t) = - 0.40276\ A_p(t)$$

For radial modes, only the radial component of the velocity perturbation is present, and it is related to the function $A_\eta(t)$ as follows:

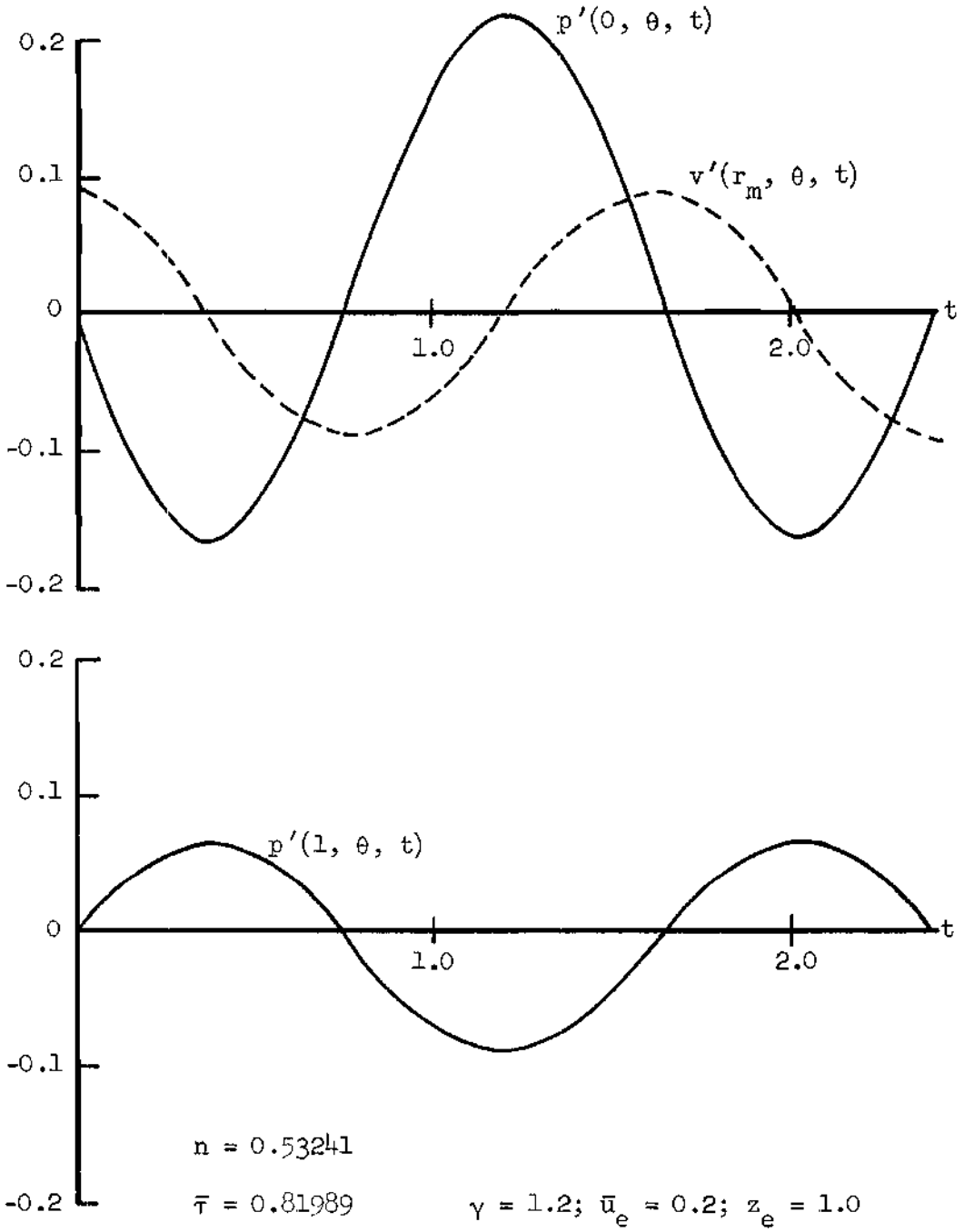

Figure 59. Third Order Pressure and Velocity Waveforms for the 1R Mode at an Unstable Limit Cycle.

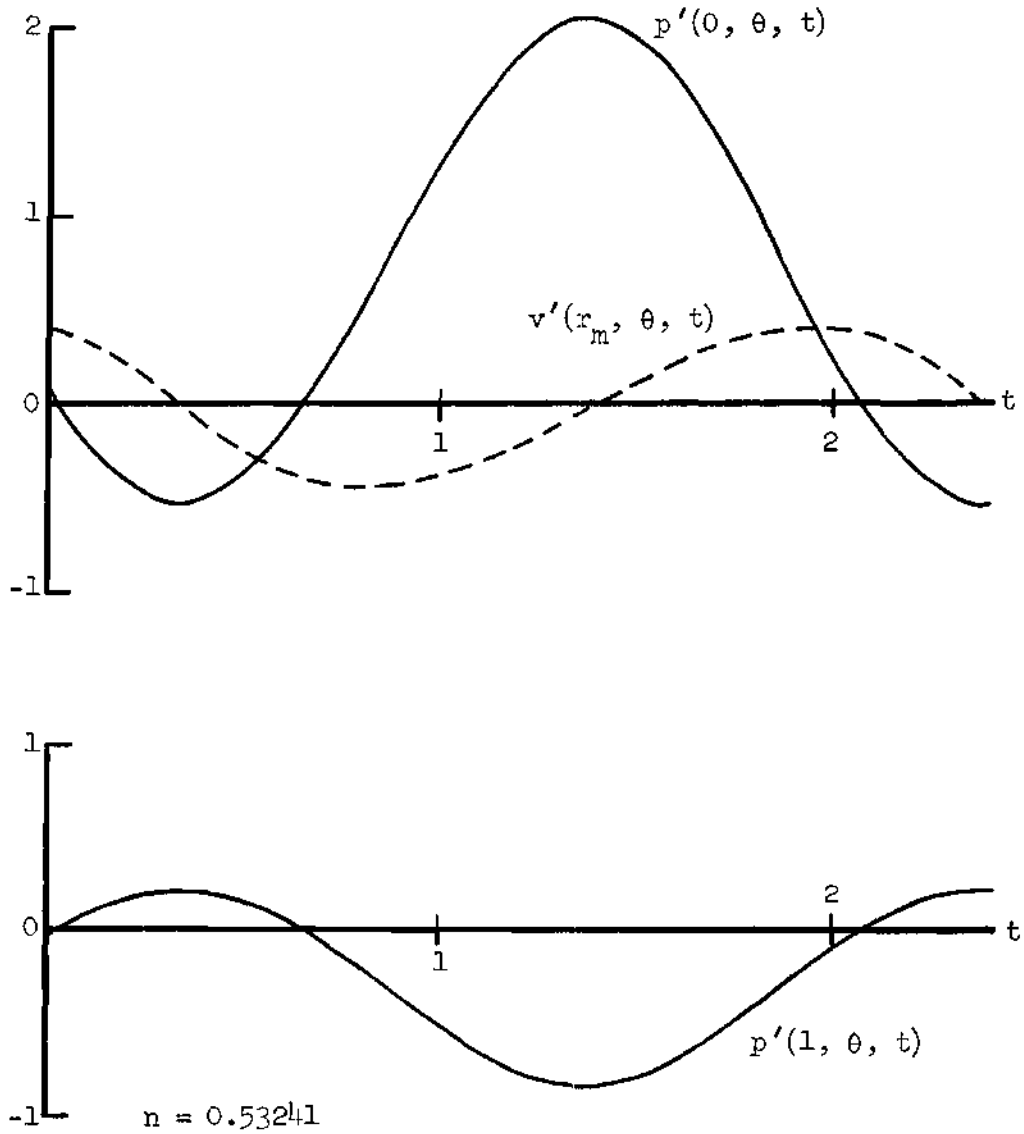

Figure 60. Third Order Pressure and Velocity Waveforms for the 1R Mode at a Stable Limit Cycle.

$$v' = \eta_r = - S_{01} J_1\left(S_{01} r\right) A_\eta(t) \tag{338}$$

From Eq. (338) it is seen that the velocity vanishes at both the axis and the wall, consequently the velocity waveforms are computed at the velocity anti-node ($r_m = 0.48051$). At this position $J_1\left(S_{01} r\right) = 0.58187$ and Eq. (338) becomes

$$v'(r_m, \theta, t) = - 2.2296\ A_\eta(t) \tag{339}$$

In contrast to the case of the 1T mode, the function $A_p(t)$ for the 1R mode was not symmetric with respect to the time axis. Instead a plot of $A_p(t)$ resembles a sine wave that has been shifted upwards, and it does not appear that $A_p(t)$ will fall below -1 even for very large peak values. According to Eqs. (337) therefore the pressure waveforms at stations between the center of the chamber and the pressure node will have high peaks and shallow troughs similar to those obtained with the second order theory. On the other hand similar waveforms at stations between the node and the wall are seen to exhibit the opposite behavior; that is, the peaks are suppressed and the minima are exaggerated. For sufficiently large peak values of $A_p(t)$ (approximately 2.48) the solution will predict a negative pressure at the wall. As in the case of the single 1T mode expansion the applicability of the theory is restricted by the occurrence of a negative pressure at some point in the chamber. In the case of the 1R mode, however, the restriction on the pressure amplitude is seen to be less severe. It is

believed that the addition of higher radial modes to the series expansion will remedy this situation.

Effect of Combustion Parameters. An investigation of the behavior of triggered first radial mode instability was made for operating conditions in the vicinity of the neutral stability limit. The results of this study are shown in Fig. (61) as plots of limiting pressure amplitude as a function of n for constant values of $\bar{\tau}$. For values of n in the linearly stable region ($\delta < 0$) each of these curves has two branches, the upper branch corresponds to stable limit cycles while the lower branch corresponds to unstable limit cycles or triggering limits. These curves show that as $\bar{\tau}$ is increased the combustion oscillations are more easily triggered and the amplitude of the resulting oscillations is higher. It is also observed that there is a minimum value of n (or δ) below which it is impossible to trigger combustion instability. This value of δ, referred to as δ_t, is seen to decrease (i.e. become more negative) with increasing $\bar{\tau}$ which indicates that the nonlinearly unstable range in n, for which triggered instability is possible, becomes larger with increasing time-lag. These results are in good qualitative agreement with those obtained for the 1R mode with the second order equations (see also Figs. (45) and (46)).

Effect of Various Types of Nonlinearities. The third order analysis of 1R mode instability is the only case considered in this investigation for which nonlinearities arising from all three major sources are included; that is, the gasdynamics of the combustor, the combustion process, and the nozzle. Furthermore it is the only case considered for which both quadratically and cubically nonlinear terms

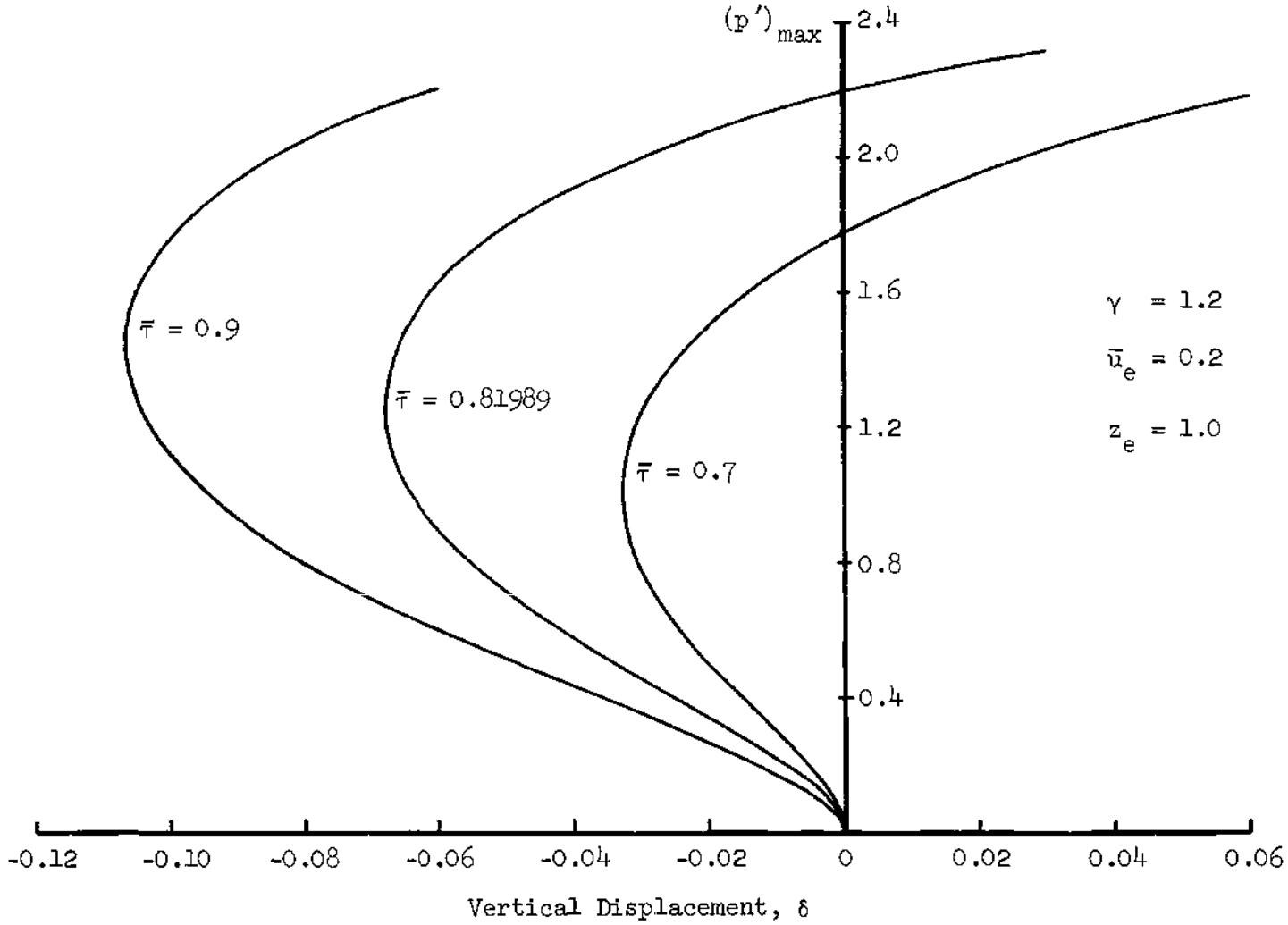

Figure 61. Third Order Stable and Unstable Limit Cycles for the First Radial Mode.

are obtained. The relative importance of these various terms was determined by considering the following three cases: (1) all terms were retained, (2) all cubically nonlinear terms were removed (the nonlinear combustion effect was quadratic and was therefore retained), and (3) the nonlinear combustion terms were dropped but all others were retained. For a point in the linearly stable region ($\bar{\tau}$ = 0.81989, n = 0.53241) with all terms retained (Case 1) a triggering limit was found with a peak chamber pressure of 0.220. An initial disturbance with a slightly larger amplitude was found to reach a stable limiting amplitude of 2.13. Dropping the cubic terms (Case 2) changed the amplitudes of both stable and unstable limit cycles by only a few percent (amplitudes of 2.04 and 0.215 respectively). However if the nonlinear driving terms are neglected (Case III) the amplitude of the triggering limit is reduced to 0.155 and the upper stable limit cycle was not obtained, that is, the solutions continued to grow indefinitely. This latter result is consistent with the third order solutions for the 1T mode, for which no nonlinear combustion terms appeared in the governing differential equations.

From the above results it can be concluded that the nonlinear combustion source is very important in determining the nonlinear stability characteristics of the first radial mode for this system, especially for determining the limiting amplitude of triggered instability. On the other hand the cubically nonlinear terms arising from the chamber gasdynamics have only a minor effect.

CHAPTER VIII

CONCLUDING REMARKS

The primary objective of the present investigation was the development of a new analytical technique to be used in the solution of nonlinear combustion instability problems. Such a method should be relatively easy to apply and should require relatively little computation time. These requirements were found to be satisfied by the Galerkin method, which was modified to accommodate the complicated boundary conditions associated with combustion instability problems.

The Galerkin method was used to obtain approximate solutions for both linear and nonlinear combustion instability problems, with emphasis on the more interesting case of nonlinear transverse instability. The applicability of the modified Galerkin method to the solution of linear problems was demonstrated by showing that the approximate solutions were in excellent agreement with those obtained by more exact mathematical techniques.

In the nonlinear studies both second order and third order theories were developed. In the second order analysis it was assumed that the amplitude of the pressure oscillations was moderate and the Mach number of the steady state flow was small. It was shown that under these conditions the unsteady flow was irrotational and it could be described with the aid of a velocity potential. The resulting second order wave equations were combined to obtain a single governing partial

differential equation which was solved with the aid of the Galerkin method. In the third order theory the amplitude restriction was relaxed, and to obtain the appropriate solutions it was necessary to solve a system of differential equations. In order to evaluate the two theories numerical solutions were obtained for the unsteady flow for a particular combustor configuration. It was assumed that the nozzle response was quasi-steady and that the combustion mass source was described by Crocco's time-lag hypothesis. In these studies particular emphasis was placed on the nonlinear behavior of the first tangential and first radial modes.

Conclusions

On the basis of the numerical results presented in this thesis the following conclusions were drawn:

(1) With a judicious choice of the assumed series expansion, the modified Galerkin method can be successfully applied in the solution of nonlinear combustion instability problems. The numerical solution of the resulting ordinary differential equations will, in most cases, require much less computer time than a finite difference solution of the original partial differential equations.

(2) The Galerkin method can predict the following experimentally observed nonlinear phenomena: (a) the final amplitude attained in an unstable engine, (b) "triggering" of instability by finite amplitude disturbances in a linearly stable engine, (c) nonlinear pressure waveforms, and (d) the dependence of the frequency on amplitude.

(3) The following nonlinear mechanisms were found to be

important in determining the nonlinear stability characteristics of the system: (a) the transfer of energy between modes, (b) the self-coupling of a mode with itself, and (c) a nonlinear combustion mass source.

(4) The self-coupling mechanism was found to be very important in the initiation of triggered instability, while the nonlinear driving mechanism was important in the determination of the final amplitude of triggered instability.

(5) With a reasonable expenditure of computer time it is possible to use the Galerkin method in the determination of the nonlinear behavior of an engine as a function of the pertinent system parameters.

Suggestions for Further Research

Additional insight into the various nonlinear aspects of combustion instability should be obtained by applying the modified Galerkin method to more general problems than those considered in this thesis. A few of these possibilities will now be briefly mentioned.

According to Crocco's time-lag model, which was used exclusively in this investigation, the burning rate was influenced only by the pressure or by properties that could be directly correlated to the pressure. Since it is known that transverse velocity effects can also be important, it is highly desirable to account for these effects by the use of more realistic combustion models. One such possibility is the use of Priem's vaporization rate model[31].

Additional problems whose solutions should be attempted with

the aid of the modified Galerkin method are as follows:

(1) The development of a third order theory in which the solutions for the dependent variables are described by multi-mode series expansions.

(2) Modification of the assumed series expansions to include the possibility of three-dimensional oscillations.

(3) Replace the quasi-steady nozzle boundary condition with a more general nonlinear nozzle admittance relation.

(4) Include the effects of the liquid droplets upon the wave motion.

It is hoped that the results presented in this thesis along with the solutions of the suggested problems will lead to a better understanding of the nonlinear aspects of combustion instability and that the modified Galerkin method will prove useful in the design of stable rocket engines.

APPENDIX A

EVALUATION OF THE COEFFICIENTS WHICH APPEAR IN THE DIFFERENTIAL EQUATIONS THAT DESCRIBE THE BEHAVIOR OF THE MODE-AMPLITUDES

Expressions for the coefficients occurring in Eqs. (220) and (221) of Chapter VI will now be derived. The acoustic, damping, and nonlinear terms will be treated separately, and the values of all coefficients will be normalized so that the coefficient of the highest order derivative is unity.

Acoustic Terms

The terms of Eqs. (220) and (221) which arise from the acoustic wave operator are obtained by evaluating the volume integrals of the residual R_{ac} (i.e. Eq. (217a)) using the weighting functions $\Psi_{A_{hjk}}$ and $\Psi_{B_{hjk}}$. Weighting with $\Psi_{A_{hjk}}$ the acoustic part of Eq. (220) becomes:

$$I_{ac} = - \sum_{\ell} \sum_{m} \sum_{n} \left\{ \left[\frac{d^2 A_{\ell mn}}{dt^2} + \left(S_{mn}^2 + \frac{\ell^2 \pi^2}{z_e^2} \right) A_{\ell mn} \right] \int_0^{2\pi} \sin m\theta \sin j\theta \, d\theta \right. \tag{A1}$$

$$\left. + \left[\frac{d^2 B_{\ell mn}}{dt^2} + \left(S_{mn}^2 + \frac{\ell^2 \pi^2}{z_e^2} \right) B_{\ell mn} \right] \int_0^{2\pi} \cos m\theta \sin j\theta \, d\theta \right\} \times$$

$$\times \int_0^{z_e} \cos \frac{\ell \pi z}{z_e} \cos \frac{h \pi z}{z_e} \, dz \int_0^1 J_m\left(S_{mn} r\right) J_j\left(S_{jk} r\right) r \, dr$$

The integrals occurring in the acoustic terms are found in any standard table of integrals and are given by:

$$\int_0^{z_e} \cos\frac{\ell\pi z}{z_e} \cos\frac{h\pi z}{z_e}\, dz = 0 \qquad (\ell \neq h) \tag{A2}$$

$$= z_e/2 \qquad (\ell = h \neq 0)$$

$$= z_e \qquad (\ell = h = 0)$$

$$\int_0^{2\pi} \sin m\theta \sin j\theta\, d\theta = 0 \qquad (m \neq j) \text{ or } (m = 0 \text{ or } j = 0)$$

$$= \pi \qquad (m = j \neq 0)$$

$$\int_0^{2\pi} \cos m\theta \cos j\theta\, d\theta = 0 \qquad (m \neq j)$$

$$= \pi \qquad (m = j \neq 0)$$

$$= 2\pi \qquad (m = j = 0)$$

$$\int_0^{2\pi} \cos m\theta \sin j\theta\, d\theta = 0$$

$$\int_o^1 J_j\left(S_{jn}r\right)J_j\left(S_{jk}r\right)rdr = 0 \qquad (n \neq k)$$

$$= \frac{S_{jk}^2 - j^2}{2S_{jk}^2}\left[J_j\left(S_{jk}\right)\right]^2 \qquad (n = k)$$

which express the orthogonality properties of the acoustic eigenfunctions. When these expressions are introduced into Eqs. (A1) it is seen that all of the terms in the series vanish except for the term corresponding to $\ell = h$, $m = j$, and $n = k$, which yields:

$$I_{ac} = -\left[\frac{d^2A_{hjk}}{dt^2} + \left(S_{jk}^2 + \frac{h^2\pi^2}{z_e^2}\right)A_{hjk}\right] \times \qquad (A3)$$

$$\times \int_o^{z_e} \cos^2\frac{h\pi z}{z_e}\,dz \int_o^{2\pi} \sin^2 j\theta\,d\theta \int_o^1 J_j^2\left(S_{jk}r\right)rdr$$

A similar expression results when the weighting functions $\Psi_{B_{hjk}}$ are used.

Equations (220) were obtained by dividing the equations resulting directly from the Galerkin method by the coefficient of the highest order derivative (i.e. d^2A_{hjk}/dt^2) so that the coefficient of this term is unity. Thus all coefficients must be normalized by the following factors:

$$N_{A_{hjk}} = -\int_o^{z_e} \cos^2\frac{h\pi z}{z_e}\,dz \int_o^{2\pi} \sin^2 j\theta\,d\theta \int_o^1 J_j^2\left(S_{jk}r\right)rdr \qquad (A4)$$

$$N_{B_{hjk}} = -\int_o^{z_e} \cos^2\frac{h\pi z}{z_e}\,dz \int_o^{2\pi} \cos^2 j\theta\,d\theta \int_o^1 J_j^2\left(S_{jk}r\right)rdr$$

which correspond to weighting the residuals with $\Psi_{A_{hjk}}$ and $\Psi_{B_{hjk}}$ respectively. The resulting expressions for the acoustic parts appear in Eqs. (220) and (221).

Terms Involving the First Derivative

The terms involving the first derivative which appear in Eqs. (220) and (221) arise from the influence of the steady state flow, the nozzle, and the combustion process. From Eq. (210) it is seen that these terms are expressed as a sum of the appropriate residuals as follows:

$$I_d = \int_o^{z_e}\int_o^{2\pi}\int_o^1 \left[-R_u - R_c\right]\Psi_n r\,dr\,d\theta\,dz - \int_o^{2\pi}\int_o^1 B_e\Psi_n(r,\theta,z_e,t)\,r\,dr\,d\theta \qquad (A5)$$

where R_u, R_c, and B_e are given by Eqs. (217) and (218). Using the weighting function $\Psi_{A_{hjk}}$ and the orthogonality properties given by Eqs. (A2) the terms appearing in Eq. (A5) become:

$$I_u = \sum_\ell \left[\gamma \int_o^{z_e} \frac{d\bar{u}}{dz} \cos\frac{\ell\pi z}{z_e} \cos\frac{h\pi z}{z_e}\,dz - 2\frac{\ell\pi}{z_e}\int_o^{z_e} \bar{u} \sin\frac{\ell\pi z}{z_e} \cos\frac{h\pi z}{z_e}\,dz\right] \times$$

$$\times \frac{dA_{\ell jk}}{dt} \int_o^{2\pi} \sin^2 j\theta \, d\theta \int_o^1 J_j^2\left(S_{jk}r\right) r dr$$

$$I_c = - \gamma n \sum_{\ell} \left[\frac{dA_{\ell jk}}{dt} - \frac{dA_{\ell jk}}{dt}(t-\bar{\tau}) \right] \int_o^{z_e} \frac{d\bar{u}}{dz} \cos\frac{\ell\pi z}{z_e} \cos\frac{h\pi z}{z_e} \, dz \times \qquad \text{(A6)}$$

$$\times \int_o^{2\pi} \sin^2 j\theta \, d\theta \int_o^1 J_j^2\left(S_{jk}r\right) r dr$$

$$I_B = \frac{\gamma-1}{2} \bar{u}_e \sum_{\ell} (-1)^{\ell+h} \frac{dA_{\ell jk}}{dt} \int_o^{2\pi} \sin^2 j\theta \, d\theta \int_o^1 J_j^2\left(S_{jk}r\right) r dr$$

where $I_d = - (I_u + I_c + I_B)$. Combining Eqs. (A6) yields the following expression for the first derivative terms appearing in Eqs. (220):

$$I_d = - \sum_{\ell} \left\{ \frac{dA_{\ell jk}}{dt} \left[\frac{\gamma-1}{2} \bar{u}_e (-1)^{\ell+h} + \gamma(1-n) \int_o^{z_e} \frac{d\bar{u}}{dz} \cos\frac{\ell\pi z}{z_e} \cos\frac{h\pi z}{z_e} \, dz \right. \right. \qquad \text{(A7)}$$

$$\left. - 2\frac{\ell\pi}{z_e} \int_o^{z_e} \bar{u}(z) \sin\frac{\ell\pi z}{z_e} \cos\frac{h\pi z}{z_e} \, dz \right]$$

$$\left. + \frac{dA_{\ell jk}}{dt}(t-\bar{\tau}) \left[\gamma n \int_o^{z_e} \frac{d\bar{u}}{dz} \cos\frac{\ell\pi z}{z_e} \cos\frac{h\pi z}{z_e} \, dz \right] \right\} \times$$

$$\times \int_o^{2\pi} \sin^2 j\theta \, d\theta \int_o^1 J_j^2\left(S_{jk}r\right) r dr$$

The integrals involving the steady state velocity which appear in Eq. (A7) are evaluated in Appendix B. The corresponding terms in Eqs. (221), which are obtained by weighting with $\Psi_{B_{hjk}}$, are found from Eqs. (A7) by replacing A_{hjk} and $\sin j\theta$ with B_{hjk} and $\cos j\theta$. The coefficients $K(\ell, h)$ and $K_\tau(\ell, h)$ are obtained by normalizing Eqs. (A7) by the appropriate factor from Eqs. (A4) which yields Eqs. (222) of Chapter VI.

Nonlinear Coupling Terms

The coefficients of the nonlinear coupling terms which appear in Eqs. (220) and (221) will now be derived by evaluating the weighted integrals of the appropriate nonlinear residuals in Eq. (210). These terms are given by:

$$I_N = -\int_o^{z_e}\int_o^{2\pi}\int_o^{1}\left[2R_{N_1} + (\gamma-1)R_{N_2}\right]\Psi_n r\,dr\,d\theta\,dz \tag{A8}$$

where R_{N_1} and R_{N_2} are defined by Eqs. (217b) and (217c). These nonlinear coefficients involve definite integrals of products of three trigonometric or Bessel functions as shown below:

$$Zi_c(\ell,\lambda,h) = \int_o^{z_e} \cos\frac{\ell\pi z}{z_e}\cos\frac{\lambda\pi z}{z_e}\cos\frac{h\pi z}{z_e}\,dz \tag{A9}$$

$$Zi_s(\ell,\lambda,h) = \int_o^{z_e} \sin\frac{\ell\pi z}{z_e}\sin\frac{\lambda\pi z}{z_e}\cos\frac{h\pi z}{z_e}\,dz$$

$$I_{sss}(m,\mu,j) = \int_0^{2\pi} \sin m\theta \, \sin\mu\theta \, \sin j\theta \, d\theta$$

$$I_{css}(m,\mu,j) = \int_0^{2\pi} \cos m\theta \, \sin\mu\theta \, \sin j\theta \, d\theta$$

$$I_{ccs}(m,\mu,j) = \int_0^{2\pi} \cos m\theta \, \cos\mu\theta \, \sin j\theta \, d\theta$$

$$I_{ccc}(m,\mu,j) = \int_0^{2\pi} \cos m\theta \, \cos\mu\theta \, \cos j\theta \, d\theta$$

$$Ji_1(m,n;\mu,\nu;j,k) = \int_0^1 J_m\left(S_{mn}r\right)J_\mu\left(S_{\mu\nu}r\right)J_j\left(S_{jk}r\right)rdr$$

$$Ji_2(m,n;\mu,\nu;j,k) = \int_0^1 J_m\left(S_{mn}r\right)J_\mu\left(S_{\mu\nu}r\right)J_j\left(S_{jk}r\right)\frac{1}{r}\,dr$$

$$Ji_3(m,n;\mu,\nu;j,k) = \int_0^1 J_m'\left(S_{mn}r\right)J_\mu'\left(S_{\mu\nu}r\right)J_j\left(S_{jk}r\right)rdr$$

Although analytical expressions for the trigonometric integrals are readily obtained, one must resort to numerical analysis to evaluate the integrals of the Bessel functions. These integrals are treated in Appendix B where analytical expressions and numerical values are presented. There it is shown that the azimuthal integrals $I_{sss}(m,\mu,j)$ and $I_{ccs}(m,\mu,j)$ vanish for all integral values of m,μ, and j.

Expressions for the coefficients C_1 and C_2 of Eqs. (220) are

obtained by using the weighting function $\Psi_{A_{hjk}}$ in Eq. (A8). The terms appearing in Eq. (A8) become:

$$I_{N_1} = \sum_{\ell,m,n} \sum_{\lambda,\mu,\nu} \Big\{ A_{\ell mn} \frac{dA_{\lambda\mu\nu}}{dt} \Big[S_{mn} S_{\mu\nu} Zi_c(\ell,\lambda,h)\, I_{sss}(m,\mu,j)\, Ji_3(m,n;\mu,\nu;j,k) + \tag{A10a}$$

$$+ m_\mu Zi_c(\ell,\lambda,h)\, I_{ccs}(m,\mu,j)\, Ji_2(m,n;\mu,\nu;j,k) +$$

$$+ \ell\lambda \left(\frac{\pi}{z_e}\right)^2 Zi_s(\ell,\lambda,h)\, I_{sss}(m,\mu,j)\, Ji_1(m,n;\mu,\nu;j,k) \Big] +$$

$$+ B_{\ell mn} \frac{dB_{\lambda\mu\nu}}{dt} \Big[S_{mn} S_{\mu\nu} Zi_c(\ell,\lambda,h)\, I_{ccs}(m,\mu,j)\, Ji_3(m,n;\mu,\nu;j,k) +$$

$$+ m_\mu Zi_c(\ell,\lambda,h)\, I_{sss}(m,\mu,j)\, Ji_2(m,n;\mu,\nu;j,k) +$$

$$+ \ell\lambda \left(\frac{\pi}{z_e}\right)^2 Zi_s(\ell,\lambda,h)\, I_{ccs}(m,\mu,j)\, Ji_1(m,n;\mu,\nu;j,k) \Big] +$$

$$+ A_{\ell mn} \frac{dB_{\lambda\mu\nu}}{dt} \Big[S_{mn} S_{\mu\nu} Zi_c(\ell,\lambda,h)\, I_{css}(\mu,m,j)\, Ji_3(m,n;\mu,\nu;j,k) -$$

$$- m_\mu Zi_c(\ell,\lambda,h)\, I_{css}(m,\mu,j)\, Ji_2(m,n;\mu,\nu;j,k) +$$

$$+ \ell\lambda \left(\frac{\pi}{z_e}\right)^2 Zi_s(\ell,\lambda,h)\, I_{css}(\mu,m,j)\, Ji_1(m,n;\mu,\nu;j,k) \Big] +$$

$$+ B_{\ell mn}\frac{dA_{\lambda\mu\nu}}{dt}\Big[S_{mn}S_{\mu\nu}Zi_c(\ell,\lambda,h)I_{css}(m,\mu,j)Ji_3(m,n;\mu,\nu;j,k) -$$

$$- m\mu Zi_c(\ell,\lambda,h)I_{css}(\mu,m,j)Ji_2(m,n;\mu,\nu;j,k) +$$

$$+ \ell\lambda\left(\frac{\pi}{z_e}\right)^2 Zi_s(\ell,\lambda,h)I_{css}(m,\mu,j)Ji_1(m,n;\mu,\nu;j,k)\Big]\Big\}$$

$$I_{N_2} = -\sum_{\ell,m,n}\sum_{\lambda,\mu,\nu}\Big\{\Big[A_{\ell mn}\frac{dA_{\lambda\mu\nu}}{dt}I_{sss}(m,\mu,j) + B_{\ell mn}\frac{dB_{\lambda\mu\nu}}{dt}I_{ccs}(m,\mu,j) + \quad \text{(A10b)}$$

$$+ A_{\ell mn}\frac{dB_{\lambda\mu\nu}}{dt}I_{css}(\mu,m,j) + B_{\ell mn}\frac{dA_{\lambda\mu\nu}}{dt}I_{css}(m,\mu,j)\Big] \times$$

$$\times \left[S_{mn}^2 + \frac{\ell^2\pi^2}{z_e^2}\right]Zi_c(\ell,\lambda,h)Ji_1(m,n;\mu,\nu;j,k)\Big\}$$

where $I_N = -\left[2I_{N_1} + (\gamma-1)I_{N_2}\right]$. Combining Eqs. (A10) and introducing the result that $I_{sss} = I_{ccs} = 0$, it is seen that the coefficients of $A_{\ell mn}\frac{dA_{\lambda\mu\nu}}{dt}$ and $B_{\ell mn}\frac{dB_{\lambda\mu\nu}}{dt}$ all vanish. The remaining coefficients are normalized by $N_{A_{hjk}}$ to obtain the following expressions:

$$C_1(\ell,m,n;\lambda,\mu,\nu;h,j,k) = \Big\{2\Big[S_{mn}S_{\mu\nu}I_{css}(\mu,m,j)Ji_3(m,n;\mu,\nu;j,k) - \quad \text{(A11)}$$

$$- m\mu I_{css}(m,\mu,j)Ji_2(m,n;\mu,\nu;j,k)\Big]Zi_c(\ell,\lambda,h) +$$

$$+\left[2\ell\lambda\left(\frac{\pi}{z_e}\right)^2 Zi_s(\ell,\lambda,h) - (\gamma-1)\left(S_{mn}^2 + \frac{\ell^2\pi^2}{z_e^2}\right)Zi_c(\ell,\lambda,h)\right] \times$$

$$\times I_{css}(\mu,m,j)\,Ji_1(m,n;\mu,\nu;j,k)\Big\}\left[\int_o^{z_e}\cos^2\frac{h\pi z}{z_e}dz\int_o^{2\pi}\sin^2 j\theta d\theta\int_o^1 J_j^2(S_{jk}r)\,rdr\right]^{-1}$$

$$C_2(\ell,m,n;\lambda,\mu,\nu;h,j,k) = \Big\{2\Big[S_{mn}S_{\mu\nu}I_{css}(m,\mu,j)\,Ji_3(m,n;\mu,\nu;j,k) - \tag{A12}$$

$$- m\mu I_{css}(\mu,m,j)\,Ji_2(m,n;\mu,\nu;j,k)\Big]Zi_c(\ell,\lambda,h) +$$

$$+\left[2\ell\lambda\left(\frac{\pi}{z_e}\right)^2 Zi_s(\ell,\lambda,h) - (\gamma-1)\left(S_{mn}^2 + \frac{\ell^2\pi^2}{z_e^2}\right)Zi_c(\ell,\lambda,h)\right] \times$$

$$\times I_{css}(m,\mu,j)\,Ji_1(m,n;\mu,\nu;j,k)\Big\}\left[\int_o^{z_e}\cos^2\frac{h\pi z}{z_e}dz\int_o^{2\pi}\sin^2 j\theta d\theta\int_o^1 J_j^2(S_{jk}r)\,rdr\right]^{-1}$$

Similarly the coefficients C_3 and C_4 of Eqs. (221) are derived by weighting the residuals with $\Psi_{B_{hjk}}$, and the corresponding expressions for I_{N_1} and I_{N_2} are given by:

$$I_{N_1} = \sum_{\ell,m,n}\sum_{\lambda,\mu,\nu}\Big\{A_{\ell mn}\frac{dA_{\lambda\mu\nu}}{dt}\Big[S_{mn}S_{\mu\nu}Zi_c(\ell,\lambda,h)\,I_{css}(j,m,\mu)\,Ji_3(m,n;\mu,\nu,j,k) + \tag{A13a}$$

$$+ m\mu Zi_c(\ell,\lambda,h)\, I_{ccc}(m,\mu,j)\, Ji_2(m,n;\mu,\nu;j,k) +$$

$$+ \ell\lambda\left(\frac{\pi}{z_e}\right)^2 Zi_s(\ell,\lambda,h)\, I_{css}(j,m,\mu)\, Ji_1(m,n;\mu,\nu;j,k)\Big] +$$

$$+ B_{\ell mn}\frac{dB_{\lambda\mu\nu}}{dt}\Big[S_{mn}S_{\mu\nu}\, Zi_c(\ell,\lambda,h)\, I_{ccc}(m,\mu,j)\, Ji_3(m,n;\mu,\nu;j,k) +$$

$$+ m\mu Zi_c(\ell,\lambda,h)\, I_{css}(j,m,\mu)\, Ji_2(m,n;\mu,\nu;j,k) +$$

$$+ \ell\lambda\left(\frac{\pi}{z_e}\right)^2 Zi_s(\ell,\lambda,h)\, I_{ccc}(m,\mu,j)\, Ji_1(m,n;\mu,\nu;j,k)\Big] +$$

$$+ A_{\ell mn}\frac{dB_{\lambda\mu\nu}}{dt}\Big[S_{mn}S_{\mu\nu}Zi_c(\ell,\lambda,h)\, I_{ccs}(j,\mu,m)\, Ji_3(m,n;\mu,\nu;j,k) -$$

$$- m\mu Zi_c(\ell,\lambda,h)\, I_{ccs}(j,m,\mu)\, Ji_2(m,n;\mu,\nu;j,k) +$$

$$+ \ell\lambda\left(\frac{\pi}{z_e}\right)^2 Zi_s(\ell,\lambda,h)\, I_{ccs}(j,\mu,m)\, Ji_1(m,n;\mu,\nu;j,k)\Big] +$$

$$+ B_{\ell mn}\frac{dA_{\lambda\mu\nu}}{dt}\Big[S_{mn}S_{\mu\nu}Zi_c(\ell,\lambda,h)\, I_{ccs}(j,m,\mu)\, Ji_3(m,n;\mu,\nu;j,k) -$$

$$- m\mu Zi_c(\ell,\lambda,h)\, I_{ccs}(j,\mu,m)\, Ji_2(m,n;\mu,\nu;j,k) +$$

$$+ \ell\lambda\left(\frac{\pi}{z_e}\right)^2 Zi_s(\ell,\lambda,h)\, I_{ccs}(j,m,\mu)\, Ji_1(m,n;\mu,\nu;j,k)\Big]\Big\}$$

$$I_{N_2} = - \sum_{\ell,m,n} \sum_{\lambda,\mu,\nu} \Big\{\Big[A_{\ell mn}\frac{dA_{\lambda\mu\nu}}{dt} I_{css}(j,m,\mu) + B_{\ell mn}\frac{dB_{\lambda\mu\nu}}{dt} I_{ccc}(m,\mu,j) \quad \text{(A13b)}$$

$$+ A_{\ell mn}\frac{dB_{\lambda\mu\nu}}{dt} I_{ccs}(j,\mu,m) + B_{\ell mn}\frac{dA_{\lambda\mu\nu}}{dt} I_{ccs}(j,m,\mu)\Big] \times$$

$$\times \left[S_{mn}^2 + \frac{\ell^2\pi^2}{z_e^2}\right] Zi_c(\ell,\lambda,h)\, Ji_1(m,n;\mu,\nu;j,k)\Big\}$$

In this case the coefficients of $A_{\ell mn}\frac{dB_{\lambda\mu\nu}}{dt}$ and $B_{\ell mn}\frac{dA_{\lambda\mu\nu}}{dt}$ disappear and the remaining terms are normalized by $N_{B_{hjk}}$ to yield the following expressions:

$$C_3(\ell,m,n;\lambda,\mu,\nu;h,j,k) = \Big\{2\Big[S_{mn}S_{\mu\nu} I_{css}(j,m,\mu)\, Ji_3(m,n;\mu,\nu;j,k) + \quad \text{(A14)}$$

$$+ m\mu I_{ccc}(m,\mu,j)\, Ji_2(m,n;\mu,\nu;j,k)\Big] Zi_c(\ell,\lambda,h) +$$

$$+ \Big[2\ell\lambda\left(\frac{\pi}{z_e}\right)^2 Zi_s(\ell,\lambda,h) - (\gamma-1)\left(S_{mn}^2 + \frac{\ell^2\pi^2}{z_e^2}\right) Zi_c(\ell,\lambda,h)\Big] \times$$

$$\times I_{css}(j,m,\mu)\, Ji_1(m,n;\mu,\nu;j,k)\Big\}\Big[\int_o^{z_e}\cos^2\frac{h\pi z}{z_e}dz \int_o^{2\pi}\cos^2 j\theta d\theta \int_o^1 J_j^2(S_{jk}r)\, r dr\Big]^{-1}$$

$$C_4(\ell,m,n;\lambda,\mu,\nu;h,j,k) = \Big\{2\Big[S_{mn}S_{\mu\nu}I_{ccc}(m,\mu,j)\,Ji_3(m,n;\mu,\nu;j,k) + \tag{A15}$$

$$+ m_\mu I_{css}(j,m,\mu)\,Ji_2(m,n;\mu,\nu;j,k)\Big]Zi_c(\ell,\lambda,h) +$$

$$+ \Big[2\ell\lambda\Big(\frac{\pi}{z_e}\Big)^2 Zi_s(\ell,\lambda,h) - (\gamma-1)\Big(S_{mn}^2 + \frac{\ell^2\pi^2}{z_e^2}\Big)Zi_c(\ell,\lambda,h)\Big] \times$$

$$\times I_{ccc}(m,\mu,j)\,Ji_1(m,n;\mu,\nu;j,k)\Big\}\Big[\int_o^{z_e}\cos^2\frac{h\pi z}{z_e}dz\int_o^{2\pi}\cos^2 j\theta d\theta\int_o^1 J_j^2(S_{jk}r)\,rdr\Big]^{-1}$$

APPENDIX B

EVALUATION OF DEFINITE INTEGRALS INVOLVING PRODUCTS OF TRIGONOMETRIC AND BESSEL FUNCTIONS

When the Galerkin method is used to obtain solutions to nonlinear problems various definite integrals arise whose integrands are products of three or more of the approximating functions used to expand the dependent variables. For a series expansion based upon the acoustic eigenfunctions for a circular cylinder integrals of products of trigonometric and Bessel functions must be evaluated. Integrals of this type appear in both the second order analysis of Chapter VI and the third order theory of Chapter VII and will be treated in this appendix.

Integrals Arising from the Second Order Theory

The integrals appearing in the coefficients of Eqs. (220) and (221) are of two types: (1) those involving products of the steady state velocity or its derivative and two trigonometric functions, and (2) those involving products of three trigonometric or Bessel functions with different arguments. Integrals of the first type appear in the coefficients $K(\ell, h)$ and $K_T(\ell, h)$ as shown in Eqs. (222) of Chapter VI, while integrals of the second type are defined by Eqs. (A9) of Appendix A.

Integrals Involving the Steady State Velocity

The integrals appearing in the coefficients K and K_T are given by the following expressions:

$$Ui_{cc}(\ell,h) = \int_o^{z_e} \frac{d\bar{u}}{dz} \cos\frac{\ell\pi z}{z_e} \cos\frac{h\pi z}{z_e}\, dz \qquad (B1)$$

$$Ui_{sc}(\ell,h) = \int_o^{z_e} \bar{u}(z) \sin\frac{\ell\pi z}{z_e} \cos\frac{h\pi z}{z_e}\, dz$$

where ℓ and h are non-negative integers. For arbitrary distributions of steady state velocity these integrals must be evaluated numerically. To avoid having to compute these integrals anew each time a change is made in the parameters $\bar{u}_e$ and z_e, Eqs. (B1) will be written in a more convenient form by making a change of variable. Introducing the new variable $\zeta = z/z_e$ the steady state velocity can be expressed in terms of the distribution function $f(\zeta) = \bar{u}(z)/\bar{u}_e$. This function varies between zero at the injector and unity at the nozzle so that the mean flow velocity and its derivative are given by:

$$\bar{u}(z) = \bar{u}_e f(z/z_e) \quad ; \quad \frac{d\bar{u}}{dz} = \frac{\bar{u}_e}{z_e} \frac{df}{d\zeta} \qquad (B2)$$

Substituting Eqs. (B2) into Eqs. (B1) and making the change of variable yields the desired expressions:

$$Ui_{cc}(\ell,h) = \bar{u}_e \int_o^1 \frac{df}{d\zeta} \cos\ell\pi\zeta \cos h\pi\zeta\, d\zeta \qquad (B3)$$

$$Ui_{sc}(\ell,h) = \bar{u}_e z_e \int_o^1 f(\zeta)\ \sin\ell\pi\zeta\ \cosh m\pi\zeta\ d\zeta$$

in which the integrands and the limits of integration are independent of the parameters $\bar{u}_e$ and z_e.

Under certain conditions analytical expressions for Eqs. (B3) can be obtained. The simplest case occurs when the velocity potential is expanded in terms of transverse modes; that is, $\ell = h = 0$. The integral Ui_{sc} then vanishes and Ui_{cc} is given by

$$Ui_{cc} = \bar{u}_e \int_o^1 \frac{df}{d\zeta}\, d\zeta = \bar{u}_e[f(1) - f(0)]$$

In view of the boundary conditions satisfied by the distribution function $f(\zeta)$, this integral reduces simply to

$$Ui_{cc}(0,0) = \bar{u}_e \tag{B4}$$

Since the influence of the steady state velocity distribution upon the solutions of Eqs. (220) and (221) appears only in the integrals given by Eqs. (B3), it is seen that the behavior of second order solutions involving only transverse modes does not depend on the distribution of the steady state velocity, but only on its value at the nozzle entrance.

The integrals Ui_{cc} and Ui_{sc} can also be evaluated analytically when the distribution function $f(\zeta)$ is a polynomial in ζ. Only the simplest case $f(\zeta) = \zeta$ will be considered here. This corresponds to a

combustor with uniformly distributed combustion for which the mean flow velocity $\bar{u}(z)$ increases linearly from zero at the injector end to its maximum value $\bar{u}_e$ at the nozzle entrance. Introducing $f(\zeta) = \zeta$ and $df/d\zeta = 1$ into Eqs. (B3) yields the following expressions:

$$Ui_{cc}(\ell,h) = \bar{u}_e \int_o^1 \cos\ell\pi\zeta \cosh m\zeta \, d\zeta \tag{B5}$$

$$Ui_{sc}(\ell,h) = \bar{u}_e z_e \int_o^1 \zeta \sin\ell\pi\zeta \cosh m\zeta \, d\zeta$$

The first of Eqs. (B5) is easily evaluated with the aid of standard integral tables to obtain:

$$Ui_{cc}(0,0) = \bar{u}_e \tag{B6}$$

$$Ui_{cc}(\ell,h) = \bar{u}_e/2 \qquad \ell \approx h$$

$$= 0 \qquad \ell \neq h$$

The integral Ui_{sc} can be evaluated by integration by parts to obtain the following expression:

$$Ui_{sc}(\ell,h) = -\frac{\bar{u}z_e}{2\pi}\left\{\zeta\left[\frac{\cos(\ell-h)\pi\zeta}{(\ell-h)} + \frac{\cos(\ell+h)\pi\zeta}{(\ell+h)}\right]_o^1 \right. \tag{B7}$$

$$- \int_0^1 \left[\frac{\cos(\ell-h)\pi\zeta}{(\ell-h)} + \frac{\cos(\ell+h)\pi\zeta}{(\ell+h)}\right] d\zeta \Bigg\}$$

where the second term vanishes (provided $\ell \neq h$) to give:

$$Ui_{sc}(\ell,h) = \frac{\bar{u}_e z_e}{2\pi}(-1)^{\ell+h+1}\left[\frac{1}{\ell-h} + \frac{1}{\ell+h}\right] \qquad (\ell \neq h) \qquad (B7)$$

for uniformly distributed combustion. For the special case $\ell = h$ the denominator in the first term of the above equation vanishes and Eq. (B7) does not represent the integral Ui_{sc}. Introducing $\ell = h$ into Eq. (B5) and again integrating by parts yields the desired result:

$$Ui_{sc}(h,h) = - 1/4h\pi \qquad (h \neq 0) \qquad (B8)$$

It is easily seen from the last of Eqs. (B5) that $Ui_{sc}(0,0) = 0$.

Integrals Appearing in the Coefficients of the Nonlinear Coupling Terms

When the Galerkin method is used to obtain approximate solutions for the velocity potential the quadratically nonlinear terms of Eq. (210) produce three types of definite integrals: (1) axial and (2) azimuthal integrals involving products of three sinusoidal functions with different arguments and (3) radial integrals of the product of a weighting function and three Bessel functions with different orders and arguments. The definitions of these integrals are given by Eqs. (A9) of Appendix A. These integrals will now be evaluated by analytical or numerical techniques.

Axial Integrals. The integrals over the length of the combustor are written in a more convenient form by making the change of variable $\varphi = \pi z/z_e$; thus:

$$Zi_c(a,b,c) = \frac{z_e}{\pi} \int_0^{\pi} \cos a\varphi \cos b\varphi \cos c\varphi \, d\varphi \tag{B9}$$

$$Zi_s(a,b,c) = \frac{z_e}{\pi} \int_0^{\pi} \sin a\varphi \sin b\varphi \cos c\varphi \, d\varphi$$

where a, b, and c are non-negative integers. Analytical expressions for Zi_c and Zi_s are readily derived with the aid of the following trigonometric relations:

$$\cos A \cos B = \frac{1}{2}\left[\cos(A-B) + \cos(A+B)\right] \tag{B10}$$

$$\sin A \sin B = \frac{1}{2}\left[\cos(A-B) - \cos(A+B)\right] \tag{B11}$$

Repeated use of Eqs. (B10) and (B11) yields the following expressions:

$$Zi_c(a,b,c) = \frac{z_e}{4\pi}\left\{\int_0^{\pi} \cos[(a-b-c)\varphi]d\varphi + \int_0^{\pi} \cos[(a-b+c)\varphi]d\varphi \right. \tag{B12}$$

$$\left. + \int_0^{\pi} \cos[(a+b-c)\varphi]d\varphi + \int_0^{\pi} \cos[(a+b+c)\varphi]d\varphi\right\}$$

$$Zi_s(a,b,c) = \frac{z_e}{4\pi}\left\{\int_0^{\pi} \cos[(a-b-c)\varphi]d\varphi + \int_0^{\pi} \cos[(a-b+c)\varphi]d\varphi \right. \quad \text{(B13)}$$

$$\left. - \int_0^{\pi} \cos[(a+b-c)\varphi]d\varphi - \int_0^{\pi} \cos[(a+b+c)\varphi]d\varphi\right\}$$

Each of the integrals in Eqs. (B12) and (B13) vanishes unless the argument of the cosine is zero, in which case its value is π. For nonzero values of a, b, and c this situation occurs only when $a = b + c$, $b = a + c$, or $c = a + b$ and even then only one of the four integrals will be nonzero. Thus the following results are obtained:

$$Zi_c(a, b, a+b) = Zi_c(a, a+c, c) = Zi_c(b+c, b, c) = z_e/4 \quad \text{(B14)}$$

$$Zi_s(a, b, a+b) = - z_e/4$$

$$Zi_s(a, a+c, c) = Zi_s(b+c, b, c) = z_e/4 \qquad (a, b, c \neq 0)$$

If any one of the integers a, b, or c is zero these integrals are more easily evaluated by returning to the original expressions given by Eqs. (B9). An inspection of the expressions for Zi_c and Zi_s reveals that

$$Zi_c(0, 0, 0) = z_e \quad \text{(B15)}$$

$$Zi_c(0, a, a) = Zi_c(a, 0, a) = Zi_c(a, a, 0) = Zi_s(a, a, 0) = z_e/2$$

where use has been made of the orthogonality properties of the sine and cosine functions. For all other values of the integers a, b, and c the integrals Zi_c and Zi_s vanish.

Azimuthal Integrals. The integrals over θ given in Eqs. (A9) are similar to those treated above; however there are four types of the azimuthal integrals and the limits of integration are different. To evaluate these integrals the trigonometric identities given by Eqs. (B10) and (B11) are needed as well as the additional relation:

$$\sin A \cos B = \frac{1}{2}\left[\sin(A + B) + \sin(A - B)\right] \tag{B16}$$

With the help of the above trigonometric relations the azimuthal integrals are expressed as the sum of four simpler integrals as follows:

$$I_{sss}(\alpha,\beta,\gamma) = \frac{1}{4}\left\{\int_o^{2\pi} \sin[(\alpha-\beta+\gamma)\theta]d\theta + \int_o^{2\pi} \sin[(\alpha+\beta-\gamma)\theta]d\theta\right. \tag{B17}$$

$$\left. - \int_o^{2\pi} \sin[(\alpha-\beta-\gamma)\theta]d\theta - \int_o^{2\pi} \sin[(\alpha+\beta+\gamma)\theta]d\theta\right\}$$

$$I_{ccs}(\alpha,\beta,\gamma) = \frac{1}{4}\left\{\int_o^{2\pi} \sin[(\alpha-\beta+\gamma)\theta]d\theta + \int_o^{2\pi} \sin[(\alpha+\beta+\gamma)\theta]d\theta\right. \tag{B18}$$

$$\left. - \int_o^{2\pi} \sin[(\alpha-\beta-\gamma)\theta]d\theta - \int_o^{2\pi} \sin[(\alpha+\beta-\gamma)\theta]d\theta\right\}$$

$$I_{css}(\alpha,\beta,\gamma) = \frac{1}{4}\left\{\int_0^{2\pi} \cos[(\alpha-\beta+\gamma)\theta]d\theta + \int_0^{2\pi} \cos[(\alpha+\beta-\gamma)\theta]d\theta \right. \tag{B19}$$

$$\left. - \int_0^{2\pi} \cos[(\alpha-\beta-\gamma)\theta]d\theta - \int_0^{2\pi} \cos[(\alpha+\beta+\gamma)\theta]d\theta\right\}$$

$$I_{ccc}(\alpha,\beta,\gamma) = \frac{1}{4}\left\{\int_0^{2\pi} \cos[(\alpha-\beta+\gamma)\theta]d\theta + \int_0^{2\pi} \cos[(\alpha+\beta-\gamma)\theta]d\theta \right. \tag{B20}$$

$$\left. + \int_0^{2\pi} \cos[(\alpha-\beta-\gamma)\theta]d\theta + \int_0^{2\pi} \cos[(\alpha+\beta+\gamma)\theta]d\theta\right\}$$

where it is observed that I_{sss} and I_{ccs} involve only the integrals of sines while the integrals I_{css} and I_{ccc} are composed only of integrals of cosines. By inspection of Eqs. (B17) and (B18) it is easily seen that

$$I_{sss}(\alpha,\beta,\gamma) = I_{ccs}(\alpha,\beta,\gamma) = 0$$

for all values of the integers α, β, and γ. The remaining integrals are similar to Eqs. (B12) and (B13) and are given by

$$I_{ccc}(\alpha, \beta, \alpha+\beta) = I_{ccc}(\alpha, \alpha+\gamma, \gamma) = I_{ccc}(\beta+\gamma, \beta, \gamma) = \pi/2 \tag{B22}$$

$$I_{css}(\alpha, \beta, \alpha+\beta) = I_{css}(\alpha, \alpha+\gamma, \gamma) = \pi/2$$

$$I_{css}(\beta+\gamma,\ \beta,\ \gamma) = -\pi/2$$

for α, β, and γ nonzero. If any one of the indices is zero (corresponding to a radial mode) the following values are obtained:

$$I_{ccc}(0,\ 0,\ 0) = 2\pi \tag{B23}$$

$$I_{ccc}(\alpha,\ \alpha,\ 0) = I_{ccc}(\alpha,\ 0,\ \alpha) = I_{ccc}(0,\ \alpha,\ \alpha) = \pi$$

$$I_{css}(0,\ \alpha,\ \alpha) = \pi$$

For all other values of α, β, and γ the integrals I_{ccc} and I_{css} are zero, for example:

$$I_{ccc}(\alpha,\ \alpha,\ \alpha) = \int_0^{2\pi} \cos^3\alpha\theta\ d\theta = 0$$

Since so many of these integrals vanish the number of nonlinear coupling terms occurring in Eqs. (220) and (221) is greatly reduced.

Radial Integrals. The radial integrals are of three types as shown below:

$$Ji_1 = \int_0^1 J_\lambda(ax)\,J_\mu(bx)\,J_\nu(cx)\,x\,dx \tag{B24}$$

$$Ji_2 = \int_o^1 J_\lambda(ax) J_\mu(bx) J_\nu(cx) \frac{1}{x} dx$$

$$Ji_3 = \int_o^1 J'_\lambda(ax) J'_\mu(bx) J_\nu(cx) x dx$$

where λ, μ, and ν are non-negative integers; a, b, and c are non-negative real numbers; and $J'_\lambda(ax)$ indicates the derivative with respect to the argument ax. In our case the numbers a, b, and c are restricted to the transverse mode frequencies as shown in Eqs. (A9). It is observed that the integrals Ji_1 and Ji_2 differ only in the form of the weighting function, while the integral Ji_3 involves the derivatives of the Bessel functions which are given by:

$$J'_m(z) = \frac{1}{2}\left[J_{m-1}(z) - J_{m+1}(z)\right] \qquad m = 1, 2, 3, \ldots$$

$$J'_o(z) = - J_1(z)$$

as found in any reference on Bessel functions.

A search of various tables of integrals and the literature on Bessel functions yielded no analytical formula for the evaluation of Eqs. (B24). These integrals however were easily calculated numerically to a sufficient degree of accuracy by using Simpson's Rule with twenty subdivisions. To save computation time it was noted that these integrals needed to be computed only for values of the integers λ, μ, and ν for which the azimuthal integrals $I_{ccc}(\lambda,\mu,\nu)$ and $I_{css}(\lambda,\mu,\nu)$ are nonzero.

The numerical evaluation of Ji_1 and Ji_3 is straightforward, but the integrand of Ji_2 is indeterminate at the lower limit of integration. If any one of the indices λ, μ, or ν is nonzero the limit of the integrand as the argument approaches zero is easily calculated with the aid of L'Hospital's Rule as follows:

$$L(\lambda,\mu,\nu) = \lim_{x\to 0} \frac{J_\lambda(ax)\,J_\mu(bx)\,J_\nu(cx)}{x}$$

$$L(\lambda,\mu,\nu) = \Big[aJ'_\lambda(ax)\,J_\mu(bx)\,J_\nu(cx) + bJ_\lambda(ax)\,J'_\mu(bx)\,J_\nu(cx) + cJ_\lambda(ax)\,J_\mu(bx)\,J'_\nu(cx) \Big]_{x=0} \qquad \text{(B25)}$$

From inspection of Eq. (B25) and the known behavior of the Bessel functions of various orders for zero arguments it is seen that the limit $L(\lambda,\mu,\nu)$ vanishes with the following exceptions:

$$L(1,\ 0,\ 0) = a/2 \qquad \text{(B26)}$$

$$L(0,\ 1,\ 0) = b/2$$

$$L(0,\ 0,\ 1) = c/2$$

For the special case $\lambda = \mu = \nu = 0$ the numerator of the integrand remains finite while the denominator vanishes and the limit $L(0,\ 0,\ 0)$ does not

exist. Fortunately in the expressions for the coefficients of the nonlinear terms the integral $Ji_2(m,n;\ \mu,\nu;\ j,k)$ is multiplied by m_μ and consequently this term vanishes if either m or μ is zero.

Numerical values of the integrals needed to compute the coefficients of the nonlinear terms when the expansion of the velocity potential consists of the first four tangential modes are presented in Table 2. In this case the integrals were computed from Eqs. (B24) with $a = S_{\lambda 1}$, $b = S_{\mu 1}$, and $c = S_{\nu 1}$. Inspection of the tabulated values reveals that as a rule these integrals are much smaller than unity with the integral Ji_3 an order of magnitude smaller than Ji_1 and Ji_2. The values of these integrals decrease as the order of the Bessel functions increases; however no conclusions regarding the dependence of the nonlinear coefficients on the order of the transverse modes can be inferred from this property of the integrals involving Bessel functions. The reason for this is the fact that in the expressions for the coefficients given by Eqs. (A11), (A12), (A14) and (A15) the radial integrals are multiplied by products or squares of the transverse mode frequencies which tends to offset the decrease in the values of the integrals. In fact the coefficients are found to increase slowly with increasing transverse mode numbers.

Integrals Arising from the Third Order Theory

The following integrals involving Bessel functions arise when the Galerkin method is applied to the third order equations (i.e., Eqs. (293) through (297)):

Table 2. Integrals of Bessel Functions

λ	μ	ν	Ji_1	Ji_2	Ji_3
1	2	1	0.04743	0.08515	0.00905
2	3	1	0.03044	0.04835	0.00538
3	4	1	0.02216	0.03272	0.00353
1	1	2	0.04743	0.08515	0.00729
1	3	2	0.03044	0.04835	0.00430
2	4	2	0.02082	0.03077	0.00297
1	2	3	0.03044	0.04835	0.00385
1	4	3	0.02216	0.03272	0.00250
1	3	4	0.02216	0.03272	0.00232
2	2	4	0.02082	0.03077	0.00246

Products of two Bessel functions:

$$J_1^{(2)} = \int_o^1 \left[J_m\left(S_{mn}r\right)\right]^2 rdr = \frac{S_{mn}^2 - m^2}{2S_{mn}^2}\left[J_m\left(S_{mn}\right)\right]^2 \qquad \text{(B27)}$$

$$J_2^{(2)} = \int_o^1 J_m\left(S_{mn}r\right)J_m'\left(S_{mn}r\right)rdr$$

$$J_3^{(2)} = \int_o^1 \left[J_m\left(S_{mn}r\right)\right]^2 \frac{1}{r}\,dr \qquad (m \neq 0)$$

Products of three Bessel functions (m = 0 only):

$$J_1^{(3)} = \int_o^1 \left[J_o\left(S_{on}r\right)\right]^3 rdr \qquad \text{(B28)}$$

$$J_2^{(3)} = \int_o^1 J_o\left(S_{on}r\right)\left[J_o'\left(S_{on}r\right)\right]^2 rdr$$

$$J_3^{(3)} = \int_o^1 \left[J_o\left(S_{on}r\right)\right]^2 J_o'\left(S_{on}r\right)rdr$$

$$J_4^{(3)} = \int_o^1 J_o\left(S_{on}r\right)J_o'\left(S_{on}r\right)J_o''\left(S_{on}r\right)rdr$$

Products of four Bessel functions:

$$J_1^{(4)} = \int_o^1 \left[J_m\left(S_{mn}r\right)\right]^4 \frac{1}{r}\,dr \qquad (m \neq 0) \qquad (B29)$$

$$J_2^{(4)} = \int_o^1 \left[J_m\left(S_{mn}r\right)\right]^4 \frac{1}{r^2}\,dr \qquad (m \neq 0)$$

$$J_3^{(4)} = \int_o^1 \left[J_m\left(S_{mn}r\right)\right]^3 J_m'\left(S_{mn}r\right) \frac{1}{r}\,dr \qquad (m \neq 0)$$

$$J_4^{(4)} = \int_o^1 \left[J_m\left(S_{mn}r\right)\right]^2 \left[J_m'\left(S_{mn}r\right)\right]^2 r\,dr$$

$$J_5^{(4)} = \int_o^1 \left[J_m\left(S_{mn}r\right)\right]^2 J_m'\left(S_{mn}r\right) J_m''\left(S_{mn}r\right) r\,dr$$

where

$$J_m'\left(S_{mn}r\right) = \frac{m}{S_{mn}r} J_m\left(S_{mn}r\right) - J_{m+1}\left(S_{mn}r\right)$$

$$J_m''\left(S_{mn}r\right) = \left[\frac{m(m-1)}{S_{mn}^2 r^2} - 1\right] J_m\left(S_{mn}r\right) + \frac{1}{S_{mn}r} J_{m+1}\left(S_{mn}r\right)$$

The integrals so indicated do not appear in the differential equations

if m = 0, and their integrands become indeterminate at the lower limit of integration for m nonzero. In each case, however, application of L'Hospital's Rule reveals that the limit is zero.

The above integrals were evaluated numerically by the use of Simpson's Rule. Numerical values of these integrals and the associated constants K_i and K_i' (as defined by Eqs. (310) and (316)) are given below for the first tangential and the first radial modes:

First tangential mode (m = 1, n = 1)

$$J_1^{(2)}(1,1) = 0.119347 \qquad K_1 = 2.352635 \tag{B30}$$

$$J_2^{(2)}(1,1) = 0.045764 \qquad K_2 = -0.154700$$

$$J_3^{(2)}(1,1) = 0.280779 \qquad K_3 = 0.613503$$

$$J_1^{(4)}(1,1) = 0.060035 \qquad K_4 = 2.013540$$

$$J_2^{(4)}(1,1) = 0.092148 \qquad K_5 = 0.043478$$

$$J_3^{(4)}(1,1) = 0.028077$$

$$J_4^{(4)}(1,1) = 0.005189 \qquad K_6 = 0.503032$$

$$J_5^{(4)}(1,1) = -0.007080$$

First radial mode (m = 0, n = 1)

$$J_1^{(2)}(0,1) = 0.081108 \tag{B31}$$

$J_2^{(2)}(0,1) = -0.021739$ $\quad$ $K_1' = 0.352279$

$J_1^{(3)}(0,1) = 0.028572$ $\quad$ $K_2' = 0.176139$

$J_2^{(3)}(0,1) = 0.014286$ $\quad$ $K_3' = 1.220311$

$J_3^{(3)}(0,1) = -0.026529$ $\quad$ $K_4' = -0.612129$

$J_4^{(3)}(0,1) = 0.013307$ $\quad$ $K_5' = -0.164783$

$J_4^{(4)}(0,1) = 0.011190$ $\quad$ $K_6' = 0.137966$

$J_5^{(4)}(0,1) = 0.003582$

APPENDIX C

NUMERICAL SOLUTION OF THE DIFFERENTIAL EQUATIONS

In applying the Galerkin method, the original set of nonlinear partial differential equations was converted to a system of nonlinear ordinary differential equations. These equations, which are given by Eqs. (223) and (224) for the second order analysis and Eqs. (305) through (309) for the third order theory, are not amenable to analytical solution. Therefore these equations must be solved by the methods of numerical analysis.

In the determination of the limiting periodic solutions of the above mentioned equations it is necessary to perform the numerical integration over a relatively large number of integration steps. It is therefore desired that the numerical method used has a small local discretization error and is not subject to numerical instability. These requirements are found to be met by the fourth order Runge-Kutta method, one of the most widely used numerical integration techniques. This method is discussed in any book on numerical analysis (e.g., see Conte[32]), from which the following formulas are taken. For the system of two differential equations given by:

$$\frac{dy}{dt} = f(y,z,t) \quad ; \quad \frac{dz}{dt} = g(y,z,t) \tag{C1}$$

the values at the next integration step are computed from the previous ones by:

$$y_{n+1} = y_n + \frac{1}{6}\left(k_1 + 2k_2 + 2k_3 + k_4\right) \tag{C2}$$

$$z_{n+1} = z_n + \frac{1}{6}\left(\ell_1 + 2\ell_2 + 2\ell_3 + \ell_4\right)$$

where

$$k_1 = hf\left(y_n,\ z_n,\ t_n\right) \tag{C3}$$

$$\ell_1 = hg\left(y_n,\ z_n,\ t_n\right)$$

$$k_2 = hf\left(y_n + k_1/2,\ z_n + \ell_1/2,\ t_n + h/2\right)$$

$$\ell_2 = hg\left(y_n + k_1/2,\ z_n + \ell_1/2,\ t_n + h/2\right)$$

$$k_3 = hf\left(y_n + k_2/2,\ z_n + \ell_2/2,\ t_n + h/2\right)$$

$$\ell_3 = hg\left(y_n + k_2/2,\ z_n + \ell_2/2,\ t_n + h/2\right)$$

$$k_4 = hf\left(y_n + k_3,\ z_n + \ell_3,\ t_n + h\right)$$

$$\ell_4 = hg\left(y_n + k_3,\ z_n + \ell_3,\ t_n + h\right)$$

where h is the integration step-size. These equations can be readily extended to a larger system of equations.

Treatment of the Time Delay

The equations which resulted from the application of the Galerkin method to our combustion instability problem differ in form from those given by Eqs. (C1). To be more specific these equations contain terms involving a retarded variable; that is, a dependent variable which is evaluated at the earlier time $t - \bar{\tau}$. Such terms arise because Crocco's time-lag model was used to describe the combustion process. Due to the presence of the retarded variables, the formulas (C3) used in the Runge-Kutta method must be slightly modified.

The appropriate formulas for applying the Runge-Kutta method to problems involving a time-delay are readily obtained by considering a single equation of the following form:

$$\frac{dx}{dt} = f(x,t) + g[x(t - \bar{\tau})] \qquad (C4)$$

Noting that at any step of the integration the value of $x(t - \bar{\tau})$ has already been determined from previous steps the function g can be considered to be a known function of time g(t) and can be combined with the time dependence of f. It then follows from Eqs. (C2) and (C3) that

$$x_{n+1} = x_n + \frac{1}{6}\left(k_1 + 2k_2 + 2k_3 + k_4\right)$$

where $$k_1 = h\left\{f(x_n,t_n) + g[x(t_n - \bar{\tau})]\right\} \tag{C5}$$

$$k_2 = h\left\{f\left(x_n + k_1/2,\ t_n + h/2\right) + g[x(t_n + h/2 - \bar{\tau})]\right\}$$

$$k_3 = h\left\{f\left(x_n + k_2/2,\ t_n + h/2\right) + g[x(t_n + h/2 - \bar{\tau})]\right\}$$

$$k_4 = h\left\{f\left(x_n + k_3,\ t_n + h\right) + g[x(t_n + h - \bar{\tau})]\right\}$$

Since $x(t)$ is computed only at discrete points $x_n(t_n)$ it is desired that the retarded variable $x(t_n - \bar{\tau})$ will coincide with such previously computed points. This can be accomplished by choosing the step-size h such that it divides the time-lag $\bar{\tau}$ into k equal increments. Thus $\bar{\tau} = kh$ and the retarded variables become

$$x(t_n - \bar{\tau}) = x(t_n - kh) = x_{n-k} \tag{C6}$$

$$x(t_n + h - \bar{\tau}) = x[t_n - (k - 1)h] = x_{n-k+1}$$

$$x(t_n + h/2 - \bar{\tau}) = x[t_n - (k - 1/2)h] = x_{n-k+\frac{1}{2}}$$

where the value $x_{n-k+\frac{1}{2}}$ is computed by interpolation. The Runge-Kutta formulas which apply to Eq. (C4) can now be written as:

$$x_{n+1} = x_n + \frac{1}{6}\left(k_1 + 2k_2 + 2k_3 + k_4\right)$$

$$k_1 = h\left\{f(x_n, t_n) + g(x_{n-k})\right\} \tag{C7}$$

$$k_2 = h\left\{f(x_n + k_1/2,\ t_n + h/2) + g(x_{n-k+\frac{1}{2}})\right\}$$

$$k_3 = h\left\{f(x_n + k_2/2,\ t_n + h/2) + g(x_{n-k+\frac{1}{2}})\right\}$$

$$k_4 = h\left\{f(x_n + k_3,\ t_n + h) + g(x_{n-k+1})\right\}$$

Equations (C7) are readily extended to a system of equations where the functions corresponding to g depend on both the dependent variables and the retarded variables. It is seen from Eqs. (C7) that k values of the dependent variables prior to the initial values are needed to start the integration.

Special Considerations

Second Order Equations

If M terms are included in the expansion for the velocity potential Eqs. (223) and (224) represent a system of M second order (in derivatives) differential equations. For application of the Runge-Kutta method these equations can be written as an equivalent system of 2M first order equations as follows:

$$\frac{dA_{jk}}{dt} = A'_{jk}$$

$$\frac{dA'_{jk}}{dt} = - S^2_{jk}A_{jk} - KA'_{jk} - K_\tau A'_{jk}(t - \bar{\tau}) \tag{C8}$$

$$- \sum_{m,n} \sum_{\mu,\nu} \left\{ C_1(m,n;\mu,\nu;j,k) A_{mn} B'_{\mu\nu} + C_2(m,n;\mu,\nu;j,k) B_{mn} A'_{\mu\nu} \right\}$$

$$\frac{dB_{jk}}{dt} = B'_{jk}$$

$$\frac{dB'_{jk}}{dt} = - S^2_{jk}B_{jk} - KB'_{jk} - K_\tau B'_{jk}(t - \bar{\tau}) \tag{C9}$$

$$- \sum_{m,n} \sum_{\mu,\nu} \left\{ C_3(m,n;\mu,\nu;j,k) A_{mn} A'_{\mu\nu} + C_4(m,n;\mu,\nu;j,k) B_{mn} B'_{\mu\nu} \right\}$$

where the dependent variables are now A_{jk}, A'_{jk}, B_{jk}, and B'_{jk}.

Third Order Equations

First consider the system of equations which govern the tangential modes as given by Eqs. (305) through (309). The continuity and momentum equations are already in the proper form for application of the Runge-Kutta method and can be expressed as follows:

$$\frac{dA_\rho}{dt} = f_\rho\left(A_\rho, A_\eta, A_\zeta, A_p, A_p(t - \bar{\tau})\right) \tag{C10}$$

$$\frac{dA_\eta}{dt} = f_\eta\left(A_\rho, A_\eta, A_\zeta, A_p\right)$$

$$\frac{dA_\zeta}{dt} = f_\zeta\left(A_\rho,\ A_\eta,\ A_\zeta,\ A_p\right)$$

where f_ρ, f_η, and f_ζ are the right hand sides of Eqs. (305), (306) and (307) respectively. On the other hand the energy equation contains the two derivatives $\frac{dA_h}{dt}$ and $\frac{dA_\rho}{dt}$ and the equation of state is an algebraic equation. These equations can be written in the required form by differentiating the equation of state and introducing the result into the energy equation to eliminate $\frac{dA_h}{dt}$. In addition other derivatives that appear are expressed in terms of Eq. (C10), which yields the result

$$\frac{dA_p}{dt} = f_p\left(A_\rho,\ A_\eta,\ A_\zeta,\ A_p,\ A_p(t - \bar{\tau})\right) \tag{C11}$$

where

$$f_p = \gamma\left\{\left[1 - \frac{\gamma-1}{2} I_u\right]f_\rho - \frac{\bar{\rho}_e \bar{u}_e}{z_e} f_h\right. \tag{C12}$$

$$- 3/8(\gamma-1)S_{mn}^2 K_5\left[2A_\rho A_\eta f_\eta + A_\eta^2 f_\rho\right] - 3/4\ S_{mn}^2 K_5 A_\rho A_\eta f_h$$

$$\left. - 1/8(\gamma-1)m^2 K_6\left[2A_\rho A_\zeta f_\zeta + A_\zeta^2 f_\rho\right] - 1/4\ m^2 K_6 A_\rho A_\zeta f_h\right\}$$

and

$$f_h = \frac{1}{I_\rho}\left\{A_p - \left[1 - \frac{\gamma-1}{2} I_u\right]A_\rho + \frac{3}{8}(\gamma-1)S_{mn}^2 K_5 A_\rho A_\eta^2\right. \tag{C13}$$

$$+ \frac{1}{8}(\gamma-1)m^2 K_6 A_\rho A_\zeta^2\Big\}$$

Applying a similar procedure to the radial mode equations yields:

$$\frac{dA_\rho}{dt} = g_\rho\Big(A_\rho,\ A_\eta,\ A_p,\ A_p(t-\bar{\tau})\Big) \tag{C14}$$

$$\frac{dA_\eta}{dt} = g_\eta(A_\rho,\ A_\eta,\ A_p)$$

$$\frac{dA_p}{dt} = g_p\Big(A_\rho,\ A_\eta,\ A_p,\ A_p(t-\bar{\tau})\Big)$$

where g_ρ and g_η are the right hand sides of Eqs. (312) and (313) respectively and g_p is given by:

$$g_p = \gamma\Big\{\Big(1 - \frac{\gamma-1}{2} I_u\Big)g_\rho - (\gamma-1)S_{on}^2 K_2' I_\rho A_\eta g_\eta \tag{C15}$$

$$- \frac{\gamma-1}{2} S_{on}^2 K_6'\Big[2A_\rho A_\eta g_\eta + A_\eta^2 g_\rho\Big] - \Big[\frac{\bar{p}_e \bar{u}_e}{z_e} - K_1' g_\rho +$$

$$+ S_{on}^2 K_2' I_\rho A_\eta + S_{on}^2 K_6' A_\rho A_\eta + \frac{n\bar{u}_e}{z_e} K_1'\Big(A_p(t) - A_p(t-\bar{\tau})\Big)\Big]g_h\Big\}$$

In Eq. (C15) the function g_h is the right hand side of Eq. (315).

One of the nonlinear combustion terms appearing in the continuity

equation (i.e., Eq. (312)) involves the integral $\int_{t-\bar{\tau}}^{t} A_p(t')\,dt'$. This expression is treated by introducing the new dependent variable:

$$A_I = \int_{t-\bar{\tau}}^{t} A_p(t')\,dt' \tag{C16}$$

which can be differentiated to obtain:

$$\frac{dA_I}{dt} = A_p(t) - A_p(t - \bar{\tau}) \tag{C17}$$

This last equation is solved numerically as part of the system of simultaneous differential equations. The initial value $A_I(0)$ is found by integrating the initial values of $A_p(t)$ over the interval $-\bar{\tau} \le t \le 0$. For initial conditions of the form $A_p(t) = P_M \cos S_{on} t$ one obtains:

$$A_I(0) = \frac{P_M}{S_{on}} \sin(S_{on}\bar{\tau}) \tag{C18}$$

Accuracy of the Numerical Calculations

One of the least desirable features of the Runge-Kutta methods is that error estimates are very difficult to obtain analytically. In this case an indication of the accuracy of the computed solutions can be obtained by comparing with exact solutions for special cases and by considering the effect of varying the step-size. In the latter case the accuracy should improve with decreasing step-size until a point is reached

where the accumulation of round-off error becomes important.

For both the second order and third order equations the numerical integration scheme was tested by considering two limiting cases: (1) the linearized equations with $\bar{u}_e = 0$ which corresponds to a harmonic oscillation, and (2) the linearized equations for $\bar{u}_e > 0$. In these tests a step-size of the order of 0.05 was used. For the case $\bar{u}_e = 0$ the calculated solution agreed with the predicted sine curve to five significant digits for the first cycle. Over longer periods of time (hundreds of cycles) the calculated results showed a negligible decay in amplitude due to error accumulation. For $\bar{u}_e > 0$ the numerical solutions exhibited the expected behavior; i.e., (1) growth of amplitude in the linearly unstable region, (2) decay in the linearly stable region, and (3) neutral oscillations on the neutral stability curve.

The accuracy of the nonlinear solutions was estimated by changing the step-size. In one particular case halving the step-size resulted in only a one percent increase in the computed limit cycle amplitude. In addition the computed amplitude remained essentially constant even when the computations were continued for several thousand cycles. In the case of unstable limit cycles (i.e., triggering limits) the solution is determined after only a few cycles of oscillation when the errors are expected to be small. On the basis of the above results it may be concluded that the errors associated with the numerical integration process are negligible for the values of the step-size used.

LITERATURE CITED

1. Sotter, J. G., and Flandro, G. A., "Resonant Combustion in Rockets," Scientific American, December 1968, pp. 95-103.

2. Hefner, R. J., "Diagnosis of High Frequency Combustion Stability Characteristics from Pressure Measurements," Third ICRPG Combustion Conference CPIA Publication No. 138, vol. I (October 1966).

3. Crocco, L., and Cheng, S. I., Theory of Combustion Instability in Liquid Propellant Rocket Motors, AGARD Monograph No. 8, Butterworths Scientific Pub., Ltd., London, 1956.

4. Scala, S. M., "Transverse Wave and Entropy Wave Combustion Instability in Liquid Propellant Rockets," Princeton University Aeronautical Engineering Report No. 380, April 1957, (Ph.D. Thesis).

5. Reardon, F. H., "An Investigation of Transverse Mode Combustion Instability in Liquid Propellant Rocket Motors," Princeton University Aeronautical Engineering Report No. 550, June 1961, (Ph.D. Thesis).

6. Culick, F. E. C., "Stability of High Frequency Pressure Oscillations in Gas and Liquid Rocket Combustion Chambers," M.I.T. Aerophysics Laboratory Report No. 480, June 1961.

7. Zinn, B. T., "A Theoretical Study of Nonlinear Transverse Combustion Instability in Liquid Propellant Rocket Motors," Princeton University AMS Technical Report No. 732, May 1966, (Ph.D. Thesis).

8. Maslen, S. H., and Moore, F. K., "On Strong Transverse Waves Without Shocks in a Circular Cylinder," Journal of Aeronautical Sciences, vol. 23, no. 6, 1956, pp. 583-593.

9. Priem, R. J., and Guentert, D. C., "Combustion Instability Limits Determined by a Nonlinear Theory and a One-Dimensional Model," NASA TN D-1409, October 1962.

10. Sirignano, W. A., "A Theoretical Study of Nonlinear Combustion Instability: Longitudinal Mode," Princeton University AMS Technical Report No. 677, March 1964, (Ph.D. Thesis).

11. Mitchell, C. E., "Axial Mode Shock Wave Combustion Instability in Liquid Propellant Rocket Engines," Princeton University AMS Technical Report No. 798, (NASA CR 72259), July 1967, (Ph.D. Thesis).

12. Burstein, S. Z., and Chinitz, W., "Nonlinear Combustion Instability in Liquid Propellant Rocket Motors," Jet Propulsion Laboratory Quarterly Reports prepared under Contract 951946.

13. Campbell, D. T., and Chadwick, W. D., "Combustion Instability Analysis at High Chamber Pressure," Rocketdyne Technical Report AFRPL-TR-68-179.

14. Finlayson, B. A., and Scriven, L. E., "The Method of Weighted Residuals -- A Review," Applied Mechanics Reviews, vol. 19, no. 9, September 1966, pp. 735-744.

15. Kaplan, W., Advanced Calculus, Addison-Wesley Publishing Company, 1952, (see pp. 417-422).

16. Ames, W. F., Nonlinear Partial Differential Equations in Engineering, Academic Press, 1965.

17. Williams, F. A., Combustion Theory, Chapter 1, Addison-Wesley Publishing Company, 1965.

18. Snyder, L. J., Spriggs, T. W., and Stewart, W. E., "Solutions of the Equations of Change by Galerkin's Methods," American Institute of Chemical Engineers Journal, vol. 10, no. 4, July 1964, pp. 535-539.

19. Shuleshko, P., "A New Method of Solving Boundary Value Problems of Mathematical Physics," Australian Journal of Applied Science, vol. 10, 1959, pp. 1-7.

20. Finlayson, B. A., and Scriven, L. E., "The Method of Weighted Residuals and its Relation to Certain Variational Principles for the Analysis of Transport Processes," Chemical Engineering Science, vol. 20, 1965, pp. 395-404.

21. Finlayson, B. A., and Scriven, L. E., "On the Search for Variational Principles," International Journal of Heat and Mass Transfer, June 1967, pp. 799-819.

22. Bolotin, V. V., Nonconservative Problems of the Theory of Elastic Stability, The MacMillan Company, New York, 1963.

23. Lighthill, M. J., "Viscosity Effects in Sound Waves of Finite Amplitude," Surveys in Mechanics, Cambridge Press, 1956, pp. 250-351.

24. Blackstock, D. T., "Approximate Equations Governing Finite-Amplitude Sound in Thermoviscous Fluids," General Dynamics GD/E Report GD-1463-52.

25. Liepmann, H. W., and Roshko, A., Elements of Gasdynamics, John Wiley and Sons, Inc., 1957.

26. Burns, S. H., "Finite-Amplitude Traveling Waves With Boundary Dissipation," Office of Naval Research Report NR-384-903, January 1966.

27. Crocco, L., and Sirignano, W. A., "Effect of the Transverse Velocity Component on the Nonlinear Behavior of Short Nozzles," American Institute of Aeronautics and Astronautics Journal, vol. 4, no. 8, August 1966, pp. 1428-30.

28. Mitchell, C. E., "High Subsonic Mach Number Extension to the Linearized Theory," Chapter VI of Nonlinear Aspects of Combustion Instability in Liquid Propellant Rocket Motors, Princeton University Aeronautical Report No. 553-d, 1964.

29. Zinn, B. T., and Savell, C. T., "A Theoretical Study of Three-Dimensional Combustion Instability in Liquid-Propellant Rocket Engines," Proceedings of the Twelfth International Symposium on Combustion, Williams and Wilkins, Co., Baltimore, 1969, pp. 139-147.

30. Kantorovich, L. V., and Krylov, V. I., Approximate Methods of Higher Analysis, Interscience Publishers, 1964.

31. Priem, R. J., and Heidmann, M. F., "Propellant Vaporization as a Design Criterion for Rocket-Engine Combustion Chambers," NASA TR R-67, 1960.

32. Conte, S. D., Elementary Numerical Analysis, McGraw-Hill Book Company, 1965.

VITA

Eugene Alexander Powell was born on July 20, 1943, in Charlotte, North Carolina. He attended public schools in Georgia and South Carolina and graduated from Sprayberry High School in Marietta, Georgia.

He entered the Georgia Institute of Technology in the fall of 1961 and was graduated with highest honors from the school of Aerospace Engineering in June of 1965. He continued his education as a graduate student at the Georgia Institute of Technology in September, 1965 and was awarded the degree of Master of Science in Aerospace Engineering in June, 1968.

He is a member of Sigma Gamma Tau, Tau Beta Pi, and Sigma Xi, and had a NASA Predoctoral Traineeship from September 1965 to September 1968 and a NSF Intermediate Traineeship from September 1968 to September 1969.